

Øystein Leif Gurandsrud Hestad

**Prebreakdown phenomena in
solids and liquids stressed by
fast transients: The effect of
additives and phase.**

Doctoral thesis
for the degree of philosophiae doctor

Trondheim, November 2010

Norwegian University of Science and Technology
Faculty of Natural Sciences and Technology
Department of Chemistry

NTNU

Norwegian University of Science and Technology

Doctoral thesis
for the degree of philosophiae doctor

Faculty of Natural Sciences and Technology
Department of Chemistry

© 2010 Øystein Leif Gurandsrud Hestad.

ISBN ISBN 978-82-471-2479-6 (printed version)
ISBN ISBN 978-82-471-2480-2 (electronic version)
ISSN 1503-8181

Doctoral theses at NTNU, 2010:243

Printed by NTNU-trykk

Contents

Contents	ii
List of papers	iii
Abstract	v
Preface	vii
Acknowledgements	ix
1 Introduction	1
1.1 Motivation	1
1.2 Hypothesis	2
1.3 Thesis outline	3
2 Field-dependent conductivity	5
2.1 Charge injection	5
2.1.1 Schottky injection	5
2.1.2 Fowler-Nordheim injection	6
2.2 High-field bulk conduction	7
2.2.1 Hopping conduction	7
2.2.2 Poole-Frenkel conduction	8
2.3 Space charge limited field	10
3 Finite element method	13
3.1 Introduction	13
3.2 Brief history	13
3.3 What is the finite element method	14
3.4 Application	15

4	Prebreakdown phenomena	17
4.1	Streamers	17
4.2	Electrical trees	22
5	Methods and materials	25
5.1	Experimental outline	25
5.2	Chemicals and procedure for sample preparation	27
6	Experimental and theoretical results	31
7	Future perspectives	35
8	Concluding remarks	39
	Bibliography	50
	Papers	51
	Paper 1	51
	Paper 2	65
	Paper 3	85
	Paper 4	99
	Paper 5	135

List of papers

1. Ø. L. Hestad, L. E. Lundgaard and D. Linhjell *New experimental system for the study of the effect of temperature and liquid to solid transition on streamers in dielectric liquids: Application to cyclohexane* IEEE Trans. Dielect. Elect. Insul., 2010, 17, 764-774.
2. Ø. L. Hestad; L. E. Lundgaard and P.-O. Åstrand *n-tridecane as a model system for polyethylene: Comparison of pre-breakdown phenomena in liquid and solid phase stressed by a fast transient* Submitted to the IEEE Trans. Dielect. Elect. Insul., 2010
3. Ø. L. Hestad, S. Ingebrigtsen, H. S. Smalø, P.-O. Åstrand and L. E. Lundgaard *Effects of N,N-dimethylaniline and trichloroethene on prebreakdown phenomena in liquid and solid n-tridecane* Submitted to the IEEE Trans. Dielect. Elect. Insul., 2010
4. H. S. Smalø, Ø. L. Hestad, S. Ingebrigtsen and P.-O. Åstrand *Field dependence on the molecular ionization potential and excitation energies compared to conductivity models for insulation materials at high electrical fields* Submitted to J. Appl. Phys.
5. Ø. L. Hestad and S. Boggs *Approximation of field, charge and extent of space charge limited field from a spheroid in a uniform background field* To be submitted.

Abstract

This study has been conducted to improve the knowledge of processes responsible for dielectric breakdown of liquid and solid insulation. This is important, as the electric power grid depends on reliable and cost effective insulation materials.

Prebreakdown phenomena in liquid and solid neat cyclohexane, neat n-tridecane, n-tridecane with 0.1 M N,N-dimethylaniline (DMA) and n-tridecane with 0.1 M trichloroethene (TCE) have been studied in a needle-plane geometry with positive and negative needle with impulse voltage. For this purpose an experimental setup for dielectric testing of insulating liquids and frozen liquids in the temperature range from -60°C to $+250^{\circ}\text{C}$ was built. The system uses a sensitive differential charge measurement technique, a computer controlled temperature regulator, a photomultiplier, and a pulse generator with a fast rise time (<40 ns, <60 kV). The electrode gap was 11.5 mm, and most experiments were conducted with a $2\ \mu\text{m}$ tip radius.

Experiments were conducted in cyclohexane to make comparison with previous results with similar experimental setups possible, n-tridecane was chosen based on the known similarities in energy bands for polyethylene and alkanes. Thus n-tridecane was used as a model system for polyethylene. The additives were chosen based on their electrochemical properties. DMA has a low ionization potential and TCE is a known electron scavenger.

Currents recorded below the inception voltage (Pre-inception currents) have been compared to finite element model calculations to obtain high-field conductivity models for liquid and frozen neat n-tridecane and neat cyclohexane. The conductivity models obtained in this way was then compared to classical conductivity models. In addition field dependent ionization and excitation energies obtained from density functional theory (DFT) simulations have been used to explain the high-field conductivity. The high-field conductivity in neat n-tridecane was found to have similar field dependence as what has been reported for cross linked polyethylene, and high-field conduction in cyclohexane can be explained by the Poole-Frenkel mechanism.

Conduction currents were observed at lower voltages in n-tridecane than in cyclohexane, corresponding to the low space charge limited field (SCLF) in n-tridecane. This may explain the lower inception voltage in cyclohexane, as the SCLF for cyclohexane is sufficient to make electron avalanches in the liquid phase plausible, while for n-tridecane the SCLF is low enough to limit the field without the creation of a streamer/electrical tree. Thus the formation of electron avalanches in n-tridecane may rely on the formation of a low density region.

Adding TCE to n-tridecane increases the pre-inception current and reduces the inception voltage for negative and positive polarity. TCE had no effect on propagation of streamers in n-tridecane. The main effect of DMA in n-tridecane is to enhance the propagation of streamers and electrical trees with positive polarity. This is in line with what has been reported for cyclohexane, and is explained by the low ionization potential of DMA.

Inception voltages, light emission and charge injection were found to be similar for liquid and solid phase in neat n-tridecane and in n-tridecane with additives, which indicates that the same processes are responsible for inception and propagation of electrical trees in solids and streamers in liquids when the material is stressed by a fast transient. The similarity between the measured properties in solid and liquid phase leads to the conclusion that electrical treeing mainly takes place in the amorphous regions of the solid phase. The scatter is generally found to increase when going from liquid to solid phase, which is explained by the inhomogeneity in the solid phase.

In another part of this thesis work, approximations for the electric field and the charge on a spheroid in a uniform background field (or semispheroid on a plane) and of the maximum extent of the SCLF region on axis of the spheroid is presented. This is relevant for electrical tree initiation, as a SCLF region of about $2 \mu\text{m}$ is needed for inception. The approximations are accurate for step voltages of finite rise time with exponentially increasing conductivity of the form $\sigma_0 \exp(k|E|^{1/n})$, where “n“ can vary from 1 to 3, which covers the range of functional dependence found in the literature, k and σ_0 are constants, and E is the electric field.

Preface

This thesis is submitted to the Norwegian University of Science and Technology (NTNU) for partial fulfilment of the degree of philosophiae doctor.

This doctoral work has been performed at the department of Chemistry, NTNU, Trondheim, with Per-Olof Åstrand as main supervisor and with co-supervisors Lars E. Lundgaard and Erling Ildstad.

This work has been funded by the Research Council of Norway through a Strategic Industry Program (164603/I30).

Acknowledgements

This thesis is dedicated to Åsta, my beloved wife.

During the work with this thesis, I have received help and support from many people. Without them, this thesis would never have been completed.

First of all, I would like to thank my supervisor, professor Per-Olof Åstrand, and my co-supervisor Lars Lundgaard. Their suggestions, insight, and support have made this work possible. They have shown great patience with me throughout this project, and have been of invaluable help while writing the articles that this thesis is based on.

Part of this work was conducted at the University of Connecticut. I want to express my gratitude to professor Steven Boggs and his students at the University of Connecticut for making my stays at UCONN so memorable. Steven always took the time to sit down and discuss with me when I was lost and did not know how to proceed. I always learned a lot at UCONN. The stays there were very inspiring. Steven has also read through part of this thesis, and patiently tried to improve my English and give me advice on how to improve the thesis. During my stay at UCONN I was very impressed by the students there, and I learned a lot from all of them. I would especially like to thank Lily, Kai, Essay and Jim, who always took very good care of me, both during daytime at the university, and after working hours. I would also like to thank them for the many good parties I was invited to during my stays in the US, and for patiently trying to teach me Chinese.

Further, I would like to thank my former and present colleagues at SINTEF Energy research and at the Department of Chemistry. I would especially like to thank my fellow PhD students, Stian, Hans Sverre and Tjasa, for many interesting and some very entertaining discussions. Dag Linhjell at SINTEF Energy Research has also been very important to this work. Calibration and testing of the experimental setup was at times extremely challenging and time consuming. Dag always took the time to discuss possible problems and solutions when I was at a dead end.

I am very grateful for the financial support that I have received from

SINTEF Energy Research and from the Research Council of Norway. SINTEF Energy Research generously provided funding for an extension of my PhD period to finish this thesis.

Finally I would like to thank my friends and my supportive family.

Chapter 1

Introduction

1.1 Motivation

High-voltage equipment constitutes an important part of the infrastructure of modern society. For transmission of electrical energy over large distances high voltages are indispensable. All high-voltage equipment depends on suitable insulating materials that can insulate conductors from other conductors and ground. Insulation material used can be gas, vacuum, liquid, solid or a combination of these.

Air is a cheap and reliable insulator, which is used extensively, for example in electric power transmission (power-lines). However, using air as insulation requires a large free volume around the conductors as the dielectric breakdown strength of air is relatively low. The dielectric properties of air and other gasses can be improved through increased pressure. In addition to air several other gasses are used in high voltage equipment, including nitrogen, CO_2 and SF_6 . In electronegative gasses, free electrons attach to neutral gas molecules are converted from light to heavy charge carriers, which reduces greatly the rate of charge carrier energy gain from the electric field. This is the case for SF_6 and explains its superior dielectric strength when compared to air, nitrogen and CO_2 . SF_6 is also the gas of choice in high voltage circuit breakers because it deionizes much more quickly than other gases after an arc. However, SF_6 is a very potent greenhouse gas, and more environmentally friendly alternatives are being pursued. High pressure gas insulation can attain high dielectric strengths, can be used with complex geometries, and the insulation is considered self healing as a discharge will not leave a permanent structure in the gas.

Liquid insulation has many of the same positive attributes as gas insulation, but in addition it can act as a more effective coolant for high voltage

equipment, as convection currents in the apparatus can bring heat from warm to cold areas. In liquids, as in gasses, dielectric breakdown is preceded by the initiation and growth of a streamer, typically growing from a defect in the insulation, or from a protrusion at the conductors. Streamers bridging the gap between conductors usually lead to dielectric breakdown of the insulation. Streamers that do not bridge the gap will typically be quenched when the field driving the phenomenon falls (either by reduction of the background field or as a result of the growing streamer). Subsequent convection of the liquid makes the insulation self healing, although repeated discharges in the liquid will cause long term ageing of the insulation. The higher density of liquids typically increases their dielectric strength compared to gasses.

The intrinsic breakdown strength of solid insulation is typically higher than for liquid or gas insulation. The main drawback with solid insulation is that it does not possess the same self-healing properties as liquid and gas. Similar structures as observed in gas and liquid are also observed at high voltages in solid insulation, where they are called electrical trees. Such trees are permanent, so that once such a structure starts to evolve, the process is cumulative and will eventually lead to dielectric breakdown. Solid electric insulators are generally poor thermal conductors, which limits their use in applications with high power density as thermal degradation and finally thermal breakdown are likely outcomes. Solid insulation is, however, needed in all power-apparatus as their mechanical strength is needed for construction of power apparatus. In many cases, as for switchgear and high voltage transformers, the solution is to combine solid and liquid or solid and gas insulation.

For improved reliability and economy, knowledge of the causes of deterioration is essential. The tendency to increase the design electric field to reduce cost as well as the push towards new more environmentally friendly insulation materials requires more knowledge of the factors influencing breakdown and prebreakdown phenomena.

1.2 Hypothesis

The fundamental hypothesis on which this project is based is that the evolution of hot electrons is the most critical component in the prebreakdown/breakdown event for both solid and liquid insulators. Our initial assumption was that the interaction between a hot electron and a molecule should not depend on the phase of the material, whether it be liquid or an amorphous solid. Therefore pre-breakdown phenomena are assumed to be

similar in the two phases. To test this hypothesis, an experimental setup was built enabling us to perform prebreakdown experiments in liquids and frozen liquids, thus making it possible to compare measurements performed in the same sample in liquid and solid states.

Hot electrons in the medium must originate either from charge injection from electrodes or through ionization of molecules in the insulation. Two additives were employed, one with a low ionization potential (IP) and one with known electron scavenging properties, to study their effect on the prebreakdown phenomena, which should be related to the creation and capture of hot electrons. For hot electrons, and possibly electron avalanches, to be created in a medium, a large electric field must exist over a sufficient volume. As the charge redistribution in the high-field region will have influence on the field, it is important to find plausible high-field conduction models that can be used to find the field distribution in which the electrons are accelerated, in order to gain knowledge of the processes responsible for inception of streamers and electrical trees.

Finally the base liquid used for most of the experiments, n-tridecane, was chosen based on its similarities with polyethylene. It is postulated that this (frozen) liquid can be used as a model system for the more complex polymeric insulator.

1.3 Thesis outline

The main part of this work is presented in five papers included at the end of this thesis. Throughout this thesis, the papers will be referred to as *paper 1-paper 5*. A list of all the papers can be found in the preface.

The thesis has been divided into 8 chapters, including this introduction. The next three chapters focus on theory after which a presentation of the experimental methods and the chemicals used is given, followed by a presentation of the experimental and theoretical results presented in the papers. In the two last chapters, some thoughts/ideas for future work and concluding remarks are given.

Chapter 2

Field-dependent conductivity

Conductivity is proportional to the product of carrier mobility and carrier density, both of which can be field-dependent. The increased conductivity typically observed when increasing the electric field can be caused by injection of charge from the electrodes, dissociation of molecules into positive and negative ions, ionization of molecules creating ion-electron pairs and/or an increase in the charge carriers mobility as a result of the electric field. For liquids stressed by high fields the liquid can be set in motion by the ions which in turn will lead to increased ion mobility in the liquid (electrohydrodynamic motion) [1].

In the following, a brief recap of some important mechanisms for charge injection from electrodes and conduction in bulk dielectrics are presented. For a more thorough discussion the reader is referred to the book by Disgado and Fothergill for solid dielectrics/polymers [2], the book by Werner F Schmidt for liquids [3], and a series of papers on this topic [4–16].

2.1 Charge injection

2.1.1 Schottky injection

Charge injection at high field electrodes requires the potential barrier, Φ , between the metal electrode and the dielectric media to be lowered sufficiently for electrons to escape. For electrodes in vacuum this barrier is given by the work function of the material, while the situation is more complex for polymers and liquids. To a first approximation the barrier that electrons need to overcome to enter the dielectric can be modelled by the electrostatic attraction between the escaping electron and the electrode. This can be formalized using the image charge method. The resulting potential as a

function of the distance from the electrode, $V(x)$, is given by [2],

$$V(x) = \frac{e^2}{16\pi\epsilon_0\epsilon_r x} \quad (2.1)$$

where e is the electron charge, ϵ_0 is the permittivity of vacuum, ϵ_r is the relative permittivity of the medium, and x is the distance from the electrode. When an external field is applied the potential will be lowered by eEx ,

$$V(x) = \frac{e^2}{16\pi\epsilon_0\epsilon_r x} - eEx \quad (2.2)$$

where E is the electric field. Eq. 2.2 can be used to find how much the barrier, Φ , is lowered by the external field. Based on this an equation for the effective potential, Φ_{eff} , the electron must overcome to enter the material can be found,

$$\Phi_{eff} = \Phi - \frac{e}{2} \sqrt{\frac{eE}{\pi\epsilon_0\epsilon_r}} \quad (2.3)$$

In order to find the current density across the electrode the rate at which electrons with sufficient energy to climb the barrier enters the material must be found. This can be done using the energy distribution of electrons in the metal (given by the Fermi-Dirac distribution), and results in the following equation for current at the electrode [2],

$$J = \frac{4\pi emk_B^2(1-R)T^2}{h^3} \cdot e^{-\frac{\Phi_{eff}}{k_B T}} \quad (2.4)$$

where m is the electron mass, k_b is Boltzmann constant, R is the reflection rate of electrons at the electrode surface ($R \leq 1$), T is the temperature, and h is Planck's constant.

2.1.2 Fowler-Nordheim injection

For a sufficiently strong electric field at the metal-dielectric interface the barrier width can be reduced sufficiently to make direct tunnelling of electrons from the electrode into the bulk possible (~ 20 MV/cm for tungsten-cyclohexane) [10]. This is called Fowler-Nordheim injection. The current density across the electrode can be found by quantum mechanics [2],

$$J = \frac{e^3 E^2}{8\pi h \phi} \cdot e^{-\frac{4}{3} \sqrt{\frac{2m}{h^2}} \frac{\phi^{3/2}}{eE}} \quad (2.5)$$

where $\phi = \Phi - E_f$, E_f is the Fermi energy and Φ is the work function of the metal. Eq. 2.5 is based on tunnelling through a triangular barrier [17], which is a good approximation of the potential at the electrode surface for field strengths of the magnitude necessary for Fowler-Nordheim injection. Currents measured in cyclohexane from very sharp negative needle electrodes ($< 0.5 \mu\text{m}$) with DC voltage have been shown to fit eq. 2.5 [10].

Fowler-Nordheim injection is observed for negative electrodes where electrons can tunnel through the barrier and into the dielectric (field emission). For positive electrodes a similar phenomena can occur where electrons can tunnel from the liquid to the metal (field ionization).

2.2 High-field bulk conduction

2.2.1 Hopping conduction

A series of common conduction models for polymers and dielectrics are termed hopping conduction [2, 18, 19]. The term hopping refers to a sudden displacement of a charge carrier from one localized site in the dielectric to another nearby site. To achieve this, the charge carrier must overcome the potential barrier between the two sites. This can be done either through thermal excitation over the barrier, tunnelling through the barrier or by a two stage process where the carrier is first thermally excited and then tunnels through the barrier to an equipotential energy level in a nearby site (thermally assisted tunnelling).

In general thermally assisted tunnelling is considered the most likely hopping mechanism, at least for moderate field strengths [2]. There are several different flavours of thermally assisted hopping conduction, two of the most important being variable-range hopping [20] and the random free-energy barrier model [21]. Variable-range hopping results in a conductivity of the form [2, 20],

$$\sigma(E) = A \exp\left(-\frac{B}{T^n}\right), \quad B = 4 \left(\frac{2\alpha^3}{9\pi k_B N(E_f)} \right) \quad (2.6)$$

where A is a constant, T is the temperature, $n = 1/4$, and $N(E_f)$ is the density of states at the Fermi level E_f . α can be derived from quantum mechanics using the WKB approximation and depends on the shape of the barrier (primarily on the barrier height and width) and the energy of the charge carrier [2, 17]. For low fields, the hopping conductivity in eq. 2.6 is primarily determined by the temperature, but as the field increases the

height and the width of the barrier that the charge carriers need to tunnel through will be decreased, thus increasing the conductivity.

Note that hopping is in some way a misleading name for thermally assisted tunnelling, as this mechanism does not require the charge carrier to jump over the barrier. The term hopping is thus best used for the case where the tunnelling between states can be neglected, and the charge carrier jumps over the potential barrier between sites. Such hopping over the barrier results in a conductivity given by [18],

$$\sigma(E) = \frac{2\nu a e n}{E} \cdot e^{-\frac{W}{k_B T}} \cdot \sinh\left(\frac{e E a}{2 k_B T}\right) \quad (2.7)$$

where ν is the escape frequency, a is the distance between traps, E is the electric field, e is the elementary charge, h is Planck's constant, k_B is Boltzmann's constant, n is the charge carrier density, T is the temperature, and W is the trap depth. The field dependence in eq. 2.7 comes from the lowering of the barrier in the direction of the field, and the increase in barrier in the opposite direction. Eq. 2.7 is only valid for a single trap depth and uniform distribution of the traps, and it assumes that tunnelling between traps can be neglected [14].

The hopping conduction models assume the charge carriers to be localized between each "jump" to a new site. As the field is increased, the barriers are lowered making each jump easier and thereby increasing the average speed of the charge carriers. Thus hopping conduction describes how the mobility of charge carriers depends on temperature and field. Generally the field dependence of the mobility derived from hopping models depends on the distribution of the traps in space and energy. A field dependent conductivity of the form given by eq. 2.7 is the classical example of hopping conduction, but more sophisticated models exist in which the mobility increase exponentially with the square root of the field [13, 14].

2.2.2 Poole-Frenkel conduction

A lowering of the barrier that localizes charge carriers is the foundation for the classical Poole-Frenkel conduction mechanism [2]. The barrier is lowered by the external electric field, thereby increasing the number of free carriers in the dielectric. This mechanism can be used for materials with wide band gaps that contain charge donors or acceptors. These charge donors and acceptors should require more energy than the available thermal energy in order to be ionized. In complex materials (i.e. polymers), regions of high or low electronegativity can be created at chemical or physical defects in the material, and these regions act as electron donors or acceptors [2, 15].

The rate of thermal excitation, r_i , over the barrier which localizes the electrons in the donor states can be found in the classical limit, [2]

$$r_i = n_D \nu_0 e^{-\frac{IP_0 - \Delta V}{k_b T}} \quad (2.8)$$

where n_D is the number density of occupied donor states, ν_0 is the attempt to escape frequency of the electrons, IP_0 is the ionization potential of the donors at zero field, and ΔV is the lowering of the potential in the field direction given by,

$$\Delta V = -2\sqrt{\frac{e^3 E}{4\pi\epsilon_0\epsilon_r}} \quad (2.9)$$

At equilibrium, the rate of ionization is equal to the rate of recombination, r_r , which is expressed as, [2]

$$r_r = n_c(N_d - n_d)vS = n_c^2 vS; \quad (n_c = N_d - n_d) \quad (2.10)$$

Here n_c is the number density of conduction electrons, N_d is the number density of donors, S is the capture cross-section of donors and v is the thermal velocity of electrons in the conduction band. Assuming that the system is in equilibrium, $r_i = r_r$,

$$n_c = \sqrt{\frac{n_D \nu_0}{vS}} e^{-\frac{IP_0 - \Delta V}{2k_b T}}. \quad (2.11)$$

The conductivity is given by: $\sigma = n_c \mu$, where μ is the mobility of free electrons in the medium. The following equation is the classical Poole-Frenkel equation, where one assumes that $\nu_0 = N_{eff} vS$,

$$\sigma(E) = \sqrt{N_{eff} N_d} \cdot e \mu \cdot e^{-\frac{IP_0}{2k_B T}} \cdot e^{-\frac{\sqrt{e^3 E}}{k_B T \sqrt{4\pi\epsilon_0\epsilon_r}}} \quad (2.12)$$

where N_{eff} is the effective density of states in the conduction band, and ϵ_r is the relative permittivity of the material. The relative permittivity is included to account for the reduction in field acting on the electron due to the screening by the dielectric. In Eq. 2.12, we have assumed that only the free electrons contribute to the conductivity. One could also envisage that bound electrons can tunnel through the barrier to a neighbouring ionized donor leaving behind an ionized donor. This is called hole conduction and can also contribute to the overall conductivity [3].

2.3 Space charge limited field

As described in the previous section, injection of charge from the electrodes and the conductivity of dielectrics are highly field dependent. Typically the conductivity increases exponentially with the field. This has a marked effect in high field regions, as the increase in conductivity leads to charge separation and charge buildup that limits the field. The resulting field is called the space charge limited field (SCLF) and was first described by Zeller et al. who used a simple model to investigate this phenomenon [22, 23]. In their model, they assume that the conductivity can be approximated by a step function with low conductivity below the SCLF and high conductivity above the SCLF. The abrupt jump in conductivity was explained by a mobility edge for electrons in the material, thus at fields above the SCLF the electrons are effectively delocalized. Clearly this is a crude approximation, as the conductivity increases gradually with field [13]. Nevertheless this simple model is very useful as it provides simple approximations for the charge distribution and extent of the SCLF from a needle electrode [23] (see *paper 5*), temperature rise near high field protrusions [22], and the electromechanical forces acting on the material in such high field regions [22].

Most high field conductivity models can be approximated to a function of the form,

$$\sigma(E) = \sigma_0 \cdot e^{(k \cdot E^{\frac{1}{n}})} \quad (2.13)$$

where σ_0 , k , and n are constants, and E is the electric field. n is typically either 1, 2 or 3, where $n = 1$ corresponds to standard hopping conduction (eq. 2.7), $n = 2$ can be explained by mechanisms such as Poole-Frenkel (eq. 2.12), Onsager-conductivity [7] and some hopping conduction models [13, 14], $n = 3$ has no established physical basis, but fits high field conduction current measurements in n-tridecane (*paper 2*) and XLPE [12]. A simple statistical-mechanics approach based on the Poole-Frenkel mechanism with field dependent excitation and ionization energies suggests that $n = 3$ for n-tridecane as a result of the field dependence of the excitation energies for n-tridecane (*paper 4*). Clearly eq. 2.13 is a simplification, as temperature is not taken into account. For impulse voltages, the temperature increase in the high field region can be substantial, and thus temperature should be included in the formula [24]. Nevertheless, a simple conductivity formula like eq. 2.13 is sufficient to gain a better understanding of the SCLF.

With a field dependent conductivity of the form given by eq. 2.13, the SCLF can be estimated from the time scale on which charge must redistribute to limit the field (dielectric time constant) compared to the frequency

of the applied voltage. The dielectric time constant must be comparable to the inverse of the voltage frequency [25],

$$\frac{1}{w} = \frac{\epsilon_r \epsilon_0}{\sigma(F_c)} \Rightarrow \sigma(F_c) = \epsilon_r \epsilon_0 w \quad (2.14)$$

where w is the frequency of the applied voltage and F_c is the SCLF. w is angular frequency if a sin/cos voltage is applied, and normal frequency for linear voltage ramps. An alternative to this approach is to compare the resistive current density, $E \cdot \sigma(E)$, and the displacement current density, $\epsilon_0 \epsilon_r \frac{dE}{dt}$. If the capacitive term is dominant, then conductivity plays a secondary role, and the field distribution is approximately Laplacian. When the field increases sufficiently to increase the conductive term to the same magnitude as the capacitive term, the SCLF is reached.

Using eqs 2.13 and 2.14, a formula for the SCLF, F_c can be derived:

$$F_c = \left(\frac{1}{k} \cdot \ln \left(\frac{\epsilon_r \epsilon_0 w}{\sigma_0} \right) \right)^n \quad (2.15)$$

Eq. 2.15 shows that for an exponentially increasing conductivity, the SCLF depends on the (angular) frequency, w . This is demonstrated in Figure 2.1, where four conductivity models with the same SCLF at 10 MHz have been plotted versus field (see *paper 5*). The four conductivity formulas plotted all give a SCLF of 1 MV/m at 10 MHz. The SCLF for 20 MHz and 1 MHz for all four models can be found from the intersection of the horizontal lines corresponding to the respective frequencies ($\epsilon_0 \epsilon_r w$) and the conductivity versus field. Note that the SCLF does not depend on frequency when the conductivity is modelled as a step-function.

SCLF and high-field conductivity are important when trying to predict the field associated with pre-breakdown phenomena. In the SCLF region, the field will be almost constant, determined by the space charge, and can be substantially lower than the calculated Laplacian field. However, the space charge increases the volume of high field (Figure 2.2). The combination of high electric field and high conductivity also results in intense energy dissipation in this region (σE^2), which can result in substantial temperature increase in the material, especially for impulse voltages [24]. The high energy dissipation and large space charge density in the high-field region leads to strong mechanical and thermal stressing of the material that can lead to degradation [22, 25].

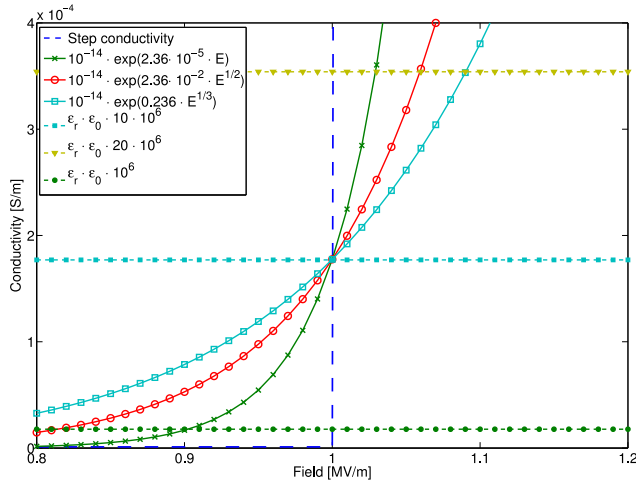


Figure 2.1: Four models for high field conductivity and $\epsilon_r \epsilon_0 w$ versus electrical field ($\epsilon_r = 2$). Note that the SCLF given by the intersections between the conductivity and $\epsilon_r \epsilon_0 w$ are low compared to typical insulators, but this plot gives the idea of how to obtain the SCLF and the frequency dependence of the SCLF. This figure is taken from *paper 5*.

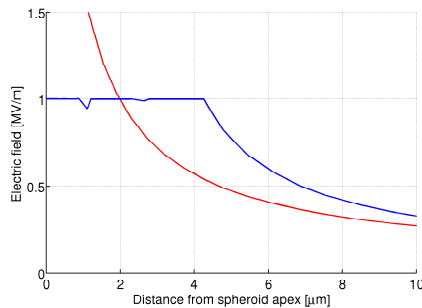


Figure 2.2: Comparison of space charge perturbed field (blue) and Laplacian field (red) along the axis from the apex of a semi-spheroid with minor axis of $10 \mu\text{m}$ and major axis of $100 \mu\text{m}$ in a uniform background field. The high-field conductivity used to obtain the blue line was a step function with step (SCLF) at 1 MV/m . Note that for XLPE the SCLF is between 200 and 300 MV/m [25].

Chapter 3

Finite element method

3.1 Introduction

The finite element method (FEM) is used in the engineering and scientific community in a wide range of disciplines ranging from civil engineering to quantum mechanics [26]. It can be used to find numerical solutions to partial differential equations with boundary values on complex geometries. When FEM is used to solve and analyse problems, it is typically referred to as finite element analysis (FEA). In this work FEM was used to model conduction currents and the field distribution in a needle-plane geometry using the commercial FEM program Comsol [27]. In the following, a brief overview of the method will be given without going into the mathematical details. A more complete introduction to the topic can be found in Ref. [28].

3.2 Brief history

FEM was developed in 1943 by the mathematician Richard L. Courant [29]. In his paper on variational methods for solving partial differential equations (PDEs) he included a short appendix where he used piecewise-linear approximation on a set of triangles, which he called elements, to solve PDEs on a set of simple two-dimensional geometries. More than ten years later the method was rediscovered and used by engineers in the aviation industry [30] from where it spread to virtually all branches of engineering and science. The name “Finite element method” was given to the method by R. W. Clough in a paper from 1960 [31], and an interesting summary of the origin of the method can be found in Ref. [32].

3.3 What is the finite element method

FEM is a numerical procedure used to find approximate solutions of partial differential equations (PDEs) on a domain with a set of boundary conditions. Such boundary value problems (BVPs) arise in mathematical modelling of many physical, chemical and biological phenomena. Very frequently, the equations under consideration, or the domain on which they should be solved are so complicated that finding their analytical solution is either impossible or impracticable.

FEM enables an approximate solution of complex BVPs by dividing the domain on which the PDEs should be solved into many sub-domains called finite elements. Thus the continuous domain is replaced by a number of subdomains in which the unknown function (for example electric potential or temperature) is represented by simple interpolation functions with unknown coefficients. These coefficients are the value of the unknown equation at a set of nodes in the finite element. The nodes are placed at each edge of the elements, and internally if a higher order shape function is used. Then a set of linear equations is created for each element using variational methods [28, 33] or weighted residual methods (for example the Galerkin method) [28, 34]. These equations are then combined into one large equation set, and solved using standard linear algebra after the boundary conditions are imposed. In some cases, where the material properties depend on the unknown function or its derivative, iterative methods are used to solve the BVP. Problems where material properties depend on the unknown function or its derivatives are called nonlinear, an example is problems involving field dependent conductivity. In this way an approximation of the unknown function are obtained at the nodes, and can be found approximately for all parts of the domain by the interpolation functions (shape functions). In summary the FEM consists of the following basic steps:

- Creating the problem geometry
- Discretization of the domain (creating the mesh)
- Selection of interpolation/shape equations
- Formulation of the system of linear equations
- Solving the equation set

The description above only explains how the PDEs are solved for a stationary system. For a time dependent problem one must also discretize time (discrete time steps are used), thus the problem is discretized in both

space and time. There are several methods for time stepping in numerical solvers of PDEs, many of which are based on so called Backward Differentiation Formulas (BDFs). BDFs are formulas that give an approximation to a derivative of the unknown function at a time t in terms of its values at t and earlier times. They are derived by forming an interpolating polynomial approximating the function using the solution from earlier time steps, differentiating it, and evaluating it at t . Picking appropriate time steps is challenging, as small time steps are beneficial to improve convergence, while larger time steps speed up the calculations as the equation set must be solved for each time step.

The accuracy of the solution can be improved by dividing the domain into smaller elements or by using a higher order shape function. However, this comes at a computational cost. A useful feature of the FEM is that the mesh does not have to be uniform. Thus a tight mesh can be used where a good approximation of the unknown function is needed or where the unknown function changes rapidly, and a coarse mesh can be used elsewhere. For time dependent problems, time stepping is typically challenging as short time steps improve convergence but at a computational cost. This can be overcome by adaptive time-stepping where short steps are used when the unknown function changes rapidly, and longer time steps are used when this is not the case. One should, for example, use short time steps during the voltage rise of a step voltage when the conductivity of the material depends on the electric field (nonlinear problem), while longer time steps can be used during time periods where the electric field changes slowly.

3.4 Application

FEM has its roots in structural and civil engineering and is still very important in these disciplines [32]. However, PDEs are central to science and can be used to describe a large range of phenomena in science and engineering. A few examples of areas where FEM is important are: acoustics [35], diffusion [36], electromagnetics [28], fluid dynamics [37], geophysics [38], heat transfer/thermal analysis [39], and quantum mechanics [26].

Within engineering, FEM is often used to test new designs before production of a test series/model. In this way, critical parameters can be tested as an integrated part of the design process prior to construction. For the aviation and car industry, the structural strength of their designs and the ability to withstand impact can be analysed, while for electrical engineering, hot spots (both thermally and electrically) in transformers and other high voltage equipment can be discovered by FEA of the design.

FEM is used extensively in electrical engineering for a wide range of problems, from simplified models of complete transformers [40–43] to models of streamer inception/propagation in dielectric liquids [44–46]. FEM has been used to model internal faults in power transformers to improve diagnostic methods of transformers in service [41, 43] and to analyse transformer failures [40]. For more fundamental studies of the effect of very high fields on dielectric materials, charge generation and transport is of vital importance. FEM can be used to find plausible high-field conduction mechanism for dielectrics by comparing results from simulations with experimental measurements [12] (*paper 2*). Such high field conductivity formulas, in combination with thermal properties of the material, can be used to calculate the field distribution, space charge buildup, electro-mechanical tension, and temperature rise in dielectrics in the vicinity of conductive protrusions for various voltage waveforms [25]. It can also be used to find the defect tolerance of the insulation [47], and the energy available for channel formation/three inception [48].

FEM has been used to find plausible mechanisms for the transition from water trees to electrical trees [49] and to model the change in dielectric response seen for cables with water trees [50]. Modelling the entire process responsible for the inception and propagation of electrical trees and streamers is, however, a daunting project as the mechanisms are very complex (see chapter 4) and the phenomenon is three dimensional. Even so, two dimensional models of streamers have been obtained with FEM for a model where free charge is assumed to be generated by field ionization [44–46]. Nevertheless, for modelling inception and propagation of streamers and electrical trees, hybrid methods are typically used. In hybrid models, FEM or other numerical methods are used to calculate the local electric field, while the propagation of the channel/tubule is controlled by a random generator and the local field [51, 52]. Such methods have been utilized to recreate the general shape of electrical trees and streamers [51–54].

Chapter 4

Prebreakdown phenomena

Stressing of dielectric liquid and solid insulation by a sufficiently strong electric field ultimately breaks down the material insulating properties, resulting in breakdown. This process can occur slowly as a result of long time ageing or rapidly at high over-voltages. Typically the dielectric strength of insulation materials used in high voltage systems is so high that extraordinary incidents (lightning impulse/switching impulse), malpractice when performing maintenance, conducting protrusions into the insulation creating regions with high fields or other contaminants reducing the mechanical or dielectric strength of the material is responsible for dielectric breakdown.

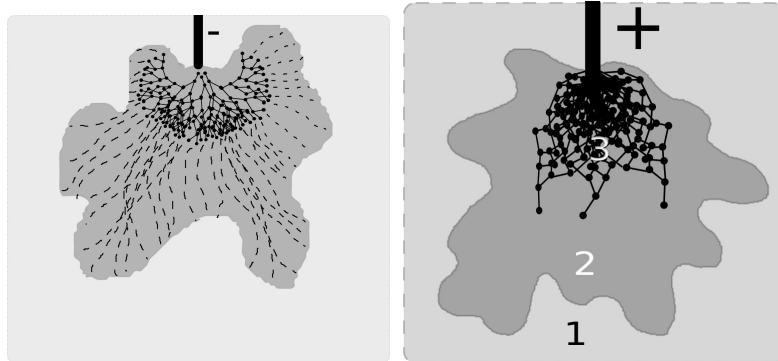
This thesis concentrates on the propagation of pre-breakdown structures in liquid and solid insulation from sharp needle electrodes in a needle-plane geometry. In liquids, all such “structures” are called streamers and are characterized by a change in refraction index making visual observation of the phenomena by schlieren or shadowgraphic techniques possible. For solid insulation, the structures are called electrical trees. In both cases, the shape of the structure can be quite diverse, depending on the experimental conditions and the sample material. However, bush or tree like structures are seen for both phases. In the following sections, some characteristics of streamers and electrical trees are presented, as well as some models used to explain the physical phenomena responsible for their inception and propagation in the insulation.

4.1 Streamers

Whereas streamers in gas discharge theory is a well defined type of discharge [55, 56], “streamers“ as related to liquids is a term used for all pre-breakdown phenomena observable by shadowgraphic or schlieren tech-

niques. As a consequence fundamentally different phenomena are classified as streamers. To differentiate among types of streamers, they are typically labelled by the polarity of the electrode from which they initiate. In addition to the division by polarity, one separates the streamers by their appearance and the speed of propagation into differing propagation modes. For positive streamers, the propagation speed increases in well defined steps as the voltage is increased, and four modes have been reported for transformer oil [57, 58]. For negative polarity the propagation speed increases more gradually, making classification into modes more difficult. In addition to visual inspection and average speeds based on pictures and oscilloscope recordings, the transition between modes can typically be seen by a clear increase in average current during streamer propagation [59]. This makes classification into different modes possible based solely on charge/current recordings. In addition to the polarity and voltage amplitude, the inception voltage (voltage level where 50% of applied impulses results in inception of streamers) is also influenced by the electrode geometry and the rise time of the applied voltage [60]. Typically the inception voltage is lower for negative polarity than for positive polarity.

The mechanism responsible for inception of streamers from negative needle electrodes in cyclohexane has been studied thoroughly, and is the same for dc and impulse voltage [10,61,62]. The first discharge occurs in the liquid phase and a shock wave develops propagating from the needle electrode. In the wake of the shock wave, a bubble develops, and subsequent discharges occur in the bubble. This theory has been supported by experiments showing that the first current pulse (electron avalanche in the liquid) does not depend on pressure, while the subsequent discharges can be quenched by increasing the hydrostatic pressure [61]. For positive streamers, even the first discharge can be quenched by increasing the hydrostatic pressure [61]. Thus the discharge responsible for inception of positive streamers probably occurs in a low density region. Such a low density region can be formed through joule heating (boiling), increased concentration of microvoids due to electromechanical forces [63], pressure reduction due to Coulomb repulsion between unipolar charges [64, 65], or a combination of these mechanisms. Although experiments suggest that electron avalanches in the liquid phase are responsible for inception of negative streamers in cyclohexane this is not necessarily the case for all liquids. Liquids with a low SCLF and a short mean-free path for free electrons require a low density region for avalanches to occur, as the field never reaches sufficient magnitudes to facilitate electron avalanches at normal densities. Thus inception for negative and positive streamers in liquids with a low SCLF and/or a short mean-free path



(a) Repetitive discharges in the gas phase feeds the streamer with the energy required for growth. Electron avalanches produce electrons that bombard the streamer-liquid interface inducing local evaporation through inelastic collisions.

(b) Positive 1st mode streamers propagate in a similar way as negative streamers. The energy required for evaporation of the liquid is provided through discharges in the gas, but the fast electrons now propagate towards the high-field electrode, leaving slower ions behind.

Figure 4.1: (a) 1st mode negative streamer propagation and (b) 1st mode positive streamer propagation

might be as described for the positive polarity above (*paper 2* and *paper 3*). An outline of the propagation mechanism for negative and positive 1st mode streamer is given in Figure 4.1

Second mode streamers propagate faster and form more filamentary structures than 1st mode streamers. Inception of 1st and 2nd mode positive streamers is probably governed by the same process [60]. For both modes, an ionized bubble is created by the first discharge, but while 1st mode streamers evolve into a dense bush-like structure 2nd mode streamers are more filamentary. Second mode positive streamers require a voltage above a threshold voltage, typically called the propagation voltage, V_p , that is independent of the point radius [60]. Thus 1st mode streamers require a sharp needle where inception can occur at voltages below the propagation voltage. For electrodes with point radius above a critical radius, r_c , no 1st mode streamers are observed [60]. An ionized low density bubble is created, but for voltages above the threshold voltage for 2nd mode streamers, the resulting field at the boundary of the bubble is large enough for ionization of the liquid-bubble interface. This results in a propagating ionization region (“streamer head”). The ionization of the liquid in front of

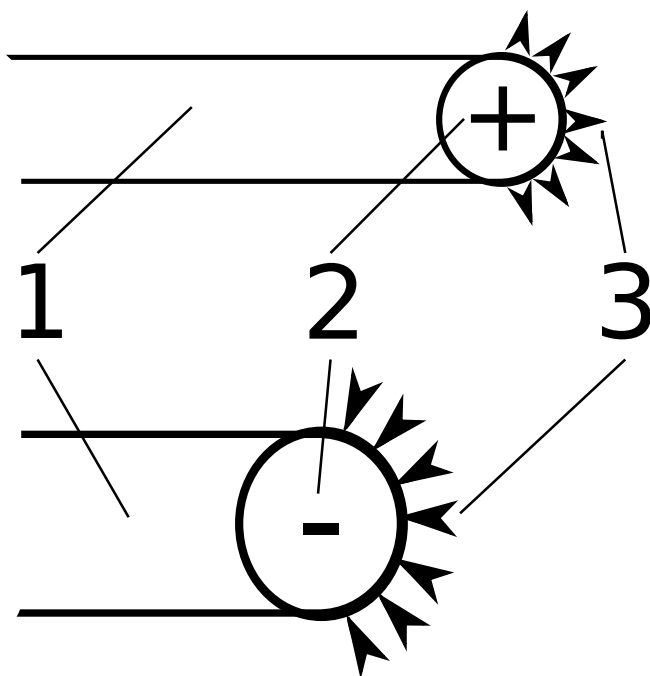


Figure 4.2: Simplified model for 2nd mode positive (upper) and negative (lower) streamer propagation. (1) Streamer channel, (2) Streamer head and (3) electron avalanches (point of arrow=start of avalanche). For this mode the field at the boundary of the streamer head created by the large space charge density in the streamer head combined with the background field is strong enough to ionize the liquid in front of it (through electron avalanches or possibly direct field ionization), thus it becomes a propagating ionization region. As the streamer head propagates it leaves behind a thin filament of conducting plasma (streamer channel) connecting it to the point electrode. The streamer head has the same polarity as the high-field electrode from which it propagates, and the streamer can be considered an electrically conductive extension of the electrode.

Table 4.1: Descriptors for streamer inception and propagation. The table has been divided into three main groups, molecular properties, bulk properties, and external properties

Descriptor	Ref
Molecular packing density and molecular branching	[69]
Functional groups/atoms	[70–73]
Molecular double and triple bonds	[73, 74]
Molecular parachor	[75]
Molecular dipole moment	[75]
Conductivity	[76]
Viscosity	[70, 77–81]
Boiling point	[82]
Hydrostatic pressure and temperature	[61, 70, 80, 81, 83] (<i>paper 1</i>)

the “streamer head” can be either by direct field ionization [66, 67] or impact ionization [16, 68]. This mode of propagation creates thin filaments of conducting plasma channels connecting the streamer head to the point electrode. The streamer head has the same polarity as the high-field electrode from which it propagates, and the streamer can be considered an electrically conductive extension of the electrode from which it propagates. In a divergent field the streamer will propagate until the field at the streamer head is reduced to a level where no further ionization of the liquid is possible. This field reduction can be caused by the voltage drop along the streamer channel or by branching of the channels resulting in a field grading. A simplified outline of the propagation mechanism believed to be responsible for 2nd mode streamers is presented in Figure 4.2.

Extensive research on prebreakdown and breakdown in liquid insulation has provided a large amount of experimental data, which is useful when attempting to understand the influence of molecular and bulk properties of liquids and additives on the inception and propagation of streamers [77, 84]. In Table 4.1 some of the proposed descriptors believed to be important for inception and/or propagation of streamers are given. In addition to the molecular and bulk properties of the liquids external factors like hydrostatic pressure and temperature are important. These properties are relevant to the energy required for the phase transition necessary for inception and propagation of streamers, as well as the viscosity of the liquid.

The energy required for inception and propagation of streamers is taken from the electric field through processes like field ionization [66] or impact ionization [16] which create free charge that can deposit the energy in the streamer structure or at the interface between the streamer and the liquid [85]. The molecular properties of the liquid influence the energy transfer from the electric field to the streamer, as the energy required for ionization (ionization potential) and the mean-free path of free electrons (determining the energy distribution of free electrons) in the liquid is determined by these factors. The bulk properties, on the other hand, determine the energy required for growth (phase transition/fluid dynamical drag). The bulk properties, as well as external properties, mainly influence the slow first-mode streamers [61, 79]. The faster more energetic 2nd mode streamers, which consist of thin plasma filaments, are typically less affected by the bulk properties of the liquid [79]. Nevertheless, bulk properties, such as viscosity/temperature, have been shown to influence the transition between the 1st and 2nd mode [80].

In addition to the molecular and bulk properties of the base liquids, it has been known for over thirty years that small concentrations of additives with electron-scavenger capabilities or low ionization potential can have a drastic effect on streamer propagation characteristics [66, 86]. During the last decades, this has been confirmed for a large variety of base liquids and additives [59, 71, 85, 87–89]. These studies have shown that electron-scavengers generally make negative streamers more filamentary and increase their propagation speed, with no effect on positive streamers. Low IP additives, on the other hand, increase the propagation speed of positive streamers, while generally having no effect on negative streamers.

4.2 Electrical trees

An electrical tree in solid insulation can be generated by slow cumulative degradation at moderate stress caused by ac or repeated impulse voltage, eventually leading to the inception of an electrical tree, or high over-voltage resulting in nearly instantaneous tree inception. This sets electrical treeing apart from streamers in liquids, as liquid insulation is self healing, which reduces the importance of cumulative degradation for the liquid phase.

Cumulative degradation of polymers has been studied thoroughly as once an initial void is created in the material, partial discharges in this void will result in an electrical tree [90]. One proposed mechanism which can cause such voids is free radical production by electron impact excitation and ionization followed by autoxidation processes [90–92]. This hypothesis

has been supported by the observed effect of oxygen [90], temperature [93], and antioxidants [94] on the inception of electrical trees in polymers. The observation of an oxidized deterioration region at protrusions which create high fields is further proof of this [95]. However, this does not mean that oxidation is a necessary condition for cumulative degradation and breakdown of the dielectrics, only that the process is enhanced by oxidation. Indeed, degassing and impregnation of the polymer with Ar or He enhances the degradation process compared to in air. This has been explained by the Penning effect, where molecules excited by the impact excitation lose their energy on impact with the polymer, breaking molecular bonds [96]. Even in degassed polymers or polymers re-impregnated with nitrogen, cumulative degradation eventually is observed, even though no oxygen is present [97]. In this case, the starting void is most likely created by hot electrons breaking polymer bonds, ultimately creating a void, without the additional aid of oxidation processes. The gradual deterioration of the material could also be caused by cracking and free volume formation due to electromechanical stress in high field regions [98].

Hot electrons with sufficient energy to cause material degradation through impact ionization, impact excitation (Penning effect) or by breaking polymer bonds require a sufficiently long mean-free path in the material for energy transfer from the electric field. Thus the deterioration process can be slowed down by reducing the mean-free path of electrons in the insulation. This can be achieved through impregnation with liquid [99], gas [91, 96, 97, 100, 101] or additives with known electron scavenger properties (i.e. SF_6) [101]. Several low molecular weight additives are effective as treeing inhibitors. This has been explained by diffusion of such molecules towards high field regions enhanced by dielectrophoresis. Thus the free volume in the most critical regions are filled with gas, thereby reducing the mean-free path of electrons [102]. The effect of some of these low molecular weight additives, typically byproducts from crosslinking, could also be explained by a reduced resistivity in the high field regions to which they will migrate, thus reducing the field in this region [102]. Such a low resistivity would lead to a low SCLF, thus reducing the strain on the insulation. An ideal dielectric should have a SCLF low enough to limit the field to safe value at protrusions/in the high-field regions without damaging the material. Such a material could only fail thermally [25, 103]

At high overvoltages, electrical trees can occur nearly instantaneously. Such trees are typically called impulse trees. Impulse treeing is a rapid process too fast to be explained by the processes typically believed to be responsible for cumulative degradation of polymers (oxidation and the Pen-

ning process). Inception and propagation of such trees are typically explained by hot electrons that form electron avalanches in the material by impact ionization, quickly deteriorating the material insulation properties and leading to the formation of a channel (tubule). Such propagation is believed to be a stepped process, where the channel acts as an extension of the electrode, and charge is injected/extracted at the tip of the tubule [2]. This process will go on until the field at the tip of the tubule falls below a threshold needed for efficient energy transfer from the field to the material through electron avalanches. Impulse treeing is affected by many of the same factors as ac-treeing (slow cumulative degradation), but processes such as dielectrophoresis, oxidation and the Penning process are too slow to influence the process. Reducing the mean-free path of electrons by impregnation as described for ac-treeing does, however, have a clear beneficial effect also for impulse treeing. Another way of reducing the likelihood of an electron avalanche occurring in the solid insulation is by redistribution of the electric field, lowering the field in the high field regions. The deterioration/oxidized region observed due to slow cumulative degradation enhances the withstand capabilities of the material to impulse treeing [95]. Oxidation of the material leads to an increased number of polar groups in the deterioration region, thus also increasing the permittivity in this region, resulting in a lower electric field in this region than what would be the case with uniform permittivity in the insulation [95]. This effect could also be explained/enhanced by increased conductivity in this region which would lower the SCLF.

Chapter 5

Methods and materials

The experimental setup and methods used are described in detail in *paper 1*; thus only a brief recap of some important aspects will be repeated here. After the experimental outline the reason for choosing cyclohexane and n-tridecane as base liquids, and N,N-dimethylaniline (DMA) and trichloroethene (TCE) as additives are given (for more information see *paper 1*, *paper 2*, and *paper 3*)

5.1 Experimental outline

A drawing of the complete experimental setup, as well as pictures of the main parts of the setup, can be seen in Figure 5.1. Experiments were performed on a sample of liquid or frozen liquid. Step-voltages with rise time of approximately 40 ns were applied to the plane in a needle-plane geometry. The grounded needle had a tip radius of 2 μm , and the gap between the electrodes was 11.5 mm. Phenomena occurring in the high field region were studied by recording the charge induced on the needle by charge injection from the electrode, and high field conduction/discharges in the dielectric. The charge on the needle electrode caused by displacement current was subtracted using a differential amplifier and a low-field (blunt) electrode (see Figure 5.2 and *paper 1*). Similar charge measurement techniques have been used to study high field phenomena in both liquid and solid dielectrics [23, 61, 104], and such measurements can be compared directly to FEM calculations [12, 25] (*paper 2*). In addition to the charge measurements, a photomultiplier was utilized to record light emission from the high field region. Light emission is closely related to the processes occurring in this region, as it is the result of relaxation from states excited by impact or thermal excitation during the redistribution of charge (*paper 3* and *paper*

4).

The needle-plane geometry results in a highly divergent field in which electrical trees and streamers can propagate without causing breakdown. For a homogeneous field, inception of streamers/electrical trees will typically result in breakdown. This is because the background field, in which the structure propagates, does not decrease as the streamer/electrical tree traverses the gap between the electrodes. The propagating phenomenon results in a field enhancement at the tip of the streamer/tree. Thus as long as the background field is constant, the phenomenon will propagate until it bridges the gap between the electrodes. For a divergent field, inception of streamers or electrical trees is not necessarily followed by breakdown, as the background field falls as the phenomenon propagates away from the needle electrode. As there is a voltage drop over the channel/tubule, and the structure is typically branched, the combined effect of field grading due to branching and potential drop over the streamer/electrical tree will reduce the field at the tip of the structure to a point where further propagation is inhibited. Thus pre-breakdown phenomena can be studied with sensitive measurement techniques (such as our differential charge measurement technique) that would be destroyed by breakdown. The needle-plane geometry also makes it possible to study the polarity effect, and since the power dissipation as a result of high-field conductivity will be limited to a small region, it is also possible to study high-field conductivity in the material without thermal breakdown. Finally, breakdown in real power apparatus typically occurs due to a defect in the insulation or at the interface with electrodes/semicon, and the needle electrode can act as a model for such a defect.

The main reason for building a new experimental setup was to control the temperature of the sample. More specifically, the goal was to conduct experiments in liquids and in frozen liquids. For experiments on liquids, the liquid was held at a constant temperature, typically 20°C, while for frozen liquids various temperature programs were used (*paper 1*, *paper 2*, and *paper 3*). When freezing the liquid a slow cooling rate was used (-1°C/min) to limit the problem of bubble formation in the ice as a result of the density difference between the liquid and the solid phase. Once a temperature well below the freezing point of the liquid was reached, one of two approaches was used. Either a single impulse was applied to the frozen liquid before reheating, or several impulses were applied until a partial discharge was detected. In this way, intrinsic properties of the frozen liquid and cumulative degradation of the material could be studied. By varying the time delay between impulses, the effect of residual space charge from

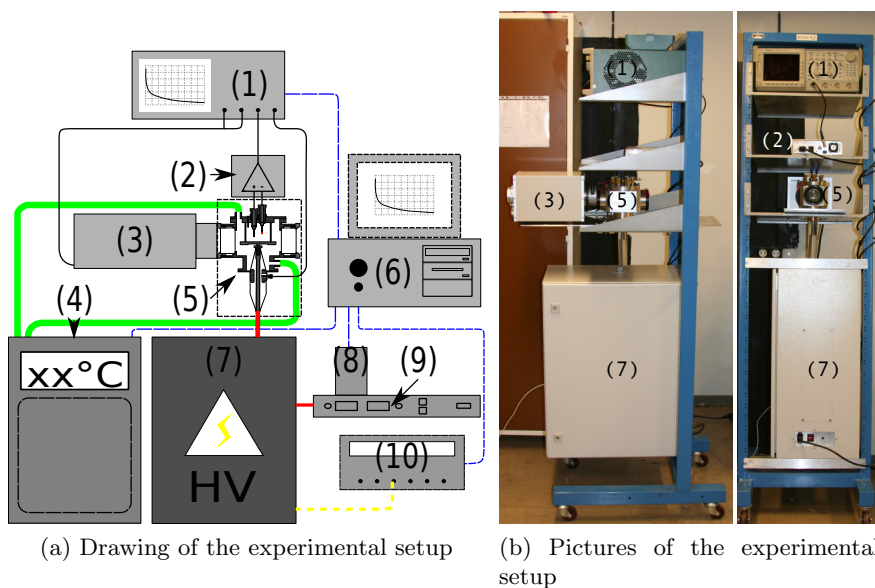


Figure 5.1: Drawing (a) and pictures (b) of the experimental setup. (1) Tektronix TDS684 Oscilloscope, (2) Lecroy DA 1855A Differential amplifier, (3) Hamamatsu R943-02 photomultiplier, (4) Julabo LH-85 Circulator, (5) Test cell, (6) Computer, (7) High voltage pulse source, (8) Fug Probus IV GPIB controlled 0-10 V DC supply, used to control the output from a HV spellman DC supply, (9) Spellman SL300 100 kV HVDC supply and (10) Stanford research systems DG535 Digital delay generator. The drawing of the experimental setup is taken from *paper 1*.

previous impulses could be studied in both liquid and frozen phase.

5.2 Chemicals and procedure for sample preparation

Experiments were conducted in neat cyclohexane and neat n-tridecane (*paper 1* and *paper 2*), as well as in 0.1 M DMA in n-tridecane and 0.1 M TCE in n-tridecane (*paper 3*). The molecular structures of the chemicals used in this study is shown in Figure 5.3.

The first experiments with the new experimental setup described in the previous section were conducted in neat cyclohexane (*paper 1*). Cyclohexane was chosen based on the extensive amount of experimental data already

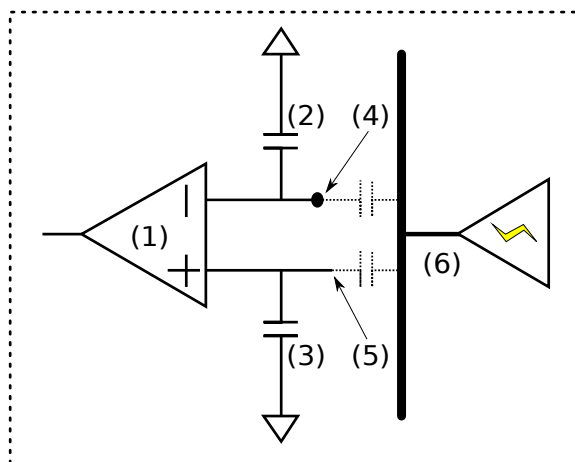


Figure 5.2: Differential charge measurement: (1) Differential amplifier (Lecroy 1855A), (2 and 3) Measurement capacitor for the probe and needle, (4) Probe electrode, (5) Needle electrode and (6) Plane electrode. (*paper 1*)

presented in the literature [59–61, 88, 89, 105, 106], which made it a good benchmark liquid to test the experimental equipment with.

The main part of the experimental work was conducted using n-tridecane as a base liquid (*paper 2* and *paper 3*). n-tridecane was chosen primarily based on its similarities with polyethylene, but also because it is available in high purity at a reasonable cost, and because it has a relatively high melting point ($-5.5\text{ }^{\circ}\text{C}$ [107]). Quantum chemical calculations have shown that the energy levels of linear alkanes converge towards the energy levels of polyethylene as the number of carbon atoms increase [15]. In addition, the morphology of n-alkanes has been studied extensively because of their importance in biological systems and as model systems for polyethylene [108, 109]. Combined, these factors made n-tridecane a logical choice as a model system for polyethylene.

The additives, DMA and TCE, were chosen based on their electrochemical properties and previous results with a similar setup where the effect of electron-attaching and electron-releasing additives on prebreakdown phenomena in cyclohexane were studied [89, 106].

DMA has a relatively low ionization potential (IP) (Table 5.1). DMA enhances positive streamer growth in cyclohexane [89]. In addition to a low IP, density functional theory (DFT) calculations in the gas phase have shown that DMA has a low first singlet-singlet excitation energy of approximately 2.4 eV (*paper 4*). TCE was chosen because of its known electron scavenger

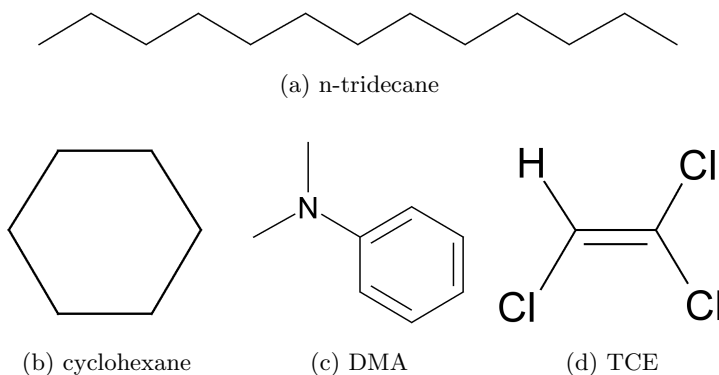


Figure 5.3: Molecular structure of chemicals used.

properties (high electron affinity and large cross section). TCE enhances negative streamer growth in cyclohexane [89]. TCE has IP and singlet-singlet excitation energy similar to cyclohexane and n-tridecane (Table 5.1).

99.9 % pure n-tridecane and cyclohexane were degassed for 24 hours, and treated with a molecular sieve (3 Å Zeochem) to reduce the content of water. During experiments, the sample volume was in contact with a 10 ml reservoir filled with air and molecular sieve, and the two volumes were connected through a syringe. This reservoir allowed the sample to expand during temperature cycling. After filling, some gas absorption from the reservoir into the sample must be expected.

As the purity of the additives was better than 99%, no pretreatment of the additives was performed. The additives were mixed with neat degassed n-tridecane overnight in a closed bottle using a magnetic stirrer.

Table 5.1: Ionization potential (IP) and electronic excitation energy (EE) for the first singlet-singlet transition. EE values are based on DFT calculations in the gas phase (*paper 4*).

Liquid	IP (eV)	EE (eV)
cyclohexane	9.86 ^b /8.4 ^a	6.4
n-tridecane	9.25 ^a	6.3
trichloroethene (TCE)	9.46 ^b	5.1
N,N-dimethylaniline (DMA)	7.12 ^b	2.4

^aLiquid phase [110, 111], ^bGas phase [107]

Chapter 6

Experimental and theoretical results

Five papers were written as part of this thesis, for four of which, I am the main author and one where I am the first coauthor. In the following, a short summary of the papers is provided.

Paper 1 presents the experimental setup used throughout the experimental part of this work, as well as initial experiments performed on cyclohexane. Cyclohexane is frequently used as a model liquid for transformer oil in prebreakdown experiments, and thus experimental data obtained in this liquid can be compared directly to results from literature to validate the experimental procedure/setup. Comparison with literature shows that the results obtained in liquid cyclohexane are similar to those obtained with similar experimental setup by other groups. Experiments were performed in liquid cyclohexane at three temperatures to investigate the temperature dependence of pre-breakdown phenomena in liquid, and in frozen cyclohexane to study the effect of the phase transition. Temperature has an effect on the injected charge for a positive needle, probably caused by the reduced energy required for bubble formation. A similar effect is expected for negative polarity, but the limited voltage range used did not give conclusive evidence for this. No temperature effect was found for pre-inception currents or inception probabilities for either polarity. Experiments performed in frozen cyclohexane were hard to interpret due to problems with the experimental setup, the inhomogeneity of the material as a result of the phase transition, and residual space charge from previous impulses.

In *paper 2* and *paper 3*, cyclohexane was replaced by n-tridecane. *Paper 2* presents experiments conducted in neat n-tridecane and compares the data for n-tridecane with results obtained in cyclohexane (*paper 1*) and re-

sults from literature. Pre-inception currents in cyclohexane and n-tridecane were compared to FEM calculations to find plausible high-field conductivity formulas for the two liquids. Cyclohexane fit a classical Poole-Frenkel mechanism, while the best fit for n-tridecane was a formula of the form $\sigma(E) = \sigma_0 \cdot \exp(k \cdot \sqrt[3]{|E|})$. The formula for conductivity in n-tridecane is of similar form as reported for XLPE [12]. The concept of space charge limited field was used to explain the large difference found for inception voltage for cyclohexane and n-tridecane. While the SCLF in cyclohexane is high enough to support electron avalanches in the liquid phase, the SCLF in n-tridecane is lower, probably requiring the formation of a low density region to facilitate electron avalanches. Still, the main finding in *paper 2* was the correlation between the pre-breakdown phenomena in liquid and frozen n-tridecane when virgin frozen samples of n-tridecane were used (meaning that the sample volume was heated and cooled down between each impulse). Based on this, it was proposed that the inception and propagation of electrical trees in frozen n-tridecane stressed by fast transients occurs in amorphous regions.

In *paper 3* the effect of two additives, N,N-dimethylaniline (DMA) and trichloroethene (TCE), on pre-breakdown phenomena is discussed. The additives were chosen based on their electrochemical properties. TCE is a known electron scavenger, while DMA has a low ionization potential. DMA increases the propagation speed and the size of positive streamers which is in line with previous results reported for DMA in cyclohexane [89]. Unlike in cyclohexane where DMA has no effect on negative streamers, DMA had an effect on negative streamers in n-tridecane. The injected charge decreased, while the emitted light increased when DMA was added. This was interpreted based on the low energy of the first excited singlet state in DMA (2.4 eV). Some of the energy from hot electrons can be absorbed by impact excitation of DMA molecules and subsequently radiated away from the high field region in the form of photons, thus not contributing to the phase transition responsible for streamer growth at the streamer-liquid interface.

Paper 4 is a theoretical paper on the effect of the electric field on ionization potential and excitation energy for a series of molecules. The main author of this paper is Hans Sverre Smalø, who has performed density functional theory (DFT) calculations which form the basis for the paper. I have contributed experimental results, FEM calculations, and classical conductivity models. Using DFT data to interpret the experimental results was a joint effort. The paper presents a new conductivity model based on the classical Poole-Frenkel mechanism. In this model the field dependence of

the conductivity is given by the difference between the ionization potential and the first excitation energy. For cyclohexane, this gives the classical Poole-Frenkel behaviour as the first excitation energy is almost independent of the electric field for low and intermediate fields, while for n-tridecane the first excitation energy decreases with increasing field, even at relatively low fields. This modified Poole-Frenkel mechanism results in a field dependence of the high-field conductivity in n-tridecane that is of similar form as the one found in *paper 2* for both cyclohexane and n-tridecane. In addition to the relevance for high field conduction, the field dependent IP and excitation energies are related to propagation of streamers and the transition between different streamer modes. For fast mode streamers, photoionization is believed to play a key role, and the reduction of the IP with field supports this hypothesis. The retardation effect of DMA on negative 1st mode streamers in n-tridecane is also discussed in this paper (*paper 4*) based on the low excitation energy of DMA.

Paper 5 presents approximations for field and charge on a spheroid in a background field with a field dependent conductivity of the form $\sigma(E) = \sigma_0 \cdot \exp(k \cdot \sqrt[n]{|E|})$ and for a conductivity that can be described as a step function with low conductivity below the SCLF and high conductivity above the SCLF. This is important as the SCLF determines the field distribution in the high-field region near a defect or at the needle electrode if a needle-plane geometry is used. In addition, the paper contains an approximation that can be used to find the extent of the SCLF in the direction of the field from a spheroid in a uniform background field. This is important, as an SCLF extent of approximately 2 μm is required for inception of electrical trees in XLPE [47].

Chapter 7

Future perspectives

The results presented in *paper 3* suggest that the reduction in injected charge measured in 0.1 M DMA may be caused by the emission of photons due to the low excitation energy of DMA. Further research to test this hypothesis can be carried out by spectral analysis of the light emitted from the streamer or by using a monochromator to determine if a substantial part of the light emitted as the streamer propagates is in the range predicted by the excitation energy. Experiments with an additive with low excitation energy (like DMA) but high IP would also be of interest. As stated above, the low excitation energy of DMA is probably the reason for the reduced size of discharges in 0.1 M DMA in n-tridecane for negative polarity. However, the low IP of DMA enhances positive streamer propagation. With an additive with a high IP and low excitation energy, one may get a positive effect for both negative and positive polarity.

The field dependent excitation and ionization energies found in *paper 4* can form the basis for future experiments. The transition between modes may be determined by the available ionization mechanisms as a function of field and the excitation energies available. Experiments with longer gaps between the electrodes and higher over-voltages should be performed to study the effect of additives on 3rd and 4th mode streamers.

Further experiments on longer alkane chains could be performed and compared to data for n-tridecane to see the effect of chain length on pre-breakdown phenomena. This would provide a more direct link to polymers. The experimental setup is capable of heating as well as cooling. Longer chain alkanes could therefore be melted between impulses, making it possible to perform experiments in melted polymers, and to heal polymer samples between consecutive impulses. In future experiments, comparing liquid and solid insulation should also be conducted with needle electrodes with large

point radius ($r_p > 10 \mu m$). The sharp needle used for these experiments resulted in large scatter in the measurements, probably caused by the inhomogeneity of the frozen liquids on the micrometer scale. A larger needle radius would improve this as it would average over a larger volume of the dielectric.

Establishing the correct physical model for high field conduction is challenging and remains one of the most important problems in dielectrics. Our work on field dependent molecular excitation and ionization energies (*paper 4*) is a step towards a better understanding, as it provides insight into how the energy required for molecular ionization/excitation depends on the local electric field. Conduction in polymers is, however, typically described by hopping theory, which assumes traps in the material (typically in the range of 1 eV and separation in the range of 3 nm [25]). Quantum chemical calculations provide an essential tool for improved understanding of how traps and conduction bands are formed in polymers, such calculations agree well with experimentally obtained data for polyethylene [15, 112, 113]. Future progress in this field may lead to material optimization for high field applications.

As described in chapter 3, hybrid models for electrical tree/streamer inception and propagation have been developed that recreate the general properties of the phenomena. The problem with these models, is that the criterion for further propagation is typically a combination of local field and a stochastic parameter. Thus the stochastic nature of the phenomenon and the importance of the local field at the tip of the streamer/tubule are taken into account, but limited information on the mechanism responsible for propagation is gained. Even so, such hybrid models might be a good start, but an essential step forward will be to improve the criteria for propagation/inception. The field dependence of the ionization potential and excitation energy derived in *paper 4* is a first step in this direction, as it can be used to find plausible mechanism for energy/charge transfer in the active region. The next step may be a complete molecular dynamics (MD) simulation of the relatively small high field region. This would require detailed knowledge of the forces between the species (neutral molecules, ions and electrons) in this region and would be computationally intensive. The complexity of the problem makes a complete simulation of the entire dielectric material in this manner intractable. A hybrid model where the local field is calculated by numerical methods like FEM, followed by a MD simulation of regions with fields above a certain threshold would reduce the computational cost of modelling. Even so, the three dimensional nature of the phenomena, the complexity of the required force field, and the number of

molecules that would have to be accounted for even in the limited high-field region makes this a demanding task. An intermediate solution might be to use a field dependent stochastic parameter and a threshold field that is based on a series of MD simulation at various field strengths. Thus the simulation could be performed in the standard way, but the parameters would be based on quantum chemical calculations and MD simulations.

Chapter 8

Concluding remarks

There is a clear correlation between measurements obtained in liquid and solid n-tridecane. The main difference is the large scatter introduced by the transition to solid phase. The increased scatter for solid phase is explained by the inhomogeneity of the solid on the micrometer scale. The morphology seems to be more important for negative than for positive polarity, indicating that electron emission from the electrode is very dependent on the interface between the electrode and the frozen liquid. The correlation between the two phases indicates that similar processes are responsible for inception and propagation of electrical trees and streamers, and that electrical trees propagate in the amorphous regions of the frozen liquid. The similar electronic properties of n-tridecane and polyethylene make n-tridecane a good choice as a simple model system for polyethylene.

The low IP additive DMA has the expected effect on positive streamers and electric trees in n-tridecane; it changes the propagation mode and enhance injected charge and light emission from the phenomenon. However, the additive also has an effect on negative streamer propagation; the injected charge is reduced while more light is emitted from the streamer. This indicates that some of the energy otherwise available for streamer growth is emitted as light, probably through excitation and de-excitation of DMA. TCE, a known electron scavenger, had no effect on negative streamers in n-tridecane. Electron scavengers are believed to facilitate negative streamer propagation through localizing energy dissipation and charge deposition at the streamer/liquid interface by shortening the thermalization length of electrons. This indicates that the thermalization length of electrons in n-tridecane is not affected by adding TCE.

The IP must be viewed as a field dependent property. The field dependence is important for all ionization processes in high electric fields and for

high-field conduction. At very high fields the reduction of the IP can significantly aid photoionization, which is probably important for fast streamers.

Bibliography

- [1] R. Tobazeon. Electrohydrodynamic instabilities and electroconvection in the transient and a.c. regime of unipolar injection in insulating liquids: A review. *J. Electrostat.*, 15:359–384, 1984.
- [2] L. A. Dissado and J. C. Fothergill. *Electrical Degradation and Breakdown in Polymers*. Material and Devices Series 9. The Institution of Engineering and Technology, London, United Kingdom, 1992.
- [3] W. F. Schmidt. *Liquid State Electronics of Insulating Liquids*. CRC Press, 1997.
- [4] A. K. Jonscher. Electronic properties of amorphous dielectric films. *Thin Solid Films*, 1:213–234, 1967.
- [5] N. J. Felici. A tentative explanation of the voltage-current characteristic of dielectric liquids. *J. Electrostat.*, 12:165–172, 1982.
- [6] V. Adamec and J. H. Calderwood. Electrical conduction in dielectrics at high fields. *J. Phys. D: Appl. Phys.*, 8:551–560, 1975.
- [7] D. M. Pai. Electric-field-enhanced conductivity in solids. *J. Appl. Phys.*, 46:5122–5126, 1975.
- [8] A. Denat, B. Gosse, and J.P. Gosse. High field dc and ac conductivity of electrolyte solutions in hydrocarbons. *J. Electrostat.*, 11:179–194, 1982.
- [9] C. W. Smith and J. H. Calderwood. The application of a classical conductivity model to dielectric liquids. *J. Electrostat.*, 12:173–178, 1982.
- [10] A. Denat, J. P. Gosse, and B. Gosse. Electrical conduction of purified cyclohexane in a divergent electric field. *IEEE Trans. Elect. Insul.*, 23:545–554, 1988.

-
- [11] Yu. N. Garstein and E. M. Conwell. High-field hopping mobility in molecular systems with spatially correlated energetic disorder. *Chem. Phys. Lett.*, 245:351–358, 1995.
- [12] G. Jiang, J. Kuang, and S. Boggs. Evaluation of high field conduction models of polymeric dielectrics. In *Ann. Rep. Conf. Elec. Insul. Diel. Phen. (CEIDP)*, volume 1, pages 187–190 vol.1, 2000.
- [13] D. Braun. Electronic injection and conduction processes for polymer devices. *J. Polym. Sci. B*, 41:2622–2629, 2003.
- [14] H. J. Wintle. Charge motion in technical insulators: facts, fancies and simulations. *IEEE Trans. Dielect. Elect. Insul.*, 10:826–841, 2003.
- [15] G. Teyssedre and C. Laurent. Charge transport modeling in insulating polymers: from molecular to macroscopic scale. *IEEE Trans. Dielect. Elect. Insul.*, 12:857–875, 2005.
- [16] A. Denat. High field conduction and prebreakdown phenomena in dielectric liquids. *IEEE Trans. Dielect. Elect. Insul.*, 13:518–525, 2006.
- [17] A. Messiah. *Quantum Mechanics, two volumes bound as one*. Dover Publications, Inc., 1999.
- [18] H. J. Wintle. Charge motion and trapping in insulators: surface and bulk effects. *IEEE Trans. Dielect. Elect. Insul.*, 6:1–10, 1999.
- [19] J. A. Anta, G. Marcelli, M. Meunier, and N. Quirke. Models of electron trapping and transport in polyethylene: Current–voltage characteristics. *J. Appl. Phys.*, 92:1002–1008, 2002.
- [20] N. F. Mott. Conduction in non-crystalline materials – iii. localized states in a pseudogap and near extremities of conduction and valence bands. *Phil. Mag.*, 19:835–852, 1969.
- [21] J. C. Dyre. The random free energy barrier model for ac conduction in disordered solids. *J. Appl. Phys.*, 64:2456, 1988.
- [22] H. R. Zeller and W. R. Schneider. Electrofracture mechanics of dielectric aging. *J. Appl. Phys.*, 56:455–459, 1984.
- [23] T. Hibma and H. R. Zeller. Direct measurement of space-charge injection from a needle electrode into dielectrics. *J. Appl. Phys.*, 59:1614–1620, 1986.

- [24] J. Kuang and S. A. Boggs. Thermal-electric field distribution around a defect in polyethylene. *IEEE Transactions on Power Delivery*, 13:23–27, 1998.
- [25] S. Boggs. Very high field phenomena in dielectrics. *IEEE Trans. Dielect. Elect. Insul.*, 12:929–938, 2005.
- [26] A. Soba. A finite element method solver for time-dependent and stationary schrödinger equations with a generic potential. *Commun. Comput. Phys. (CiCP)*, 5:914–927, 2009.
- [27] Comsol Multiphysics® ver. 3.5a with AC/DC module. Comsol AB. Regnergatan 23. SE-111 40 Stockholm. Sweden. www.comsol.com.
- [28] J. Jin. *The Finite Element Method in Electromagnetics*. Wiley, New York, 2002.
- [29] R. L. Courant. Variational methods for the solution of problems of equilibrium and vibration. *Bulletin of the American Mathematical Society*, 49:1–23, 1943.
- [30] M. J. Turner, R. W. Clough, H. C. Martin, and L. J. Topp. Stiffness and deflection analysis of complex structures. *J. Aeronaut. Sci.*, 23:805–823, 1956.
- [31] R. W. Clough. The finite element method in plane stress analysis. In *Second conference on electronic computation*, 1960.
- [32] R. W. Clough. The finite element method after twenty-five years: A personal view. *Computers & structures*, 12:361–370, 1980.
- [33] Z. Zheng and S.A. Boggs. Efficient solution of transient nonlinear field problems. In *Ann. Rep. Conf. Elec. Insul. Diel. Phen. (CEIDP)*, 2002.
- [34] A. C. Polycarpou. *Introduction to the Finite Element Method in Electromagnetics*. Morgan & Claypool Publishers, 2006.
- [35] L. L. Thompson. A review of finite-element methods for time-harmonic acoustics. *J. Acoust. Soc. Am.*, 119:1315–1330, 2006.
- [36] S. M. Hellesø, V. C. Henoen, and S. Hvidsten. Simulation of water diffusion in polymeric cables using finite element methods. In *ISEI*, pages 595–598, 2008.

- [37] K. S. Surana, S. Allu, P. W. Tenpas, and J. N. Reddy. k-version of finite element method in gas dynamics: higher-order global differentiability numerical solutions. *Int. J. Numer. Meth. Engng.*, 69:1109–1157, 2007.
- [38] M. E. Everett, E. A. Badea, L. C. Shen, G. A. Merchant, and C. J. Weiss. 3-d finite element analysis of induction logging in a dipping formation mark. *IEEE Trans. Geosci. Remote Sens.*, 39:2244–2252, 2001.
- [39] H. Brakelmann and J. Stammen. Thermal analysis of submarine cable routes: Lsm or fem? In *PECON 2006*, pages 560–565, 2006.
- [40] F. E. Elliott, B. E. Lavier, W. P. Kuehn, and A. Kuechler. Fem-study on converter transformer failures in the celilo hvdc converter station. In *Power Engineering Society*, 1999.
- [41] H. Wang and K. L. Butler. Finite element analysis of internal winding faults in distribution transformers. *IEEE. Trans. Power Del.*, 16:422–428, 2001.
- [42] B. Feng, N. Zhong-Xia, S. Yu-Jie, and Z. Dong-Fang. Finite element analysis of high voltage planar transformer. In *ISAPE*, 2006.
- [43] E. Bjerkan and H. K. Høidalen. High frequency fem-based power transformer modeling: Investigation of internal stresses due to network-initiated overvoltages. *Electric Power Systems Research*, 77:1483–1489, 2007.
- [44] F. M. O’Sullivan. *A Model for the Initiation and Propagation of Electrical Streamers in Transformer Oil and Transformer Oil based Nanofluids*. PhD thesis, MIT, Cambridge, MA, USA, 2007.
- [45] J.G. Hwang, F. O’Sullivan, M. Zahn, O. Hjortstam, L.A.A. Pettersson, and Rongsheng Liu. Modeling of streamer propagation in transformer oil-based nanofluids. In *Ann. Rep. Conf. Elec. Insul. Diel. Phen. (CEIDP)*, 2008.
- [46] J. G. Hwang, M. Zahn, L. A. A. Pettersson, O. Hjortstam, and R. Liu. Modeling streamers in transformer oil: The transitional fast 3rd mode streamer. In *ICPADM*, 2009.
- [47] Z. Zheng and S. Boggs. Defect tolerance of solid dielectric transmission class cable. *IEEE Electric. Insul. Mag.*, 21:34–41, 2005.

- [48] G. Jiang, J. Kuang, and S. Boggs. Tree channel formation in solid dielectrics. low variance observations and mechanism of formation. In *Ann. Rep. Conf. Elec. Insul. Diel. Phen. (CEIDP)*, 1999.
- [49] S. Boggs. Mechanisms for reduction of impulse strength resulting from small water trees. In *Ann. Rep. Conf. Elec. Insul. Diel. Phen. (CEIDP)*, 2000.
- [50] S. Hvidsten, E. Ildstad, J. Sletbak, and H. Faremo. Understanding water treeing mechanisms in the development of diagnostic test methods. *IEEE Trans. Dielect. Elect. Insul.*, 5:754–760, 1998.
- [51] K. E. Seralathan, A. Mahajan, and N. Gupta. Modelling of electric tree progression due to space charge modified fields. *Journal of Physics D: Applied Physics*, 41:105501, 2008.
- [52] G. E. Vardakis and M. G. Danikas. Simulation of electrical tree propagation using cellular automata: the case of conducting particle included in a dielectric in point-plane electrode arrangement. *J. Electrostat.*, 63:129–142, 2005.
- [53] L. A. Dissado, J. C. Fothergill, N. Wise, and J. Cooper. A deterministic model for branched structures in the electrical breakdown of solid polymeric dielectrics. *J. Phys. D: Appl. Phys.*, 33:L109, 2000.
- [54] H. A. Fowler, J. E. Devaney, and J. G. Hagedorn. Growth model for filamentary streamers in an ambient field. *IEEE Trans. Dielect. Elect. Insul.*, 10:73–79, 2003.
- [55] J. A. Rees. *Electrical breakdown in gases*. The Macmillan Press LTD, 1973.
- [56] R. S. Sigmond. The residual streamer channel: Return strokes and secondary streamers. *J. Appl. Phys.*, 56:1355–1370, 1984.
- [57] O. Lesaint and G. Massala. Positive streamer propagation in large oil gaps: experimental characterization of propagation modes. *IEEE Trans. Dielect. Elect. Insul.*, 5:360–370, 1998.
- [58] L. Lundgaard, D. Linhjell, G. Berg, and S. Sigmond. Propagation of positive and negative streamers in oil with and without pressboard interfaces. *IEEE Trans. Dielect. Elect. Insul.*, 5:388–395, 1998.

- [59] S. Ingebrigtsen, H. S. Smal, P.-O. Astrand, and L. E. Lundgaard. Effects of electron-attaching and electron-releasing additives on streamers in liquid cyclohexane. *IEEE Trans. Dielect. Elect. Insul.*, 16:1524–1535, 2009.
- [60] P. Gournay and O. Lesaint. A study of the inception of positive streamers in cyclohexane and pentane. *Journal of Physics D (Applied Physics)*, 26:1966–74, 1993.
- [61] L. Dumitrescu, O. Lesaint, N. Bonifaci, A. Denat, and P. Notingher. Study of streamer inception in cyclohexane with a sensitive charge measurement technique under impulse voltage. *J. Electrostat.*, 53:135–146, 2001.
- [62] R. Kattan, A. Denat, and O. Lesaint. Generation, growth, and collapse of vapor bubbles in hydrocarbon liquids under a high divergent electric field. *J. Appl. Phys.*, 66:4062–4066, 1989.
- [63] T. J. Lewis. A new model for the primary process of electrical breakdown in liquids. *IEEE Trans. Dielect. Elect. Insul.*, 5:306–315, 1998.
- [64] H. Sueda and K. C. Kao. Prebreakdown phenomena in high-viscosity dielectric liquids. *IEEE Trans. Elect. Insul.*, EI-17:221–227, 1982.
- [65] R. Tobazeon. Prebreakdown phenomena in dielectric liquids. *IEEE Trans. Dielect. Elect. Insul.*, 1:1132–1147, 1994.
- [66] J. C. Devins, S. J. Rząd, and R. J. Schwabe. Breakdown and pre-breakdown phenomena in liquids. *J. Appl. Phys.*, 52:4531–4545, 1981.
- [67] P. Biller. A simple qualitative model for the different types of streamers in dielectric liquids. In *Proc. IEEE Int. Conf. Diel. Liq. (ICDL)*, pages 189–192, 1996.
- [68] H. M. Jones and E. E. Kunhardt. Development of pulsed dielectric breakdown in liquids. *J. Phys. D: Appl. Phys.*, 28:178–188, 1995.
- [69] T. Schutte. The influence of the molecular packing on electrical breakdown strength of liquids. In *Nordic Insulation Symposium*, 1994.
- [70] H. Yamada and T. Sato. High-speed electro-optical measurement of pre-breakdown current in dielectric liquids. *IEEE Trans. Elect. Insul.*, EI-20:261–267, 1985.

- [71] S. Sakamoto and H. Yamada. Optical study of conduction and breakdown in dielectric liquids. *IEEE Trans. Elect. Insul.*, EI-15:171–181, 1980.
- [72] Y. Nakao, T. Yamazaki, H. Tagashira, K. Miyagi, and Y. Sakai. Propagation of streamer discharge in dielectric liquids with various molecular structure by using high-speed schlieren photography. In *Proc. IEEE Int. Conf. Diel. Liq. (ICDL)*, pages 261–264, 1999.
- [73] Y. Nakao, T. Yamazaki, K. Miyagi, Y. Sakai, and H. Tagashira. The effect of molecular structure on prebreakdown phenomena in dielectric liquids under a nonuniform field. *IEEEJ*, 139, 2002.
- [74] N. Hamano, Y. Nakao, T. Naito, Y. Nakagami, R. Shimizu, Y. Sakai, and H. Tagashira. Influence of molecular structure on propagation of streamer discharge in hydrocarbon liquids. In *Proc. IEEE Int. Conf. Diel. Liq. (ICDL)*, pages 119–122, 2002.
- [75] Y. Nakao, H. Nagasawa, R. Yamaoka, H. Itoh, Y. Sakai, and H. Tagashira. Influence of molecular structure on the propagation of streamer discharge in dielectric liquids. *J. Electrostat.*, 40-41:199–204, 1997.
- [76] J. Nieto-Salazar. Breakdown and pre-breakdown phenomena in water under impulse voltage. *ISH*, 2003.
- [77] V. Ya. Ushakov. *Impulse Breakdown of Liquids*. Springer, 2007.
- [78] P. K. Watson, W. G. Chadband, and M. Sadeghzadeh-Araghi. The role of electrostatic and hydrodynamic forces in the negative-point breakdown of liquid dielectrics. *IEEE Trans. Elect. Insul.*, 26:543–559, 1991.
- [79] W. G. Chadband. Electrical breakdown—from liquid to amorphous solid. *J. Phys. D: Appl. Phys.*, 24:56–64, 1991.
- [80] R. Badent, K. Kist, and A. J. Schwab. The effect of viscosity on streamer propagation in insulating oil under impulse conditions. In *Proc. IEEE Int. Conf. Diel. Liq. (ICDL)*, 1996.
- [81] Y. Katayama, T. Nakayashiki, and H. Yamashita. The effect of viscosity on the negative streamer inception in pfpe. In *Ann. Rep. Conf. Elec. Insul. Diel. Phen. (CEIDP)*, 1999.

- [82] F. M. J. McCluskey and A. Denat. Bubble formation in synthetic insulating liquids in a pulsed divergent electric field. *IEEE Trans. Dielect. Elect. Insul.*, 1:672–679, 1994.
- [83] R. Badent, K. Kist, and A. J. Schwab. The effect of hydrostatic pressure on streamer inception and propagation in insulating oil. In *Proc. IEEE Int. Symp. El. Insul. (ISEI)*, 1994.
- [84] A. Beroual, M. Zahn, A. Badent, K. Kist, A.J. Schwabe, H. Yamashita, K. Yamazawa, M. Danikas, W.D. Chadband, and Y. Torshin. Propagation and structure of streamers in liquid dielectrics. *IEEE Electric. Insul. Mag.*, 14:6–17, 1998.
- [85] O. Lesaint and P. Gournay. Initiation and propagation thresholds of positive prebreakdown phenomena in hydrocarbon liquids. *IEEE Trans. Dielect. Elect. Insul.*, 1:702–8, 1994.
- [86] J. C. Devins, S. J. Rzađ, and R. J. Schwabe. Prebreakdown phenomena in liquids: electronic processes. *J. Phys. D: Appl. Phys.*, 9:87–91, 1976.
- [87] W. G. Chadband and T. M. Sufian. Experimental support for a model of positive streamer propagation in liquid insulation. *IEEE Trans. Elect. Insul.*, EI-20:239–246, 1985.
- [88] O. Lesaint and M. Jung. On the relationship between streamer branching and propagation in liquids: influence of pyrene in cyclohexane. *J. Phys. D: Appl. Phys.*, 33:1360–, 2000.
- [89] S. Ingebrigtsen, L. E. Lundgaard, and P. O. Astrand. Effects of additives on prebreakdown phenomena in liquid cyclohexane: Ii. streamer propagation. *J. Phys. D: Appl. Phys.*, 40:5624–5634, 2007.
- [90] N. Shimizu and C. Laurent. Electrical tree initiation. *IEEE Trans. Dielect. Elect. Insul.*, 5:651–659, 1998.
- [91] C. Laurent, C. Mayoux, and S. Noel. Dielectric breakdown of polyethylene in divergent field: Role of dissolved gases and electroluminescence. *J. Appl. Phys.*, 54:1532–1539, 1983.
- [92] L. A. Dissado. Understanding electrical trees in solids: from experiment to theory. *IEEE Trans. Dielect. Elect. Insul.*, 9:483–497, 2002.

- [93] K. Uchida and N. Shimizu. The effect of temperature and voltage on polymer chain scission in high-field region. *IEEE Trans. Elect. Insul.*, 26:271–277, 1991.
- [94] Y. Sekii, D. Tanaka, M. Saito, N. Chizuwa, and K. Kanasawa. Effects of antioxidants on the initiation and growth of electrical trees in xlpe. In *Ann. Rep. Conf. Elec. Insul. Diel. Phen. (CEIDP)*, pages 661–665, 2003.
- [95] N. Shimizu, K. Uchida, and S. Rasikawan. Electrical tree and deteriorated region in polyethylene. *IEEE Trans. Elect. Insul.*, 27:513–518, 1992.
- [96] N. Shimizu and H. Sato. Role of electron impact in ac electrical tree initiation. In *Proc. Int. Conf. Prop. App. Diel. Mat. (ICPADM)*, 1997.
- [97] N. Tohyama, Y. Tateno, H. Sato, and N. Shimizu. Tree initiation in polyethylene absorbing helium gas. In *Int. Symp. El. Insul. Mat. (ISEIM)*, pages 455–458, 1995.
- [98] J. P. Jones, J. P. Llewellyn, and T. J. Lewis. The contribution of field-induced morphological change to the electrical aging and breakdown of polyethylene. *IEEE Trans. Dielect. Elect. Insul.*, 12:951–966, 2005.
- [99] N. Shimizu and T. Suzuki. Suppression of high field degradation and electrical tree by n-hexane impregnation in xlpe. In *Ann. Rep. Conf. Elec. Insul. Diel. Phen. (CEIDP)*, pages 253–256, 2001.
- [100] J. Andrianjohaninarivo, M. R. Wertheimer, and A. Yelon. Nucleation of electrical tress in polyethylene. *IEEE Trans. Elect. Insul.*, EI-22:709–714, 1987.
- [101] N. Shimizu, Y. Muramoto, and Y. Kamiya. Suppression of electrical tree in silicone rubber by gas impregnation. In *Proc. IEEE Int. Symp. El. Insul. (ISEI)*, pages 599–602, 2008.
- [102] N. Shimizu and H. Tanaka. Effect of liquid impregnation on electrical tree initiation in xlpe. *IEEE Trans. Dielect. Elect. Insul.*, 8:239–243, 2001.
- [103] S. Boggs and J. Kuang. High field effects in solid dielectrics. *IEEE Electric. Insul. Mag.*, 14:5–12, 1998.

-
- [104] Y. Cao, G. G. Jiang, and S. Boggs. Guarded needle for “charge injection” measurement. *Review of Scientific Instruments*, 73:3012–3017, 2002.
- [105] H. Yamashita, K. Yamazawa, and Y. S. Wang. The effect of tip curvature on the prebreakdown streamer structure in cyclohexane. *IEEE Trans. Dielect. Elect. Insul.*, 5:396–401, 1998.
- [106] S. Ingebrigtsen, L. E. Lundgaard, and P. O. Astrand. Effects of additives on prebreakdown phenomena in liquid cyclohexane: I. streamer initiation. *J. Phys. D: Appl. Phys.*, 40:5161–5169, 2007.
- [107] D. R. Lide. *Handbook of Chemistry and Physics*. CRC Press, 2004.
- [108] K. Shigematsu, Y. Saito, K. Saito, and Y. Takahashi. Pressure effect on the solid-liquid equilibrium forms of odd normal alkanes. *Journal of Crystal Growth*, 310:4681–4684, 2008.
- [109] G. Ungar and X. Zeng. Learning polymer crystallization with the aid of linear, branched and cyclic model compounds. *Chemical Reviews*, 101:4157–4188, 2001.
- [110] W. F. Schmidt. Charge carrier energetics and dynamics in nonpolar liquids. *Nucl. Instr. Meth. A*, A327:83–86, 1993.
- [111] J. Casanovas, R. Grob, D. Delacroix, J. P. Guelfucci, and D. Blanc. Photoconductivity studies in some nonpolar liquids. *J. Chem. Phys.*, 75:4661–8, 1981.
- [112] A. Huzayyin, S. Boggs, and R. Ramprasad. Quantum mechanical studies of carbonyl impurities in dielectric polyethylene. *IEEE Trans. Dielect. Elect. Insul.*, 17:920–925, 2010.
- [113] A. Huzayyin, S. Boggs, and R. Ramprasad. Density functional analysis of chemical impurities in dielectric polyethylene. *IEEE Trans. Dielect. Elect. Insul.*, 17:926–930, 2010.

Paper 1

New experimental system for the study of the effect of temperature and liquid to solid transition on streamers in dielectric liquids: Application to cyclohexane

Ø. L. Hestad, L. E. Lundgaard and D. Linhjell

IEEE Trans. Dielect. Elect. Insul., 2010, 17, 764-774.

New Experimental System for the Study of the Effect of Temperature and Liquid to Solid Transition on Streamers in Dielectric Liquids: Application to Cyclohexane

Ø. L. Hestad

Department of Chemistry
Norwegian University of Science and Technology (NTNU)
7491 Trondheim, Norway

L. E. Lundgaard and D. Linhjell

Department of Electric Power Technology
SINTEF Energy Research
7465 Trondheim, Norway

ABSTRACT

An experimental setup for dielectric testing of insulating liquids in the temperature range from $-60\text{ }^{\circ}\text{C}$ to $+250\text{ }^{\circ}\text{C}$ has been built. The system uses point-plane geometry, a sensitive differential charge measurement technique, a computer controlled temperature regulator, a photomultiplier and a pulse generator with a fast rise time. This paper presents a detailed overview of the functionality of the system and results obtained in cyclohexane under positive and negative polarity below and above freezing point. Pre-inception current, inception probabilities, streamer charge and emitted light from streamers are reported. The results found in cyclohexane at room temperature compares well to results obtained in other similar setups. A temperature dependence on the injected streamer charge for liquid cyclohexane under positive polarity was observed. No polarity differences were observed for any of the measured quantities in frozen cyclohexane.

Index Terms — Test equipment, charge injection, charge measurement, temperature control, dielectric materials, cyclohexane.

1 INTRODUCTION

DIELECTRIC materials are used as electrical insulation in all power systems. It is therefore of vital importance to understand the limitations and possibilities of these materials. In order to do so, good experimental procedures for testing of dielectrics under high electrical fields are needed. Several different test-setups have been proposed, and have formed the basis of international standards for testing dielectric liquids [1]-[3]. These standard tests have many shortcomings [4], and non-standardized tests have been used extensively to study pre-breakdown phenomena in liquids [5]-[13] and similar setups have also been used to study pre-breakdown phenomena in solids (electrical trees/carrier mobilities/partial discharges) [14].

In the following sections an experimental setup based on a widely used non-standardized point-to-plane gap test for

dielectric liquids, adapted to a temperature controlled test setup, is described. Results from first experiments on cyclohexane for both liquid and frozen cyclohexane are presented. In the future the capability of testing frozen liquids will be used in model systems for solid insulation using pure hydrocarbons with additives to control the chemical, electrical and/or morphological properties of the system. Before going into details about the experiments and experimental setup a short discussion of the background for working on frozen liquids, and a short review of the theories for pre-breakdown phenomena in liquids are given.

2 BACKGROUND

2.1 PREBREAKDOWN PHENOMENA

In liquids all pre-breakdown phenomena which lead to a phase transition (vaporisation) that can be observed through schlieren/shadow graphics methods are called streamers. Streamers from positive needles are called positive and

streamers from negative needles are denoted negative. Similar structures can be observed in solids, but are typically referred to as electrical trees.

Streamers in dielectric liquids and electrical trees in solid insulation have been extensively studied during the last decades [12], [15]-[17]. The processes responsible for electrical treeing and streamer growth are not well known and no unified theory for the inception and propagation of streamers and electrical trees are known. Most knowledge on this is based on investigations of the field necessary for inception, the speed and length of propagation, and the charge/current injection and light emission from the streamer. There has also been more qualitative research on the chemical composition of the channels in the electrical trees and spectroscopic measurements of light emitted from the streamer/tree channels [18]. During the last decades modeling has improved, but no models capable of predicting the entire process are available at this time [19]-[21]. The following will focus on inception and propagation in liquids since most of the experimental data presented later have been recorded in liquids.

2.1.1 STREAMER MODES IN LIQUIDS

Inception and propagation of a streamer is polarity dependent. Inception voltage is governed by point radius and voltage rise time [10], and is typically lower for negative than for positive streamers.

Polarity and amplitude of the voltage have been shown to be of importance for propagation. In addition to the polarity, the streamers are classified based on the propagation mode and speed. For positive polarity the speed increases in steps as the voltage is increased; these steps are referred to as propagation modes [22]. For negative polarity the speed variation is more gradual. The difference of the speed between modes are typically a factor of ten, where the slow first mode travels at speeds from a hundred m/s to a few hundred m/s and the very fast 4th mode travels at speeds higher than 100 km/s [23].

In the present experiment only 1st mode streamers are studied.

2.1.2 INCEPTION AND PROPAGATION OF 1st MODE STREAMERS

In negative polarity the initiation mechanism is well known, and is seen to be the same for impulse [11] as for dc [24], [25]. When the field in the high field region reaches a critical value the following is observed (at atmospheric pressure):

- Micrometer sized bubbles are induced by an electron avalanche in the liquid.
- A shock wave follows the avalanche (after a few ns), and a bubble develops in its wake [11].
- Discharges occur inside the gas phase, producing fast current pulses in the gas, and supporting the growth of the slow bush like streamer [24], [25]

Experiments in pressurized cyclohexane have shown that the discharges and bubble growth can be suppressed by

increasing the pressure. Only the initial electron avalanche remained. This shows that the avalanche takes place in the liquid, whereas the following discharges take place in a gas phase [11], [25].

For positive polarity the process leading to streamer initiation is not yet fully revealed, while several theories have been proposed. Among these are:

- Local joule heating from a micro-region on the electrode can cause boiling; subsequent discharges can take place in the gas [11].
- Electromechanical forces can cause a high concentration of sub-micron cavities in the high field region [26].
- Pressure reduction caused by electrohydro-dynamic motion and/or pressure reduction caused by Coulomb repulsion between unipolar charges can facilitate the phase transition from liquid to gas [12], [27].

All theories assume that gas or low density regions where discharges can occur are created. This is also supported by the finding that elevated hydrostatic pressures increases the inception voltage for positive polarity in liquids [11]. For 1st mode streamers dissociation into plasma is not likely to occur.

2.1.3 ELECTRICAL TREEING IN SOLIDS

Solids used for insulation of power apparatus typically have very high intrinsic breakdown strengths. The onset of a tree thus requires a defect within the material, typically being voids, particles or protrusions. In practice sharp protrusions will be the most important. Some important aspects are discussed here. For a more detailed and extensive treatment we refer to the work of Dissado [16], [17].

Electrical trees propagating from one of the electrodes are called vented trees, while trees propagating from contaminants/voids in the insulation are called bow-tie trees. The trees are typically divided into tree types by their appearance: bush, bush-branched and branched trees. Like for liquids the treeing is divided into two stages, the inception stage and the propagation stage.

Slow cumulative processes under moderate stress caused by ac or repeated impulse voltages can result in degradation and finally tree formation. Free radical production, caused by electron impact excitation and ionization, followed by autoxidation process are believed to play an essential role in long term tree inception in polymers [17], [28].

For higher fields electrical trees can occur without prestressing the solid. In this case the field needs to be above the threshold-field for impact ionization by hot electrons in the solid.

Hot electrons are believed to play a key role for both cumulative and instant treeing. To gain sufficient energy from the field to get impact excitations or ionization of the molecules in the solid the electrons depend on a long mean free path. The mean free path can be reduced by impregnating the solid to reduce free volume, or by introducing electron scavengers [16]. For cumulative processes degassing also has

a beneficial effect because it suppresses the autoxidation of the sample [28]. Furthermore morphology, temperature, chemical composition (additives and base polymer) have an effect on inception and propagation of electrical trees.

Once a channel (tubule) is formed the electric tree can start to propagate. The propagation is believed to be a stepped process where the channel acts as an extension of the electrode, and charge is injected into/extracted from the solid at the tip of the tubule. Continued propagation requires the field at the tip to be above the threshold required for forming hot electrons [17].

Quantum mechanical calculations using density functional theory (DFT) has shown that the energy levels for linear hydrocarbons approach the energy bands found in polyethylene when the number of carbon atoms are increased [29]. A model hydrocarbon liquid like e.g. tridecane can thus constitute a model system of a more complicated polymer when frozen. Obviously the polymer will have different mechanical, morphological and thermodynamic properties, but for an electron moving in the solid the location of the energy bands will be quite similar. Knowledge gained from such a model system can subsequently be used to explain the observations made in more complicated systems. For cyclohexane, studied here, the correlations to a real polymer are not that evident. Cyclohexane was used because it has been thoroughly studied with similar setups in its liquid phase previously, and thus presents a good basis for comparison.

2.2 EXPERIMENTS IN LIQUIDS AND SOLIDS

2.2.1 LIQUIDS

The study of streamers in liquids has several advantages compared to experiments in solid insulation:

- Most liquids are transparent making visual observation of streamer propagation possible.
- Liquids are self healing (no permanent structures).
- Liquids fill the entire test volume. This ensures good contact between electrodes and the sample.
- Additives can easily be added.

2.2.2 SOLIDS/FROZEN LIQUIDS

Additives in liquids have previously been studied by several groups [5]-[9]. Starting with a liquid and freezing it makes similar experiments possible in solids. Many of the benefits from experiments in liquids can be directly transferred to the study of solid insulation. The main difference is that in most cases the frozen liquid will no longer allow visual observation of the electrical tree growth because they freeze into a crystalline/semi-crystalline form. However, trees can be analyzed in solids after slicing the object, which is not possible in a frozen liquid.

A correlation between charge injection and streamer length has been found in liquids [7]. Charge recordings can therefore reveal information about the propagation of the streamers, as well as the speed of the phenomena and the energy involved. Light emission can be measured using a photomultiplier even

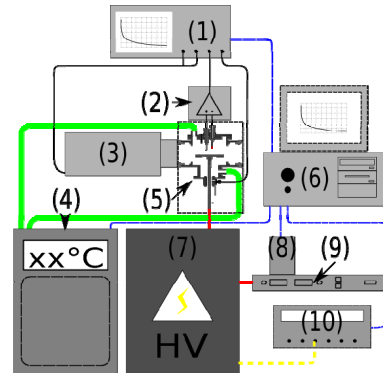


Figure 1. Drawing of the experimental setup. (1) Tektronix TDS684 Oscilloscope, (2) Lecroy DA 1855A Differential amplifier, (3) Hamamatsu R943-02 photomultiplier, (4) Julabo LH-85 Circulator, (5) Test cell, (6) Computer, (7) High voltage pulse battery, (8) Fug Probus IV GPIB controlled 0-10V DC supply, used to control the output from a HV Spellman DC supply, (9) Spellman SL300 100kV HVDC supply and (10) Stanford research systems DG535 Digital delay generator.

in crystalline materials. Since light is mainly emitted during inception and propagation it can be used as an indicator of tree growth.

Adding chemicals to a polymer is a complicated process. Our setup allows us to easily add substances that change the properties of the insulator (by acting as electron traps or electron donors) or changes the morphology of the base material (by breaking the symmetry and thus making it harder to form crystalline materials). In reality adding chemicals (e.g. oxidation stabilizers, crosslinking catalysts, remains from crosslinking, nanofillers etc.) will typically change both these properties, making it challenging to look at only one effect at a time.

The ability to easily go from solid to liquid phase by melting it and then freezing it again makes a sample self-healing. This allows automatic data collection. By cooling the liquid slowly one can also limit the problems with voids at the electrodes that may form when a needle is pressed into a polymer sample. This also reduces the mechanical tension at the electrode surfaces.

3 EXPERIMENTAL SETUP

The experimental setup is shown in Figure 1, and consists of six main parts:

- Test cell (section 3.1)
- Charge measurement (3.2)
- Photomultiplier (3.3)
- Temperature control (3.4)
- High voltage pulse source (3.5)
- Computer control/Data acquisition (3.6)

Each part is described in detail below.

3.1 TEST CELL

The test cell is shown in Figure 2. The main body is made from aluminum, the plane electrode and the two feedthroughs

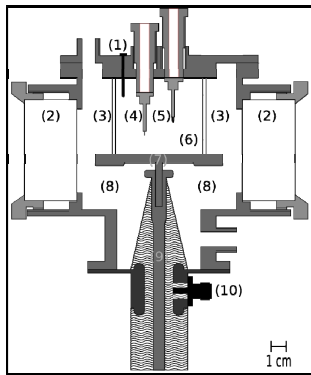


Figure 2. Drawing of the test cell used. (1) PT 100 temperature sensor, (2) Evacuated windows, (3) Glass cylinder separating the sample volume from the circulation volume, (4) Needle electrode, (5) Probe electrode, (6) Sample volume, (7) Plane electrode $\varnothing=90\text{mm}$, (8) Circulation volume, used for temperature control, (9) High voltage feed through and (10) Capacitive high voltage probe

for the probe and needle electrodes are made of stainless steel. The test cell is divided into a 3 dl sample volume and a surrounding volume for temperature controlling liquid. The test cell is covered in thermal insulating material and the observation windows are double pane evacuated windows.

3.1.1 SIMULATIONS

Simple finite element simulations were run in Comsol [30] with axial symmetric point-plane geometries, to check the validity of the often used field estimation by hyperbolic geometry proposed in the paper by Coelho et al [31] and to verify that the fields at other sharp edges were sufficiently below the field at the point apex. The actual field seems to be about half the field calculated by the simple analytic formula, which is caused by the surrounding grounded surfaces and the tip shielding arrangement.

The influence of the low-field probe on the field outside the needle also needed attention. A 3D simulation with the entire test cell was run, in order to look at the cross coupling between the two electrodes. The meshing of a 3D model with a range of sizes from 2 μm (point radius) to 45 mm (plane radius) (1:22500), is challenging. Using a rather crude mesh the field at the point was found to fall by only one percent when introducing the probe and the effect of the probe is therefore neglected.

3.2 CHARGE MEASUREMENT

In principle the charge measurement technique is quite simple. A similar charge measurement setup has been described in [11]. It consists of two electrodes (probe and needle) connected to a differential amplifier, see Figure 3. The needle-plane and probe-plane capacitance are adjusted to be almost equal and the two measurement capacitors (C_m) are equal giving equal time constants for the two bridge branches. When the step voltage is applied to the plane electrode the displacement current will be the same on the point and the probe electrodes, provided no streamer occur, and the signals cancels each other.

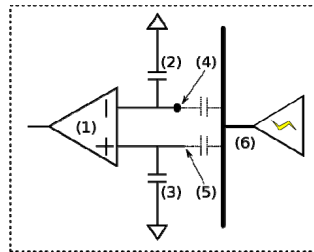


Figure 3. Schematics showing how the differential charge measurement works. (1) Differential amplifier (Lecroy 1855A), (2 and 3) Measurement capacitor for the probe and needle, C_m , (4) Probe electrode, (5) Needle electrode and (6) Plane electrode

At higher fields charge will be induced on the needle electrode either from charge injection from the needle into the dielectric, or from charges moving in the gap. This charge, Q_{ind} , on the needle will give a voltage, over the measurement capacitor, C_m , given by:

$$dV = \frac{Q_{ind}}{C_m}$$

If the system is properly calibrated this is the only signal that gets through the differential amplifier, and the charge induced on the needle by the activity in the high field region can thus be found by multiplying the recorded voltage signal by the measurement capacitor.

3.2.1 ELECTRODES

A figure showing how the needle and probe electrodes were constructed can be seen in Figure 4. The needle electrodes were electrochemically etched from a 100 μm thick wolfram wire to a point radius of 1-2 μm curvature. The tungsten wire was inserted in a 0.7 mm thick steel canulla. The probe was made by a steel canulla only.

The probe was polished with fine sand paper, and then electrochemically etched till it was found to be smooth under examination in a normal light microscope and subsequently with a scanning electron microscope (SEM). It is important to avoid sharp edges on the probe, because this could elevate the field at the probe to values comparable to the field at the point.

The needle electrodes were also studied before and after experiments with a SEM in order to find sharp points not revealed under a light microscope. New needle electrodes sometimes had sharp tungsten fibers sticking out which would wear down after use. This explains a conditioning effect often observed in streamer inception. The additional “etching” was, however, never seen to affect the overall mean radius of the needles.

A simple 2D simulation was run to find the optimal shielding of the point electrode. One basically wants low capacitance between the needle and the plane. If this is achieved a small measurement capacitor can be used which will improve the sensitivity of the system. It was found that the capacitance increases nearly linearly with the distance from the needle tip to the edge of the shield (the silver epoxy

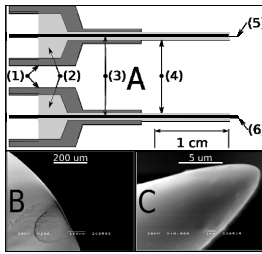


Figure 4. A: Schematics showing the needle and probe electrodes. (1) SMA connectors, (2) PTFE insulation, (3) Steel cannula, (4) Silver epoxy coating (shielding), (5) point electrode (electrochemically etched wolfram) and (6) etched and polished probe electrode. B: SEM image of the tip of a probe electrode. C: SEM image of the tip of a needle electrode

coating shown in Figure 4). To be sure that the edge of the shield did not create a high field region it was decided to keep the distance from the point apex to the edge of the shield at 1 mm or more. The capacitance between the plane and the needle electrodes created were typically around 0.02 pF with a distance between the plane and the needle of 11.5 mm.

3.2.2 MEASURING CAPACITORS

The measuring capacitors used are class 1 ceramic plate capacitors from BC Components. The real and imaginary capacitance was measured from 1Hz to 1MHz by a Novocontrol Alpha A dielectric spectrometer. The capacitors have a flat frequency response over the measured frequency range and very low losses.

3.3 PHOTOMULTIPLIER

A photomultiplier from Hamamatsu (R943-02) mounted in a Hamamatsu C4877 cooler was used. A simple filter with a time constant of 200 μ s was designed to increase the fall time of the signals from the photomultiplier. This was done to achieve an integration effect allowing a lower sampling frequency and easy measurement of integrated light during streamer/electric tree propagation. The circuit can be seen in Figure 5.

3.4 TEMPERATURE CONTROL

Temperature control of the test cell was achieved by circulation of silicon oil through the volume surrounding the sample in the test cell. The circulator used was an LH-85 from Julabo with a temperature range from -85 $^{\circ}$ C to 250 $^{\circ}$ C. The test cell was designed with materials allowing it to be cooled to -60 $^{\circ}$ C.

3.5 HIGH VOLTAGE PULSE SOURCE

The impulse source consisted of a fast high voltage MOSFET switch that can be controlled with a standard TTL signal, see Figure 6.

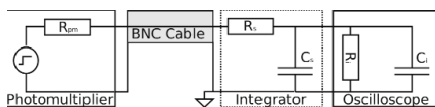


Figure 5. Measurement circuit for the photomultiplier. $R_{pm}=10$ k Ω , $R_s=50$ Ω , $C_s=100$ pF, $R_i=1$ M Ω and $C_i=10$ pF. Simulations show that in order to minimize oscillations in the circuit C_s should be equal to the capacitance of the cable and R_s should be 50 Ω .

The rise time of the high voltage impulse was approximately 40 ns. The duration of the pulse could be arbitrarily long, but would decay with time constant of 4450 μ s. The switching off time constant was 80 μ s. The circuit used for this can be seen in Figure 6, and a typical voltage recording is shown in Figure 7.

A simple passive filter was used for the high voltage measurement [32].

3.6 COMPUTER CONTROL/DATA ACQUISITION

The system is controlled from a computer running Labview linked to the central parts of the setup by GPIB and serial links. It controls the temperature control, oscilloscope, level and timing of the voltage source, see Figure 1. A flowchart of a typical test sequence can be seen in Figure 8. Initially parameters like voltage levels, timing and number of applied pulses and temperature sequences are set. The test is run automatically. All information about the test sequence and the recordings from each shot is stored. It is possible to adapt the test routines to the outcome of an oscilloscope recording; (e.g. stop a test after a large discharge). After one test sequence is completed test conditions (e.g voltage levels) will be adjusted and the sequence rerun as decided. Matlab files for further processing of the recorded data are created.

The programs ability to act based on data recorded during the experiment is a significant feature. The program can, for example, act when a discharge above a certain magnitude occurs and melting of the system is required.

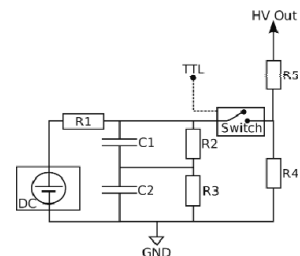


Figure 6. Pulse battery. DC=High voltage DC supply, Spellman SL300 100kV. $R_1=70$ M Ω . $R_2=R_3=500$ M Ω . $C_1=C_2=9900$ pF (3x Ceramic 3300 in parallel), total capacitance is 4450 pF. Switch=High voltage MOSFET switch. $R_4=1$ M Ω . $R_5=1$ k Ω .

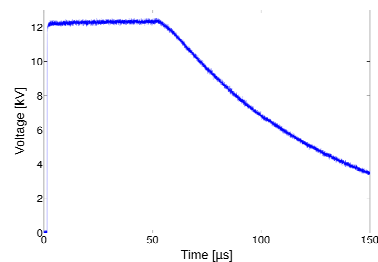


Figure 7. Typical pulse used in the experiments, rise time of approximately 40 ns, nearly constant voltage for 50 μ s and then a tail with a time constant of 80 μ s

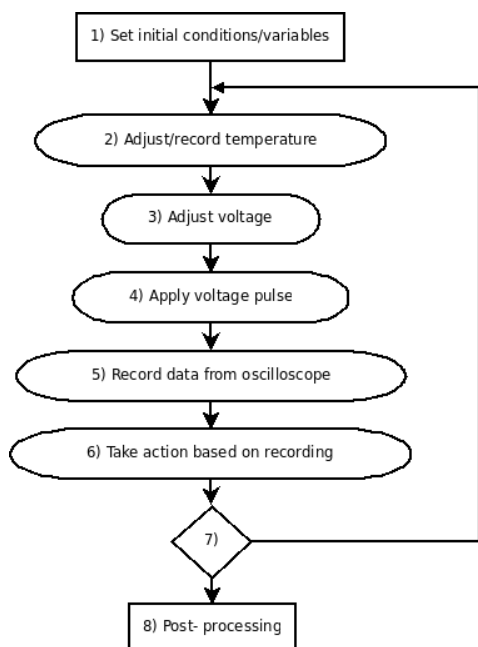


Figure 8. Flowchart illustrating a typical program sequence. The main part of the program (2-7) is inside a loop that repeats several times.

It is clear that space charge will have a long life in a solid compared to a liquid. Thus if one wants to study virgin systems one can melt the liquid after each applied impulse, while if one wants to study the effect of space charge one can apply several consecutive impulses before the sample is melted. If several impulses are applied consecutively it is important to stop the test before a growing tree results in breakdown.

4 EXPERIMENTAL RESULTS FROM CYCLOHEXANE

4.1 PROCEDURE

Experiments in liquid and in solid cyclohexane were done. Point radii of respectively 2 μm in liquid and 1 μm in solid cyclohexane were used. A needle-plane distance of 11.5 mm was used in both cases. The liquid was of spectroscopic grade (99.9 % pure), without further preconditioning.

The voltage pulse used can be seen in Figure 7, it has a fast rise time to limit charge injection prior to inception and a nearly constant voltage level lasting 50 μs to allow streamer propagation until self extinction. The pulse duration is limited to reduce energy/charge injection. Measuring capacitors of 106 pF were used, which together with the capacitance of the cables gave a total integrating capacitance of 141 pF. With the

sensitivity of the amplifiers the sensitivity of the charge measurement ended up below 0.07 pC.

4.1.1 TESTS ON LIQUID

The voltage amplitude was increased in steps of 500 V starting at 7 kV. At each step the liquid was tested at 20, 40 and 60 $^{\circ}\text{C}$. Part of the experimental sequence can be seen in Figure 9. Between each applied impulse there was a pause of three minutes during which the plane was grounded. The same temperature sequence was used for both polarities, but the voltage range was changed from 7 to 12 kV used under positive needle polarity to 7 to 9 kV used for negative polarity. 40 impulses were applied at each voltage and temperature level.

4.1.2 TESTS ON SOLID

Cyclohexane freezes to a crystalline solid at 6.6 $^{\circ}\text{C}$. When doing experiments on frozen cyclohexane the cell was cooled at linear rate from 10 $^{\circ}\text{C}$ to 0 $^{\circ}\text{C}$ during 20 minutes. Then the temperature was kept constant for five minutes before the first impulse was applied. If the charge recording then showed a particularly large jump (above 1.4 pC) the temperature was increased to ten degrees and kept constant for five minutes before the process was repeated. This was done in order to heal/reset the sample at pd-levels well below breakdown. The threshold for melting the sample was intentionally set small to limit the influence of space charge and thus making comparison to the results obtained in liquid cyclohexane easier.

Occasionally the calibration of the differential charge measurement was affected by the temperature cycling. The charge measurement is so sensitive that even very small tensions in the cables or a slight displacement of the wolfram wire when the liquid is frozen result in a slight imbalance in the charge measurement setup which might give a jump in the charge measurement larger than the 1.4 pC limit chosen for melting the sample. For this reason some "false" alarms occurred after the liquid was refrozen even though no partial discharge had taken place.

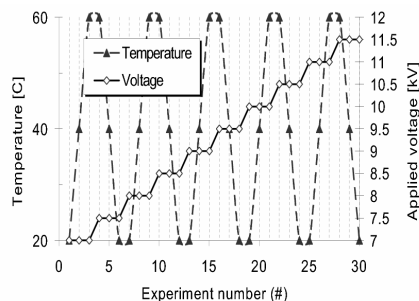


Figure 9. Experimental procedure followed for the test in liquid cyclohexane. The impulse voltage was applied 20 times at each voltage and at each temperature (20 impulses were applied at each experiment number). Only the first part of the procedure is shown in this graph. The same program was used in "reverse" going from high voltage to low voltage, giving a total of 40 impulses at each voltage. This experimental procedure ensures that the tests at different temperatures are done with as equal experimental conditions as possible.

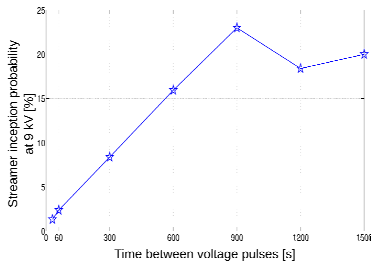


Figure 10. Positive streamer inception probability in frozen cyclohexane at 9 kV versus time between voltage pulses.

In some cases after freezing (less than 5%) it seemed clear that there was a void just outside the point electrode. This was seen by a very much larger discharge than normal with a very rapid rise time occurring with no time lag and additionally a large signal from the photomultiplier, both saturating the measuring system. These cases have been discarded.

Systematic tests with 30, 60, 600, 900, 1200 and 1500 seconds waiting time between each applied high voltage pulse was done under positive polarity to study effects of space charge accumulation. It was found that space charge had a noticeable effect on the inception probabilities (in the range between 7 and 9 kV) for resting times shorter than 900 s. For the full test a rest time of 900 s (15 minutes) between applied impulses was therefore used, see Figure 10.

4.2 RESULTS

4.2.1 PRE-INCEPTION CURRENT

Pre-inception currents recognized by a slow rise time during the whole pulse duration, were observed in both liquid and frozen cyclohexane, usually without corresponding light emission. They appeared quite different in the two phases. For liquid cyclohexane there is a marked polarity effect in these currents. For solid cyclohexane no such difference could be seen. Above freezing point reproducible signals are recorded for both polarities, whereas the situation is far more stochastic below the freezing point. We assume this stochastic behavior to be partly due to difficulties with the setup and partly due to the phase change. The material is not as homogeneous after freezing as before and the signal recorded will be highly dependent on the properties close to the point. Additionally, the material may gradually change as a result of the electrical stressing from previous voltage pulses. It is also reasonable to assume that some residual space charge remains from earlier pulses. This will have great influence on the pre-inception measurement. The difficulties with the setup were mainly occurrence of water condensation in the void between the coaxial measuring cables from the electrodes and the steel wall in the feedthroughs. This reduced the accuracy of the system for frozen liquids, mainly causing a problem for the pre-inception current measurements. After these experiments this was solved by filling the feedthroughs with epoxy.

In many cases very small currents were recorded for the first few applied impulses in solid cyclohexane, but then the current gradually increased until the first partial discharge,

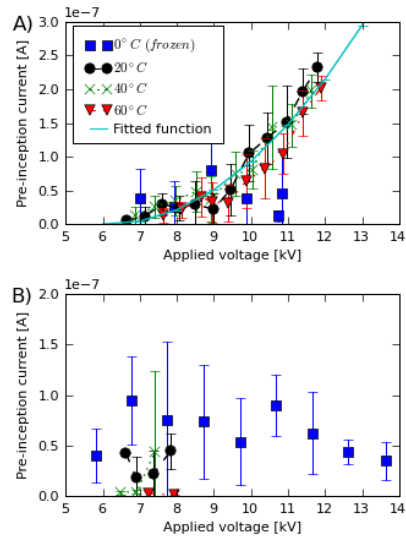


Figure 11. Pre-inception current in liquid and frozen state. A) Positive polarity, the data for liquid cyclohexane was fitted to a function of the form $k*(V-V_0)^2$. B) Negative polarity.

recognized as a stepped increase in the charge recording, was recorded. In cases where discharges did not occur at a voltage application following a discharge observation, the pre-inception current level was observed to be reduced. This is probably due to residual space charge from the discharge.

The differences between current measurements in liquid and frozen state for both polarities can be seen in Figure 11. For positive polarity the pre-inception current in the liquid state increases with increasing voltage and is proportional to $(V-V_0)^2$, with $V_0=6$ kV. The pre-inception current in the frozen state stays low, but with a larger scatter. Under negative polarity the pre-inception current is at the limit of the sensitivity of the setup. For solid cyclohexane the recorded currents are in the same range as under positive polarity, with a similar scatter and no voltage dependence.

4.2.2 INCEPTION PROBABILITIES

The probability for inception of a partial discharge from a streamer, characterized by a step in the charge recording, was studied. 50% inception probability in liquid cyclohexane for all three temperatures lies within 9-10 kV for positive polarity and 7-8 kV for negative polarity, see Figure 12. The differences from temperature changes seen in the graph are small, and no systematic trend could be found.

For frozen cyclohexane a sharper point electrode was used, and the laplacian fields are therefore not directly comparable. It has previously been shown that in dielectric liquids the point radius primarily influences inception and has little or no effect on propagation of streamers [10]. In the same study it was shown that the inception field for streamers in cyclohexane falls by approximately 20% when the needle radius is increased from 1 to 2 μm . From FEM simulations

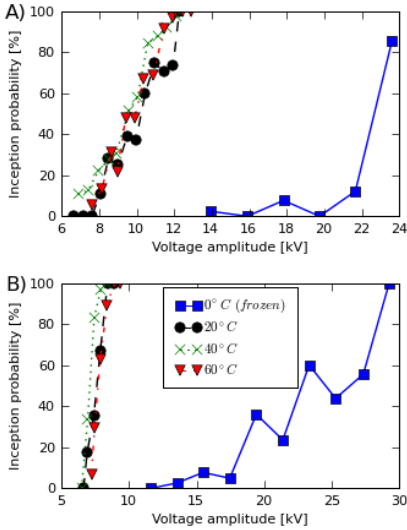


Figure 12. Inception probability versus applied voltage. A) Positive polarity, B) negative polarity. Applied voltage for frozen cyclohexane is multiplied by two in both plots to simplify comparison with liquid cyclohexane.

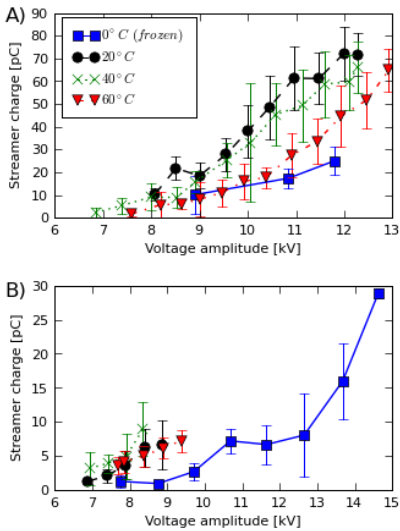


Figure 13. Injected streamer charge versus applied voltage. A) Positive polarity, B) negative polarity

and analytical calculations the field is found to be approximately twice the magnitude at the needle apex with 1 μm radius compared to 2 μm radius at the same voltage. We have therefore normalized the inception probability plots (Figure 12 and Figure 14) based on the field at the point apex by multiplying the voltage values for frozen cyclohexane by two. For frozen cyclohexane, 50% inception probability is between 11 and 12 kV for both polarities (between 22 and 24 kV after normalization).

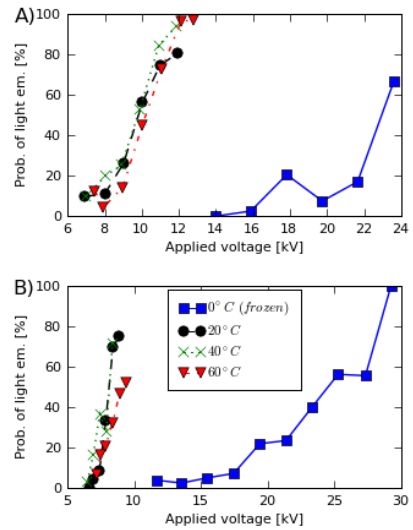


Figure 14. Probability of emitted light versus applied voltage. A) Positive polarity, B) negative polarity. Applied voltage for frozen cyclohexane is multiplied by two in both plots to simplify comparison with liquid cyclohexane.

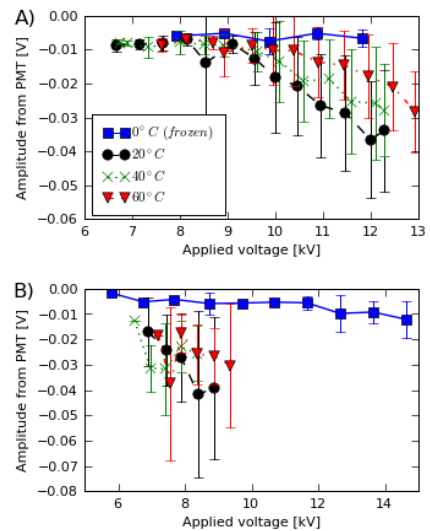


Figure 15. Signal amplitude from photomultiplier versus voltage. A) Positive polarity, B) negative polarity

4.2.3 STREAMER CHARGE/SIZE

There is a trend towards lower streamer charge for higher temperatures under positive polarity, but the differences are small and the scatter in the measurements is quite large. Nevertheless the trend is quite clear, Figure 13.

No temperature dependence was found for streamer charge injection in liquid cyclohexane under negative polarity.

In frozen cyclohexane no polarity effect was found on the discharge magnitudes. Under negative polarity where higher voltages were applied, a large increase in the injected charge was found at voltages above 13 kV. Under positive polarity tests were not performed above 13 kV due to the risk of getting breakdown.

4.2.4 LIGHT EMISSION

Light was observed from streamers in cyclohexane almost every time they occurred. In a few cases an electrical discharge was observed without any recorded light emission. Only in a few cases was light observed from the pre-inception currents, and then only for pre-inception currents at voltages in the inception voltage range.

The probability for recorded light as a function of the applied voltage can be seen in Figure 14. It is clear that light recordings are as good as charge recordings for partial discharge observation. The probability for streamers versus voltage plot in Figure 12 corresponds well to the probability of light emission versus voltage. No temperature effect on the probability of recorded light was found.

The signal amplitude from the photomultiplier is shown in Figure 15. One might assume that the amount of emitted light is correlated to the energy injected to the streamer. The similarity with the plot for streamer charge versus applied voltage is striking. The emitted light from the streamer is seen to be closely related to the injected charge. As for charge most light is observed at 20 °C and then the trend goes towards less emitted light for higher temperatures.

The emitted light in frozen cyclohexane is much lower than for the liquid phase. This is also in good agreement with the charge recordings, but in addition to this it is likely that more light is absorbed by the less transparent frozen cyclohexane.

5 DISCUSSION

5.1 PRE-INCEPTION CURRENT

5.1.1 LIQUID

Dumitrescu et al. found that the pre-inception current recorded with positive polarity in cyclohexane is proportional to $(V - V_0)^2$, with a value for V_0 slightly below what was found in this experiment (4.5 versus 6 kV) [11]. Similar measurements have also been reported in [6]. The onset voltages (V_0) for pre-inception current in these two studies are similar to the ones found in this study. Since the onset voltage is highly dependent on the electrode geometry and the test cell, slight deviations between the values obtained from different test series using different equipment should be expected. The general trend seen in the three studies are nevertheless consistent for positive polarity.

Negative streamers occur at voltages just a few kV above the voltage where the first pre-inception currents are recorded. The transition from 0-100% streamer probability occurs over a small voltage range (compared to positive polarity). Pre-inception currents can thus only be recorded in a narrow voltage range with a negative needle electrode. No pre-inception

currents were found in [11], while pre-inception current with negative polarity have been reported before in [6].

The magnitude of the pre-inception currents measured under negative polarity are in the same range as the pre-inception currents measured with positive polarity at the same voltages, and the first signals are recorded at approximately the same voltage. The conduction mechanism responsible for pre-inception current can therefore be the same under both polarities.

5.1.2 SOLID

The most consistent current measurements in solid cyclohexane were obtained for virgin samples (i.e. the first impulse after a sample had been frozen) Further investigations to study pre-inception currents should be done for cases where the sample is heated between each measurement to avoid the interference of space charge or ageing of the material from previous stresses. Comparison between the measurements and simulations in comsol shows that the currents for virgin samples could be explained by a Poole-Frenkel mechanism. However, the large scatter seen in the current magnitude makes final conclusions hazardous. New experiments with virgin samples would make more direct comparison between the liquid and solid phase possible.

5.2 STREAMER INCEPTION

50 % streamer inception probability was found at 9-10 kV for positive polarity and 7-8 kV for negative polarity. This corresponds well to results obtained in pure cyclohexane with similar experimental setups [6], [11].

No temperature dependence was found for streamer inception. Inception requires enough energy to vaporize a small volume at the needle electrode. Negative streamers have been found to be initialized by an electron avalanche in the liquid. At ambient pressure and room temperature this avalanche is always followed by a low density (gas) region observable by shadowgraphics [11]. If one increases the temperature less energy is required for vaporization. The lack of temperature dependence thus indicates that the onset field for the avalanche in the liquid to form is not influenced by the temperature change, and that the energy deposited by the avalanche is enough to vaporize a small volume of the liquid for all three temperatures used in this study.

Inception under positive polarity has been shown to depend on hydrostatic pressure, but from 0.1 to 1 MPa no measurable increase in the inception voltage has been reported, even higher hydrostatic pressures must be applied to quench streamers [11]. The change in pressure from 0.1 to 1 MPa corresponds to an increase in the boiling point of cyclohexane from 80.74 °C to approximately 184 °C. This corresponds to a large increase in the required energy for bubble formation. The fact that no increase in inception voltage was found for this case corresponds well with the lack of temperature dependence in the range from 20 to 60 °C at atmospheric pressure. This indicates that the vaporization of the region at the needle point is not a simple boiling process but is most likely due to a more complex mechanism. The mechanism responsible for streamer inception under positive polarity might be a combination of all three mechanisms referred to in section 0.

5.3 STREAMER CHARGE/SIZE

The streamer charge measurements presented in Figure 13 correspond well to similar measurements with similar setups in cyclohexane [7].

The temperature dependence for streamer charge seen under positive polarity can be explained quantitatively by looking at the temperature dependence of energy required for bubble formation. The energy injected into the liquid at the high field region will be proportional to the charge injection. On average approximately 50 % less charge is injected at the same applied voltage for 60 °C compared to 20 °C, see Figure 13, and thus less energy is injected at higher temperatures.

1st mode streamers are believed to be gas discharges in an expanding bubble of vaporized liquid. Energy is required for heating the liquid to the boiling point and for the phase transition; in addition some energy is deposited in the liquid phase in the form of a pressure wave from the expanding bubble. At higher temperatures less energy is required to heat the liquid to the boiling point, thus less energy is required to form a bubble of the same size when the temperature is increased. Since energy transfer from the electric field to the bubble is assumed to be by discharges in the vaporized liquid the bubble will expand only until the field in the bubble falls below a threshold where no new discharges can occur. It can be assumed that the field in the bubble primarily depends on the size of the bubble, thus the size of the bubble at the same voltage will be the same for all three temperatures. If this assumption holds the vaporized volume will be the same for all three temperatures at the same voltage while the energy (and thus charge) required for vaporization of that volume will decrease when the temperature is increased.

Under negative polarity no clear temperature dependence was observed, but this could be due to the more limited voltage range used under negative polarity. It has been reported that the first pulse observed for negative streamers are in the liquid phase, while subsequent pulses are in the gas bubble [11]. It is therefore logical to assume that if higher voltages had been applied resulting in larger bubbles one would measure less charge for higher liquid temperatures.

6 CONCLUSION

An experimental setup for pre-breakdown testing of liquids in liquid and frozen phase has been built and tested. The system records light emission using a photomultiplier and charge injection using a sensitive differential charge measurement technique. The temperature of the test sample can be varied within a large range (-60 to 250 °C) allowing the effect of phase transitions to be studied. The setup was tested on cyclohexane, and the results at room temperature correspond well with what is found in literature.

Four phenomena were studied: Pre-inception current, inception probability, streamer charge and emitted light from the high field region. In liquid cyclohexane a clear effect of the polarity on all the measured phenomena were found, but for frozen cyclohexane no such effect was found.

Streamer charge was found to decrease for increasing temperatures in liquid phase with a positive point electrode. No temperature dependence was found under negative polarity.

Charge and light measurements show a clear correlation. The light recordings can be used to find the inception voltage and the size of the discharge. This was observed under both polarities and for both phases.

The test set-up is expected to be a good tool for studying insulation and what occurs under phase transitions. It can be a tool for testing and developing model systems for thermoplastic insulation.

REFERENCES

- [1] ASTM D3300-00, "Standard Test Method for Dielectric Breakdown Voltage of Insulating Oils of Petroleum Origin Under Impulse Conditions".
- [2] IEC 60897, "Methods for the determination of the lightning impulse breakdown voltage of insulating liquids".
- [3] IEC 61294, "Insulating liquids – Determination of the partial discharge inception voltage (PDIV) – Test procedure".
- [4] L. E. Lundgaard, Ø. L. Hestad, and S. Ingebrigtsen, "Review of test methods for dielectric properties of liquids for HV transformer application", Nordic Insulation Symposium (Nord-IS), pp. 83-87, 2005
- [5] J. C. Devins, S. J. Rzad and R. J. Schwabe, "Breakdown and prebreakdown phenomena in liquids", J. Appl. Phys., Vol. 52, pp. 4531-4545, 1981.
- [6] S. Ingebrigtsen, L. E. Lundgaard and P. O. Åstrand, "Effects of additives on prebreakdown in liquid cyclohexane: I. Streamer initiation", J. Phys. D: Appl. Phys., Vol. 40, pp. 5161-5169, 2007.
- [7] S. Ingebrigtsen, L. E. Lundgaard and P. O. Åstrand, "Effects of additives on prebreakdown in liquid cyclohexane: II. Streamer propagation", J. Phys. D: Appl. Phys., Vol. 40, pp. 5624-5634, 2007.
- [8] Y. Nakao, H. Itoh, S. Hishino, Y. Sakai and H. Tagashira, "Effects of Additives on Prebreakdown Phenomena in n-Hexane", IEEE Trans. Dielectr. Electr. Insul., Vol. 1, pp. 383-390, 1994.
- [9] O. Lesaint and M. Jung, "On the relationship between streamer branching and propagation in liquids: influence of pyrene in cyclohexane", J. Phys. D: Appl. Phys., Vol. 33, pp. 1360-1368, 2000.
- [10] P. Gournay and O. Lesaint, "A study of the inception of positive streamers in cyclohexane and pentane", J. Phys. D: Appl. Phys., Vol. 26, pp. 1966-1974, 1993.
- [11] L. Dumitrescu, O. Lesaint, N. Bonifaci, A. Denat and P. Notinger, "Study of streamer inception in cyclohexane with a sensitive charge measurement technique under impulse voltage", J. Electrostat., Vol. 53, pp. 135-146, 2001.
- [12] R. Tobazeon, "Prebreakdown phenomena in dielectric liquids", IEEE Trans. Dielectr. Electr. Insul., Vol. 1, pp. 1132-1147, 1994.
- [13] H. Yamashita, K. Yamazawa and Y. Wang, "The effect of tip curvature on the prebreakdown streamer structure in cyclohexane", IEEE Trans. Dielectr. Electr. Insul., Vol. 5, pp. 396-401, 1998.
- [14] Y. Cao, G. G. Jiang and S. Boggs, "Guarded needle for "charge injection measurement", Rev. Sci. Instruments, Vol. 73, pp. 3012-3017, 2002.
- [15] A. Beroual, M. Zahn, A. Badent, K. Kist, A. Schwabe, H. Yamashita, K. Yamazawa, M. Danikas, W. Chadband, and Y. Torshin, "Propagation and structure of streamers in liquid dielectrics", IEEE Electr. Insul. Mag., Vol. 14, No. 2, pp. 6-17, 1998.
- [16] L. A. Dissado and J. C. Fothergill, *Electrical Degradation and Breakdown in Polymers*, P. Peregrinus for IEE, London, ISBN 0 86341 1967. 1992.
- [17] L. A. Dissado, "Understanding electrical trees in solids: from experiment to theory", IEEE Trans. Dielectr. Electr. Insul., Vol. 9, pp. 483-497, 2002.
- [18] A. Denat, N. Bonifaci and M. Nur, "Spectral analysis of the light emitted by streamers in hydrocarbon liquids", IEEE Trans. Dielectr. Electr. Insul., Vol. 5, pp. 382-387, 1998.
- [19] T. Aka-Nguni and A. Beroual, "Modelling of multi-channel streamers propagation in liquid dielectrics using the computation electrical network", J. Phys. D: Appl. Phys., Vol. 34, pp.794-805, 2001.

- [20] F. M. O'Sullivan, *A Model for the Initiation and Propagation of Electrical Streamers in Transformer Oil and Transformer Oil Based Nanofluids*, Ph.D. dissertation, MIT, Cambridge, MA, USA, 2007.
- [21] M. Kim, R. Hebner and G. Hallock, "Modeling the Growth of Streamers During Liquid Breakdown", *IEEE Trans. Dielectr. Electr. Insul.*, Vol. 15, pp. 547-553, 2008.
- [22] O. Lesaint and G. Massala, "Positive streamer propagation in large oil gaps: experimental characterization of propagation modes", *IEEE Trans. Dielectr. Electr. Insul.*, Vol 5, pp. 360-370, 1998.
- [23] L. Lundgaard, D. Linhjell, G. Berg and S. Sigmond, "Propagation of positive and negative streamers in oil with and without pressboard interfaces", *IEEE Trans. Dielectr. Electr. Insul.*, Vol. 5, pp. 388-395, 1998.
- [24] A. Denat, J.P. Gosse and B. Gosse, "Electrical conduction of purified cyclohexane in a divergent electric field", *IEEE Trans. Electr. Insul.*, Vol. 23, pp. 545-554, 1988.
- [25] R. Kattan, A. Denat and O.Lesaint, "Generation, growth and collapse of vapor bubbles in hydrocarbon liquids under a high divergent electric field", *J. Appl. Phys.*, Vol. 66, pp. 4062-4066, 1989.
- [26] T.J. Lewis, "A new model for the primary process of electrical breakdown in liquids", *IEEE Trans. Dielectr. Electr. Insul.*, Vol 5, pp. 306-315, 1998.
- [27] H. Sueda and K. C. Kao, "Prebreakdown Phenomena in High-Viscosity Dielectric Liquids", *IEEE Trans. Electr. Insul.*, Vol. 17, pp. 221-227, 1982.
- [28] N. Shimizu and C. Laurent, "Electrical tree initiation", *IEEE Trans. Dielectr. Electr. Insul.*, Vol. 5, pp. 651-659, 1998.
- [29] G. Teyssedre and C. Laurent, "Charge Transport Modeling in Insulating Polymers: From Molecular to Macroscopic Scale", *IEEE Trans. Dielectr. Electr. Insul.*, Vol. 12, pp. 857-875, 2005.
- [30] Comsol Multiphysics® ver. 3.4 with AC/DC module from the Comsol Group. Comsol AB. Regnergatan 23. SE-111 40 Stockholm. Sweden. www.comsol.com
- [31] R. Coelho and J. Debeau, "Properties of the tip-plane configuration", *J. Phys. D: Appl. Phys.*, Vol. 4, pp. 1266-1280, 1971.
- [32] R. S. Sigmond, "Simple passive electrical filter for discharge diagnostics", 11th Symp. on Elementary Processes and Chem. Reactions in Low Temp. Plasma, Bratislava, pp. 256-259, 1998.



Øystein L. Hestad was born in Mo I Rana, Norway in 1978. He received the M.Sc. degree in physics at the Norwegian university of science and technology in 2003. From 2003 to 2006 he worked at SINTEF Energy Research. He is currently studying for the Ph.D. degree in physical chemistry at the Norwegian university of science and technology.



Lars E. Lundgaard was born in Copenhagen, Denmark on 24 May 1952. He took his M.Sc in power electric engineering at The Norwegian Institute of Technology in 1976. Since 1980 he has worked with SINTEF Energy Research. He is working on material science for electric power apparatus, relating to design, diagnostics and maintenance. He is also working on electro-separation of water-oil emulsions. His main experiences are in the field of GIS and transformer insulation. He is active within SC D1 in CIGRÉ.



Dag Linhjell was born in Trondheim, Norway on 14 March 1955. He received the Ph.D. degree in 1985 on electron and ion physics. Since 1986 he has been with SINTEF Energy Research. He has mainly worked on high voltage measurements and high voltage insulation for power apparatus.

Paper 2

n-tridecane as a model system for polyethylene: Comparison of pre-breakdown phenomena in liquid and solid phase stressed by a fast transient

Ø. L. Hestad; L. E. Lundgaard and P.-O. Åstrand

Submitted to the *IEEE Trans. Dielect. Elect. Insul.*, 2010

n-tridecane as a model system for polyethylene: Comparison of pre-breakdown phenomena in liquid and solid phase stressed by a fast transient

Ø. L. Hestad, P.-O. Åstrand

Department of Chemistry,
Norwegian University of Science and Technology (NTNU)
7491 Trondheim, Norway

and L. E. Lundgaard

Department of Electric Power Technology
SINTEF Energy Research
7465 Trondheim, Norway

ABSTRACT

Pre-breakdown phenomena in pure n-tridecane in liquid and solid state have been investigated experimentally in a needle-plane geometry with impulse voltage. Light emission and charge injection from the high-field electrode were measured. Pre-inception currents in liquid and solid state were recorded and compared to finite element calculations to find plausible high-field conduction models for n-tridecane and cyclohexane.

n-tridecane was chosen as a model system for polyethylene based on the known similarities in energy bands for polyethylene and alkanes. The results obtained in pure n-tridecane were compared to similar experiments in cyclohexane and polymer systems. High field conduction in liquid n-tridecane was found to have a similar field dependence as previously reported for cross linked polyethylene (XLPE). Conduction currents and inception probabilities were found to be almost independent of polarity in frozen and liquid n-tridecane, which is also in line with results obtained in XLPE. Conduction currents were observed at lower voltages in n-tridecane than in cyclohexane, reflecting the lower space charge limited field (SCLF) in n-tridecane. Inception of streamers in liquid cyclohexane occurs at lower voltages than in liquid n-tridecane, and stronger polarity dependence for all phenomena was observed in cyclohexane compared with n-tridecane. A possible explanation for the differences between n-tridecane and cyclohexane is given based on the field needed for electron avalanches and the SCLF in the two liquids.

Inception voltages, light emission and charge injection were found to be similar in liquid and solid n-tridecane. This indicates that the same processes are responsible for inception and propagation of electrical trees in solids and streamers in liquids when the material is stressed by a fast transient. The similarity between the measured properties in solid and liquid phase leads to the conclusion that electrical treeing mainly takes place in the amorphous regions of the solid phase.

Index Terms — Pre-breakdown phenomena, streamer, electrical tree, cyclohexane, n-tridecane, space charge limited field, high field conductivity.

1 INTRODUCTION

ELECTRICAL degradation and breakdown in dielectric

materials is a broad and complex topic. Mechanical, electrical and thermal properties of the materials have all been shown to be of importance [1]. In addition to the material properties of the dielectric, external properties like the electrode geometry (homogeneous or in-homogeneous field), type of applied voltage (AC, DC, transient), temperature and relative

humidity in the laboratory are also of importance for degradation and breakdown.

Mechanisms leading to discharges and breakdown in gases are relatively well understood [2,3], and theories for breakdown in liquid and solid materials are often discussed along the same lines [4-6]. However, no unified theory exists for condensed matter. While pre-breakdown phenomena normally are denoted streamers in liquids similar phenomena are called electrical trees or discharges in solids. Here we will also refer to these phenomena as partial discharges, where a partial discharge is recognized by a sudden large increase in charge and emitted light.

When fast rising transient voltages are applied hot electrons are conjectured to play an important role for discharges in both liquid and solid insulation [1, 7, 8]. Our initial assumption was that the interaction between a hot electron and a molecule should not depend on the phase of the material; whether it being liquid or an amorphous solid. Therefore pre-breakdown phenomena are assumed to be similar in the two phases. To test this assumption an experimental setup with temperature control that enables pre-breakdown experiments in liquids and frozen liquids was built and results from experiments on liquid and frozen cyclohexane have been presented [9]. For the experiments presented in this paper n-tridecane was used because of its similarities with polyethylene (e.g. similar energy levels and crystalline structure) [10, 11], and the results for liquid and solid phase have been compared to results obtained with the same setup with liquid cyclohexane. The main focus of this paper is on how pre-breakdown phenomena are affected by the transition from liquid to solid phase.

In the following section we provide some theoretical background. This paper is not intended as a review paper for theories describing pre-breakdown phenomena, but a short recapitulation for liquid and solid insulation will be given. For a more complete discussion of pre-breakdown phenomena in liquids several review papers exist [12-14], and for solid insulation the reader is referred to the book by Dissado and Fothergill [1]. The background section also describes the reasoning for choosing n-tridecane as a model for polyethylene. After the theory section a brief description of the experimental setup and procedures used will be given. The experimental setup has been described in detail previously [9]. Finally the main part of this paper is the experimental results and discussion given in two separate sections. Both sections are divided into three subsections dealing with pre-inception currents, inception probabilities and propagation of partial discharges in the two phases. In the discussion, our results are discussed based on high-field conduction models, and the influence of high-field conduction on the electrical-field distribution and energy dissipation in the high-field region.

2 BACKGROUND

2.1 PRE-BREAKDOWN PHENOMENA IN SOLIDS AND LIQUIDS

Streamers in dielectric liquids and electrical trees in solid insulation have been extensively studied during the last decades [1, 13-17]. Investigations document e.g. the field needed for inception, speed and length of propagation, and charge/current injection and light emission from discharges in various geometries. There has also been more qualitative research on the chemical composition of the channels in the electrical trees [18, 19] and spectroscopic measurements of light emitted from the discharges [16, 20]. Some progress has been made in modelling of the phenomena [21-25].

2.2 STREAMER INCEPTION AND PROPAGATION IN LIQUIDS

2.2.1 *Streamer modes*

Inception and propagation of a streamer is dependent on the polarity, and the streamers are thus labelled by the polarity of the electrode from which they propagate. Inception voltage is governed by electrode geometry and rise time of the applied voltage [26], and is typically lower for negative than for positive streamers. The propagation modes of the streamer are usually classified by polarity, propagation speed and streamer shape, and are dependent on the voltage. For positive polarity the speed increases in quite well defined steps as the voltage is increased, defining the propagation modes [27], while for negative polarity the speed variation is more gradual making classification into different modes more uncertain. The variation of propagation speed for the different modes for positive streamers are typically a factor of ten, where the slow first mode travels at speeds from a hundred m/s to a few hundred m/s while the fast 4th mode propagates at speeds higher than 100 km/s [28]. The present experiment only deals with 1st and 2nd mode streamers.

2.2.2 *Inception and propagation of 1st mode streamers*

For negative polarity the initiation mechanism is known, and is the same for impulse as for dc [7, 8, 29], i.e. when the field reaches a critical value an electron avalanche in the liquid creates a shock wave and a bubble develops in its wake, discharges occur inside the bubble created by the avalanche, producing fast current pulses and supporting the growth of a slow bush-like streamer. This theory has been supported by experiments showing that the first current pulse (electron avalanche in the liquid) does not depend on pressure, while the subsequent discharges can be quenched by increasing the hydrostatic pressure [7].

Experiments have shown that the inception voltage for positive polarity can be increased by increasing the hydrostatic pressure [7]. Thus the discharges probably occur in a low density/gas region. The origin of this low density region is unknown, but might be caused by:

- Boiling (local joule heating) [7].
- Increased concentration of microvoids due to

electromechanical forces [30].

- Pressure reduction facilitating phase transition from liquid to gas caused by electrohydrodynamic motion and/or pressure reduction by Coulomb repulsion between unipolar charges [12, 31].

2.2.3 Inception and propagation of 2nd mode streamers

It has been shown that inception of 2nd mode streamers requires a threshold voltage, V_p , for a given gap distance that is independent of the electrode point radius, r_p , and that above a critical radius, r_c , 1st mode streamers are not observed [26]. With sharp points ($r_p < r_c$), inception can occur at voltages below V_p , but the resulting streamer will then be a 1st mode streamer. With a larger radius, $r_p > r_c$, the voltage required for inception will be higher than the threshold voltage, and thus 1st mode streamers cannot occur [26].

It has been proposed that the inception mechanism is identical for 1st and 2nd mode streamers [26]. In both cases an ionized low density bubble is created, but for voltages above the threshold voltage for 2nd mode streamers the resulting field at the boundary of the bubble is large enough for ionization of the liquid-bubble interface. This results in a propagating ionization region ("streamer head"), the ionization of the liquid in front of the "streamer head" can be either by direct field ionization [17] or impact ionization [32]. This mode of propagation creates thin filaments of conducting plasma channels connecting the streamer head to the point electrode. The streamer head has the same polarity as the high-field electrode from which it propagates and the streamer can be considered to be an electrically conductive extension of the electrode from which it propagates. In a divergent field the phenomena will propagate until the field at the streamer head is reduced to a level where no further ionization of the liquid is possible. This field reduction can be caused by the voltage drop over the streamer channel, or by branching of the channels resulting in a field grading.

2.3 ELECTRICAL TREEING IN SOLIDS

Solids used for insulation of power apparatus typically have very high intrinsic breakdown strengths [1]. The onset of an electrical tree or a breakdown thus requires a defect within the material typically being voids, particles or protrusions. In practice sharp protrusions will be the most important [16].

Electrical trees propagating from one of the electrodes are called vented trees, while trees propagating from contaminants/voids in the insulation are called bow-tie trees. The trees are typically divided into categories based on their appearance: bush, bush-branched and branched trees. As for liquids it is common to distinguish between the inception and a propagation stage of electrical treeing.

In contrast to liquids, which are considered to be self-healing, solids are exposed to slow, gradual, cumulative

processes under moderate stress caused by ac or repeated impulse voltages that can result in permanent degradation and finally tree formation. Free radical production, caused by electron impact excitation and ionization, followed by autoxidation process are believed to play an essential role in long-term tree inception in polymers [15, 16, 33]. The gradual deterioration of the material could also be caused by cracking and free volume formation due to electromechanical stress [34].

At higher fields, electrical trees can occur instantaneously. This threshold field for instantaneous electrical treeing can be explained by impact ionization caused by generation of hot electrons in the solid. This requires a high field over a sufficient length so that electron avalanches have sufficient energy to damage the material.

Hot electrons are believed to play a key role for both cumulative and instantaneous treeing. Impact excitations or ionization of the molecules in the solid by hot electrons depend on a relatively long mean free path where the electrons can be accelerated by the electrical field. The mean free path can be reduced by impregnating the solid to reduce the free volume, or by introducing electron scavengers [1]. For cumulative processes degassing is observed to have a positive effect because it suppresses the autoxidation of the sample [16]. Furthermore, morphology, temperature, and chemical composition (additives and base polymer) have an effect on inception and propagation of electrical trees.

Once a channel (tubule) is formed, the electric tree can start to propagate. The propagation is believed to be a stepped process where the channel acts as an extension of the electrode, and charge is injected into/extracted from the solid at the tip of the tubule. Continued propagation requires the field at the tip to be above the threshold required for forming hot electrons [1].

2.3.1 High-field conductivity

Insulation materials have a very low conductivity at low and intermediate electrical fields. Many theories exist for describing high-field conductivity in dielectric materials, and common for many of them is the prediction of an exponential increase in conductivity with field [1, 35]. The increased conductivity may be caused by free charge injected from the electrodes, delocalization of charge carriers in the bulk material, increased charge carrier mobility or a combination of these factors. Table 1 contains some important mechanisms. Notice the similarities between the field dependence of the Poole-Frenkel model (bulk conductivity) and the Schottky model (charge injection from electrode). It is generally hard to tell these two mechanisms apart since they have the same field dependence, i.e. in general the data will fit both models equally well for homogeneous fields. In addition, several high-field bulk conduction mechanisms exist with similar field dependence as predicted by the Poole-Frenkel mechanism, for example are the Onsager model and some hopping conduction models [38, 39]. When a divergent

Table 1. Models for charge injection from electrodes/bulk conductivity.

Name	Equation ^(a)	Ref.
Schottky injection	$J(E) = \frac{4\pi emk_B^2(1-R)T^2}{h^3} \cdot e^{-\frac{\Phi}{k_B T}} \cdot e^{-\frac{e}{2k_B T} \sqrt{\pi\epsilon_0\epsilon_r} \sqrt{eE}}$	[1, 35, 36]
Fowler-Nordheim	$J(E) = \frac{e^3 E^2}{8\pi h \phi} \cdot e^{-\frac{4}{3} \sqrt{\frac{2m}{h^2}} \frac{\phi^{3/2}}{eE}}$	[1]
Hopping conduction	$\sigma(E) = \frac{2vaen}{E} \cdot e^{-\frac{W}{k_B T}} \cdot \sinh\left(\frac{eEa}{2k_B T}\right)$	[37]
Poole-Frenkel	$\sigma(E) = \sqrt{N_{eff} N_D} e \mu e^{-\frac{\Phi}{2k_B T}} \cdot e^{\frac{e^{3/2} \sqrt{E}}{\sqrt{4\pi\epsilon_0\epsilon_r} k_B T}}$	[1, 35]

^(a) ϵ_0 is the permittivity of vacuum, ϵ_r is the relative permittivity, μ is the charge carrier mobility, v is the escape frequency, ϕ is the work function, Φ is the barrier height, a is the distance between traps, E is the electric field, e is the elementary charge, h is Planck's constant, k_B is Boltzmann's constant, m is the electron mass, n is the charge carrier density, N_{eff} is the effective density of states in the conduction band, N_D is the number of potential donors, R is the reflection coefficient, T is the temperature, and W is the trap depth.

geometry is used one can assume that the Schottky and Fowler-Nordheim models contribute when the high-field electrode is negative, but electrons must be taken from the bulk when the high-field electrode is positive (field ionization). One can therefore look at the polarity dependence of the measured conduction currents when trying to separate bulk and electrode contribution to the amount of free charge in the dielectric. Since several high-field conduction mechanisms have a similar field dependence, it is hard to distinguish between them based on measurements of high-field conduction currents. In the discussion, measured conduction currents in the liquid and the solid phase will be compared to the Poole-Frenkel mechanism. Note that a fit to this model does not rule out other models with the same field dependence.

2.3.2 Effect of high-field conductivity

As described in the previous section the conductivity of a material is typically a function highly dependent on the electric field. When sufficiently high conductivity in the high-field region occurs, the field in this region will be limited to a space charge limited field (SCLF). The field strength at which this happens is dependent on the frequency of the applied voltage. For a given high-field conductivity the SCLF can be derived by calculating the field strength that gives the same time constant for the relaxation of charge and for the applied voltage rise [40]:

$$\tau = \frac{\epsilon_0 \epsilon_r}{\sigma(E_{lim}, T)} = \frac{1}{\omega}, \quad (1)$$

where τ is the relaxation time constant, σ is the conductivity, E_{lim} is the SCLF, ϵ_r is the relative permittivity of the medium, ϵ_0 is the permittivity of vacuum, and T is the temperature.

An idealized example illustrates the physical basis for this [40], in cross-linked polyethylene (XLPE) typical trap depths are 0.8 eV and the average distance between traps are 2.8 nm [41]. At an electric field of 285 MV/m the energy gained by charge carrier between the traps will be

the same as the depth of the traps, effectively delocalizing the charge carriers. This stress is often referred to as the mobility edge for electrons. At this field the polymer will behave like a metal, restricting the maximum electrical field in the dielectric to values close to the mobility edge.

SCLF and high-field conductivity are an important issue for dielectrics as it gives a more realistic picture of the field distribution and energy dissipation in the stressed regions of a material than a charge-free electrostatic Laplacian field distribution. In a high-field region the field will be almost constant, determined by the space charge, and can be substantially lower than the calculated Laplacian field. However, the space charge increases the volume of high stress. The combination of high electric field and high conductivity also results in intense energy dissipation in this region (σE^2). The high energy dissipation and large space charge density in the high-field region leads to strong mechanical and thermal stressing of the material that can lead to degradation [40, 42].

2.4 N-TRIDECANE AS A MODEL SYSTEM

n-tridecane is a short linear hydrocarbon, . It freezes at -5.5°C and boils at 234°C [43]. Quantum chemical calculations have shown that the energy levels of linear alkanes quickly converges towards the energy levels of polyethylene as the number of carbon atoms increase (see section 2.4.1 and [10]). The morphology of n-alkanes have been studied extensively because of their importance in biological systems and as model systems for polyethylene (see section 2.4.2 and [11, 44]). The simple structure of n-tridecane, its high melting point, and similarities with polyethylene, combined with availability in high purity at a reasonable price, makes it a logical choice as a model system for polyethylene.

2.4.1 Energy levels

The relationship between the energy bands in short linear hydrocarbons and polyethylene has been studied [10]. For n-alkanes of finite length there will be a finite number of

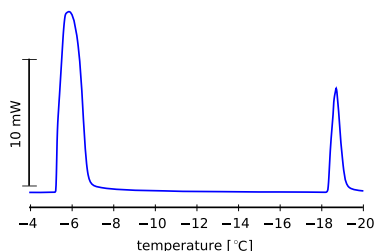


Figure 1. DSC measurement of pure n-tridecane. The measurement was performed with a constant cooling rate of $-1^{\circ}\text{C}/\text{min}$. The two exothermic peaks in the DSC cooling curve correspond to a liquid-solid transition and a solid-solid transition. DSC heating curves are similar, but the transitions are shifted towards higher temperatures. The peaks occur at -16°C (solid-solid) and -2°C (solid-liquid) when the temperature is increased by $1^{\circ}\text{C}/\text{min}$.

energy levels, but they will approach the continuous bands found in polyethylene as the number of carbon atoms increases.

The use of energy band theory for semi-crystalline materials like polymers are controversial and clearly solid state physics can at best be used as an approximation [1, 10]. Polyethylene is usually branched to some degree making it difficult to form a perfect crystalline material. Imperfections in the crystalline lattice are typically referred to as physical defects/disorder, and will typically result in a region of higher electron affinity or lower ionization potential (electron trap/donor) compared with the rest of the lattice. Similarly such imperfections can be introduced by additives with "active" molecular groups of high electron affinity or low ionization potential, creating electron traps or donors.

Quantum chemical calculations using tridecane as a model system for polyethylene have shown that electrons travel more easily in the amorphous phase compared with crystalline phase, the energy barrier between the two phases were estimated to be around 0.6 eV [10].

2.4.2 Morphology

The morphology of n-alkanes and mixtures of n-alkanes is a broad and complex field [11, 45-47]. When cooling n-tridecane from room temperature to -40°C it passes two first-order phase transitions. A differential scanning calorimetry (DSC) cooling curve showing this can be seen in Figure 1. The first transition is from the liquid phase to a rotator/plastic phase. The second transition is from the rotator phase to a fully ordered solid phase. Rotator phases are found for all odd-numbered n-alkanes having from 9 to approximately 43 carbon atoms [45]. The rotational states are layered and are typically crystals with long-range positional order. Here, the molecules are free to rotate around their main axis. These states are also known as plastic crystals or highly ordered smectics. Frozen n-tridecane is polycrystalline. Polycrystalline materials consist of crystallites held together by thin layers of amorphous solid at the boundaries between the crystallites.

In n-tridecane only one rotator phase ("rotator phase R1") exists between the liquid and the fully ordered

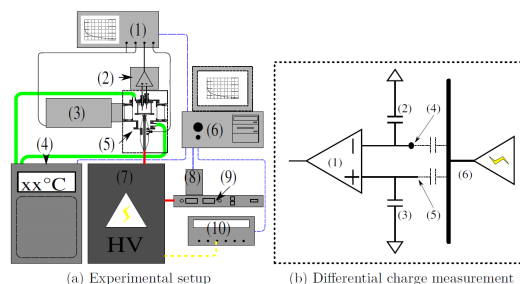


Figure 2. (a) **Experimental setup:** (1) Tektronix TDS684 Oscilloscope, (2) Lecroy DA 1855A Differential amplifier, (3) Hamamatsu R943-02 photomultiplier, (4) Julabo LH-85 Circulator, (5) Test cell, (6) Computer, (7) High voltage pulse source, (8) Fug Probus IV GPIB controlled 0-10-V DC supply, used to control the output from a HV spellman DC supply, (9) Spellman SL300 100-kV HVDC supply and (10) Stanford research systems DG535 Digital delay generator. (b) **Differential charge measurement:** (1) Differential amplifier (Lecroy 1855A), (2 and 3) Measurement capacitor for the probe and needle, (4) Probe electrode, (5) Needle electrode and (6) Plane electrode.

crystalline phase [45, 46]. This rotator phase has an orthorhombic structure similar to that below the solid-solid transition, but with a marked increase in unit-cell volume almost entirely due to transverse expansion [45]. There is thus an increase in free volume as a result of the loss of orientational order (weaker bonds between molecules).

The mechanical properties of two n-alkanes (n-heneicosane and n-tricosane) and a binary mixture of the two were measured using dynamic mechanical spectroscopy (DMS) [48], which showed that the observed viscoelasticity in the rotator phases is largely due to the transition between rotator phases. For a system with only one rotator phase the properties below and above the solid-solid transition were similar. Based on this one can assume that the mechanical properties for n-tridecane in its rotator phase is similar to its properties in the fully ordered phase. Thus, the main difference will be the reduced free volume in the fully ordered phase.

3 EXPERIMENTAL TECHNIQUE

3.1 EXPERIMENTAL SETUP

The experimental setup is shown in Figure 2 [9]. It comprises a high voltage pulse source, a temperature control system, a differential charge measurement setup, and a photomultiplier tube (PMT). Needle-plane electrode geometry with a needle radius of $2\ \mu\text{m}$ and a gap distance of $11.5\ \text{mm}$ was used. The plane electrode has a diameter of $90\ \text{mm}$. The sample volume was approximately 2 dl. The temperature can be varied between -60°C and $+260^{\circ}\text{C}$.

The voltage source connected to the plane electrode gave stepped voltages with rise time of 40 ns, constant high voltage for 50 μs and switching off time constant of 80 μs , hereafter called impulses. Two electrodes, a sharp needle and a blunt probe, were used for differential charge recordings during the applied impulses, see Figure 2. The system has sensitivity better than 0.1 pC [9].

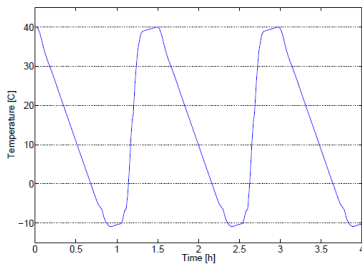


Figure 3. Temperature program used for experiments in frozen n-tridecane.

3.2 TEMPERATURE SEQUENCE

The temperature sequence used to study the effect of phase transition from liquid to solid state is shown in Figure 3. The sample was cooled to -10°C using a linear cooling rate of $-1^{\circ}\text{C}/\text{min}$. Once the desired temperature was reached it was kept constant for ten minutes before the first impulse was applied. Once a discharge with magnitude above 10 pC was recorded the sample was melted (heated to 40°C) and then frozen again to produce a new virgin sample before new impulses were applied. In some experiments the sample was melted and frozen between each applied impulse, giving a virgin sample for every impulse. All experiments performed in liquid n-tridecane were done at 20°C .

3.3 DELAY BETWEEN IMPULSES

In the studies on the liquid phase, delays between each impulse application of 60, 180 and 600 s were used for both polarities. A short delay does not allow charge injected during an impulse time to drain away before the next impulse is applied. The influence of remaining space charge can thus be studied.

For frozen n-tridecane delays of 60, 300, 600 and 1500 s were used for positive polarity, while only 600 s delays were used for negative polarity. Test series where the sample was melted between each impulse were also performed.

3.4 ELECTRODES

Experiments were performed with wolfram electrodes electrochemically etched from wolfram wire with $100\text{ }\mu\text{m}$ diameter to point radius of $2\text{ }\mu\text{m}$. Special concern was given to the submicroscopic properties of the electrode surface as effects attributed to this were seen in the initial pre-inception current experiments:

One test series at low voltages was conducted with electrodes made of wolfram with a fine layer of gold. This was done because SEM images of wolfram needles sometimes revealed small protrusions or very thin filaments extending from the needle surface. The surface of the needle electrodes appeared smoother after a layer of gold was sputtered on to the wolfram. In addition to the improved surface of the needle, the gold coating will also

Table 2. Experiments performed for n-tridecane. Polarity is the polarity of the needle electrode, delay is the delay between impulses (Melt=sample was melted between each impulse), and electrode material is the material of the needle electrode. The temperature of the sample and the voltage range used are also shown.

Polarity	T ($^{\circ}\text{C}$)	Delay (s)	Electrode material	V (kV)
Positive	20	60	Wolfram	14-24
		180	Wolfram	5-31
		600	Wolfram	12-24
		600	Wolfram (new)	5-24
		600	Gold on Wolfram (new)	2, 8-15
Negative	20	60	Wolfram	15-25
		180	Wolfram	15-25
		600	Wolfram	14-30
		600	Wolfram (new)	5-32
		600	Gold on Wolfram (new)	2, 5-12
Positive	-10	60	Wolfram	15-20
		300	Wolfram	15-20
		600	Wolfram	15-25
		1500	Wolfram	12-20
		600	Gold on Wolfram (new)	2, 5-10
Negative	-10	Melt	Wolfram (new)	5-26
		600	Wolfram	9-14
		600	Wolfram (new)	9-15
		Melt	Wolfram (new)	9-28
		Melt	Gold on Wolfram (new)	5-8

slightly increase the work function of the electrode (wolfram: $4.32\text{-}5.22\text{ eV}$, gold: $5.1\text{-}5.47\text{ eV}$ [43]).

It has previously been shown that the radius of the point electrode is of importance only before inception, and of little or no practical relevance for propagation of streamers [26]. The experiments performed with gold coated electrodes were therefore limited to fields below the inception field for discharges to look at the influence on pre-inception phenomena.

3.5 PROCESSING OF SAMPLE

The liquid used was 99.9% pure n-tridecane, degassed for 24 hours, and treated with a molecular sieve (3 \AA Zeochem) to reduce the content of water in the sample. During experiments the sample volume was in contact with a 10 ml reservoir filled with air and molecular sieve, the two volumes were connected through a syringe. This reservoir allowed the sample to expand during temperature cycling. After filling, some gas absorption from the reservoir into the sample must be expected.

3.6 EXPERIMENTS PERFORMED

Experiments to study the effect of delay between impulses, phase (liquid/frozen liquid) and the electrode material (gold/wolfram) on pre-breakdown phenomena were conducted. The results for frozen cyclohexane obtained previously with this experimental setup were hard to interpret due to some problems with the experimental setup, and residual space-charge from previous impulses in the sample [9]. To compare the two phases one should use virgin frozen samples, i.e. the sample should be melted between each applied voltage impulse to eliminate the influence from residual space charge and cumulative degradation. Table 2 lists all the experiments performed.

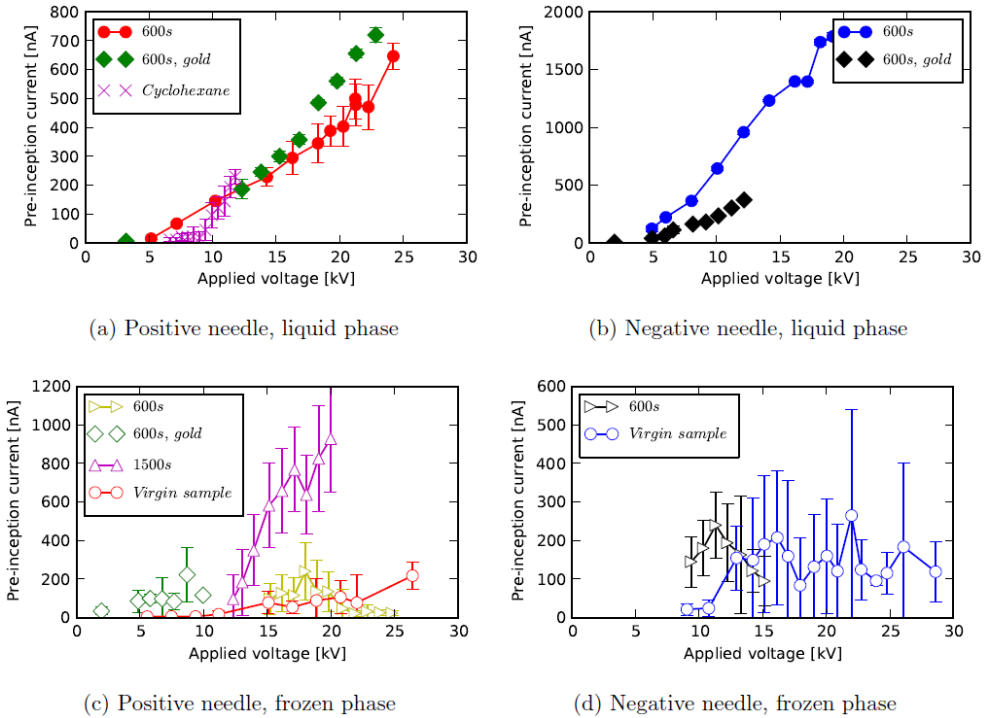


Figure 4. Average pre-inception current during the first 50 μ s after applied voltage.

4 FINITE ELEMENT METHOD SIMULATIONS

The finite element method (FEM) simulations were done with Comsol [49] using a 2D axial symmetrical geometry representing a simplified version of the test cell. The field distribution at the needle was compared to a 3D simulation of the test cell to make sure that the simplified geometry is a good approximation of the real case [9].

The simulations were performed to compare measured currents at voltages below inception (pre-inception currents) to simulations using different conductivity models. FEM simulations of pre-inception currents in liquid phase are difficult and requires coupling of at least three sets of equations: thermal, electrical and hydrodynamic. Here only the thermal and electrical parts of the problem were taken into account. This means that the currents found from FEM simulations gives smaller values than obtained from experiments since the increase in ion mobility as a result of electrohydrodynamic motion of the liquid is not taken into account. For solids the main problem in direct comparison of experimental results and results from simulations is the inhomogeneity on the micrometer scale. The charge recordings will be influenced by the morphology of the material in the high field region [40].

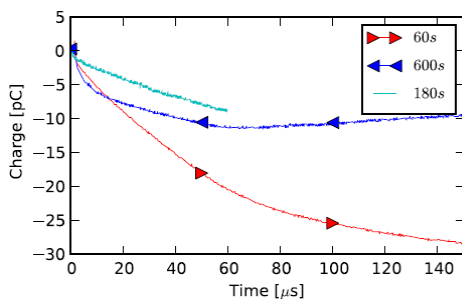
5 RESULTS

5.1 PRE-INCEPTION CURRENT

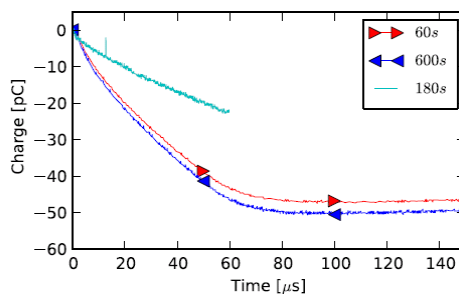
Pre-inception currents were measured for both polarities and both phases. The average current, recorded during the time of constant voltage (first 50 μ s after applied voltage), can be seen in Figure 4 for positive and negative polarity in liquid and solid phase respectively. The effect of delay between impulses and the effect of electrode material and surface were studied. For positive polarity in liquid phase the results are compared to the results obtained in cyclohexane, for negative polarity and solid phase only results in n-tridecane are shown. First, a conditioning effect observed while conducting experiments in liquid n-tridecane with positive polarity will be discussed.

5.1.1 Conditioning effect of discharges

Typical examples of pre-inception currents in liquid n-tridecane with positive polarity are shown in Figure 5. All the charge recordings shown at 14 and 24 kV were obtained with the same needle. The difference between the charge recordings cannot be explained by the difference in delay between impulses alone. The charge injection with a delay of 180 s between impulses is lower than for both 60 s and 600 s delays at the same applied voltage. The experiments were done in the following sequence: 60 s (14-20 kV), 600 s (14-24 kV), 60 s (21-24 kV) and 180 s (4-32 kV) delay



(a) 14 kV



(b) 24 kV

Figure 5. Typical examples of pre-inception current. The same needle was used for all these charge recordings. Experiments with 180 s delay were performed with higher sampling rate which is why there is only data for the first 60 μ s.

between impulses. Examination of the obtained recordings, in liquid n-tridecane, was influenced primarily by the voltage amplitude, and the number of impulses/discharges the needle electrode had been subjected to. The effect of the number of discharges/impulses must be due to conditioning of the needle, and thus a thorough examination of the needle surface for new and aged needles was done. Two phenomena that could explain the conditioning effect were observed. For used needles evidence of a polymer layer growing on the needle were found, while for newly etched needles some very fine wolfram filaments were observed under an electron microscope.

A fine filament at the tip of the needle electrode will cause a strong field enhancement at the tip. Such a protrusion will result in increased charge injection. We believe that this is what is seen for the 60 s and 600 s charge recordings in Figure 5a. The shape of the 600 s recording at 14 kV shows a large increase during the first μ s, corresponding to charge injection, and then levelling off as the field is limited by the space charge (slow increase of charge due to spreading of the charge in the high field region). For 60 s delays at 14 kV the charge increase during the first microseconds is less marked, and the charge recording is most likely influenced by charge left behind from previous impulses. No evidence of wolfram filaments were found for used needles, indicating that the filaments were electrochemically etched or melted by the discharges. In Figure 5b, only the effect of the polymer layer on the 180 s recording can be seen, and no effect of the difference in delay between impulses for the 60 and 600 s series was found, indicating that at that time there was no protrusion at the tip of the needle.

The polymer observed after several hundred discharges in n-tridecane was clearly visible under an electron microscope, indicating that the layer is at least semi-conductive. This can explain the reduced charge injection observed for the last test series (180 s delay) because a semi-conductive layer on the electrode would have the same effect as replacing the needle with a blunter needle.

As a result of these findings the surface of the needle electrodes was always thoroughly studied under an electron microscope prior to experiments.

5.1.2 Positive polarity, liquid

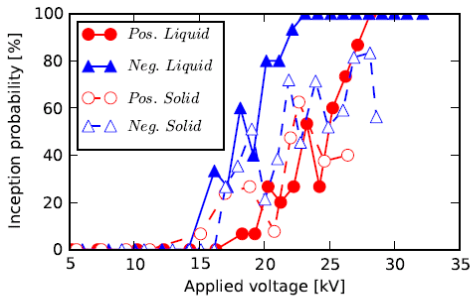
The average pre-inception current in n-tridecane starts to increase at a lower voltage/field and increases more slowly than what is found for cyclohexane as seen in Figure 4. In n-tridecane, using a gold needle, pre-inception currents were recorded at voltages as low as 2 kV, whereas in cyclohexane no currents were recorded for voltages below 5 kV. Even though the increase in average current versus applied voltage is slower in n-tridecane than in cyclohexane, higher current levels are reached in n-tridecane, but at voltages well above the inception voltage in cyclohexane. In contrast to cyclohexane where pre-inception currents have been shown to behave like a space charge limited current ($I=k(V-V_0)^2$) [7, 9], the pre-inception current increases almost linearly with applied voltage for n-tridecane as seen in Figure 4a.

5.1.3 Negative polarity, liquid

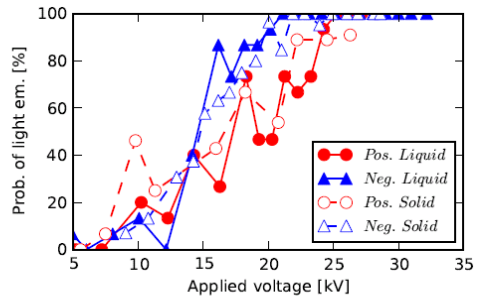
Two measurement series of average pre-inception current versus voltage for negative needle polarity are shown in Figure 4b. Both were obtained with the same delay between impulses, but with different point electrodes. The first electrode was a newly etched wolfram electrode checked under an electron microscope while the second electrode had a gold coating. Both electrodes had a radius of $2.0 \pm 0.1 \mu\text{m}$. For the wolfram needle, the pre-inception current with negative polarity were almost a factor of ten higher than with positive polarity, while gold coating reduced the current to magnitudes similar to what was measured with positive polarity.

The shape of the charge recordings was similar for both electrodes. However, for the two wolfram electrodes very small steps in the charge recordings were seen at voltages near the inception voltage. These steps were at the limit of the sensitivity of the experimental setup. The large pre-inception current might be caused by small discharges below the sensitivity of the setup.

5.1.4 Positive polarity, frozen

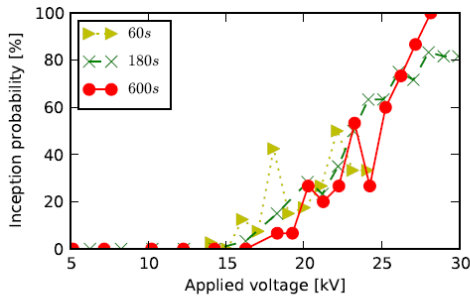


(a) Inception probability versus voltage

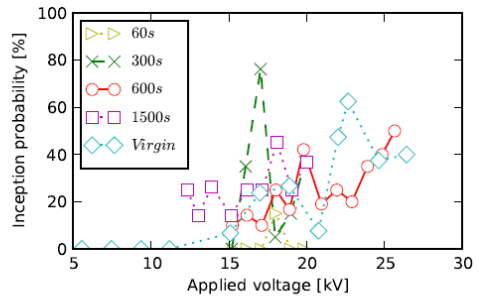


(b) Probability of emitted light versus voltage

Figure 6. Partial discharge probability and probability of light emission versus applied voltage for liquid and solid phase. Delays between impulses were 600 s for liquid phase, for solid phase the samples were melted between each impulse.



(a) Liquid



(b) Solid

Figure 7. Comparison of partial discharge inception probability for test series where different delays between impulses were used with positive polarity.

In frozen n-tridecane, pre-inception currents were not reproducible when short time delays between impulses were used. For 60, 300 and 600 s between impulses the effect of space charge left behind from previous impulses have a large effect on the charge recordings: No good correlation between the applied voltage and the measured pre-inception current was found, and for short delays the average current was actually found to decrease at higher voltages.

For the longest delay used, 1500 s, the pre-inception

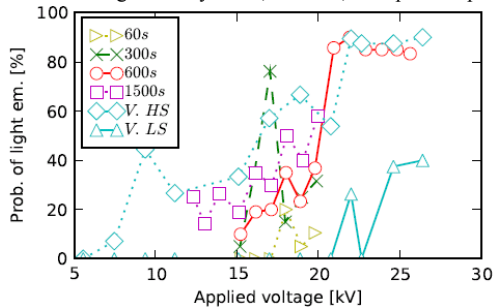


Figure 8. Probability of light emission versus applied voltage for frozen n-tridecane. All recordings were done with the same photomultiplier with default settings. The same input sensitivity of the oscilloscope were used for all recordings except the one marked "V HS" where a higher sensitivity were used (10 mV/div versus 200 mV/div). V = virgin sample, HS = high sensitivity, LS = low sensitivity (same as other series).

current was found to increase nearly linearly with applied voltage, which corresponds to the observed behaviour in liquid phase indicating that the cumulative ageing makes frozen n-tridecane more like liquid n-tridecane. One hypothesis that could explain this is that the long-range order of the frozen phase is reduced as a result of the cumulative ageing, resulting in an amorphous region near the point electrode. This has been observed in polymers and silicon rubber before and the aged region is typically referred to as the degradation zone [18, 33, 50, 52].

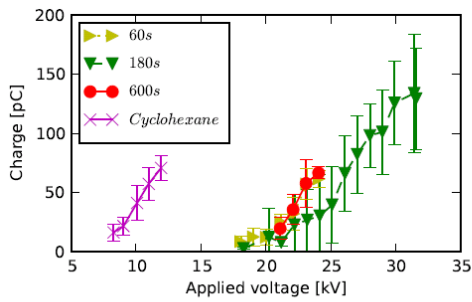
In the case with virgin samples, i.e. samples melted between each voltage impulse, the current was also seen to increase with increased applied voltage, but it increased more slowly than what was found for liquid and for solid phase with 1500 s delay between impulses.

5.1.5 Negative polarity, frozen

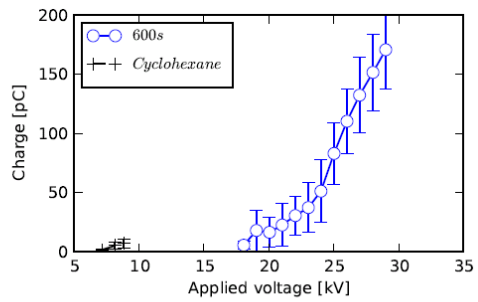
The pre-inception current measured in frozen phase negative polarity shows a large scatter, even for virgin samples. The current recorded was approximately one tenth of what was recorded in liquid phase with the same polarity, but around the same order of magnitude as the current recorded for positive polarity in frozen phase with similar conditions.

5.2 INCEPTION

Inception probability versus voltage is shown in Figure



(a) Positive polarity



(b) Negative polarity

Figure 9. Comparison of measured charge for partial discharges versus applied voltage for the liquid phase.

6. The Figure shows the results obtained with 600 s delay between impulses in liquid phase. For the frozen phase, results obtained with virgin samples are shown. Partial discharges were observed at lower voltages for negative polarity than for positive polarity. Light emission was observed at voltages below the level where the first partial discharges were observed. Both inception probability for discharges and probability for light emission were similar for both phases and both polarities.

Comparing the results obtained in n-tridecane with cyclohexane [9], light emission in liquid cyclohexane and

n-tridecane are observed at approximately the same voltage (5-6 kV), whereas partial discharges (streamers) occurs at much lower voltages in liquid cyclohexane compared with liquid n-tridecane.

5.2.1 Effect of delay between impulses

Figure 7 shows the effect of delay between each impulse on the inception probability. In liquid phase no effect of changing the delay was found. In solid phase the effect of the delay was only apparent for the shortest delay, 60 s, where only a few discharges were observed.

Figure 8 shows the probability of light emission versus voltage in frozen n-tridecane. The same trend is seen as in Figure 7. Note that when the same input sensitivity on the oscilloscope (200 mV/div) was used light was observed only at higher voltages for virgin samples compared with samples subjected to several impulses between each time they were melted. When higher oscilloscope sensitivity (10 mV/div) was used for virgin samples the results were similar to those observed with several consecutive pulses. The photomultiplier tube was operated at recommended voltage in all experiments, thus the sensitivity of the photomultiplier was constant while the sensitivity of the oscilloscope varied

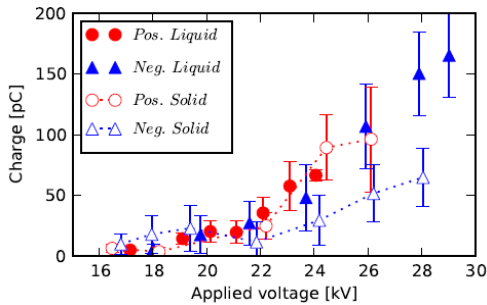


Figure 10. Measured charge versus applied voltage. Comparison of charge injected into liquid and solid n-tridecane with negative and positive polarity respectively. Only virgin frozen samples are included in the plot.

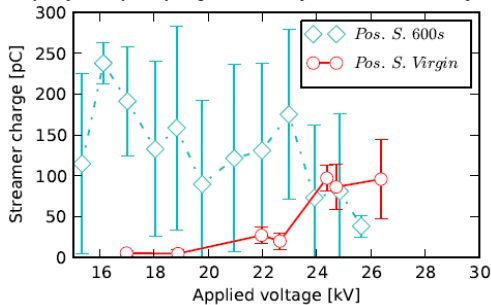


Figure 11. Measured charge versus applied voltage, positive polarity, solid phase. Comparison between charge recorded in a virgin samples and charge recorded in a sample that have been subjected to several impulses with a 600 s delay between each impulse. In the latter case, several of the charge measurements reached saturation, which means that the charge is larger than what is indicated in this figure.

5.3 PROPAGATION

5.3.1 Charge measurement

The charge injection from partial discharges versus voltage is presented in Figure 9 for liquid n-tridecane. In Figure 10, the results from the liquid and the solid phase are compared. Only measurements with virgin samples have been included in this Figure.

Using several impulses in solid phase without melting between each impulse, the discharge amplitude increased significantly, saturating the measuring equipment. This was seen for both polarities. A plot of average charge injection for partial discharges versus voltage for virgin samples, and samples where a delay of 600 s between each impulse were used can be seen in Figure 11.

The main finding is that the phase transition from liquid to solid phase does not change the size of the discharge (measured charge) when virgin solid samples are used as seen in Figure 10.

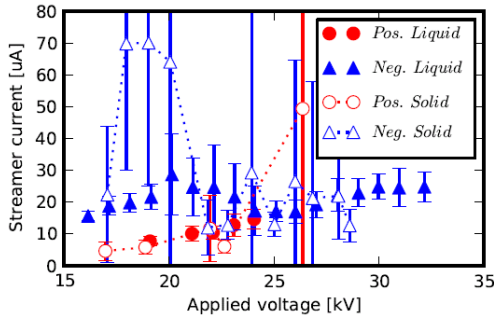


Figure 12. Comparison of average discharge current versus applied voltage for both phases and both polarities.

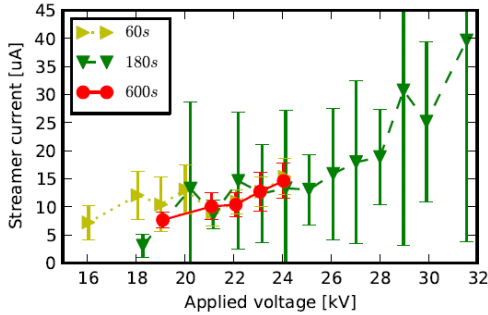


Figure 13. Comparison of average discharge current versus applied voltage for positive polarity in liquid n-tridecane with different delays between impulses. The same needle was used for all experiments, no effect of ageing was seen.

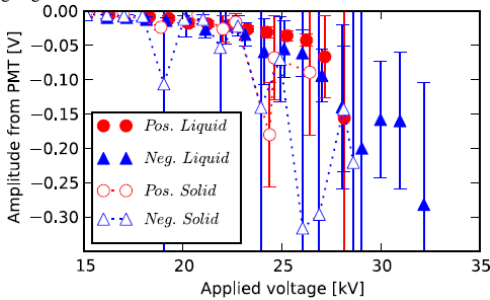


Figure 14. Light emission versus applied voltage. Comparison of negative and positive polarity for liquid (600 s delay) and frozen (virgin samples) phase.

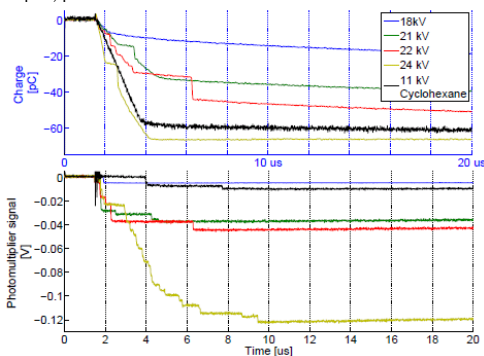


Figure 15. Typical examples of charge recordings with corresponding photomultiplier signal for streamers in n-tridecane compared to a typical example in cyclohexane.

The average discharge current found by dividing the measured charge of the discharge by the propagation time is shown in Figure 12. For positive polarity an increase in discharge current with increased applied voltage was found, while for negative polarity the discharge current was found to be approximately constant. The results presented in Figure 13 shows that the delay between impulses and conditioning effect of the needle had no effect on the average discharge current.

5.3.3 Light emission measurement

Figure 14 shows the amplitude of the signal from the photomultiplier tube (pmt) versus the applied voltage. Signal increase vs time and signal duration behaved similarly for the charge recordings and for the pmt recordings for both phases and both polarities.

In liquid phase the delay between impulses does not have a clear influence on the emitted light. For non-virgin frozen samples the light emission signals corresponding to partial discharges tend to be very large, as for the charge recordings, resulting in a graph corresponding to Figure 11.

5.3.4 Shape of streamer recordings, comparison with cyclohexane

Typical charge recordings for positive polarity in liquid phase with the corresponding signal from the photomultiplier are shown in Figure 15. Compared with cyclohexane the charge injection is more stepwise in n-tridecane. Averaged over the propagation time the average streamer current for comparable discharges are approximately the same in the two liquids, but discharges occurs at much lower voltages in cyclohexane. Discharges in n-tridecane emit much more light than comparable discharges in cyclohexane. Most charge and light recordings show a combination of two phenomena: A constant increase of charge during the discharge superimposed with steps in the charge recordings. For cyclohexane only the approximately constant increase in charge versus time is seen.

6 DISCUSSION

6.1 PRE-INCEPTION CURRENTS

The pre-inception current can be explained by one or a combination of the following:

- Increased bulk conductivity in the high-field region [1, 13].
- Charge injection from the electrode by field ionization/field emission at the electrode-dielectric boundary [1].
- Micro-discharges/electron avalanches and subsequent drift of the charge [13, 52].
- Electrohydrodynamic motion (for liquid) [53]

It is generally hard to separate between these effects. Careful examination of the effect of polarity and voltage can give some insight into the possible mechanisms. In

addition, FEM simulations can be a way to indicate likely mechanisms.

6.1.1 Liquid cyclohexane

Measurements of current density versus applied voltage in solutions of triisomyllammonium picrate in cyclohexane obtained using a homogeneous field have been presented (planar electrodes with 0.25 mm distance between the electrodes) [54]. These results are compared to FEM simulations in Figure 16. Thermal and electrical properties for cyclohexane are obtained from [43]. The following conductivity model, based on a classical Poole-Frenkel model was used:

$$\sigma(E) = 1.3 \cdot 10^{-4} \cdot e^{\frac{-5454 + 0.33 \cdot \sqrt{E}}{T}} \quad (2)$$

The temperature dependence is taken from [55] where the activation energy for conductivity in cyclohexane at low fields was obtained. Equation (2) is very close to the theoretical Poole-Frenkel equation based on the low-field conductivity for the electrolyte given by equation (3).

$$\sigma(E) = 2.9 \cdot 10^{-4} \cdot e^{\frac{-5454 + 0.3 \cdot \sqrt{E}}{T}} \quad (3)$$

Comparing the two equations, the low-field conductivity deviates by a factor of two, which could be caused by electrohydrodynamic motion increasing the mobility of the ions.

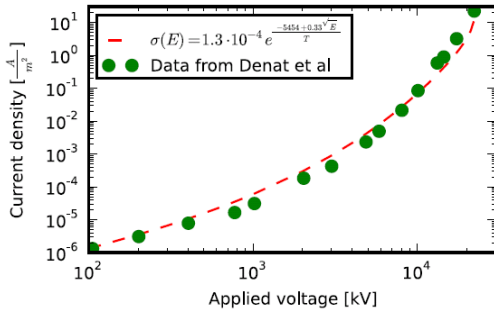


Figure 16. Comparison of stationary injection current density in a solution of triisomyllammonium picrate in cyclohexane ($7 \cdot 10^{-4}$ M) with FEM simulations with a conductivity given by equation (2). Data were obtained from fig. 1 in [52].

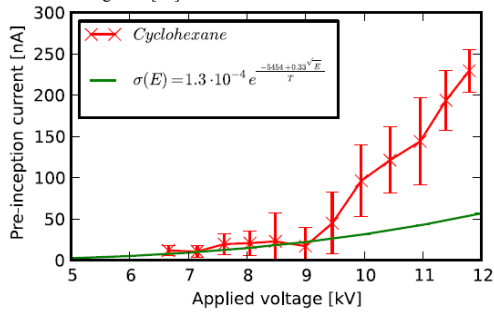


Figure 17. Comparison of measured pre-inception currents in cyclohexane at room temperature and positive polarity with FEM simulations with a similar geometry and conductivity given by equation (2).

The conductivity given in equation (2) gives an SCLF of 285 MV/m, at 10 MHz and 300 K, which is approximately the field at which pre-inception currents in pure cyclohexane with point-plane geometry is observed. Based on this, a simulation with geometry similar to that of our experiments was performed with the conductivity given in (2). This resulted in a good fit for the results obtained up to voltages of 9 kV where the pre-inception currents increase rapidly in cyclohexane (Figure 17). The field dependence of the current thus indicates that Poole-Frenkel conductivity is responsible for the current observed up to around 9 kV. As noted in section 2.3.1 there are several high-field conduction models that predicts the same field dependence as the Poole-Frenkel model. Above 9 kV, the current can no longer be explained by the field dependence predicted by these models.

The low-field conductivity obtained from (2) is too high for low fields. It has previously been reported that no clear correlation exists between low-field conductivity and the pre-inception current observed in liquid cyclohexane [52].

The difficulty in fitting the pre-inception currents in cyclohexane to known high field conduction mechanism above 9 kV could mean that the currents are results of not fully developed avalanches in the liquid phase and subsequent drift of the charge [52]. It has been suggested that a field of at least 200 MV/m over a sufficient path is needed for electron avalanches to occur in liquid cyclohexane [4]. This is below the SCLF for cyclohexane, and thus the SCLF region, which will increase with increased applied voltage, will give ideal conditions for electron avalanches.

The Poole-Frenkel mechanisms do not depend on the polarity of the needle, and thus similar currents should be measured for both polarities. For voltages below the inception voltage the recorded pre-inception currents with negative polarity in cyclohexane is in the same range as those recorded at the same voltages with positive polarity [9]. Negative streamers have lower inception voltage than positive streamers in cyclohexane, and at 9 kV the inception probability for negative streamers reaches 100 %. Thus the increase in pre-inception current for positive polarity at around 9 kV can not be observed for negative polarity.

6.1.2 Liquid n-tridecane

For n-tridecane currents are observed at low fields, while for cyclohexane a threshold voltage of 5-6 kV is needed for a measurable current (Figure 4). Comparison of the pre-inception currents in liquid n-tridecane with positive polarity with a FEM simulation using the following equations for conductivity,

$$\sigma(E) = 1.0 \cdot 10^{-12} \cdot e^{0.0015 \sqrt{E}} \quad (4)$$

$$\sigma(E) = 1.0 \cdot 10^{-12} \cdot e^{0.03 \sqrt[3]{E}} \quad (5)$$

is shown in Figure 18. Equation (4) corresponds to an SCLF of approximately 160 MV/m, and equation (5) gives

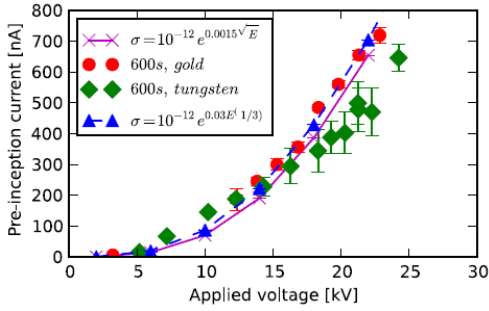


Figure 18. Comparison between measured average pre-inception currents and simulated current for liquid n-tridecane with positive polarity.

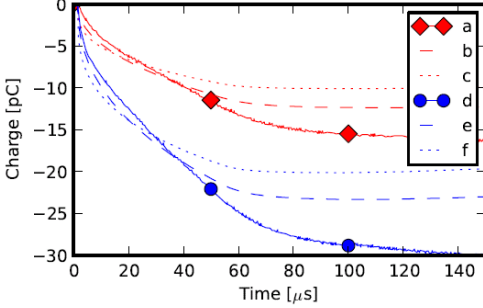


Figure 19. Comparison of recorded charge injection and simulated charge injection for positive polarity. (a) Charge recording at 14 kV, (b) simulation based on equation (5), (c) simulation based on equation (4), (d) charge recording at 18 kV, (e) simulation based on equation (5), (f) simulation based on equation (4).

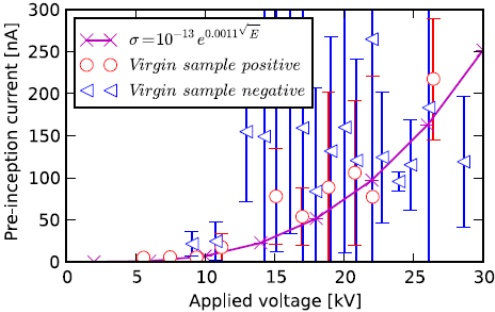


Figure 20. Comparison between measured average pre-inception currents and simulated current based on standard Poole-Frenkel theory for frozen virgin samples of n-tridecane with both polarities.

an SCLF of approximately 255 MV/m at 10 MHz. Equation (4) is similar to Poole-Frenkel conductivity, but the constant in the exponential is somewhat high, since classical Poole-Frenkel theory gives $\sigma_0 \exp(0.0011\sqrt{E})$ at room temperature. Equation (5) is not based on any known conductivity theory, but similar field dependence for the conductivity has previously been reported for polyethylene [56]. The magnitude of the SCLF is also in good agreement with what has been measured in XLPE [40]. The simulations based on the two formulas have been compared to charge recordings in Figure 19. Equation (5) fits the measured results better than equation (4), but for the last part of the charge recording the fit is rather poor. Again,

this could be due to electrohydrodynamic motion resulting in increased ion mobility. Both equations give a lower SCLF than what was measured for cyclohexane which corresponds to the lower voltages needed for pre-inception currents to occur in n-tridecane compared with cyclohexane. The low voltage at which the first current is recorded in n-tridecane indicates that the SCLF in the liquid is probably closer to 160 MV/m than 255 MV/m.

The reason for the differences in high-field conductivity observed for n-tridecane and cyclohexane is still unknown. Density functional theory (DFT) calculations have been performed looking at the first excited states and ionization potential for both n-tridecane and cyclohexane as a function of field. The main difference between n-tridecane and cyclohexane is in the way the first excited state is influenced by an electric field. In cyclohexane the first excited state stays constant at moderate electric fields while in n-tridecane it decreases with increased field. This decrease in excitation energy could explain why n-tridecane has a higher conductivity at lower fields than cyclohexane. It could also be the reason why the field dependence of high-field conductivity in n-tridecane deviates from the field dependence predicted by Poole-Frenkel theory. This will be the topic of a separate paper where the field dependence of the conductivity in materials consisting of relatively simple molecules is discussed based on quantum chemical calculations [57].

For negative polarity, small steps in the measured charge have been observed for high fields, which could be interpreted as very small discharges. The increased current measured with a wolfram point compared to a gold point under negative polarity (Figure 4b), is believed to be caused by an emission point/protrusion on the electrode surface, rather than by the change in material (since the difference in work function is small). The main effect of the gold-coating is to create a smoother and more uniform surface.

6.1.3 Frozen n-tridecane

The experimental results obtained in frozen n-tridecane are compared to simulations in Figure 20. A Poole-Frenkel conductivity mechanism was used in the simulations:

$$\sigma(E) = 1.0 \cdot 10^{-13} \cdot e^{0.0011 \cdot \sqrt{E}} \quad (6)$$

The constant in the exponential can be obtained directly from classical Poole-Frenkel theory and is only dependent on the permittivity of the medium and the temperature [1, 35].

The increased scatter in the results for negative polarity compared with positive polarity is of unknown origin. The conductivity model used in the simulations is only dependent on the bulk properties of the material, but the difference for positive and negative polarity must be caused by the electrode. Effects of emissive spots where field emission of electrons from a negative electrode have previously been found in vacuum [58]. In liquids a similar effect is believed to be responsible for the "surface effect"

(i.e. the lowering of the apparent inception field for streamers with increased point radius) [59]. The increased scatter for negative polarity could thus be caused by emission of electrons from the negative electrode. However, like for gold electrodes in liquid n-tridecane the magnitude of the recorded currents are comparable under both polarities in frozen n-tridecane. This indicates that the SCLF is approximately independent of polarity, as has previously been reported to be the case for XLPE [40].

In liquid n-tridecane the currents are 2-3 times larger than for frozen virgin n-tridecane (Figure 4). The lower current recorded in solid phase can be explained by the reduced conductivity in crystalline regions, and the reduced ion mobility compared with liquid phase. In some cases the recorded charge is of the same magnitude as for the liquid phase, while in other cases the recorded charge is at the threshold of the experimental sensitivity, the scatter of the recordings are larger for frozen phase. This indicates that the material is not homogeneous on the micrometer scale, and that the SCLF depends on the morphology in the vicinity of the needle electrode, as has been shown to be the case for polyethylene [60].

Figure 6b shows that the inception voltage for light emission is the same in liquid and solid n-tridecane. A clear correlation between luminescence and the SCLF has previously been found for polymers [61]. The light emission measurements thus indicate that the SCLF should be about the same in liquid and solid n-tridecane. However, the comparison of measured average pre-inception currents in solid phase and liquid phase indicates a higher SCLF in the frozen phase. One possible interpretation of this is that the SCLF in the amorphous parts of the solid is similar to the SCLF in the liquid, thus the current flows in the amorphous regions and the light is emitted from these regions.

6.1.4 Influence of delay between impulses

An extensive study to look at the influence of delay between impulses was conducted with positive polarity. This was done to see how residual space-charge would influence the pre-breakdown phenomena. The results for liquid n-tridecane was, nevertheless, hard to interpret due to the polymer layer being deposited on the needle electrode. The general picture seems to be that the delay between impulses mainly influenced the pre-inception currents in frozen n-tridecane as shown in Figure 4c (the effects seen in liquid can be accounted for by the polymer coating).

The current recorded with 1500 s between impulses in frozen n-tridecane with positive polarity were found to increase with applied voltage. For shorter delays between impulses the current was found to increase with increasing voltage up to a maximum at which point further increase of the applied voltage resulted in a decrease in average current (Figure 4c). This is most likely caused by residual injected homo space-charge in the material effectively screening the high field region.

The average currents recorded with 1500 s between

impulses are of similar magnitude as what was recorded in the liquid. One can assume that the continued stressing of the material with high field strengths will break up the structure of the material and reduce the long-range order and introduce local defects as have been reported for polyethylene and silicone rubber [18, 50]. The increased current is most likely caused by a combination of the reduced crystallinity, increased crack and void formation, and the creation of donors/traps in the material as a result of the cumulative degradation.

6.2 INCEPTION

6.2.1 Liquid phase, negative polarity

One hypothesis is that the inception of negative streamers in cyclohexane is caused by an avalanche in the liquid phase followed by discharges in a low density region created by the avalanche [7]. The SCLF in cyclohexane (280 MV/m) is larger than the minimum field where avalanches in the liquid phase are believed to be plausible (fields stronger than 200 MV/m in liquid cyclohexane and pentane [4]). Thus as the voltage is increased the SCLF region will be ideal for electron avalanches (region of nearly constant field with field strength above the threshold for avalanches in the liquid phase.) The value of the SCLF in cyclohexane therefore supports the hypothesis that the onset of negative streamers in cyclohexane is the result of an electron avalanche in the liquid phase.

Inception of negative streamers in n-tridecane occurs at much higher voltages than in cyclohexane (inception voltage in n-tridecane is approximately 20 kV (Figure 6), in cyclohexane it is approximately 7 kV [9]). This can be explained by the lower SCLF in n-tridecane that effectively reduces the electric field to a value below the necessary field for electron avalanches to occur in liquid n-tridecane. The onset of streamers in n-tridecane is thus probably caused by an avalanche in a low density/vaporized region created by the large energy dissipation ($\sigma(E) \cdot E^2$) in the high-field region.

Based on the observed difference in inception voltage for n-tridecane and cyclohexane, the difference in SCLF for the two liquids and the field required for electron avalanche formation in the liquid, different inception mechanisms are proposed for negative streamers in liquids:

If the SCLF is above the necessary field for avalanche formation, as our results indicate for cyclohexane, the following mechanism is proposed:

- An avalanche occurs in the liquid phase.
- A bubble is created by the avalanche
- Discharges in the vaporized region can lead to further growth of the streamer.

This is similar to the hypothesis usually used to explain negative streamer inception in cyclohexane [7], but the influence of the SCLF has not been included in this hypothesis before.

For liquids with an SCLF below the necessary field for avalanche formation in liquid phase (i.e. n-tridecane) the

following inception mechanism is proposed:

- Local joule heating creates a region with low density liquid or a bubble.
- In the low density region/bubble the mean free path of electrons will increase, thus avalanches can occur in this region at a field below the field needed for electron avalanches in liquid phase at normal density.
- Discharges in the low density region/bubble can lead to further growth of the streamer.

Since the electrical discharge/avalanche occurs in a low density region for this hypothesis it can be tested by increasing the hydrostatic pressure.

6.2.2 Liquid phase, positive polarity

Inception of positive streamers in liquid cyclohexane is believed to be caused by discharges in a low density region. The SCLF for cyclohexane is higher than the necessary field for electron avalanches in liquid cyclohexane, making electron avalanches in the liquid phase possible. For an avalanche to form a seed electron in a location that is far enough from the electrode to give the necessary path length, and close enough to be in a region with a field above the necessary field for electron avalanches is needed. For negative polarity such seed electrons can be taken from the negative electrode, where they will be ideally located to create large avalanches (long path with high electric field). For positive polarity such electrons can be created anywhere in the high-field region (by field ionization, cosmic radiation, thermal excitation etc.) and the avalanches will be terminated when the electrons reach the positive electrode. As a result of this most avalanches will start too close to the electrode, and therefore not have enough energy to vaporize the liquid. As the voltage is increased the high-field region also increases and larger/more avalanches can occur since the volume where seed electrons can create avalanches will increase. The energy dissipation in the high-field region as a result of these micro-discharges can form a low density region/bubble where larger discharges/avalanches can occur resulting in streamer inception. The creation of seed electrons in the liquid is highly stochastic, which can explain why the transition of streamer inception probability from 0 to 100 is slower for positive polarity than for negative polarity where the inception mechanism is more deterministic (transition occurs over a small voltage range) [9].

Positive streamers in liquid n-tridecane are observed at somewhat higher voltages than negative streamers, but besides this slight shift in inception voltage the onset occurs over a similar voltage range (Figure 6). We propose that the same mechanism is responsible for negative and positive streamer inception in n-tridecane. The lower inception voltage for negative polarity can be caused by the availability of electrons from the negative electrode. These electrons are probably the reason for the higher currents

recorded under negative polarity as seen in Figure 4 (giving a higher energy dissipation), and they will also be available as seed electrons to create electron avalanches in the low density region.

6.2.3 Solid phase, virgin n-tridecane samples

Comparing inception probabilities in frozen and liquid n-tridecane shows a great similarity between the two phases (Figure 6). We believe that this indicates that the same mechanism is responsible for inception of partial discharges in the two phases. No clear influence of polarity were found for frozen n-tridecane, which is in good agreement with results obtained in XLPE [40, 62]

The amorphous regions are the weakest both mechanically and electrically, and will be where most of the pre-inception current flows (there is a barrier of approximately 0.6 eV that electrons need to ascend to enter crystalline regions [10]). Thus inception is likely to be initiated in amorphous regions at or very close to the needle electrode. In polymers the inception and propagation of electrical trees have been found to primarily occur in amorphous regions [1, 62]. Formation of a low density region will in this case require a phase transition from solid to gas/low density liquid, and thus more energy than needed for liquid phase is required. The pre-inception recordings indicate that the SCLF is higher for frozen phase than for liquid phase. Thus in the high-field region the power dissipation will be even greater than for liquid n-tridecane, but in a smaller region. However, the charge recordings will depend on the average morphology at the needle surface, and the SCLF in the amorphous region could be close to the one found for liquid phase. It should also be noted that the boiling point for n-tridecane is high (234°C), and the energy required to reach the boiling point is large compared with the extra energy required for the phase transition from solid to liquid phase, this can explain the similarity between the two phases.

6.3 PROPAGATION

6.3.1 Liquid phase

Charge recordings for positive streamers in cyclohexane have the same main feature as charge recordings in n-tridecane, see Figure 15. For both liquids the main feature is a nearly linear increase in charge during the period of streamer growth. For n-tridecane some small steps in the charge recordings were observed. The main characteristic of the streamer charge recordings for both liquids corresponds well to what has been reported for 1st mode positive streamers [26]. The observed steps in the charge recordings for n-tridecane indicate that the streamers in n-tridecane are a mixture of 1st and 2nd mode streamers. The transition to 2nd mode streamers is typically seen in the charge recordings by a clear increase in the average streamer current with increased voltage [52]. No such change was observed for n-tridecane (Figure 12). It is known that the observation of 1st mode streamers requires a sharp tip ($r_p < 6 \mu\text{m}$ in cyclohexane) that gives a large

enough field for inception at voltages below the "propagation voltage" for the liquid [26]. The propagation voltage is the threshold voltage for 2nd mode streamer propagation and depends on the liquid and the distance between the needle electrode and the plane but is independent of the point radius [26]. The fact that we observe 1st mode streamers in n-tridecane means that the radius of the needle electrode, 2 μm , is below the critical radius for n-tridecane. We also observe what we interpret as the start of a transition to 2nd mode streamers indicating that the propagation voltage in n-tridecane for our geometry is around 25-30 kV.

Negative streamers in n-tridecane are clearly of 1st mode, no transition to 2nd mode was observed. The streamer current was found to be almost constant over the entire voltage range (15-30 kV). The charge recordings obtained with negative polarity are similar to the ones obtained with positive polarity with more steps in the recordings.

6.3.2 Solid phase

The charge obtained with virgin n-tridecane (melted between each applied impulse) falls within the same range as for liquid n-tridecane for both positive and negative polarity (Figure 10). The charge recordings also shows the same characteristic (quasilinear increase of charge with some steps), and the average streamer currents falls within the same range for both phases and both polarities (Figure 12). The relatively small effect of the phase transition makes it reasonable to assume that the propagation mechanism for streamers and electrical trees under transient voltage are similar. Most likely the structure grows in the weak "liquid-like" amorphous regions of the solid, as reported for polymers [1, 18]. Thus once propagation starts the electrical tree will choose the path of least resistance along the amorphous regions, and create structures similar to those observed in liquid phase. This indicates that for instantaneous ageing the amorphous region is the most important, as it constitutes the weak part of the material, and the liquid and solid phases show similar behaviour.

When frozen n-tridecane was stressed by several consecutive impulses the discharges were found to be large even for low applied voltages. The cumulative degradation of the system degrades the high-field region, leading to a weak region where electrical trees can grow, thus lowering the inception voltage. This has previously been reported for polymers stressed by ac voltage, where a degradation zone at the needle electrode has been reported [18]. The large discharges in the degradation zone could be caused by the formation of voids and cracks in the high field region giving the discharges the characteristics of discharges in gas/voids.

7 CONCLUSION

The main result obtained in this study is the clear correlation between inception and propagation of streamers

and electrical trees in the liquid and frozen phases for n-tridecane. Based on this it is proposed that the inception and propagation in the frozen phase occur in an amorphous region.

An SCLF of approximately 160 MV/m was found for tridecane based on the recorded pre-inception currents. This value is low compared to the one obtained for cyclohexane (280 MV/m), and may explain the large difference in inception voltage for the two liquids. In cyclohexane the SCLF is large enough to facilitate electron avalanches in the liquid, while the lower obtainable fields in n-tridecane makes avalanche formation in the liquid phase unlikely. If this is the case then discharges in n-tridecane requires a low density liquid or gas region which is created by other means than electron avalanches in the liquid. One likely way of creating such a low density region is by local joule heating.

Comparison between our results in n-tridecane and results obtained by others using polyethylene show similar values for the SCLF and the field required for inception of electrical trees. The similarity between positive and negative polarity is also similar to results obtained in polyethylene. The similar electronic properties of n-tridecane and polyethylene make n-tridecane a good choice as a simple model system for polyethylene.

ACKNOWLEDGMENT

Support from the Norwegian Research Council through a Strategic Industry Program (164603/130) is acknowledged.

REFERENCES

- [1] L. A. Dissado and J. C. Fothergill. "Electrical Degradation and Breakdown in Polymers." Material and Devices Series 9. The Institution of Engineering and Technology, London, United Kingdom, 1992.
- [2] M. Goldman and R. S. Sigmond. "Corona and insulation." IEEE Trans. Elect. Insul., EI-17:90-105, 1982.
- [3] R. S. Sigmond. "The residual streamer channel: Return strokes and secondary streamers." J. Appl. Phys., 56:1355-1370, 1984.
- [4] M. Haidara and A. Denat. "Electron multiplication in liquid cyclohexane and propane." IEEE Trans. Elect. Insul., 26:592-597, 1991.
- [5] E.O. Forster. "Electrical breakdown in liquid hydrocarbons." J. Electrostat., 12:1-12, 1982.
- [6] W. G. Chadband. "On variations in the propagation of positive discharges between transformer oil and silicone fluids." J. Phys. D: Appl. Phys., 13:1299-307, 1980.
- [7] L. Dumitrescu, O. Lesaint, N. Bonifaci, A. Denat, and P. Notinger. "Study of streamer inception in cyclohexane with a sensitive charge measurement technique under impulse voltage." J. Electrostat., 53:135-146, 2001.
- [8] A. Denat, J. P. Gosse, and B. Gosse. "Electrical conduction of purified cyclohexane in a divergent electric field." IEEE Trans. Elect. Insul., 23:545-554, 1988.
- [9] Ø. L. Hestad, L. E. Lundgaard, and D. Linhjell. "New experimental system for the study of the effect of temperature and liquid to solid transition on streamers in dielectric liquids: Application to cyclohexane." IEEE Trans. Dielect. Elect. Insul., 17:767-777, 2010.
- [10] G. Teyssedre and C. Laurent. "Charge transport modeling in insulating polymers: from molecular to macroscopic scale." IEEE Trans. Dielect. Elect. Insul., 12:857-875, 2005.

- [11] G. Ungar and X. Zeng. "Learning polymer crystallization with the aid of linear, branched and cyclic model compounds." *Chem. Rev.*, 101:4157–4188, 2001.
- [12] R. Tobazeon. "Prebreakdown phenomena in dielectric liquids." *IEEE Trans. Dielect. Elect. Insul.*, 1:1132–1147, 1994.
- [13] A. Denat. "High field conduction and prebreakdown phenomena in dielectric liquids." *IEEE Trans. Dielect. Elect. Insul.*, 13:518–525, 2006.
- [14] A. Beroual, M. Zahn, A. Badent, K. Kist, A. J. Schwabe, H. Yamashita, K. Yamazawa, M. Danikas, W. D. Chadband, and Y. Torshin. "Propagation and structure of streamers in liquid dielectrics." *IEEE Electric. Insul. Mag.*, 14:6–17, 1998.
- [15] L. A. Dissado. "Understanding electrical trees in solids: from experiment to theory." *IEEE Trans. Dielect. Elect. Insul.*, 9:483–497, 2002.
- [16] N. Shimizu and C. Laurent. "Electrical tree initiation." *IEEE Trans. Dielect. Elect. Insul.*, 5:651–659, 1998.
- [17] J. C. Devins, S. J. Rzed, and R. J. Schwabe. "Breakdown and prebreakdown phenomena in liquids." *J. Appl. Phys.*, 52:4531–4545, 1981.
- [18] K. Uchida and N. Shimizu. "The effect of temperature and voltage on polymer chain scission in high-field region." *IEEE Trans. Elect. Insul.*, 26:271–277, 1991.
- [19] A. S. Vaughan, I. L. Hosier, S. J. Dodd, and S. J. Sutton. "On the structure and chemistry of electrical trees in polyethylene." *J. Phys. D: Appl. Phys.*, 39:962–978, 2006.
- [20] A. Denat, N. Bonifaci, and M. Nur. "Spectral analysis of the light emitted by streamers in hydrocarbon liquids." *IEEE Trans. Dielect. Elect. Insul.*, 5:382–387, 1998.
- [21] K. Tavernier, B. R. Varlow, and D. W. Auckland. "Electrical tree modelling in non-linear insulation." In *Ann. Rep. Conf. Elec. Insul. Diel. Phen. (CEIDP)*, pages 661–664 vol. 2, 1998.
- [22] T. Aka-Ngnui and A. Beroual. "Modelling of multi-channel streamers propagation in liquid dielectrics using the computation electrical network." *J. Phys. D: Appl. Phys.*, 34:794, 2001.
- [23] F. M. O'Sullivan. "A Model for the Initiation and Propagation of Electrical Streamers in Transformer Oil and Transformer Oil based Nanofluids." PhD thesis, MIT, Cambridge, MA, USA, 2007.
- [24] M. Kim, R. E. Hebner, and G. A. Hallock. "Modeling the growth of streamers during liquid breakdown." *IEEE Trans. Dielect. Elect. Insul.*, 15:547–553, 2008.
- [25] A. L. Kupershtokh and D. I. Karpov. "Models of pulse conductivity of streamers propagating in dielectric liquid." In *Proc. IEEE Int. Conf. Diel. Liq. (ICDL)*, pages 87–90, 2005.
- [26] P. Gournay and O. Lesaint. "A study of the inception of positive streamers in cyclohexane and pentane." *J. Phys. D: Appl. Phys.*, 26:1966–74, 1993.
- [27] O. Lesaint and G. Massala. "Positive streamer propagation in large oil gaps: experimental characterization of propagation modes." *IEEE Trans. Dielect. Elect. Insul.*, 5:360–370, 1998.
- [28] L. Lundgaard, D. Linhjell, G. Berg, and S. Sigmond. "Propagation of positive and negative streamers in oil with and without pressboard interfaces." *IEEE Trans. Dielect. Elect. Insul.*, 5:388–395, 1998.
- [29] R. Kattan, A. Denat, and O. Lesaint. "Generation, growth, and collapse of vapor bubbles in hydrocarbon liquids under a high divergent electric field." *J. Appl. Phys.*, 66:4062–4066, 1989.
- [30] T. J. Lewis. "A new model for the primary process of electrical breakdown in liquids." *IEEE Trans. Dielect. Elect. Insul.*, 5:306–315, 1998.
- [31] H. Sueda and K. C. Kao. "Prebreakdown phenomena in high-viscosity dielectric liquids." *IEEE Trans. Elect. Insul.*, EI-17:221–227, 1982.
- [32] H. M. Jones and E. E. Kunhardt. "Development of pulsed dielectric breakdown in liquids." *J. Phys. D: Appl. Phys.*, 28:178–188, 1995.
- [33] C. Laurent, C. Mayoux, and S. Noel. "Dielectric breakdown of polyethylene in divergent field: Role of dissolved gases and electroluminescence." *J. Appl. Phys.*, 54:1532–1539, 1983.
- [34] J. P. Jones, J. P. Llewellyn, and T. J. Lewis. "The contribution of field-induced morphological change to the electrical aging and breakdown of polyethylene." *IEEE Trans. Dielect. Elect. Insul.*, 12:951–966, 2005.
- [35] V. Adamec and J. H. Calderwood. "Electrical conduction in dielectrics at high fields." *J. Phys. D: Appl. Phys.*, 8:551–560, 1975.
- [36] A.K. Jonscher. "Electronic properties of amorphous dielectric films. *Thin Solid Films*", 1:213–234, 1967.
- [37] H.J. Wintle. "Charge motion and trapping in insulators: surface and bulk effects." *IEEE Trans. Dielect. Elect. Insul.*, 6:1–10, 1999.
- [38] D. M. Pai. "Electric-field-enhanced conductivity in solids" *J. Appl. Phys.*, 46:5122–5126, 1975.
- [39] Y. N. Garstein and E. M. Conwell. "High-field hopping mobility in molecular systems with spatially correlated energetic disorder" *Chemical Physics Letters*, 245:351–358, 1995.
- [40] S. Boggs. "Very high field phenomena in dielectrics." *IEEE Trans. Dielect. Elect. Insul.*, 12:929–938, 2005.
- [41] K. Iida, J. S. Kim, S. Nakamura, and G. Sawa. "Effects of molecular structure on electrical conduction in low-density polyethylene above its melting point." *IEEE Trans. Elect. Insul.*, 27:391–398, 1992.
- [42] H. R. Zeller and W. R. Schneider. "Electrofracture mechanics of dielectric aging." *J. Appl. Phys.*, 56:455–459, 1984.
- [43] "Handbook on Chemistry and Physics." CRC Press, 84th edition, 2004.
- [44] K. Shigematsu, Y. Saito, K. Saito, and Y. Takahashi. "Pressure effect on the solid-liquid equilibrium forms of odd normal alkanes." *J. Cryst. Growth*, 310:4681–4684, 2008.
- [45] G. Ungar. "Structure of rotator phases in n-alkanes." *J. Phys. Chem.*, 87:689–695, 1983.
- [46] E. B. Sirota, Jr. H. E. King, D. M. Singer, and H. H. Shao. "Rotator phases of the normal alkanes: An x-ray scattering study." *J. Chem. Phys.*, 98:5809–5824, 1993.
- [47] S. Y. Chazhengina, E. N. Kotelnikova, I. V. Filippova, and S. K. Filatov. "Phase transitions of n-alkanes as rotator crystals." *J. Mol. Struct.*, 647:243–257, 2003.
- [48] M. J. Nowak and S. J. Severson. "Dynamic mechanical spectroscopy of plastic crystalline states in n-alkane systems." *J. Mat. Sci.*, 36:4159–4166, 2001.
- [49] Comsol Multiphysics® ver. 3.5a with AC/DC module. Comsol AB. Regnergatan 23. SE-111 40 Stockholm. Sweden. www.comsol.com.
- [50] Y. X. Zhou, Q. Nie, Z. Z. Chen, and R. Liu. "Analysis of electrical tree ageing in silicone rubber by physicochemical approach." *J. Phys. Conf. Ser.*, 183:012013–, 2009.
- [51] N. Shimizu, K. Uchida, and S. Rasikawan. "Electrical tree and deteriorated region in polyethylene." *IEEE Trans. Dielect. Elect. Insul.*, 27:513–518, 1992.
- [52] S. Ingebrigtsen, L. E. Lundgaard, and P.-O. Åstrand. "Effects of additives on prebreakdown phenomena in liquid cyclohexane: I. streamer initiation." *J. Phys. D: Appl. Phys.*, 40:5161–5169, 2007.
- [53] R. Tobazeon. "Electrohydrodynamic instabilities and electroconvection in the transient and a.c. regime of unipolar injection in insulating liquids: A review." *J. Electrostat.*, 15:359–384, 1984.
- [54] A. Denat, B. Gosse, and J. P. Gosse. "High field dc and ac conductivity of electrolyte solutions in hydrocarbons." *J. Electrostat.*, 11:179–194, 1982.
- [55] H. Polak and B. Jachym. "Mobility of excess charge carriers in liquid and solid cyclohexane." *J. Phys. C: Solid State Phys.*, 10:3811–3818, 1977.
- [56] G. Jiang, J. Kuang, and S. Boggs. "Evaluation of high field conduction models of polymeric dielectrics." In *Ann. Rep. Conf. Elec. Insul. Diel. Phen. (CEIDP)*, 2000.
- [57] H. S. Smalø, Ø. L. Hestad, S. Ingebrigtsen, and P.-O. Åstrand. "Ionization potential of molecules in an electric field." Submitted.
- [58] R. V. Latham. "A new perspective on the origin of prebreakdown electron emission processes." *IEEE Trans. Elect. Insul.*, 23:9–16, 1988.
- [59] P. Biller. "A simple qualitative model for the different types of streamers in dielectric liquids." In *Proc. IEEE Int. Conf. Diel. Liq. (ICDL)*, 1996.
- [60] G. Jiang, J. Kuang, and S. Boggs. "Critical parameters for electrical tree formation in xlpe." *IEEE Trans. Power Deliv.*, 13:292–296, 1998.
- [61] Y. Cao and S. Boggs. "Electroluminescence based determination of the space charge limited field." In *Ann. Rep. Conf. Elec. Insul. Diel. Phen. (CEIDP)*, pages 236–240, 2001.

- [62] R Sarathi and K Sridhar. "Investigation in to growth of electrical trees in xlpe cables under transient voltages." IEEE ICSD, pages 329–332, 1998.



Øystein L. Hestad was born in Mo I Rana, Norway in 1978. He received the M.Sc. degree in physics at the Norwegian university of science and technology in 2003. From 2003 to 2006 he worked at SINTEF Energy Research. He is presently pursuing his Ph.D. in physical chemistry at the Norwegian University of Science and Technology.



Per-Olof Åstrand, was born in Sättila, Sweden in 1965. He is Professor in theoretical chemistry at the Department of Chemistry, Norwegian University of Science and Technology, Trondheim, Norway. He received the Ph.D. degree at the University of Lund in 1995 with Prof. Gunnar Karlström as the thesis supervisor, and he spent seven years in Denmark at Aarhus University, University of Copenhagen and Risø National Laboratory before he moved to Norway in 2002. His research interests include the construction of molecular mechanics models for intermolecular forces, reactive force fields and optical properties, with applications in optics, nanoscience, catalysis and electrical breakdown of dielectric liquids.



Lars E. Lundgaard was born in Copenhagen, Denmark on 24 May 1952. He took his M.Sc in power electric engineering at The Norwegian Institute of Technology in 1976. Since 1980 he has worked with SINTEF Energy Research. He is working on material science for electric power apparatus, relating to design, diagnostics and maintenance. He is also working on electro-separation of water-oil emulsions. His main experiences are in the field of GIS and transformer insulation. He is active within SC D1 in CIGRÉ.

Paper 3

Effects of N,N-dimethylaniline and trichloroethene on prebreakdown phenomena in liquid and solid n-tridecane

Ø. L. Hestad, S. Ingebrigtsen, H. S. Smalø, P.-O. Åstrand and
L. E. Lundgaard

Submitted to the *IEEE Trans. Dielect. Elect. Insul.*, 2010

Effects of N,N-dimethylaniline and trichloroethene on prebreakdown phenomena in liquid and solid n-tridecane

Ø. L. Hestad, H. S. Smalø, P.-O. Åstrand

Department of Chemistry
Norwegian University of Science and Technology (NTNU)
7491 Trondheim, Norway

S. Ingebrigtsen and L. E. Lundgaard

Department of Electric Power Technology
SINTEF Energy Research
7465 Trondheim, Norway

ABSTRACT

Prebreakdown phenomena in 0.1 M N,N-dimethylaniline (DMA) and 0.1 M trichloroethene (TCE) in n-tridecane have been investigated experimentally in liquid and solid phases in a needle-plane geometry with impulse voltage. Light emission and charge injection from the high-field electrode were measured. Results have been compared with results obtained in neat n-tridecane and in cyclohexane with the same additives. Adding TCE to n-tridecane increase the pre-inception current and reduce the inception voltage for negative and positive polarity. The increase in pre-inception current is probably caused by trap assisted conduction, and may be responsible for the decrease in inception voltage. TCE had no effect on propagation of streamers in n-tridecane. The main effect of DMA in n-tridecane is to enhance the propagation of streamers and electrical trees with positive polarity. This is in line with what has been reported for cyclohexane, and is explained by the low ionization potential of DMA. Charge injection for negative streamers is reduced by the addition of DMA in n-tridecane, while the emitted light is increased. This indicates that some of the energy otherwise used for propagation is emitted as light. A low electronic excitation energy for DMA at 2.4 eV supports this hypothesis. The additives have the same effect on prebreakdown phenomena in solid and liquid phases with positive polarity, and thus the same mechanism is suggested to be responsible for electrical treeing and streamer inception and propagation. The scatter is generally found to increase when going from liquid to solid phase, which is explained by the inhomogeneity in the solid phase. The transition to solid phase with negative polarity typically results in an even larger scatter than for positive polarity. The effect of additives seems to be secondary to the morphology at the point electrode with negative polarity.

Index Terms — Prebreakdown phenomena, streamer, electrical tree, additives, phase transition.

1 INTRODUCTION

Modern society depends upon reliable high-voltage insulation. Electrical degradation and breakdown of gas, liquid, and solid-state insulators have been studied extensively during the last decades [1-3]. Each study has typically been focused on one of the phases because of the physical differences between the phases, and three separate research branches have thus developed. Even so, the well-known discharges in gas phase

have typically been the foundation for proposed mechanisms in the condensed phases [4], and it has been shown that pre-breakdown and breakdown phenomena in a series of dielectric liquids and polyethylene are similar [5-7]. Occasionally all three phases have been linked based on the many similarities for pre-breakdown phenomena regardless of phase [8].

Pre-breakdown phenomena are observed in condensed phases at voltages below the breakdown voltage. In liquids the electrical stress creates a low density region, a streamer, observable by shadowgraphic techniques [3,9-12]. A similar process occurs in solids where a permanent structure, an electrical tree, is created [2,7]. In both phases the structures have a low dielectric strength

compared with that of the bulk insulation material. When such a structure bridges the entire gap between the electrodes, it typically induces a breakdown. The properties of streamers and electrical trees depend on a series of external factors, among them are: electrode geometry, voltage polarity (divergent fields), and voltage waveform (ac, dc, impulse, step voltage etc.) [2,11].

Hot electrons play an important role in degradation and breakdown of dielectrics exposed to fast voltage transients [2,3,13]. One hypothesis is that hot electrons will behave similarly in liquids and amorphous solids due to similar density and molecular arrangement in the two phases. Our experimental work on liquids and their frozen counterparts have been done to test this hypothesis [14,15]. This paper is the third paper in a series describing experiments performed in liquid and solid (frozen) phase. The first paper presents the experimental setup and experiments performed in liquid and frozen cyclohexane [14]. The second paper investigates pre-breakdown processes in neat n-tridecane (i.e. purified n-tridecane with no additives), and how the liquid-solid phase transition affects the pre-breakdown phenomena [15]. It was found that for virgin samples, i.e. samples that were melted between each applied voltage impulse, the main effect of the phase transition was an increased scatter in the measurements due to the increased inhomogeneity when going from liquid to solid phase [15]. The present paper focuses on the effect of two additives, trichloroethene (TCE) and N,N-dimethylaniline (DMA), on pre-breakdown phenomena in liquid and solid n-tridecane. The additives were chosen based on their ionization potential (IP) and electron scavenger properties that have been shown to be of importance for streamer propagation in cyclohexane [16,17].

2. THEORY

Pre-breakdown phenomena in solid and liquid phases are complex. There are several review papers/books on the topic [2,3,11], and a brief description of the processes responsible for inception and propagation of streamers and electrical trees were given previously [15]. Here, we focus on the effect of additives and base liquid/solid properties.

2.1. ADDITIVES IN LIQUID AND SOLID INSULATION

Additives are common in both solid and liquid insulation. Cross-linked polyethylene (XLPE) typically contains a mixture of chemical additives either left behind from cross linking (i.e. acetophenone, cumylalcohol, etc.) or included to inhibit oxidation (typically antioxidants of the phenolic or amine type). The material properties are also modified by additives, fillers and cross-linking [2,18].

For liquid insulation a similar picture arises, but in addition to the controlled additives added to increase stability, the composition is often not well defined for liquid insulation as it is typically based on mineral oil. Mineral oils are produced by refining crude oil, and are complex mixtures of paraffinic, naphthenic and aromatic hydrocarbons. Small amounts of sulphur compounds, nitrogen compounds, and oxygen

compounds also occur naturally in a mineral oil. Different additives like oxidation inhibitors, pour-point depressants, gas absorbers and metal captivators may also be added [19].

2.2. IMPORTANT FACTORS FOR STREAMER INCEPTION/PROPAGATION IN LIQUIDS

A large number of prebreakdown/breakdown experiments have been performed in a variety of liquids [11,12], and the results have been interpreted based on one or more of the molecular or bulk properties of the liquids: Molecular packing density and molecular branching [20], functional groups/atoms [5,21-23], molecular double and triple bonds [23,24], molecular parachor [25], molecular dipole moment [25], conductivity [26], viscosity [5,12,27-30], and boiling point [31]. In addition, external factors like the hydrostatic pressure and temperature have been shown to be of importance for streamer inception and propagation [5,14,29,30,32,33], these properties will influence the energy required for evaporation and the viscosity of the liquid. The energy required for inception and propagation of streamers are taken from the electric field through processes like field ionization [10] or impact ionization [3] creating free charge that can deposit the energy in the streamer structure or at the interface between the streamer and the liquid [34]. The molecular properties in the list above will influence the energy transfer from the electric field to the streamer, while the bulk properties mainly influence are on the energy required for growth. The bulk properties, as well as external properties, mainly influence the slow first-mode streamers [28,32]. The faster more energetic 2nd mode streamers are typically less affected by bulk properties [28]. Nevertheless, bulk properties, like viscosity/temperature, can affect the transition between the 1st and 2nd mode [29].

It is known that electron scavengers and low ionization potential additives can have a large effect on streamer propagation [35], which has subsequently been confirmed for a large variety of base liquids and additives, showing that even a small concentration of additives with specific electrochemical properties can drastically change the propagation characteristics of streamers [17,21,34,36-38]. The general trend found is that molecules with low ionization potential speed up positive streamers, while molecules with electron scavenger properties makes negative streamers more filamentary and faster.

2.3. IMPORTANT FACTORS FOR ELECTRICAL TREE INCEPTION IN SOLIDS

For solid insulation much emphasis have been on slow cumulative degradation, unlike streamers in dielectric fluids, once an electrical tree is initiated further growth will occur through partial discharges eventually leading to breakdown [13]. The first void in which partial discharges can occur is believed to be caused by hot electrons breaking polymer bonds followed by autoxidation [13,39,40].

The importance of oxidation processes for long-term treeing has been confirmed through the observed influence of oxygen [13], temperature [41] and antioxidants on inception [42]. The observation of a deterioration region at high-field regions

showing clear evidence of oxidation is further proof of this [43]. Degassing and subsequent impregnation with Ar or He has been shown to increase the rate of deterioration of the polymer, which has been ascribed to the Penning effect [44].

Oxidation and the Penning effect both rely on hot electrons with sufficient energy to either break polymer bonds or excite molecules. Therefore, the deterioration process is slowed down by reducing the mean-free path of the electrons, thus reducing the number of hot electrons [40,45]. This can be achieved by impregnation with liquid [46] or gas [39,44,45,47,48] which reduces the free volume in the insulation material, or by electron scavenger additives (i.e. SF₆) [45]. Additives with low molecular weight and byproducts from crosslinking have also been shown to be effective as treeing inhibitors, explained by diffusion into voids thus reducing the free volume [49]. The diffusion of such molecules to high-field regions could be enhanced by dielectrophoresis, and these molecules could lower the resistivity in the high-field region, thus reducing the field in this region [49]. This would lead to a low space charge limited field (SCLF). An ideal dielectric should have a SCLF low enough to limit the field to safe values in the high-field region without damaging the dielectric, such a material could only fail thermally [50,51].

Impulse treeing is affected by many of the same factors as ac-treeing, but dielectrophoresis, oxidation and the Penning process are too slow to have any effect on impulse trees. Thus for impulse treeing one can increase the inception voltage either by reducing the mean-free path of electrons, or by reducing the field in the high-field region. For example the inception voltage for impulse electrical trees in polymers are higher after the formation of a deterioration/oxidation region by slow cumulative degradation [43]. This has been explained by the large number of polar groups in this region, leading to a higher dielectric constant of the material. This will alter the field distribution, lowering the field in this region [43]. An increased conductivity in the deterioration region could also explain the result through a reduced SCLF [51].

3. METHODS AND MATERIALS

3.1. EXPERIMENTAL SETUP

The experimental setup has been described in detail previously [14]. It comprises a high voltage pulse source, a temperature control system, a differential charge measurement setup, and a photomultiplier tube (PMT). Needle-plane electrode geometry with a needle radius of 2 μm and a gap distance of 11.5 mm was used. The plane electrode has a diameter of 90 mm. The sample volume was approximately 2 dl. The temperature can be varied between -60°C and $+260^\circ\text{C}$.

The voltage source connected to the plane electrode gives step voltages with a rise time of 40 ns, constant high voltage for 50 μs and switching off time constant of 80 μs , hereafter called impulses. Two electrodes, a sharp needle and a blunt probe, were used for differential charge recordings during the applied impulses. The system has sensitivity better than 0.1 pC [14].

The sharp needle electrodes were made of 100 μm wolfram wires electrochemically etched to a point radius of 2 μm . Special concern was given to the submicroscopic properties of the electrode surface as this has been shown to be of importance for the experimental results [15]. All electrodes used were studied under a scanning electron microscope prior to the experiments. New needles were made for each test series, as previous experiments have shown that multiple discharges in n-tridecane deposit a polymer layer on the needle that affects the measurements [15].

3.2. MATERIALS

Experiments were performed in 0.1 M DMA in n-tridecane, and 0.1 M TCE in n-tridecane and were compared to previous results obtained in neat n-tridecane (i.e. n-tridecane with no additives) with the same setup [15]. The additives were chosen based on their electrochemical properties, and on previous results with a similar setup where electron-attaching and electron-releasing additives in cyclohexane were studied [16,17].

The linear alkane, n-tridecane, was chosen based on its known similarities with polyethylene. The energy levels in linear alkanes approach the continuous energy bands found for polyethylene as the number of carbon atoms in the chain increases [52]. In addition, linear alkanes have been used as model systems to study the morphology of polyethylene [53]. Tridecane has an IP of 9.25 eV in the liquid phase [54], and a first singlet-singlet excitation energy of 6.3 eV in the gas phase [55].

DMA was chosen because of its relatively low IP of 7.12 eV in the gas phase [56]. It has been shown to enhance streamer growth from positive needle electrodes in cyclohexane [17]. In addition to a low IP, density functional theory (DFT) calculations in the gas phase have shown that DMA has a low first singlet-singlet excitation energy of approximately 2.4 eV [55].

TCE was chosen because of its known electron scavenger properties (high electron affinity and large cross section). This substance has been shown to enhance streamer growth from negative needle electrodes in cyclohexane [17]. TCE has an IP of 9.46 eV in the gas phase [56], and a first singlet-singlet excitation energy of 5.1 eV in the gas phase [55].

The base liquid was 99.9 % pure n-tridecane, degassed for 24 hours, and treated with a molecular sieve (3 \AA Zeochem) to reduce the content of water in the sample. 0.1 M solutions of n-tridecane and TCE or DMA were made by mixing the degassed n-tridecane with the additive overnight using a magnetic stirrer. During experiments the sample volume was in contact with a 10 ml reservoir filled with air and molecular sieve, the two volumes were connected through a syringe. This reservoir allowed the sample to expand during temperature cycling.

Frozen n-tridecane is a polycrystalline material, meaning that it is mainly crystalline, but with amorphous regions at the boundaries between crystallites. As the additives will not fit into the crystalline structure, they will primarily be located at the boundaries between crystallites, and will therefore reduce the overall crystallinity of the frozen liquid.

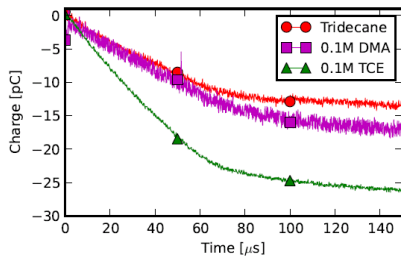


Figure 1. Typical examples of charge recordings in neat n-tridecane and the two mixtures at 16 kV, positive needle polarity and 20°C.

3.3. TEMPERATURE SEQUENCE

The sample was cooled to -15°C with a linear cooling rate of -1°C/min. Once the desired temperature was reached, it was kept constant for ten minutes before the impulse was applied. After each impulse the sample was melted (heated to 20°C and held at that temperature for 10 minutes) and then frozen again to produce a new virgin sample before new impulses were applied. This temperature sequence is similar to the one used previously with neat n-tridecane [15], but with neat n-tridecane the sample was only cooled to -10°C. The lower temperature was used since the freezing point is lowered by the additives. A short test with neat n-tridecane was conducted to be sure that the two temperature programs gave similar results for neat n-tridecane. All experiments on the liquid phase were done at 20°C.

3.4. NUMBER OF AND DELAY BETWEEN IMPULSES

For all experiments at least 20 impulses were applied at each voltage level. For the liquid phase a delay of 600s was used between each applied impulse, while for the solid phase virgin samples were used (section 3.3).

4. EXPERIMENTAL RESULTS

This section is divided into three subsections corresponding to the different stages observed for streamers/electrical trees at increasing voltage levels:

- Pre-inception currents: Currents recorded when no streamers/electrical trees were created are presented.
- Inception: Probability for initiation of streamers and electrical trees versus voltage level, and the probability for recorded light emission versus voltage level are given in this section.
- Propagation: The last section gives the characteristic measurements describing the propagation of the structures in liquid and solid phases. Since no visual observation was possible this is limited to the magnitude and duration of the measured charge, emitted light and the average current for streamers and electrical trees.

4.1. PRE-INCEPTION CURRENTS

Charge recordings that showed no evidence of discharges, i.e. no sudden increase in current or steps in the charge recordings, were classified as "pre-inception currents". Typical examples

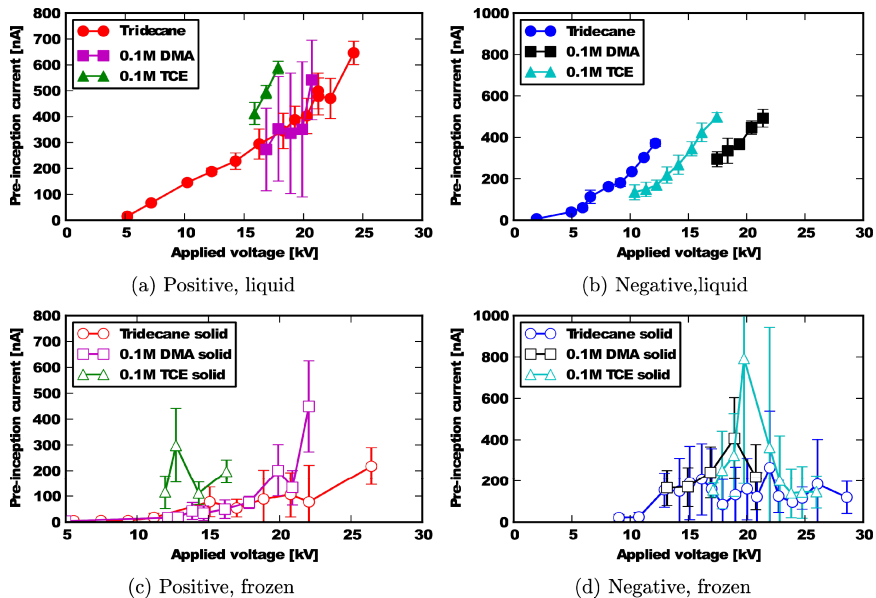


Figure 2. Average pre-inception current during the first 50 μ s after applied voltage. At least 20 impulses were applied at each voltage, but at the highest voltages some of the impulses resulted in streamers, thus reducing the number of recordings of pre-inception currents at high voltages. Each point corresponds to at least five data points. Experiments in the solutions were conducted in a limited voltage range, from a few kV below the inception voltage (50% streamer inception probability, table 1).

Table 1. Voltage range corresponding to 10-90% streamer/electrical tree inception probability and inception voltage, V_i (50% inception probability). In some cases 90% inception voltage was not reached within the voltage range used (up to 28 kV).

	Positive polarity (kV)				Negative polarity (kV)			
	Liquid		Frozen		Liquid		Frozen	
	10 – 90 %	V_i	10 – 90 %	V_i	10 – 90 %	V_i	10 – 90 %	V_i
Neat n-tridecane	19 - 27.5	24	16 -	23	14.5 - 22	18.5	16.5 -	20
0.1 M DMA	17 - 21	20	12.5 - 23	20	18.5 - 22	20.5	14 - 20	17.5
0.1 M TCE	16 - 19	17.5	16 - 18.5	17	13.5 - 18	15	16 - 20.5	18

recorded at 16 kV and 20°C with positive polarity are shown in figure 1. Such currents have been reported in similar experiments with other liquids and solids before [16,32,57]. Pre-inception currents were measured in all materials at both polarities and both phases (figure 2). The general shape of the charge recordings, from which the pre-inception currents presented in figure 2 were calculated, was similar to the ones shown in figure 1 regardless of the phase and polarity.

In the frozen phase with positive polarity, neat n-tridecane and 0.1 M DMA were found to yield the same current-voltage characteristic up to 22 kV, where the current in 0.1 M DMA became larger than in neat n-tridecane (figure 2c). In the liquid phase, a similar increase at 22 kV is observed, but within the standard deviation of the measurements in neat n-tridecane (figure 2a). TCE was found to increase the pre- inception current with positive polarity for both phases (figures 2a and 2c).

Higher voltages were needed to induce the same pre-inception current in the solutions compared to neat n-tridecane with negative polarity. An average current of approximately 300 nA was recorded at 12 kV, 15 kV and 17 kV, for n-tridecane, 0.1 M DMA and 0.1 M TCE respectively (figure 2b). Comparing the results obtained with 0.1 M DMA and 0.1 M TCE with negative polarity to the results obtained in the same liquids under positive

polarity, shows that the pre-inception currents in these liquids are unaffected by the polarity, while the currents in neat n-tridecane are higher for negative than for positive polarity at the same voltage.

For the frozen phase, the scatter in the measurements are too large to recognize any difference between the three liquids (figure 2d). The general trend for all three frozen liquids is that the pre-inception currents stay low even at high voltages. No clear correlation with voltage level was found.

4.2. INCEPTION

The voltage range where streamer/electrical tree inception probabilities increase from 10 to 90% as well as the inception voltage (50% inception probability) for positive and negative polarity with both phases are given in Table 1. Inception probabilities were found by counting the voltage impulses that resulted in streamer/electrical trees characterised by a step/step increase in charge versus time in the charge recordings at a given voltage.

Both additives were found to lower the inception voltage in the liquid phase with positive polarity (Table 1). However, the lowest voltage for which streamer inception occurred was found to be similar for all three liquids. The rise from 10 to 90%

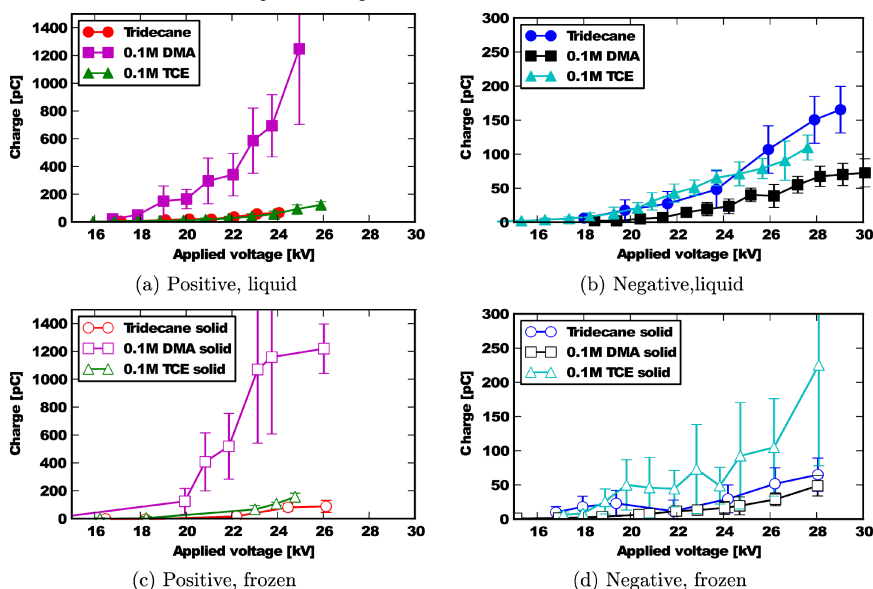


Figure 3. Average injected charge versus applied voltage for streamers and electrical trees. The charge is based on the total charge increase from the first step in the charge recording to the last. Charge recordings of streamers in combination with shadowgraphic imaging of the phenomenon in liquids have shown a clear correlation between the charge and the spatial size of streamers [17].

streamer probability occurs over a larger voltage range in neat n-tridecane than in n-tridecane with additives. The same trend was observed for the solid phase, but the first electrical tree occurs at lower voltages than the first streamer in the liquid phase. However, the 20-90% voltage range is similar for the liquid and solid phase.

Inception probabilities with negative polarity in neat n-tridecane were found to fall between those obtained with the two mixtures in the liquid phase (Table 1). The onset voltage (10% streamer probability) in neat n-tridecane is about the same as what is observed in 0.1 M TCE, while 100% probability was found to coincide with the results found for 0.1 M DMA. As for positive polarity the increase from 10 to 90% inception probability occurred over the largest voltage range for neat n-tridecane.

For the solid phase and negative polarity, the only clear distinction between the three liquids is that only 0.1 M DMA reaches 100 % inception probability within the voltage range used (up to 28 kV). In contrast to what was found in the liquid phase, discharges were observed at lower voltages in 0.1 M DMA than in the other two materials.

4.3. PROPAGATION

Propagation of streamers and electrical trees were measured indirectly through charge and light emission measurements (figures 3 and 4). Several studies where the extension of streamers into dielectric liquids have been measured indicate that there is a clear correlation between the spatial extension of the streamers and the measured charge [17]. In the liquid phase it has been shown that the transition from one propagation mode to another is followed by a sharp increase in the average streamer

current [17]. The streamer/electrical tree current have therefore been plotted in figure 5.

The charge versus voltage plots in figure 3 are based on the total charge increase from the first step in the charge recording to the last. Figure 4 simply shows the amplitude recorded by the photomultiplier versus voltage. The average streamer current versus voltage level shown in figure 5 was calculated by dividing the streamer charge by the propagation time.

Adding DMA to n-tridecane increases the injected charge for positive polarity both for the frozen and the liquid phase (figures 3a and 3c). At voltages near the inception voltage, the smallest discharges are about the same size as those recorded in neat n-tridecane, but they grow faster with applied voltage. At 25 kV, the size of the discharges was found to be around 8-10 times larger in 0.1 M DMA compared to neat n-tridecane. For negative polarity, DMA has the opposite effect. In the liquid phase the discharges increase more slowly with increasing voltage in 0.1 M DMA compared to what was observed in neat n-tridecane (figure 3b). In the liquid phase at 26 kV, approximately twice as much charge is injected into a streamer in neat n-tridecane compared to 0.1 M DMA. In the solid phase, the average injected charge is reduced when adding DMA, but the effect is smaller than in the liquid phase, and typically lies within the standard deviations of the results obtained for neat n-tridecane (figure 3d).

Adding TCE to n-tridecane has no effect on the injected charge for positive polarity neither for the liquid nor for the frozen phase (figures 3a and 3c). In contrast to what was observed for the liquid phase, for negative polarity and frozen phase TCE was found to increase the average injected charge and the observed scatter (figure 3d). At 26 kV, the average discharges

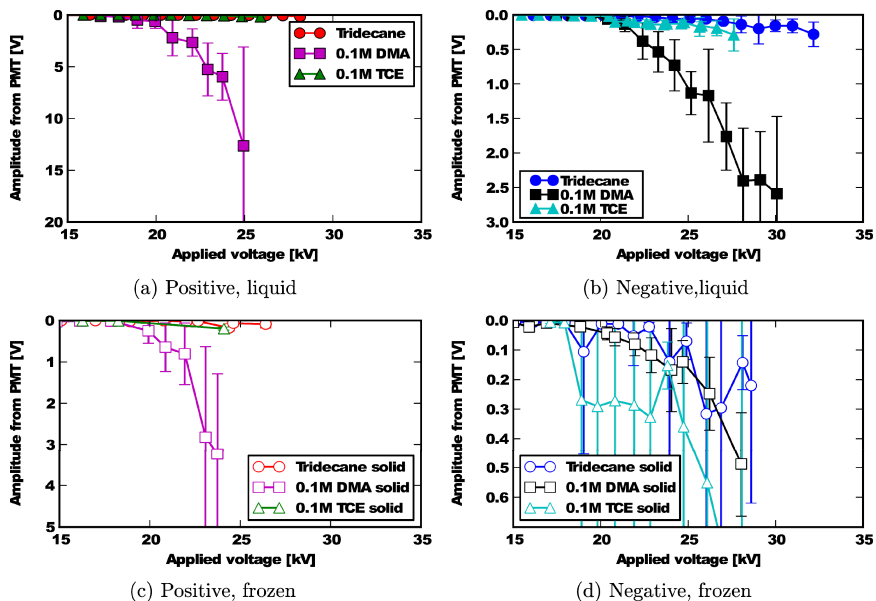


Figure 4. Average photomultiplier amplitude versus applied voltage. The plots above are based on photomultiplier amplitudes measured for streamers/electrical trees. Note the different y-scales.

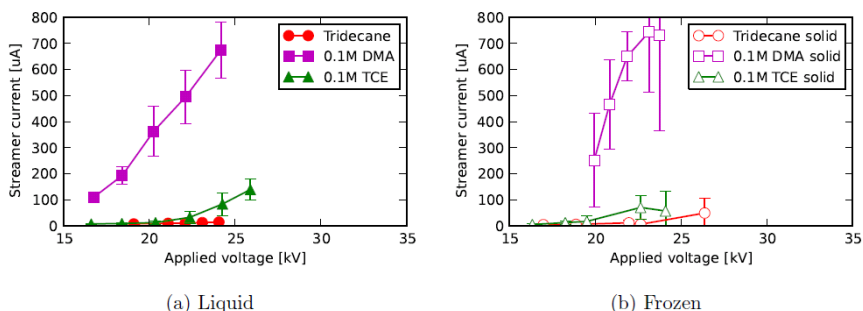


Figure 5. Average streamer current versus voltage level for positive polarity. No effect of the additives was found for negative polarity, thus only results for positive polarity are presented above. The streamer current was calculated by dividing the streamer charge by the propagation time (time from first to last discharge/step in the charge recording).

are twice as large in 0.1 M TCE compared to the average discharges in neat n-tridecane in the frozen phase (figure 3d).

Light emission from 0.1 M DMA was much larger than for neat n-tridecane with positive polarity for both phases and for negative polarity in the liquid phase (figures 4a, 4b and 4c). For the solid phase with negative polarity, the results for 0.1 M DMA and neat n-tridecane were similar (figure 4d). No clear effect of TCE on light emission were found, only a small increase within standard deviations for negative polarity in solid phase was observed (figure 4d).

The streamer current recorded in both phases with positive polarity were more than 100 times larger in 0.1 M DMA than the currents recorded in neat n-tridecane (figures 5a and 5b). For negative polarity, no effect of DMA were observed.

TCE has a much weaker effect on the streamer current, but for voltages above 22 kV with positive polarity in the liquid phase, the streamer current was found to increase faster in 0.1 M TCE than in neat n-tridecane (figure 5a). No effect of TCE was found for frozen phase and positive polarity (figure 5b). The measurements performed in 0.1 M TCE were within standard deviations of measurements performed in neat n-tridecane for both phases with negative polarity.

5. DISCUSSION

In our previous paper on discharges in neat n-tridecane, we discussed the following mechanism for inception of streamers in liquids where the space charge limited field (SCLF) is below the necessary field for electron avalanche formation in the liquid phase [15]:

- Local joule heating creates a region with low density liquid or a bubble.
- In the low density region/bubble the mean-free path of electrons will increase, thus avalanches can occur in this region.
- Discharges in the low density region/bubble can lead to further growth of the streamer.

Additives can influence this process by changing the required mean-free path, changing the SCLF/high-field conductivity, or

changing the energy required for the creation of a low density region.

The effect of phase transition from liquid to solid phase was found to be small for both inception and propagation in n-tridecane, the main effect of the phase transition being an increased scatter in all measured quantities [15]. Therefore it was proposed that similar phenomena occurs in liquid and frozen n-tridecane, but the increased scatter is caused by the inhomogeneity of the material in the solid phase. The amorphous regions are probably weaker than the crystalline regions (lower yield strength and lower dielectric strength). The morphology at the needle apex is therefore important for the inception of electrical trees.

In the following the effect of DMA and TCE on inception of streamers/electrical trees will be discussed for both polarities and phases. In addition the effect of the additives on the growth of streamers and electrical trees is discussed.

For positive polarity the same general trends were found for both phases. Thus we start by discussing the effect of the additives followed by a brief discussion about the limited effect of phase transition for positive polarity.

The probability for streamers in 0.1 M DMA follows the inception probability in neat n-tridecane up to about 20 kV where the inception probability increases more rapidly resulting in a somewhat lower inception voltage than for neat n-tridecane (Table 1). This corresponds to the increase in pre-inception current seen at 21-22 kV in 0.1 M DMA (figures 2a and 2c) which may be caused by electron avalanches with insufficient energy to start a streamer. The increase in pre-inception current at lower voltages in 0.1 M DMA compared to n-tridecane is expected as a low-IP material will facilitate electron avalanches [38]. DMA will make formation of avalanches more efficient than in neat n-tridecane because less energy is required for impact ionization of DMA (a shorter mean-free path is required).

The low IP of DMA enhances the probability for impact ionization making electron avalanches larger [38], which may explain both the large measured charge and the enhanced light emission in 0.1 M DMA compared to in neat n-tridecane (figures 3a, 3c, 4a and 4c). It should be noted that the first excitation

energy for DMA is approximately 2.4 eV, which is in the area of visible light. Therefore, the DMA molecules are easily excited, and one possible way of relaxation is through emission of light. The plot of the streamer current for both phases shows that the average streamer current is much larger in 0.1 M DMA than in 0.1 M TCE and n- tridecane (figures 5a and 5b). The increased streamer current indicates faster streamer propagation when DMA is added (higher streamer mode). This is in line with what has previously been reported for low IP molecular additives in dielectric liquids [10,17,34].

For positive polarity, TCE was found to increase the pre-inception current in both phases (figures 2a and 2c). TCE is a known electron scavenger, thus it creates traps in the material (regions of higher electron affinity). One would expect this to reduce the mobility of the electrons and thus reduce the measured current by localizing free electrons in traps. Such traps in combination with a strong electric field can, on the other hand, lead to effective conduction through mechanisms such as trap assisted tunnelling or hopping conduction [2]. Some traps may be occupied by free electrons produced by background radiation. For the liquid phase, these electron scavengers could also result in more space charge being left behind from previous impulses. However, the same trend is seen for the frozen phase where the sample goes through two phase transitions between each measurement (approximately 1.5 hours between each impulse). Even a small number of filled traps would increase the conductivity in the material thus explaining the larger current measured in 0.1 M TCE. The lower inception voltage in 0.1 M TCE compared with n-tridecane for both phases corresponds with the increase in pre-inception currents which results in an increased energy dissipation in the high-field region creating a low- density region at lower voltages (Table 1). Comparing the pre-inception current in the liquid phase at the inception voltage in n-tridecane (24 kV) and in 0.1 M TCE (17.5 kV) gives approximately equal values (figure 2a). The pre-inception current increases at a higher rate with increasing voltage in 0.1 M TCE than in n-tridecane, corresponding to the faster rise from 0 to 100 % streamer probability in 0.1 M TCE. In addition to the more efficient creation of a low density region the filled traps in 0.1 M TCE may provide seeding electrons for avalanche initiation.

Electron scavengers like TCE have only minor effects on positive streamers in cyclohexane and other dielectric liquids [10,17,34], and the same is true for TCE in n-tridecane in solid and liquid phase (figures 3, 4, and 5). However, at voltages above 22 kV the current increases faster in 0.1 M TCE than in n-tridecane in the liquid phase (figure 5a), indicating a transition to 2nd mode streamers. There is some evidence for a transition from 1st to 2nd mode for neat n-tridecane as well [15], thus the effect of TCE might be relatively small. The effect could be caused by filled traps in the material which could easily give up their electrons. This could cause transition to 2nd mode streamers by the same mechanism believed to be responsible for the change in propagation mode caused by low IP additives.

The same general trends are seen for both phases with positive polarity for all measured quantities. Thus the main processes

responsible for pre-inception currents, inception and propagation are most likely similar for the two phases. Most of the current probably flows in the amorphous regions [52] and this might quickly melt these regions. n- tridecane is a substance with a high boiling point, and the energy required for phase transition from solid to liquid phase is small compared to the energy required to go from room temperature to vapour phase. This explains why the phase transition is found to be of minor importance. The main difference when going from liquid to frozen phase is that higher voltages are required to reach 100% inception probability for all three liquids after they are frozen, and all measured quantities have larger standard deviations. This can be explained by the fluctuations of dielectric strength at the needle apex (pre-inception and inception) and in the material in general (propagation) caused by the inhomogeneity of the material in the solid phase.

For negative polarity the phase transition has a larger effect, and pre-inception, inception and propagation/growth of streamers must thus be discussed based on both additives and phase. The findings for negative polarity are also compared to what was found with positive polarity.

The polarity dependence of the pre-inception currents in the liquid phase in n-tridecane (higher currents with negative polarity at the same voltage level) disappeared when the additives were introduced (figures 2a and 2b). Reproducibility can be a problem for pre-inception current measurements with negative polarity, as the measured current is strongly dependent on the surface of the needle electrode [15]. The insensitivity to polarity in the two solutions could thus be caused by smoother electrodes being used. However, similar procedures were used to produce and check all the needle electrodes (see section 3.1), which makes it reasonable to assume that the similar behaviour for both polarities are caused by the additives. We propose that the additives thermalize the electrons emitted from the negative needle electrode before they gain enough energy to create more free electrons by impact ionization. In the case of TCE this can be explained by its electron scavenger properties, while the low excitation energy for DMA means that it can take up energy from hot electrons through electronic excitation [55].

The large scatter in pre-inception current recordings for negative polarity and frozen phase indicates that, unlike for positive polarity, the interface between the electrode and the material is of higher importance than the voltage level as long as the voltage is above a certain threshold (figures 2c and 2d). From DFT calculations on n-tridecane, it is known that electrons travel primarily in the amorphous regions [52]. Thus the morphology at the needle apex will be of importance for electron emission. From the recordings, it is evident that a threshold voltage of 10 kV is needed for charge injection to occur (figure 2d), but the average current was not found to increase with voltage above this threshold. This could be explained by low mobility in the frozen phase effectively localizing the injected charge reducing the field at the needle to a value below the one needed for electron emission.

The faster increase from 10% to 90% streamer probability in n-tridecane with negative compared to positive polarity (Table 1) can be explained by the availability of seeding electrons from the electrode, and the higher recorded pre-inception currents [15]. A similar inception mechanism as the one suggested for n-tridecane is proposed for the two solutions, but contradictory to what was observed in n-tridecane the polarity of the electrode hardly has any effect on the inception probability in the two solutions (Table 1). This can be explained by more seeding electrons in the bulk for the two solutions, thus reducing the effect of the needle polarity.

For the frozen phase the inception probability versus voltage is harder to interpret. The inception voltage for 0.1 M TCE and neat n-tridecane is increased by a few kV (Table 1), whereas the results for 0.1 M DMA is reduced by approximately 3 kV. The phase transition reduces the difference between the three liquids. Generally negative polarity frozen phase seems to be more dependent on the morphology at the needle apex than on the additives.

For negative polarity, the addition of DMA has a much smaller effect on the propagation of streamers and electrical trees than observed for positive polarity as expected [17]. For the frozen phase, no significant effect was found, while for the liquid phase the injected charge is reduced in 0.1 M DMA compared to neat n-tridecane (figures 3b and 3d).

In the liquid phase much more light is emitted as a result of streamer propagation in 0.1 M DMA than in n-tridecane and 0.1 M TCE (figure 4b). No mode transition was observed as a result of DMA (the streamer current did not increase), and the streamers were thus 1st mode streamers. For such streamers the electron avalanches/discharges are believed to take place in the gas vapour inside the streamer "bubble" and the electrons from these discharges bombard the liquid at the streamer liquid interface causing vaporization of the liquid and further growth of the streamer [58]. The discharges seen may be corona discharges with an ionization region at the point electrode, and a drift region from the ionization region to the streamer-liquid interface where the electron energy is too low for impact ionization. Clearly a portion of the hot electrons will lose their energy due to inelastic collisions with insufficient energy to cause impact ionization. Normally this would release the energy in form of heat, thus also contributing to the streamer growth, but in some cases the energy might be emitted as photons. At high fields with hot electrons in the streamer region it is likely that a fraction of the DMA molecules will be excited, and the relaxation of these excited molecules will occur through heat transfer or emission of photons in the visible range. Photons in this range will escape from the streamer region in an optically clear liquid like n-tridecane. Thus the effect of DMA is probably to hinder the propagation of the streamer by emission of parts of the energy dissipated in the streamer region as photons. This hypothesis could be checked by spectroscopy. The low IP of DMA should enhance electron multiplication in the streamer, thus increase the amount of charge bombarding the streamer-liquid interface, but this effect seems to be secondary to the emission of energy for

1st mode streamers. A more complete discussion of this is given elsewhere [55].

Adding DMA does not affect the frozen phase, both charge and light emission is within standard deviations of the values recorded for neat n-tridecane (figures 3d and 4d). The absent effect of DMA may indicate that fewer DMA molecules are excited or that a larger fraction of excited DMA molecules release their energy as heat in a discharge in the solid phase compared to the liquid phase. If, on the other hand, the discharges in the solid and liquid phase are similar then the absent effect of DMA in the solid phase indicates that most of the energy that is emitted as photons is absorbed in the electrical tree, or at the boundary between the electrical tree and the frozen solid, thus the energy is contained in the vicinity of the tree and will contribute to further growth of the tree. The reason for the difference between the liquid and the solid phase may be increased scattering in the solid, and a larger DMA concentration in the amorphous phase between crystallites where electrical tree growth is assumed to take place (thus photons emitted by relaxation of DMA molecules can excite DMA molecules in the solid, which can in turn release the energy as heat). This would increase the absorption of photons in the region close to the discharge in the solid compared to the liquid phase.

No effect of TCE was found for negative polarity in the liquid phase. For the solid phase a small increase in injected charge and emitted light within standard deviations of measurements in neat n-tridecane were observed. However, TCE has been reported to have a clear effect on propagation of negative streamers in cyclohexane [17], and adding electron scavengers to dielectric liquids generally makes negative streamers propagate faster and be more filamentary [10]. The reason for this is believed to be that the electron scavengers focuses the energy transfer and space charge build-up from hot electrons to a smaller region near the streamer/liquid interface, while electrons can travel further in liquids with no electron scavengers [17]. This indicates that n-tridecane already focuses the energy and charge of the hot electrons to a small volume, and that the addition of TCE does not further enhance this. Thus the mean free path and thermalization distance of electrons in n-tridecane is probably short compared with cyclohexane. This is in line with the high inception voltage found for n-tridecane which indicates that a low density region is required for sufficiently long mean-free paths for electron avalanches [15].

6. CONCLUSIONS

The effect of a low-IP additive (DMA) and an electron-scavenger additive (TCE) in n-tridecane on pre-breakdown phenomena for liquid and solid phases have been studied. The main effect of DMA was to change the propagation mode of positive streamers and enhance the injected charge and emitted light from the phenomena with positive polarity for both phases. For negative polarity in the liquid phase, the addition of DMA reduced the injected charge and increased the emitted light from the streamer. This indicates that some of the energy otherwise available for streamer growth is emitted as light with negative

polarity, probably through excitation and de-excitation of DMA which has a low excitation energy (2.4 eV).

TCE had no effect on negative streamer propagation, unlike what has been reported for TCE and other electron scavengers in cyclohexane. Electron scavengers are believed to facilitate negative streamer propagation through localizing energy dissipation and charge deposition at the streamer/liquid interface. The fact that no such effect was found for n-tridecane indicates that the thermalization distance for electrons in n-tridecane is short, thus effectively localizing the energy transfer and space charge build-up to a limited region at the interface even with no electron scavenger additive. This is supported by the similar characteristics of positive and negative streamers in neat n-tridecane, and the very high inception voltage in n-tridecane.

Pre-breakdown phenomena are similar for the liquid and solid phases, the main difference being the large scatter introduced by the transition to solid phase. This is explained by the inhomogeneity of the solid on the micrometer scale. The morphology seems to be more important for negative than for positive polarity. Electron emission from the needle electrode is probably very dependent on the interface between the needle apex and the frozen liquid. The similarity between the phases suggests that electrical trees grow in the amorphous regions of the solid.

ACKNOWLEDGMENT

Support from the Norwegian Research Council through a Strategic Industry Program (164603/130) is acknowledged.

REFERENCES

- J. M. Meek and J. D. Craggs, editors. "Electrical Breakdown of Gases." John Wiley & Sons, 1978.
- L. A. Dissado and J. C. Fothergill. "Electrical Degradation and Breakdown in Polymers." Material and Devices Series 9. The Institution of Engineering and Technology, London, United Kingdom, 1992.
- A. Denat. "High field conduction and prebreakdown phenomena in dielectric liquids." *IEEE Trans. Dielect. Elect. Insul.*, 13:518-525, 2006.
- M. Haidara and A. Denat. "Electron multiplication in liquid cyclohexane and propane." *IEEE Trans. Elect. Insul.*, 26:592-597, 1991.
- H. Yamada and T. Sato. "High-speed electro-optical measurement of pre-breakdown current in dielectric liquids." *IEEE Trans. Elect. Insul.*, EI-20:261-267, 1985.
- H. Yamada, S. Kimura, T. Fujiwara, and T. Sato. "Prebreakdown current and breakdown propagation velocity in polyethylene under a highly nonuniform field condition." *J. Phys. D: Appl. Phys.*, 24:392, 1991.
- H. Yamada, T. Fujiwara, and Y. Suzuoki. "Electrical breakdown time delay and breakdown propagation velocity in polypropylene under a highly non-uniform field condition." *J. Phys. D: Appl. Phys.*, 26:1328, 1993.
- E.O. Forster. "Electrical breakdown in liquid hydrocarbons." *J. Electrostat.*, 12:1-12, 1982.
- S. S. Hakim and J. B. Higham. "Phenomena in n-hexane prior to its electric breakdown." *Nature*, 189:996, 1961.
- J. C. Devins, S. J. Rzad, and R. J. Schwabe. "Breakdown and prebreakdown phenomena in liquids." *J. Appl. Phys.*, 52:4531-4545, 1981.
- A. Beroual, M. Zahn, A. Badent, K. Kist, A. J. Schwabe, H. Yamashita, K. Yamazawa, M. Danikas, W. D. Chadband, and Y. Torshin. "Propagation and structure of streamers in liquid dielectrics." *IEEE Electric. Insul. Mag.*, 14:6-17, 1998.
- V. Ya. Ushakov. "Impulse Breakdown of Liquids." Springer, 2007.
- N. Shimizu and C. Laurent. "Electrical tree initiation." *IEEE Trans. Dielect. Elect. Insul.*, 5:651-659, 1998.
- Ø. L. Hestad, L. E. Lundgaard, and D. Linhjell. "New experimental system for the study of the effect of temperature and liquid to solid transition on streamers in dielectric liquids: Application to cyclohexane." *IEEE Trans. Dielect. Elect. Insul.*, 17:767-777, 2010.
- Ø. L. Hestad, L. E. Lundgaard, and P.-O. Åstrand. "n-tridecane as a model system for polyethylene: Comparison of pre-breakdown phenomena in liquid and solid phase stressed by a fast transient." Submitted, 2010.
- S. Ingebrigtsen, L. E. Lundgaard, and P.-O. Åstrand. "Effects of additives on prebreakdown phenomena in liquid cyclohexane: I. streamer initiation." *J. Phys. D: Appl. Phys.*, 40:5161-5169, 2007.
- S. Ingebrigtsen, L. E. Lundgaard, and P.-O. Åstrand. "Effects of additives on prebreakdown phenomena in liquid cyclohexane: II. streamer propagation." *J. Phys. D: Appl. Phys.*, 40:5624-5634, 2007.
- T. L. Hanley, R. P. Burford, R. J. Fleming, and K. W. Barber. "A general review of polymeric insulation for use in hvdc cables." *IEEE Electric. Insul. Mag.*, 19:13-24, 2003.
- J. Webster. "Dielectrics and Electrical Insulation, Wiley Encyclopedia of Electrical and Electronics Engineering." John Wiley & Sons, 2007.
- T. Schutte. "The influence of the molecular packing on electrical breakdown strength of liquids." In *Nord-is*, pages 147-160, 1994.
- S. Sakamoto and H. Yamada. "Optical study of conduction and breakdown in dielectric liquids." *IEEE Trans. Elect. Insul.*, EI-15:171-181, 1980.
- Y. Nakao, T. Yamazaki, H. Tagashira, K. Miyagi, and Y. Sakai. "Propagation of streamer discharge in dielectric liquids with various molecular structure by using high-speed schlieren photography." *Proc. IEEE Int. Conf. Diel. Liq. (ICDL)*, pages 261-264, 1999.
- Y. Nakao, T. Yamazaki, K. Miyagi, Y. Sakai, and H. Tagashira. "The effect of molecular structure on prebreakdown phenomena in dielectric liquids under a nonuniform field." *Electrical engineering in Japan*, 139, 2002.
- N. Hamano, Y. Nakao, T. Naito, Y. Nakagami, R. Shimizu, Y. Sakai, and H. Tagashira. "Influence of molecular structure on propagation of streamer discharge in hydrocarbon liquids." In *Proc. IEEE Int. Conf. Diel. Liq. (ICDL)*, 2002.
- Y. Nakao, H. Nagasawa, R. Yamaoka, H. Itoh, Y. Sakai, and H. Tagashira. "Influence of molecular structure on the propagation of streamer discharge in dielectric liquids." *J. Electrostat.*, 40-41:199-204, 1997.
- J. Nieto-Salazar. "Breakdown and pre-breakdown phenomena in water under impulse voltage." *Int. Symp. on High Voltage Engineering (ISH)*, 2003.
- P. K. Watson, W. G. Chadband, and M. Sadeghzadeh-Araghi. "The role of electrostatic and hydrodynamic forces in the negative-point breakdown of liquid dielectrics." *IEEE Trans. Dielect. Elect. Insul.*, 26:543-59, 1991.
- W. G. Chadband. "Electrical breakdown-from liquid to amorphous solid." *J. Phys. D: Appl. Phys.*, 24:56-64, 1991.
- R. Badent, K. Kist, and A. J. Schwab. "The effect of viscosity on streamer propagation in insulating oil under impulse conditions." *Proc. IEEE Int. Conf. Diel. Liq. (ICDL)*, 1996.
- Y. Katayama, T. Nakayashiki, and H. Yamashita. "The effect of viscosity on the negative streamer inception in pfp." In *Ann. Rep. Conf. Elec. Insul. Diel. Phen. (CEIDP)*, 1999.
- F. M. J. McCluskey and A. Denat. "Bubble formation in synthetic insulating liquids in a pulsed divergent electric field." *IEEE Trans. Dielect. Elect. Insul.*, 1:672-679, 1994.
- L. Dumitrescu, O. Lesaint, N. Bonifaci, A. Denat, and P. Notinger. "Study of streamer inception in cyclohexane with a sensitive charge measurement technique under impulse voltage." *J. Electrostat.*, 53:135-146, 2001.
- R. Badent, K. Kist, and A. J. Schwab. "The effect of hydrostatic pressure on streamer inception and propagation in insulating oil." In *Proc. IEEE Int. Symp. El. Insul. (ISEI)*, 1994.
- O. Lesaint and P. Gournay. "Initiation and propagation thresholds of positive prebreakdown phenomena in hydrocarbon liquids." *IEEE Trans. Dielect. Elect. Insul.*, 1:702-8, 1994.
- J. C. Devins, S. J. Rzad, and R. J. Schwabe. "Prebreakdown phenomena in liquids: electronic processes." *J. Phys. D: Appl. Phys.*, 9:87-91, 1976.

- [36] W. G. Chadband and T. M. Sufian. "Experimental support for a model of positive streamer propagation in liquid insulation." *IEEE Trans. Dielect. Elect. Insul.*, EI-20:239-246, 1985.
- [37] O. Lesaint and M. Jung. "On the relationship between streamer branching and propagation in liquids: influence of pyrene in cyclohexane." *J. Phys. D: Appl. Phys.*, 33(11):1360-, 2000.
- [38] S. Ingebrigtsen, H. S. Smalø, P.-O. Åstrand, and L. E. Lundgaard. "Effects of electron-attaching and electron-releasing additives on streamers in liquid cyclohexane." *IEEE Trans. Dielect. Elect. Insul.*, 16:1524-1535, 2009.
- [39] C. Laurent, C. Mayoux, and S. Noel. "Dielectric breakdown of polyethylene in divergent field: Role of dissolved gases and electroluminescence." *J. Appl. Phys.*, 54:1532-1539, 1983.
- [40] L. A. Dissado. "Understanding electrical trees in solids: from experiment to theory." *IEEE Trans. Dielect. Elect. Insul.*, 9:483-497, 2002.
- [41] K. Uchida and N. Shimizu. "The effect of temperature and voltage on polymer chain scission in high-field region." *IEEE Trans. Elect. Insul.*, 26:271-277, 1991.
- [42] Y. Sekii, D. Tanaka, M. Saito, N. Chizuwa, and K. Kanasawa. "Effects of antioxidants on the initiation and growth of electrical trees in xlp." In *Ann. Rep. Conf. Elec. Insul. Diel. Phen. (CEIDP)*, 2003.
- [43] N. Shimizu, K. Uchida, and S. Rasikawan. "Electrical tree and deteriorated region in polyethylene." *IEEE Trans. Elect. Insul.*, 27:513-518, 1992.
- [44] N. Shimizu and H. Sato. "Role of electron impact in ac electrical tree initiation." In *Proc. Int. Conf. Prop. App. Diel. Mat. (ICPADM)*, 1997.
- [45] N. Shimizu, Y. Muramoto, and Y. Kamiya. "Suppression of electrical tree in silicone rubber by gas impregnation." In *Proc. IEEE Int. Symp. El. Insul. (ISEI)*, pages 599-602, 2008.
- [46] N. Shimizu and T. Suzuki. "Suppression of high field degradation and electrical tree by n-hexane impregnation in xlp." In *Ann. Rep. Conf. Elec. Insul. Diel. Phen. (CEIDP)*, 2001.
- [47] J. Andrianjohanarivo, M. R. Wertheimer, and A. Yelon. "Nucleation of electrical tress in polyethylene." *IEEE Trans. Elect. Insul.*, EI-22:709-714, 1987.
- [48] N. Tohyama, Y. Tateno, H. Sato, and N. Shimizu. "Tree initiation in polyethylene absorbing helium gas." In *Proc. IEEE Int. Symp. El. Insul. (ISEI)*, 1995.
- [49] N. Shimizu and H. Tanaka. "Effect of liquid impregnation on electrical tree initiation in xlp." *IEEE Trans. Dielect. Elect. Insul.*, 8:239-243, 2001.
- [50] S. Boggs and J. Kuang. "High field effects in solid dielectrics." *IEEE Electric. Insul. Mag.*, 14:5-12, 1998.
- [51] S. Boggs. "Very high field phenomena in dielectrics." *IEEE Trans. Dielect. Elect. Insul.*, 12:929-938, 2005.
- [52] G. Teyssedre and C. Laurent. "Charge transport modeling in insulating polymers: from molecular to macroscopic scale." *IEEE Trans. Dielect. Elect. Insul.*, 12:857-875, 2005.
- [53] G. Ungar and X. Zeng. "Learning polymer crystallization with the aid of linear, branched and cyclic model compounds." *Chem. Rev.*, 101:4157-4188, 2001.
- [54] W. F. Schmidt. "Charge carrier energetics and dynamics in nonpolar liquids." *Nucl. Instr. Meth. A*, A327:83-86, 1993.
- [55] H. S. Smalø, Ø. L. Hestad, S. Ingebrigtsen, and P.-O. Åstrand. "Field dependence on the molecular ionization potential and excitation energies compared to conductivity models for insulation materials at high electrical fields." Submitted.
- [56] *Handbook on Chemistry and Physics*. CRC Press, 84th edition, 2004.
- [57] Y. Cao, G. G. Jiang, and S. Boggs. "Guarded needle for "charge injection" measurement." *Rev. Sci. Instr.*, 73:3012-3017, 2002.

- [58] N. J. Felici. "Blazing a fiery trail with the hounds." *IEEE Trans. Elect. Insul.*, 23:497-503, 1988.



Øystein L. Hestad was born in Mo I Rana, Norway in 1978. He received the M.Sc. degree in physics at the Norwegian university of science and technology in 2003. From 2003 to 2006 he worked at SINTEF Energy Research. He is presently pursuing his Ph.D. in physical chemistry at the Norwegian University of Science and Technology.



Stian Ingebrigtsen, Ph.D., was born in Bergen, Norway in 1978. He received his M.Sc. degree in physics in 2002 and his Ph.D. degree in chemistry in 2008, both from the Norwegian University of Science and Technology (NTNU), Trondheim, Norway. Since 2002 he has worked with SINTEF Energy Research in Trondheim. His research interests include dielectric performance of materials for electrical insulation purposes.



Hans Sverre Smalø was born in 1978 in and grew up in Trondheim, Norway. In 2002 he obtained his M.Sc. degree in physics at the Norwegian University of Technology (NTNU) in Trondheim. He is currently a Ph.D. student in the Department of Chemistry at NTNU, and is working with computational chemistry and molecular modelling.



Per-Olof Åstrand, was born in Sättila, Sweden in 1965. He is Professor in theoretical chemistry at the Department of Chemistry, Norwegian University of Science and Technology, Trondheim, Norway. He received the Ph.D. degree at the University of Lund in 1995 with Prof. Gunnar Karlström as the thesis supervisor, and he spent seven years in Denmark at Aarhus University, University of Copenhagen and Risø National Laboratory before he moved to Norway in 2002. His research interests include the construction of molecular mechanics models for intermolecular forces, reactive force fields and optical properties, with applications in optics, nanoscience, catalysis and electrical breakdown of dielectric liquids.



Lars E. Lundgaard was born in Copenhagen, Denmark on 24 May 1952. He took his M.Sc in power electric engineering at The Norwegian Institute of Technology in 1976. Since 1980 he has worked with SINTEF Energy Research. He is working on material science for electric power apparatus, relating to design, diagnostics and maintenance. He is also working on electro-separation of water-oil emulsions. His main experiences are in the field of GIS and transformer insulation. He is active within SC D1 in CIGRÉ.

Paper 4

**Field dependence on the molecular ionization potential and
excitation energies compared to conductivity models for
insulation materials at high electrical fields**

H. S. Smalø, Ø. L. Hestad, S. Ingebrigtsen and P.-O. Åstrand

Submitted to *J. Appl. Phys.*

Field dependence on the molecular ionization potential and excitation energies compared to conductivity models for insulation materials at high electrical fields

Hans S. Smalø¹, Øystein Hestad¹, Stian Ingebrigtsen² and Per-Olof Åstrand¹ *

¹ *Department of Chemistry, Norwegian University of Science and Technology (NTNU), N-7491 Trondheim, Norway and*

² *Department of Electric Power Technology, SINTEF Energy Research, N-7465 Trondheim, Norway*

Abstract

The aim of this study is to improve the understanding of high-field phenomena (such as pre-inception currents/conduction, streamer initiation and propagation) in insulating materials in terms of the molecular properties of the substances involved. In high electric fields, ionization is a likely process, and in all such processes, the ionization potential is an important parameter. A fundamental question is how these processes depend on the electric field, and therefore, based on the interaction between a negative point charge and a molecular cation as modelled by density functional theory, a field-dependent model for the ionization potential is developed. In addition, the first excitation energies as a function of the electric field are calculated using time-dependent density functional theory.

It is demonstrated that empirical high-field conduction models for cyclohexane and *n*-tridecane can be explained in terms of the difference between the ionization potential and the first excitation energy. It is also suggested that the reduction of the ionization potential with electric fields, can help explain how fast-mode streamers propagate.

* Corresponding author: per-olof.aastrand@chem.ntnu.no

I. INTRODUCTION

Pre-breakdown phenomena in liquids and solids have been studied extensively during the last decades to gain insight into the processes responsible for breakdown in dielectric media as a result of high applied voltage. A thorough investigation of pre-breakdown phenomena in cyclohexane and *n*-tridecane stressed by a fast transient in a highly divergent field has been reported.¹⁻⁸ With increasing applied voltage, the measured current-voltage characteristics go through three stages⁸:

- Slow increase in recorded current with applied voltage. This is caused by increased conductivity in the high-field region (average currents are in the range up to 1 μA).
- Large increase in current at a threshold voltage. The average current increases to several μA during the formation of a low density region (streamer/electrical tree). This is observed as steps in the charge recordings and a low density/vaporized region can be seen in the liquid phase. For a frozen phase an electrical tree starts to grow in the high-field region, causing lasting damage to the insulation.
- As the voltage is increased further the streamer/electrical tree grows until it traverses the electrode gap at a sufficiently high voltage. This may result in breakdown, resulting in a large step in the recorded current.

This is a simplified description of the phenomena. The conduction current recorded below inception of streamer/electrical trees goes through many stages and the streamer/electrical trees have been observed to go through several stages/modes as well.^{4,9} For a more thorough discussion of the pre-breakdown phenomena in liquids and solids, the reader is referred to several review papers on the two topics.⁹⁻¹¹ In this paper, we focus on the currents recorded below the threshold for inception of electrical trees/streamers in the material. These currents are typically referred to as ‘pre-inception currents’, and can be compared to transient nonlinear finite element method (FEM) simulations based on high-field conduction models.^{8,11}

A high electric field induces an increased conductivity which may be caused by^{9,12}:

- Increased charge carrier density due to injection of charge from the electrodes in an experimental setup.

- Dissociation of molecules into molecular fragments
- Ionization of molecules creating ion-electron pairs.
- Increased charge mobility.
- Increased ion mobility in a liquid due to electrohydrodynamic (EHD) motion.

The field and temperature-dependent conductivity is important, since the high-field conductivity determines the electric-field distribution and the amount of energy dissipated in the material due to joule heating.¹¹ Four important high-field conductivity models are given in Table I, where the two first (Schottky and Fowler-Nordheim) describe charge injection from the electrode, and the last two (Hopping conduction and Poole-Frenkel) describe the high-field conductivity in the bulk material. These mechanisms are all based on the lowering of the potential barrier localizing the charge due to an external electric field. If a sufficiently high electric field is applied, the charge can either climb the reduced barrier by thermal excitation (Schottky and Poole-Frenkel) or tunnel through the barrier (Fowler-Nordheim and Hopping conduction).¹²⁻¹⁷

The focus of this paper is mainly on the calculation of the ionization potential, IP, of molecules subjected to a high background field, which is used to interpret current measurements in cyclohexane and *n*-tridecane. The hypothesis is that electrons/holes are the main charge carriers in dielectrics stressed by fast transients (ions are too slow to contribute significantly during the first microseconds). The electrons are localized in molecules prior to the application of the step voltage, and the increase in free electron concentration depends on how much the escape barrier, i.e. the IP, is lowered.

The IP of a molecule *A* is defined as the energy to remove an electron and create a cation A^+ ,



where U_A is the energy of molecule *A* and U_{A^+} is the energy of its cation. Quantum chemistry provides molecular properties (polarizability, dipole moment, excitation energies, ionization potential, etc.) with good accuracy, and through advances in methodology and computer power, quantum chemistry can be used for increasingly larger systems. Density functional theory (DFT) has been used to calculate the IP accurately.¹⁸⁻²⁰ Earlier work,^{21,22} demonstrated how quantum chemistry can be used to calculate the IP, and how the IP is important

Table I. Conductivity models with charge injection from electrodes/bulk

Name	Equation ^a	Ref.
Schottky injection	$J(E) = \frac{4\pi emk_B^2(1-R)T^2}{h^3} \cdot e^{-\frac{\Phi}{k_B T}} \cdot e^{\frac{e}{2k_B T} \sqrt{\frac{eE}{\pi\epsilon_0\epsilon_r}}}$	12,14,15
Fowler-Nordheim	$J(E) = \frac{e^3 E^2}{8\pi h \phi} \cdot e^{-\frac{4}{3} \sqrt{\frac{2m}{h^2}} \frac{\phi^{3/2}}{eE}}$	12
Hopping conduction	$\sigma(E) = \frac{2\nu a e n}{E} \cdot e^{-\frac{W}{k_B T}} \cdot \sinh\left(\frac{eEa}{2k_B T}\right)$	17
Poole-Frenkel	$\sigma(E) = \sqrt{N_{eff} N_D} e \mu \cdot e^{-\frac{\Phi}{2k_B T}} \cdot e^{\frac{e^{3/2} \sqrt{E}}{\sqrt{4\pi\epsilon_0\epsilon_r k_B T}}}$	12,14,15

^a ϵ_0 is the permittivity of vacuum, ϵ_r is the relative permittivity, μ is the charge carrier mobility, ν is the escape frequency, ϕ is the work function, Φ is the barrier height, a is the distance between traps, E is the electric field, e is the elementary charge, h is Planck's constant, k_B is Boltzmann's constant, m is the electron mass, n is the charge carrier density, N_{eff} is the effective density of states in the conduction band, N_D is the number of potential donors, R is the reflection coefficient, T is the temperature, and W is the trap depth.

for interpreting streamer propagation. However, if the molecule is in an external electric field, the definition of the IP given in Eq. (1) is problematic since the energy of an ion in an electric field is dependent on the choice of origin. Intuitively, a high external electric field should make ionization processes easier, and thus the effect of the external field cannot be neglected. In this paper, the IP is obtained so that it becomes a useful descriptor when the field is different from zero, while Eq. (1) is retained in the limit of zero field. DFT is used to calculate the field dependence of the IP for a few molecules, such as cyclohexane and n -tridecane.

The paper is divided into six sections (including this introduction). The next section describes the theoretical foundation for the quantum chemical calculations of the IP and excitation energies when molecules are placed in a high background field. The theory section includes a discussion of how microscopic properties can be linked to conduction models. The third section describes ionization mechanisms. Section four contains the results obtained from the DFT calculations (IP, excitation energies and ground state energies). Section five presents a brief discussion which links the results obtained from DFT with experimental measurements of high-field conduction currents. Finally a conclusion is given.

In this work, atomic units²³ are used in the theory section while eV is used for energies and MV/cm is used for electric fields in the section with the results. It is also noted that the terms *high* and *low* electric fields always depend on a reference field. Intermolecular fields can be an order of magnitude greater than any macroscopic field. Thus even *extremely high* electric fields ($100 MV/cm$) may be small compared to intermolecular fields.

II. THEORY

A. Classical system

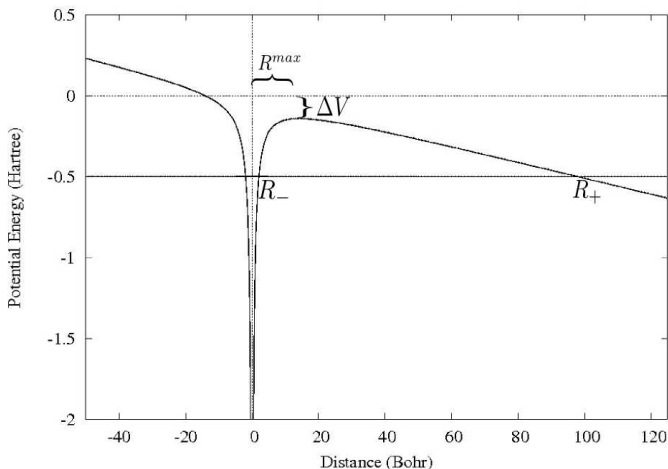


Figure 1. The Coulomb potential energy in an electric field, $E=0.005$ au, and ground-state energy of the hydrogen atom. In this illustration, the classical turning points, R_{\pm} , the distance to the maximum potential, R^{max} , and the maximum potential, $V_e^{max} = \Delta V$, are indicated.

In high electric fields, free electrons can be created by ionization.

A simple quantum-mechanical (QM) system, the hydrogen atom, is considered in the following. In a negative homogeneous external electric field, $-E$, the one-electron potential energy, V_e (illustrated in Figure 1) is

$$V_e = -\frac{1}{|R_e|} - ER_e \quad (2)$$

where R_e is the position of the electron relative to the proton (not distance since the potential is not symmetric about the origin). In this work, we assume that the main effect of the field

is described by a simplified one-dimensional problem along the electric field. This potential has a maximum at

$$R_e^{max} = 1/\sqrt{E} , \quad (3)$$

and an electron is bound to the proton only when the total energy of the electron ε_e is less than the potential at the maximum, V_e^{max} . When $E \rightarrow 0$, $R_e^{max} \rightarrow \infty$ and $V_e^{max} \rightarrow 0$. Thus without an electric field the electron is free when $\varepsilon_e \geq 0$. However, when $E \neq 0$, the maximum potential is decreased as

$$V_e^{max} = -\Delta V = -2\sqrt{E} \quad (4)$$

and thus if ε_e is larger than V_e^{max} , the electron is no longer bound by the hydrogen atom. This is true both when the electron is treated quantum mechanically and classically. Eq. (4) represents a reduction of the potential barrier which can release an electron from the hydrogen atom.

A conduction mechanism based on Eq. (4) is the classical Poole-Frenkel mechanism. The barrier between donors is lowered by the external electrical field, thus increasing the number of free charge carriers in the dielectric which increases the conductivity of the material.¹² This mechanism applies to materials with wide band gaps that contain charge donors and/or acceptors. These charge donors and acceptors should require more energy than what is generally available in order to be ionized. In complex materials (i.e. polymers) regions of high or low electronegativity can be created at chemical or physical defects in the material where electrons can be more easily ionized or captured, and these regions will then act as electron donors or acceptors.^{12,16}

If one assumes that the source of free electrons are molecules with $IP = IP_0$ at zero field the classical Poole-Frenkel equation is,¹²

$$\sigma(E) = \sqrt{N_{eff}N_d} \cdot \mu \cdot e^{-\frac{IP_0}{2k_B T}} \cdot e^{-\frac{\sqrt{E}}{k_B T \sqrt{\epsilon_r}}} \quad (5)$$

where N_{eff} is the effective density of states in the conduction band, N_d is the number density of donors (molecules), μ is the mobility of free electrons, and ϵ_r is the relative permittivity of the material. Eq. (5) assumes that only free electrons contribute to the conductivity. One could also envisage that bound electrons in a molecule can tunnel through the barrier to a neighbouring ionized molecule leaving behind an ionized molecule at the previous location. This is termed hole conduction and also contributes to the overall conductivity.¹³ If

one assumes that the mobility of the holes is not field dependent, this contribution to the conductivity can be included in the constant preceding the exponential function in Eq. (5) since the number of holes will be equal to the number of free electrons.

The Poole-Frenkel mechanism assumes that the source of electrons is the bulk material. In a similar mechanism, Schottky injection, the source of electrons is a metal electrode.¹² To a first approximation, the barrier that electrons need to overcome to enter the dielectric can be estimated by the electrostatic attraction between the electron and the electrode, and the contribution from the work function of the metal is thus neglected. The electrostatic attraction can be calculated using the image charge method, and the resulting potential barrier as a function of the distance from the electrode as augmented by the external electric field is given by,¹²

$$V_e = -\frac{1}{4 \cdot |R_e| \epsilon_r} - ER_e \quad (6)$$

Based on a similar analysis as for the Poole-Frenkel model, the current density at the electrode surface as a function of the applied field is¹²

$$J = 4\pi k_B^2 (1 - R) T^2 \cdot e^{-\frac{\Phi}{k_B T}} \cdot e^{\frac{\sqrt{E}}{k_B T \sqrt{\epsilon_r}}}, \quad (7)$$

where R is the proportion of electrons which are reflected by the surface of the metal, Φ is the barrier height in the absence of a field, and T is the temperature. Distinguishing between currents caused by the Poole-Frenkel mechanism or Schottky injection is generally difficult, since both are exponential functions which depend on the square root of the field.

Several other conductivity mechanisms giving similar field dependence as the Poole-Frenkel mechanism have been proposed,^{24,25} as phonon assisted tunnelling²⁶ and the Onsager mechanism.²⁷ For the Onsager mechanism, as for the Poole-Frenkel model, the field dependence stems from the lowering of the Coulomb potential between localized electrons/charges by the external field as in Eq. (4). However the phonon assisted tunnelling model is more involved, since the traps are modelled as dipoles/induced dipoles, and the energetic and spatial distribution of such traps govern the field-dependent mobility.²⁶ The field dependence of the IP will be important for the Onsager and Poole-Frenkel models, while phonon assisted tunnelling is a pure mobility model that does not require ionization of molecules/traps (it explains the field dependent conductivity by a field dependent mobility, not by creation of more free charge).

B. Quantum mechanical system

In a hydrogen atom, the lowering of the barrier by an electric field is given by Eq. (4), which is here regarded as a model system for a many-electron system. If the system can be simplified in analogy to the Hartree approximation²⁸ as an effective one-electron potential for the escaping electron, the electron may escape from the molecule if the energy is above the maximum of this effective one-electron potential. Here, the exchange between the escaping electron and the rest of the electrons is neglected, and the escaping electron is regarded as a negative point charge and not a charge distribution. We assume that

$$U_{A^++e^-} = U_{A^+} + V_e \quad (8)$$

such that the one-electron potential V_e (see Figure 1) at position R_e can be calculated from the interaction energy between a negative point charge, e^- , placed at R_e and a cation A^+ . Since the total system ($A^+ + e^-$) is electrically neutral, the energy in an electric field for the combined system is origin independent. If the electric field is small, R_e^{max} is relatively large such that exchange effects are small. For typical fields (below some tens of MV/cm), a model in terms of effective local one-electron potentials should be a good approximation since for example $R_e^{max} \approx 7\text{\AA}$ for $E = 30\text{MV/cm}$ using Eq. (3). The difference between this QM approach and the classical approach is caused by two effects, a molecular ion is not a point charge, and secondly a molecular ion may be polarized both by the external electric field and by the ionized electron.

In this model, the IP is given as

$$IP = U_{A^++e^-}^* - U_A \quad (9)$$

where $U_{A^++e^-}^*$ is the total energy of the combined system $A^+ + e^-$ at R_e^{max} . A three-dimensional potential is more complicated since the electron has many possible escape paths. The most probable path is in general not a straight line, and $U_{A^++e^-}^*$ is a first-order saddle point defined by the maximum of the energy along the simplest escape path. In the present work, only the distance between the point charge and the cation was varied, and a three dimensional search to find $U_{A^++e^-}^*$ was not carried out. This is reasonable since the energy $U_{A^++e^-}$ depends mostly on the distance between A^+ and the point charge along the field direction. At separation distances close to R_e^{max} , the potential is necessarily relatively flat

since $dU/dR \approx 0$, and it is thus not critical to find R_e^{max} with high accuracy. The point charge was placed a certain distance along the direction of the field from a given atom chosen more or less at random (test calculations showed that which atom the electron was pulled out of had little influence on the results). For the smallest fields, $E = 0.001$ au = 5.14 MV/cm a maximum was generally found between 10 Å and 20 Å from the closest atom, while for the largest fields, $E = 0.02$ au = 102.8 MV/cm a similar maximum was found between 1.5 Å and 4 Å from the closest atom. The main objective of this study is to calculate the IP as a function of electric field using Eq. (9), and then compare it to the classical results in Eq. (4) to see if the field dependence of the IP can be used to aid in the interpretation of experimental results.

For the DFT calculations the BLYP^{29,30} functional with the augmented TZP basis set^{31,32} was used. All calculations were carried out using the ADF software package,^{33,34} and the geometries was obtained from a geomtry optimization of the neutral molecules in gas phase. The calculations on the cation were carried out using both the restricted and unrestricted open-shell method. However, only results for the unrestricted open-shell method are presented since the difference between the results of the two methods is small. On a practical note, the interaction energy between the point charges and the external electric field is not included in the energy obtained in ADF and this energy contribution has to be added manually.

To study the effect of the electric field on the neutral molecule in greater detail, excitation energies as a function of electric field were calculated using time-dependent density functional theory^{35,36} (TD-DFT) with the same functional and basis set. For these calculations, especially for the high electric fields, a further augmentation of the basis set might have been beneficial, since some excited states may be relatively diffuse, especially in an external electric field. Furthermore, it is noted that TD-DFT is regarded to give accurate excitation energies as long as the excitation is characterized as local, however for charge-transfer states (which are biradical), or Rydberg states (the excited state is very diffuse) large errors may be obtained for many of the contemporary functionals.^{37,38} However, only the lowest singlet-singlet excitation energy whose accuracy is relatively unproblematic is included here.

C. Effect of a dielectric medium

All calculations in this work were done in the gas phase, however the corresponding experiments have been carried out in the liquid phase,⁸ and thus a central question is how gas-phase calculations can be compared to relevant experiments. Representing the medium by a dielectric continuum, the Clausius-Mossotti equation gives the relation between the local field E_L felt by an atom/molecule in a spherical cavity and the average macroscopic field E_M as³⁹

$$E_L = \frac{\epsilon_r + 2}{3} E_M . \quad (10)$$

The relative permittivity, ϵ_r of cyclohexane, *n*-tridecane and other non-polar liquids are typically around 2, and thus $E_L \approx 1.3E_M$. The local field felt by a single molecule is therefore similar to the macroscopic field in an experimental setup. However, using $R_e^{max} = 1/\sqrt{E}$ one obtains $R_e^{max} \approx 7 \text{ \AA}$ at $E = 0.005 \text{ au} \approx 25 \text{ MV/cm}$. Thus, with this model, the escaping electron may be far into the medium before it is released from the attractive potential from the positive ion. Therefore it is not only the local field inside the cavity that is important, but also the field outside. Outside the cavity the medium will screen the cation and thus the escaping electron will feel a smaller field from the cation. Classically in a medium, the reduction of the potential barrier is given by¹²

$$\Delta V = -2\sqrt{\frac{E}{\epsilon_r}} \quad (11)$$

which reduces the IP by a factor of $\sqrt{\epsilon_r}$ in the medium compared to in vacuum (Eq. (4)). Furthermore, by using the polarizable continuum model (PCM) without an electric field, it is found that liquid cyclohexane ($\epsilon_r \approx 2$), reduces the IP by about 1 eV for a large number of molecules.²²

So, on one hand, without the presence of an electric field, a liquid/solid medium decreases the IP, but on the other hand the electric field reduces the IP less in a medium. The total effect of the medium is not clear and therefore the results of the calculations should only be compared qualitatively with experimental result.

III. IONIZATION MECHANISMS

For a hydrogen atom in the gas phase, the classical result in Eq. (4) gives

$$IP = IP_0 - 2 \frac{e^2}{4\pi\epsilon_0\alpha_0} \sqrt{\frac{4\pi\epsilon_0\alpha_0^2 E}{e}} \quad (12)$$

where α_0 is the Bohr radius which is 1 in atomic units. In Eq. (12) the square root is dimensionless and independent of the set of units used. The prefactor is a pure energy term, and it is easy to transform between the different units used. Experimental evidence for a field dependence like the one in Eq. (12) have been reported.^{40,41}

The IP is important for all ionization mechanisms, which can be grouped into three main categories, impact ionization, photoionization and field ionization. All are used to explain the various conductivity and streamer propagation mechanisms. Streamers are assumed to have 4 modes of propagation,⁴² and different mechanism dominate for the various modes. For example photoionization is believed mainly to be connected to the 4th mode streamers (fast event) but could be of importance also for 2nd and 3rd mode streamers.⁴³

A. Impact ionization

Impact ionization is given by the following reaction



For this process to occur, the energy of the incoming electron must be higher than the IP of the molecule. If the IP is high compared to the typical electron energy, the energy of the electrons will be the limiting factor. Thus the probability for such a process to occur can be modelled as being proportional to the number of electrons with energy above the IP,²¹

$$\int_{IP}^{\infty} f_e(\varepsilon) d\varepsilon \quad (14)$$

where f_e is the energy distribution of the electrons. The field dependence of the IP can be estimated by Eq. (4), but to find the field dependence of impact ionization, the field dependence of f_e is also needed, which in general is unknown.

An important type of discharge in gases based on impact ionization is the Townsend discharge,^{44,45} which is often used to explain discharges in voids in solid insulation.¹² If

a free electron on average creates more than one new free electron before it releases its energy and is localized, an electron avalanche may be created. Such a mechanism depends on a relatively long mean-free path so that free electrons (accelerated by the electric field) gain sufficient kinetic energy before they collide with a molecule that is ionized by impact ionization. For the discharge to be self-sustained, each electron avalanche must create at least one new avalanche through some form of feedback mechanism. Electron avalanches in condensed phase is controversial due to the higher medium density, and thus lower mean-free path for electrons.¹ Even so, experimental results with negative polarity in cyclohexane under impulse and DC voltage suggests that the onset of streamers in the liquid is caused by an electron avalanche in the liquid phase.^{3,46}

B. Photoionization

In photoionization, a single photon is absorbed by a molecule and an electron is released,



This process requires a photon with energy $h\nu$, equal to or higher than the IP of the molecule. If $h\nu$ is higher than the IP of the molecule, the energy conservation may be obtained by either giving the ionized electron more kinetic energy, by allowing the molecule to emit a photon with lower energy, $h\nu'$ or by leaving the cation in an excited state.

Streamers are observed to emit a large amount of visible light,⁴³ and therefore it is reasonable to assume that the typical photon energies emitted are in the visible light spectrum, which is between 1.8 and 3.1 eV. On the other hand, the IP of typical molecules used as electric insulation materials is of the order 10 eV.²² However, if the molecule interacts with a high electric field in addition to a single high-energetic photon, the IP is predicted to fall according to Eq. (12). Thus, for sufficiently strong electric fields, photoionization is plausible, and it has been speculated that photoionization might be responsible for the fast-mode streamer propagation.⁴³

For atomic systems, with nonrelativistic energies and without an electric field, the photoionization differential cross-section σ , per unit solid angle, Ω is⁴⁷

$$\frac{d\sigma}{d\Omega} \propto \sin^2 \theta_e \quad (16)$$

where θ_e is the angle between the direction of the photon and the emitted electron. The electron is most probably emitted at an angle around $\theta_e \approx 90^\circ$, which is reasonable since the electric field of an electromagnetic wave is perpendicular to the propagation direction. To find the total ionization cross-section, Eq. (16) is integrated over all angles. However, if a permanent external electric field is applied to the system in addition to an electromagnetic wave, there is only a limited angle which is classically available for ionization (i.e. angles where the kinetic energy of the escaping electron is above the maximum potential in that direction), and it can be assumed that only these angles contribute to ionization. Integrating Eq. (16) over the classically available angles could thus serve as a simplified model for atomic photoionization in the presence of an electric field. The size of the classically available area depends on the energy of the photon, while in what region it lies depends on the direction of the photon compared to the direction of the static electric field. If the photon and the static electric field is parallel, the classically available angles are around $\theta_e = 0^\circ$, while if the photon and the static electric field is perpendicular, the classical available angle is around $\theta_e = 90^\circ$. Thus, one could expect that photoionization is more effective if the external electric field is perpendicular to the photon. This is also reasonable from a classical point of view since in this case the static and the time dependent electric fields are parallel. Streamers are observed as tree structures with various degree of branching, depending on the liquid in which they propagate as well as electrochemical additives in the base liquid.^{9,48,49} The angle dependence of photoionization may be important to understand the highly branched structures often observed at high voltages where several of the branches propagate in directions deviating from the direction of the external field. Such branching has been shown to be enhanced by low IP additives in cyclohexane.⁴⁹

C. Field ionization

The third fundamental mechanism, field ionization, is dependent on tunnelling.¹³ It is therefore of interest to study tunnelling with a Coulomb potential in an external electric field. In contrast to impact ionization, which requires the knowledge of the electron energy distribution, $f_e(\varepsilon)$, tunnelling is only dependent on the local electric field and therefore easier to model.

In an electric field, the tunnelling probability, τ , from an electrode has been found to

follow^{12,50}

$$\ln \tau \propto \frac{1}{E} \quad (17)$$

both theoretically and experimentally. Eq. (17) assumes that the work function, or potential barrier height is independent of the electric field, but the width of the barrier is reduced when the field increases. This has been found to be a good approximation for removing electrons from metals, field emission, at high fields (20 MV/cm).⁴⁶ Therefore, if the charge carriers are dominated by electrons donated from a negative electrode, a tunnelling mechanism given by Eq. (17) may describe the conductivity as found for very sharp tips.⁴⁶ This mechanism is termed Fowler-Nordheim injection, and is observed for negative electrodes where electrons can tunnel through the barrier and into the dielectric. For positive electrodes a similar phenomena can occur where electrons can tunnel from the liquid to the metal.¹³

However if the barrier height depends on the field, a different field dependence is obtained. Let the potential be given by Eq. (2), ε_i be the energy of the electron in state i , and ψ_i be the corresponding wavefunction. The tunnelling probability τ is proportional to²⁸

$$\tau \propto \frac{\psi_i(R_-)}{\psi_i(R_+)} \quad (18)$$

where R_{\pm} are the points where the energy of the electron ε_i is equal to the potential $V(R)$ (Figure 1). For the hydrogen atom $\varepsilon_0 = -1/2$ hartree, and the classical turning points is given when $V(R_{\pm}) = \varepsilon_i$. When the field is assumed to be small ($E \ll \varepsilon_i$), the classical turning points are given by

$$R_+ = -1/\varepsilon_i \quad (19)$$

and

$$R_- = -\varepsilon_i/E - 1/\varepsilon_i \quad (20)$$

The tunnelling probability as a function of the electric field may be analyzed using the Wentzel-Kramers-Brillouin (WKB) approximation, and the WKB wavefunction is given by²⁸

$$\psi_i(R) = \frac{B_{\pm}}{(\varepsilon_i - V_e(R))^{1/4}} e^{\pm \int \sqrt{2(V_e(R) - \varepsilon_i)} dR} \quad (21)$$

where B_{\pm} are constants. Since the wavefunction before tunnelling is assumed to be close to the stationary solution, B_+ is zero and only B_- is considered. The solution with B_+ could be interpreted as important for tunnelling probability into the atom, i.e. the recombination of electrons and positive charged ions. Here we focus on tunnelling out of the Coulomb

barrier, representing a field ionization of a neutral molecule in gas phase, where the electron tunnels out into vacuum.

Exactly at the classical turning points, $R = R_{\pm}$, the WKB wavefunction has a problem as the prefactor has a singularity at $R = R_{\pm}$. However, the divergence disappears for $\psi_i(R_-)/\psi_i(R_+)$

$$\frac{\psi_i(R_-)}{\psi_i(R_+)} = \exp\left(-\int_{R_+}^{R_-} \sqrt{2(V_e(R) - \varepsilon_i)} dR\right) \quad (22)$$

As an approximation, the integral is proportional to the length given by $R_- - R_+ = \varepsilon_i/E$, and multiplied by the height given by the maximum of $\sqrt{V_e(R) - \varepsilon_i}$. If this maximum is field independent, the field dependence of the tunnelling probability is given by Eq. (17). However, for the Coulomb potential, $V_e^{max}(r) - \varepsilon_i = -\varepsilon_i - 2\sqrt{E}$, and assuming $\sqrt{E} \ll \varepsilon_i$

$$\int_{R_+}^{R_-} \sqrt{2(V_e(R) - \varepsilon_i)} dR \propto -\frac{\varepsilon_i}{E} \sqrt{-\varepsilon_i - 2\sqrt{E}} = \frac{(-\varepsilon_i)^{3/2}}{E} \left(1 - \frac{\sqrt{E}}{-\varepsilon_i} + \dots\right) \quad (23)$$

$$= \frac{(-\varepsilon_i)^{3/2}}{E} - \sqrt{\frac{-\varepsilon_i}{E}} + \dots \quad (24)$$

and thus the tunnelling probability, τ_i , given that the electron starts in the electronic state i is

$$\ln \tau_i = -C \left(\frac{(-\varepsilon_i)^{3/2}}{E} - \sqrt{\frac{-\varepsilon_i}{E}} \right) \quad (25)$$

where C is a constant. In very small electric fields the potential is triangular, and thus the first term should be equal to the term obtained from a triangular potential^{12,50}

$$\ln \tau_i = -\frac{4\sqrt{2}}{3} \frac{(-\varepsilon_i)^{3/2}}{E}. \quad (26)$$

Comparing Eqs (25) and (26) it is seen that $C = 4\sqrt{2}/3$. Another way of obtaining the same result is to assume that the shape of the potential is almost triangular for larger electric field, but the height is given by $\varepsilon_i - 2\sqrt{E}$. The field dependence of the tunnelling probability has also been found elsewhere.⁵⁰

Here it is important to note that $-\varepsilon_0$ can be interpreted as the IP at zero electric field (Koopmann's theorem) while $\varepsilon_0 - \varepsilon_1$ is the first excitation energy. Typically $|\varepsilon_1|$ is much smaller than $|\varepsilon_0|$ such that τ_1 is much larger than τ_0 .

1. Two-stage process

In ionization processes by strong low-frequency fields, a tunnelling mechanism may be dominating. However for the hydrogen atom, a pure tunnelling mechanism does not fit

with numerical solutions of the time-dependent Schrödinger equation, and it is indicated that an indirect tunnelling mechanism is important.^{51,52} This is in line with the fact that in conductivity models, two-stage processes are often adopted.¹² Thus, first the molecule is excited, then an electron is released by tunnelling. The total tunnelling probability τ can be modelled as

$$\tau = \sum_i f_i \tau_i \quad (27)$$

where f_i is the probability that the molecule is in excited state i , and τ_i is the probability to tunnel out of state i . The probabilities f_i can be modelled by a Boltzmann distribution

$$f_i = \frac{e^{\frac{-\varepsilon_i}{k_b T}}}{\sum e^{\frac{-\varepsilon_i}{k_b T}}} \quad (28)$$

However, these probabilities assume equilibrium, which, depending on the situation, may be questionable. Generally, electrons react faster to changes in for example electric field compared to the heavier protons. Therefore, in the presence of a time-dependent electric field (for example as a step-function), it may not be unreasonable to assume that the number of excited states f_i is far greater than the equilibrium value.

2. Hopping

A series of common conduction models for polymers and dielectrics are termed hopping conduction.^{12,17,53} The term hopping refers to a sudden displacement of a charge carrier from one localized site in the dielectric to another nearby site. This can occur either by thermal excitation of the carrier over the barrier or by tunnelling through the barrier between localized sites. In general, a combination is considered the most likely mechanism.¹² First the carrier is excited and then tunnels to a neighbouring site with the same energy level. Thus hopping is in some way a misleading name for this mechanism actually describing thermally assisted tunnelling between two sites, and not hopping over the energy barrier. Hopping is thus best used for the special case where the tunnelling between states can be neglected, and the charge carrier must actually jump over the potential barrier between the two sites/traps.

There are several different flavours of thermally assisted hopping conduction that includes tunnelling through the barrier, two of the most important being variable-range hopping⁵⁴

and the random free-energy barrier model.⁵⁵ Hopping is typically viewed as an increase in charge mobility with field, not the charge density as the charge is localized between each jump across the barriers. Thus the average speed/mobility of the carriers is increased with increased field but the average free charge density is not changed. The field dependence of the resulting mobility depends on the distribution of the traps in space and in energy, typically the mobility will increase exponentially with the square root of the field.^{24,25}

The hopping model given in Table I is based on hopping from one site to another site over a potential barrier lowered by the electric field. The model is only valid for a single trap depth and uniform distribution of the traps, and it assumes that tunnelling between traps can be neglected. This simple model results in a conductivity that increases exponentially with the field.²⁴

However these exponentially increasing mobilities are based on lowering of the barriers between two sites and that it is the crossing of these barriers that limits the mobility. If for example a cyclohexane cation is surrounded by neutral cyclohexane molecules, all neighbouring molecules are potential electron donors. Depending on the distance between the sites and the energy of the electron involved, there might be only a very small barrier or even not a barrier at all. In Figure 2, the potential barrier between two hydrogen atoms is compared to the ground state energy of the hydrogen atom for different separation distances. As seen from the figure, if the distance between two sites is too small, there is no barrier to cross and the mobility must be limited by other factors. Thus in these cases, the hole mobility does not necessarily increase exponentially with the electric field.

IV. RESULTS

Excitation energies and IPs were calculated for the following molecules: *n*-tridecane, cyclohexane, 2-propanol, *p*-diaminobenzene, benzene, *N,N*-dimethylaniline and tetracyanoethene. Benzene was added as a reference molecule, and *n*-tridecane was included because experiments on conduction currents in neat *n*-tridecane have been compared to conductivity models.⁸ The rest of the molecules, were chosen based on a previous experimental study on pre-breakdown phenomena in cyclohexane with additives.^{5,6,21} Cyclohexane is used as a model liquid for mineral oil, and additives with known electron scavenger properties or low IP were chosen as additives. It was found that the IP of the additives is an impor-

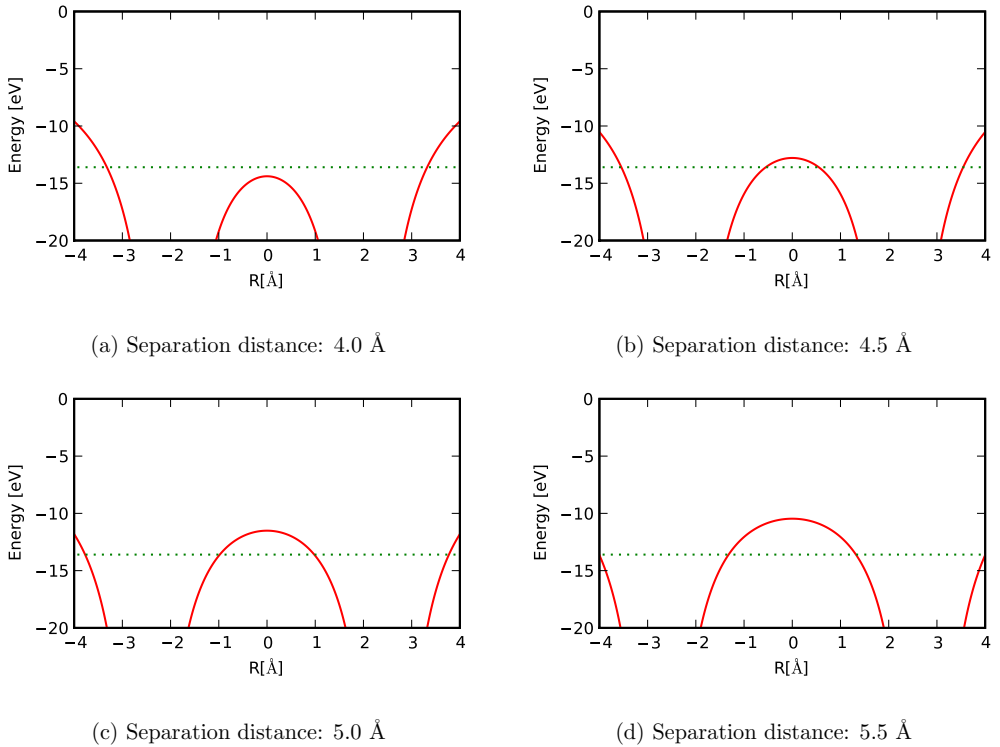
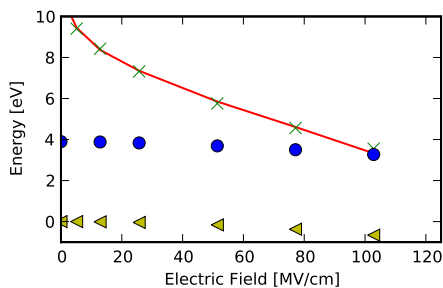


Figure 2. Potential (—) between two protons at different separation distance compared to the ground state of the hydrogen atom (\cdots) for different separation distances.

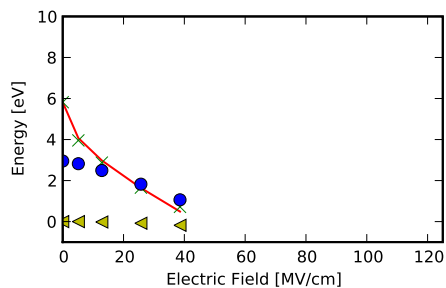
tant descriptor for the effect on pre-breakdown phenomena²¹. Based on the Poole-Frenkel mechanism and DFT calculations, it is possible, as is shown in this paper, to compare the experimental results directly to the results obtained from DFT calculations.

The results from the DFT calculations are summarized in Figures 3 and 4. The calculations show that the direction of the electric field is only of minor importance for these properties for most of the molecules (not shown in the figures). The direction of the electric field is therefore only specified in the cases where it was found to be of importance. The ground state energy of the molecules was not significantly altered by the electric field on this energy scale. This is illustrated in Figures 3(c), 4(c) and 4(d) which shows that the ground state energy is only a relatively weak function of the electric field even for polar molecules like 2-propanol and N,N-dimethylaniline.

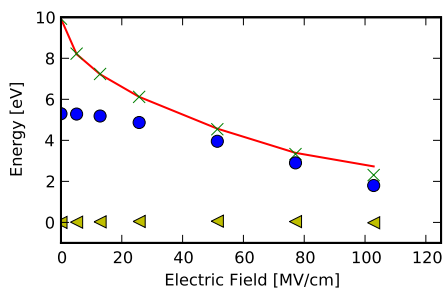
The first excitation energy changes very little with the electric field for weak fields



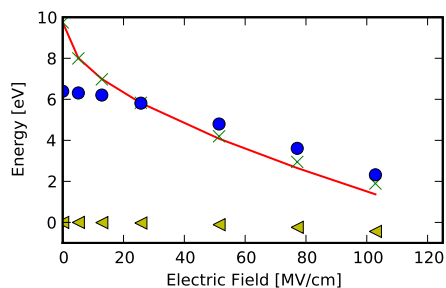
(a) Tetracyanoethene



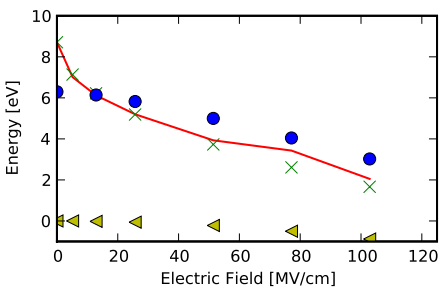
(b) p-diaminobenzene



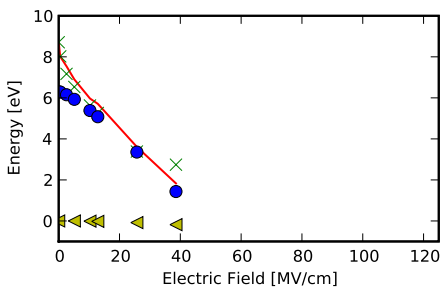
(c) 2-propanol



(d) Cyclohexane



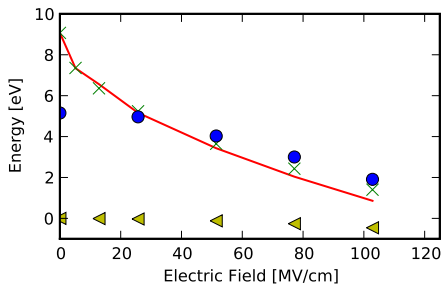
(e) *n*-Tridecane, Electric field perpendicular to chain



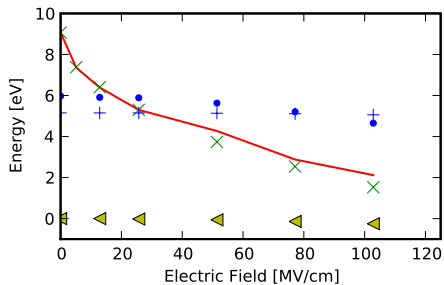
(f) *n*-Tridecane, Electric field parallel to the chain

Figure 3. Ground state energies (\triangleleft), lowest singlet-singlet excitation energies (\bullet), IP ($—$) and model IP given by Eq. (29) (\times), for different molecules.

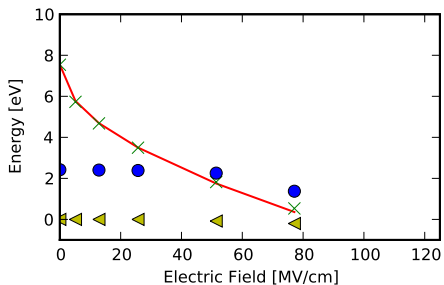
(<20 MV/cm) for all molecules included in the study except for *n*-tridecane. The IP on the other hand decreases rapidly even for a relatively small increase in the electric field for all molecules, and above a certain field it approaches the first excitation energy. When the field is increased further the IP and the first excitation energy falls at the same rate. The excita-



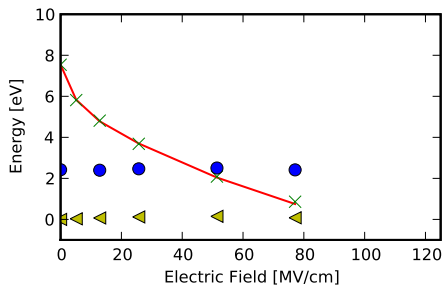
(a) Benzene, Electric field in-plane



(b) Benzene, Electric field out-of-plane



(c) N,N-dimethylaniline, Electric field in-plane



(d) N,N-dimethylaniline, Electric field out of plane

Figure 4. Ground state energies (◁), lowest singlet-singlet excitation energies (●), IP (—) and model IP given by Eq. (29) (×), for different molecules. In figure (b) the lowest excitation energies for two different symmetry groups (+ and ●) are presented.

tion energies for N,N-dimethylaniline and tetracyanoethene are low, but stays constant up to higher electric fields than for the other molecules. Thus larger electric fields are needed to decrease the IP to the first excitation energy (see Figures 3(a) and 4(c)).

It seems to be a general trend that above a certain field strength the first excitation energy as calculated by TD-DFT approaches the IP. Thus above this field the molecule can either be in its ground state or in a state with energy at or above the IP. The basis set used can in principle only describe bound states (states where the wavefunction far from the molecule decreases exponentially with distances). A description of free electrons, which are dependent on $\cos(kx)$ and $\sin(kx)$ functions, are not included in the basis set. Therefore, in theory the basis set limits TD-DFT to bound states only. In practice, however, the basis set may be able to approximate the behavior of a non-bound state locally around the molecule,

but what happens at large separations is unclear. Furthermore, an ionization can be viewed as an excitation to a delocalized state, and therefore the lowest excitation energy should be at the IP or lower. It has been exploited to calculate the IP by adding a very diffuse basis function in coupled-cluster response theory,⁵⁶ which is a reasonable approach without an external electric field. For a more detailed discussion on the behavior of TD-DFT at the ionization limit, see Ref 57.

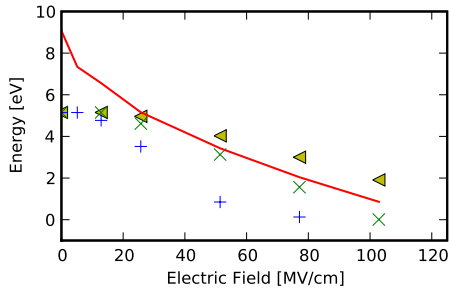
For the planar molecules in this study, the excitation energies are nearly independent of the electric field when the field points out of the plane, as exemplified in Figures 4(b) and 4(d) and above a certain electric field, the IP becomes lower than the first excitation energy. In Figure 5, the basis set dependence of the lowest excitation energies of benzene is shown. For the QZ3P-2D basis set, the excitation energies are always smaller than the IP, regardless of field direction. Thus, the reason for the constant excitation energies for planar molecules is a too small basis set to describe the out-of-plane orbitals.

However since the electric field gives an energy term linear in R_e , there exist a continuum of delocalized states with energy below the IP (see Figure 1) in addition to the continuum above the IP. Therefore, it is difficult to interpret the excitation energies for high fields when using the large basis sets (see Figure 5). Although in theory the same problem exist for low fields, it is of less importance, since the distance to R_+ (see Figure 1) is much higher and the *negative* continuum at large R may be ignored. All basis sets give approximately the same results for low fields (see Figure 5), and qualitatively the same basis set dependence is seen for cyclohexane and *n*-tridecane. Therefore, we restrict our discussion on the excitation energies to fields below 15 *MV/cm*. The IP on the other hand is trivial to interpret, and applying larger basis sets had small effects on the results.

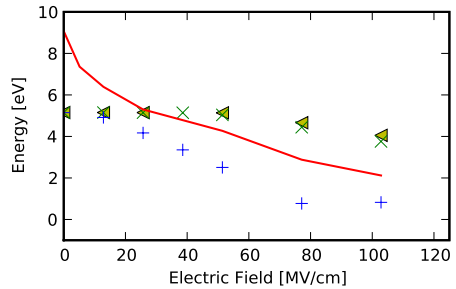
To validate the classical treatment of the IP in Eq. (12), the calculated IP is compared to,

$$IP = IP_0 - \beta_{PF} \sqrt{\gamma E} \quad (29)$$

where β_{PF} is treated as a parameter and $\gamma = 4\pi\epsilon_0\alpha_0^2/e$. Linear regression was used to fit the calculated IP to an IP of the form given in Eq. (29) for fields below 30 *MV/cm*. Above this field strength, larger deviations from the classical results are expected and when comparing to pre-inception currents,⁸ it is the behaviour below 30 *MV/cm* which is interesting. For all molecules, an IP of the form in Eq. (29) gives a good fit with an RMSD below 0.1 *eV*, and the value of β_{PF} is close to the classical result, see Table II. Neither the type of molecule nor



(a) Benzene, Electric field in-plane



(b) Benzene, Electric field out-of-plane

Figure 5. Basis set dependence of the excitation energy: IP using aug-TZP basis set (—), the lowest excitation energy using aug-TZP (\blacktriangle), QZ3P-1D (\times) and QZ3P-2D ($+$) basis set.³²

the direction of the field is important. This supports an assumption that the difference in IP between two different molecules does not depend on the electric field.²¹ Above 30 MV/cm , the fitted curve typically deviates only slightly from the calculated IP. Since these results are not included in the linear regression, it indicates that the classical result gives the main contribution even for relatively high fields. Thus, even for large fields the monopole is the dominating interaction term. For both n -tridecane and cyclohexane, $\epsilon_r \approx 2$, and so to compare these results with experiments, the fitted β_{PF} is divided by $\sqrt{\epsilon_r}$ in Table II, following Eq. (11).

For n -tridecane, unlike the other molecules studied here, the direction of the electric field is important. Two cases are presented here, one where the field is perpendicular to the chain and one where the field is parallel to the chain. If the electric field is perpendicular to the chain, n -tridecane behaves like the other molecules, see Figure 3 (e). The results obtained for an electric field parallel to the chain is more interesting, see Figure 3 (f). Here the excitation energy seems to approach zero at much lower fields than the other molecules. But also in this case, the IP approaches the first excitation energy for fields above 20 MV/cm .

n -tridecane also differs from the other molecules in terms of the β_{PF} coefficients in Table II. An electric field perpendicular to the n -tridecane molecule decreases the IP less than the other molecules, but an electric field parallel to n -tridecane decreases the IP more. In the latter case, it is also noted that an IP of the form Eq. (29) gives larger deviations, and thus the classical results is not a perfect approximation in this case. The main reason for these

Table II. Field dependence of IP

Molecule	$\beta_{PF}(eV)^a$	RMSD ^b (eV)	$\beta_{\epsilon_r=2}(eV)^c$
Classically	54.4	-	38.5
Cyclohexane ^d	53.8	0.05	38.0
<i>n</i> -Tridecane ^e	68.9	0.31	48.7
<i>n</i> -Tridecane ^f	49.8	0.09	35.2
Tetracyanoethene ^d	53.6	0.03	37.9
2-propanol ^d	54.4	0.01	38.4
N,N-dimethylaniline ^d	56.1	0.03	37.7
p-diaminobenzene ^d	54.5	0.06	38.5
Benzene ^d	54.0	0.07	38.1

^a Eq. (29)

^b Root mean square deviation (RMSD) between calculated IP and a model IP given in Eq. (29), for fields below 30 MV/cm

^c $\beta_{\epsilon_r=2} = \beta_{PF}/\sqrt{2}$

^d Averaged over the three different directions of the electric field

^e Electric field parallel to the chain

^f Electric field perpendicular to the chain

deviations is the results obtained for the two largest fields, where the IP approaches the excitation energies (Figure 3(f)). If omitting the two highest fields in the linear regression, $\beta_{PF} = 59.6 eV$ and an RMSD below 0.1 eV is obtained, which indicates that the classical results fits better for lower fields.

V. DISCUSSION

Based on symmetry arguments, a natural initial guess for the charge distribution in for example the cyclohexane cation, is to place the positive charge evenly among all carbon atoms. However, as Figure 6 shows, the reduction of the IP with the electric field would be too large for such a charge distribution compared to the IP obtained from a point charge and DFT. The IP would fall to zero at about 30 MV/cm , so that cyclohexane would ionize completely at such fields. Furthermore, Figure 7(a) shows that such a model fails to repro-

duce the interaction energy between a point charge and a cyclohexane cation. On the other hand, a model where only the closest carbon atom is charged, reproduces the interaction energy almost perfectly. A similar plot for *n*-tridecane (Figure 7(b)) shows slightly larger deviations for the one-charge model. However, even for *n*-tridecane, a one-charge model fits rather well. The IP in general fits a one-charge model, even for very high electric fields (see Figures 3 and 4 and Table II).

In quantum chemistry many models exist to obtain atomic charges, and many of them rely on a Mulliken-type of division of the charge distribution.⁵⁸ The calculated atomic charges in an electric field could not be used to verify Figures 6 and 7. For example, for cyclohexane these models give an unphysically large charge transfer between the carbon and hydrogen atoms. It has been noted repeatedly that Mulliken charges are highly dependent on the basis set used, see for example Ref 59.

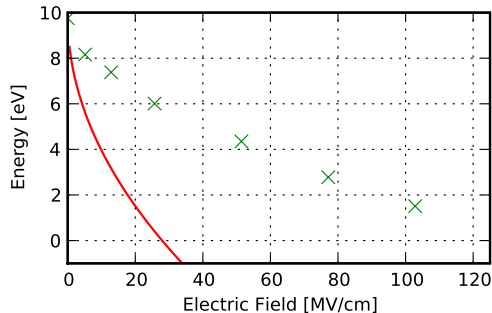


Figure 6. The reduction of IP in cyclohexane as a function of the electric field, both with respect to DFT data (\times) and with respect to a model where each carbon gets 1/6 charge (—)

Measurements of high-field conduction currents in cyclohexane have been compared to FEM simulations.⁸ The following conductivity model, based on Poole-Frenkel conductivity, was found to fit the experimental data (see Eq. (5)),

$$\sigma(E) = \sigma_0 \cdot e^{\frac{W}{k_B T}} \cdot e^{\frac{\beta_{PF} \sqrt{\gamma E}}{2k_B T}} \quad (30)$$

where $\sigma_0 = 1.3 \cdot 10^{-4} S/m$, $W = 0.47 eV$ is the thermal activation energy,⁶⁰ $\beta_{PF} = 40.7 eV$, and $\gamma = 1.9 \cdot 10^{-12} m/V$. The parameter β_{PF} and the constant γ are introduced in Eq. (29). The proposed high-field conductivity for cyclohexane based on experiments⁸ supports an IP of the form given in Eq. (29). There is a good agreement between β_{PF} found experimentally

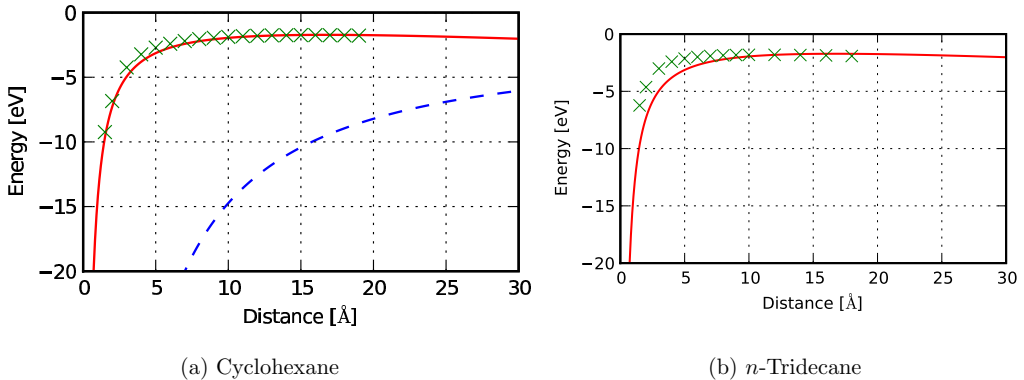


Figure 7. The potential energy between a point charge and a cyclohexane/*n*-tridecane cation in an electric field of $0.001 \text{ au} = 5.14 \text{ MV/cm}$, as a function of the distance between the point charge and the closest carbon atom, with respect to DFT data (\times), a one-charge potential ($-$) and for cyclohexane a model potential where each carbon atom get $1/6$ charge ($- -$). In (b) the field is parallel to the chain.

of $\beta_{PF} = 40.7 \text{ eV}$ and in calculations when the medium is taken into account by dividing the calculated value by $\sqrt{\epsilon_r}$. This suggest that the effect of a medium can be adequately modelled as a dielectric continuum, at least for relative small electric fields ($< 10 \text{ MV/cm}$). Thus, the reduction of the IP with increasing fields in liquid cyclohexane with $\epsilon_r \approx 2$, will be lower than in the gas phase.

FEM simulation using the following equations for conductivity,

$$\sigma(E) = \sigma_0 \cdot e^{\frac{\beta_{PF}\sqrt{\gamma E}}{2k_B T}} \quad (31)$$

and

$$\sigma(E) = \sigma_0 \cdot e^{\frac{\beta_{1/3}\sqrt[3]{\gamma E}}{2k_B T}} \quad (32)$$

where $\sigma_0 = 1.0 \cdot 10^{-12} \text{ S/m}$, $\beta_{PF} = 54.3 \text{ eV}$, $\beta_{1/3} = 12.4 \text{ eV}$, $\gamma = 1.9 \cdot 10^{-12} \text{ m/V}$, have been shown to give pre-inception currents that fits experimental results in neat *n*-tridecane with needle plane geometry (positive needle).⁸ Eq. (31) is similar to a Poole-Frenkel conductivity, but β_{PF} is somewhat high. It is interesting to note that the value for β_{PF} obtained from DFT calculations is also high compared to the classical result (see Table II). Thus the DFT calculations points in the same direction as the experimental results.

To our knowledge, Eq. (32) is not based on any known conductivity theory, but similar

field dependence for conductivity have previously been reported for polyethylene.⁶¹ Direct comparison of experimental charge recordings and the results from FEM simulations have shown that Eq. (32) fits the measured results better than Eq. (31).⁸ The direction of the electric field is important in *n*-tridecane since the IP is reduced more when the electric field is parallel to the chain than when the field is perpendicular to the chain. It is therefore assumed that the parallel component is more important when interpreting experimental data. The DFT results show that the main difference between *n*-tridecane and cyclohexane is in the way the excitation energy depends on the electric field for fields below 20 *MV/cm*. In cyclohexane, the excitation energy is almost constant up to such field strengths (see Figure 3(d)), while it is reduced even at lower fields in *n*-tridecane (see Figure 3(f)). This is probably, as discussed below, why a conductivity given by Eq. (32) fits better than a conductivity given by Eq. (31) for *n*-tridecane.

In order to explain the difference between the experimental conductivity for *n*-tridecane and cyclohexane the difference, Δ , between the first excitation energy, ε_1 , and the IP is examined,

$$\Delta(E) = IP(E) - \varepsilon_1(E) \quad (33)$$

Linear regression was used to compare two ansatzes for Δ ,

$$\Delta(E) = \Delta(0) - \beta_{PF}\sqrt{\gamma E} \quad (34)$$

and

$$\Delta(E) = \Delta(0) - \beta_{1/3}\sqrt[3]{\gamma E} \quad (35)$$

where $\Delta(0)$ is the energy difference between the first excitation energy and the IP at zero field, γ is given by Eq. (29), and β_{PF} and $\beta_{1/3}$ are pure energy terms. Fitting the two equations above to the DFT calculations is a way to find the energy terms that can be compared directly to the experimentally obtained conductivity models, $\beta_{1/3}$ in Eq. (32) and β_{PF} in Eqs. (31) and (30). For cyclohexane, ε_1 does not depend on the electric field for fields below 30 *MV/cm*. Thus results obtained from linear regression compared to the IP, and compared to Δ would give the same field dependence, and thus the same value for β_{PF} (Table II).

The result for *n*-tridecane, see Figure 8, is interesting as it gives a different dependence on electrical field than what was found for cyclohexane. For *n*-tridecane, a Δ as in Eq. (35)

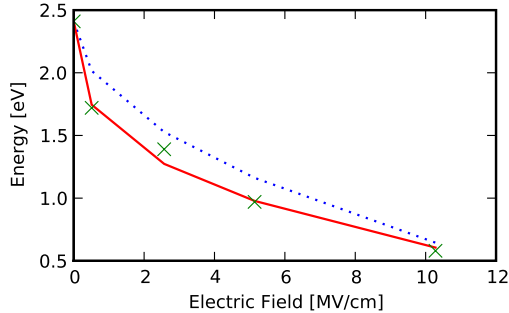


Figure 8. Difference between the IP and the excitation energy for *n*-tridecane, with the electric field parallel to the chain, obtained by DFT (\times), model in Eq. (34) (—), and model in Eq. (35) (\cdots). With linear regression, the following coefficients are obtained; $\beta_{PF} = 39.5$ eV and $\beta_{1/3} = 14.3$ eV.

fits almost perfectly with the DFT data, while a Δ as in Eq. (34) (which gives a good fit for cyclohexane) yields a poor fit. The coefficients obtained from linear regression, $\beta_{1/3}$ (see Figure 8) is close to the experimental value,⁸ $\beta_{1/3}^{\text{EXP}} = 12.4$ eV, without a modification given by the relative permittivity of the medium. Since the excitation energy is field-dependent even for small fields, it is reasonable to assume that it is also dependent on ϵ_r , and that an increased ϵ_r will decrease the excitation energy. Therefore the difference between the IP and the excitation energy may be less dependent on the medium compared to the individual properties. For cyclohexane, the excitation energy is not dependent on the electric field for small fields (<30 MV/cm), and thus in this case one can assume that the excitation energy is also less dependent on the dielectric constant. If this is the case only the IP will be dependent on the medium.

A conductivity given by

$$\sigma = \sigma_0 e^{\frac{\Delta}{2k_b T}} \quad (36)$$

similar to the Poole-Frenkel model,¹² explains both a conductivity given by Eq. (31) and (32). This model assumes equilibrium between the first excitation energy and the IP. However, to obtain a conductivity model given by Eq. (36) there cannot be an equilibrium between the ground state and the first excitation energy. If that had been the case, the conductivity would only be dependent on the IP, not Δ . However in the Born-Oppenheimer approximation electron responses are immediate, and thus when electric field is suddenly applied, it is

Table III. The lowest singlet (S_1 and S_2) and triplet (T_1 and T_2) excitation energies for n -tridecane and N,N-dimethylaniline (in eV)

Excitation	n -tridecane	N,N-dimethylaniline
S_1	6.29	2.42
S_2	6.36	3.38
T_1	6.28	1.34
T_2	6.35	2.61

not unreasonable to assume that the number of excited electrons are far greater than the equilibrium value.

One possible reason for the non-equilibrium between the ground state and the first electronic excitation energy might be impact excitation, where a free electron collides with a molecule and excites it. Experimental evidence indicating that impact excitation is important have been found for negative streamers in n -tridecane with N,N-dimethylaniline (DMA),⁶² where 0.1 M DMA in n -tridecane reduces the injected charge and increases the emission of light for negative first mode streamers. For such streamers, the streamer growth is believed to occur through evaporation of the streamer-liquid interface by inelastic collisions of free electrons created in an ionization region at the needle electrode (glow discharges).⁶³ These electrons will be slowed down by inelastic collisions with molecules in the streamer and at the streamer-liquid interface. Energy transferred from the electrons by these collisions can either be released as heat or by photon emission. Emission of energy in the form of photons that are transmitted through the liquid or absorbed at safe distances, do not contribute to the phase transition and will thus reduce the streamer growth.

It is important to note that a collision with a free electron may excite the molecule to states which are unlikely through excitation by light. Thus, both the singlet-singlet excitation energies and the singlet-triplet excitation energies may be of importance. In both cases, the free electron will lose a large portion of its energy, but if a molecule is excited to a singlet state, it may relax by emitting a single photon in addition to heat. A molecule excited to a triplet state on the other hand, relaxes in a more complicated way, and the probability for emitting photons is smaller. Thus a larger portion of the energy is released locally as heat.

The lowest singlet state for DMA is as low as 2.42 eV (Table III), and a relaxation from this state would emit photons in the visible range where an optical liquid like *n*-tridecane would not absorb it. Clearly higher energy excitations will also contribute, but energies of that order is probably only available for electrons which lie in the high energy tail of a Maxwell distribution in the region with highest field close to the needle electrode (ionization region). Thermal excitation are unlikely as it requires very high temperatures (at 5000 K 5% of the DMA molecules would be excited to the lowest triplet state, and 0.4% would be in the lowest singlet state using a Boltzmann distribution), thus impact excitation is probably dominant.

Photoionization has been proposed as a possible feedback mechanism during streamer propagation occurring at voltages above the breakdown voltages in liquids.⁴³ These are the 4th mode streamers propagating with speeds from some tens to above one hundred kilometres per second and are clearly highly field-dependent events. The order of magnitude of the threshold fields may be estimated from threshold voltages reported in the literature.⁴⁹ In neat cyclohexane, the 4th mode streamer appears suddenly above 120 kV in a 5 cm point-to-plane gap.⁴⁹ By assuming an ideal step voltage and a hyperbolically shaped streamer tip radius of 6 μm ,⁴⁹ the corresponding Laplacian field magnitude at the propagating streamer tip is about 40 MV/cm . This field magnitude, indicative as it is, lies well within the field range where our calculations show a drastic reduction of the IP, and very close to the typical magnitudes where there are no excitation energies between the IP and the ground state. Thus, through the reduction of the IP, the electric fields in a micrometer region in front of the streamer could significantly aid a photoionization mechanism. Consequently, the study of the field-dependent IP of molecules typically present in insulating liquids can be important to understand the occurrence of fast-mode streamers.

VI. CONCLUSION

Ionization processes, by impact, photon or tunnelling are not trivial, and it is not necessarily easy to predict probabilities for ionization even though the IP is known. However, for all three types of processes, the IP is the single most important parameter.

The model with the calculation of the interaction energy between a cation and a negative point charge gives a reduction of the IP as a function of the electric field which agrees

qualitatively with experimental results, both with respect to conductivity models for pre-inception currents and for fast-mode streamers. Furthermore, the difference in pre-inception currents for cyclohexane and *n*-tridecane suggest that the field dependence of the first excitation energy is important. Specifically, a conduction which is dependent on the difference between the first excitation energy and the IP, explains both a conduction proportional to $e^{-\beta_{PF}\sqrt{E}/kT}$ and a conduction proportional to $e^{-\beta_{1/3}\sqrt[3]{E}/kT}$, where the first is obtained if the excitation energy is independent of E and the latter is obtained if the excitation energy depends on the electric field.

Furthermore, free electrons will lose energy by exciting molecules electronically, and when an excited molecule relaxes, it may emit light. Thus additives with low excitation energies as N,N-dimethylaniline, can retard 1st mode negative streamer growth by emission of energy in the form of light.

It is a general trend that the difference between the IP calculated by Eq. (9), and the first excitation energy, calculated by TD-DFT, become small above a specific electric field. Thus, above this electric field, the molecules may either be in its ground state or have energy at or above the IP. Furthermore for such high electric fields (~ 40 MV/cm), a reduction of the IP can significantly aid photoionization, which is believed to be the dominant mechanism for fast streamers.

Thus it is concluded that the IP must be viewed as a field-dependent property, and that the field dependence of the IP is important for all ionization processes in high electric fields and for high-field conduction models.

ACKNOWLEDGEMENTS

Support from the Norwegian Research Council through a Strategic Industry Program (164603/I30) and grants of computer time are acknowledged. We would also like to thank Steven Boggs and Ramamurthy Ramprasad for helpful feedback, and Anna I. Krylov for fruitful discussions regarding Ref. 57.

¹ M. Haidara and A. Denat. IEEE Trans. Elect. Insul., **26**, 592–597, (1991).

² A. Denat, N. Bonifaci, and M. Nur. IEEE Trans. Dielect. Elect. Insul., **5**, 382–387, (1998).

- ³ L. Dumitrescu, O. Lesaint, N. Bonifaci, A. Denat, and P. Notinghamer. *J. Electrostat.*, **53**, 135–146, (2001).
- ⁴ P. Gournay and O. Lesaint. *J. Phys. D: Appl. Phys.*, **26**, 1966–74, (1993).
- ⁵ S. Ingebrigtsen, L. E. Lundgaard, and P.-O. Åstrand. *J. Phys. D: Appl. Phys.*, **40**, 5161–5169, (2007).
- ⁶ S. Ingebrigtsen, L. E. Lundgaard, and P.-O. Åstrand. *J. Phys. D: Appl. Phys.*, **40**, 5624–5634, (2007).
- ⁷ Ø. L. Hestad, L. E. Lundgaard, and D. Linhjell. *IEEE Trans. Dielect. Elect. Insul.*, **17**, 767–777, (2010).
- ⁸ Ø. L. Hestad, L. E. Lundgaard, and P.-O. Åstrand. Submitted, (2010).
- ⁹ A. Denat. *IEEE Trans. Dielect. Elect. Insul.*, **13**, 518–525, (2006).
- ¹⁰ L. A. Dissado. *IEEE Trans. Dielect. Elect. Insul.*, **9**, 483–497, (2002).
- ¹¹ S. Boggs. *IEEE Trans. Dielect. Elect. Insul.*, **12**, 929–938, (2005).
- ¹² L. A. Dissado and J. C. Fothergill. *Electrical Degradation and Breakdown in Polymers*. Material and Devices Series 9. The Institution of Engineering and Technology, London, United Kingdom, (1992).
- ¹³ W. F. Schmidt. *Liquid State Electronics of Insulating Liquids*. CRC Press, (1997).
- ¹⁴ A. K. Jonscher. *Thin Solid Films*, **1**, 213–234, (1967).
- ¹⁵ V. Adamec and J. H. Calderwood. *J. Phys. D: Appl. Phys.*, **8**, 551–560, (1975).
- ¹⁶ G. Teyssedre and C. Laurent. *IEEE Trans. Dielect. Elect. Insul.*, **12**, 857–875, (2005).
- ¹⁷ H.J. Wintle. *IEEE Trans. Dielect. Elect. Insul.*, **6**, 1–10, (1999).
- ¹⁸ C. Zhan, J. A. Nichols, and D. A. Dixon. *J. Phys. Chem. A.*, **107**, 4184–4194, (2003).
- ¹⁹ V. Lemierre, A. Chrostowska, A. Dargelos, and H. Chermette. *J. Phys. Chem. A.*, **109**, 8348–8355, (2005).
- ²⁰ L. A. Curtiss, P. C. Redfern, K. Raghavachari, and J. A. Pople. *J. Chem. Phys.*, **109**, 42–55, (1998).
- ²¹ S. Ingebrigtsen, H. S. Smalø, P.-O. Åstrand, and L. E. Lundgaard. *IEEE Trans. Dielect. Electr. Insul.*, **16**, 1511, (2009).
- ²² H. S. Smalø, S. Ingebrigtsen, and P.-O. Åstrand. *IEEE Trans. Dielect. Electr. Insul.*, **17**, 733–741, (2010).

- ²³ Atomic units (au) are defined by $|e| = 1$, $\hbar = 1$, $m_e = 1$, $1/4\pi\epsilon_0 = 1$. Energy in au is 1 hartree which is given by $E_h = m_e e^4 / (4\pi\epsilon_0 \hbar)^2 \approx 4.36 \times 10^{-18} J$.
- ²⁴ H. J. Wintle. IEEE Trans. Dielect. Elect. Insul., **10**, 826–841, (2003).
- ²⁵ D. Braun. J. Polym. Sci. B, **41**, 2622–2629, (2003).
- ²⁶ Yu. N. Garstein and E. M. Conwell. Chem. Phys. Lett., **245**, 351–358, (1995).
- ²⁷ D. M. Pai. J. Appl. Phys., **46**, 5122–5126, (1975).
- ²⁸ A. Messiah. *Quantum Mechanics, two volumes bound as one*. Dover Publications, Inc., (1999).
- ²⁹ A. D. Becke. Phys. Rev. A, **38**, 3098, (1988).
- ³⁰ C. Lee, W. Yang, and R. G. Parr. Phys. Rev. B, **37**, 785, (1988).
- ³¹ E. van Lenthe and E. J. Baerends. J. Comput. Chem., **24**, 1142–1156, (2003).
- ³² D. P. Chong. Mol. Phys., **103**, 749–761, (2005).
- ³³ G. te Velde, F. M. Bickelhaupt, E. J. Baerends, C. Fonseca Guerra, S. J. A. van Gisbergen, J. G. Snijders, and T. Ziegler. J. Comput. Chem., **22**, 931–967, (2001).
- ³⁴ C. Fonseca Guerra, J.G. Snijders, G. te Velde, and E.J. Baerends. Theor. Chem. Acc., **99**, 391–401, (1998).
- ³⁵ G. Zhang and C. B. Musgrave. J. Phys. Chem. A, **111**, 1554–1561, (2007).
- ³⁶ R. Bauernschmitt and R. Ahlrichs. Chem. Phys. Lett., **256**, 454–464, (1996).
- ³⁷ C. Adamo, G. E. Scuseria, and V. Barone. J. Chem. Phys., (1999).
- ³⁸ M. J. G. Peach, P. Benfield, T. Helgaker, and D. J. Tozer. J. Chem. Phys., **128**, (2008).
- ³⁹ J. D. Jackson. *Classical electrodynamics*. John Wiley & Sons, Inc., (1999).
- ⁴⁰ N. Erdmann, M. Nunnemann, K. Eberhardt, G. Herrmann, G. Huber, S. Köhler, J. V. Kratz, G. Passler, J. R. Peterson, N. Trautmann, and A. Waldek. J. Alloys Compd., **271–273**, 837–840, (1998).
- ⁴¹ S. Douin, P. Parneix, and P. Brechignac. Z. Phys. D, **21**, 343–348, (1991).
- ⁴² O. Lesaint and G. Massala. IEEE Trans. Dielect. Elect. Insul., **5**, 360–370, (1998).
- ⁴³ L. Lundgaard, D. Linhjell, G. Berg, and S. Sigmond. IEEE Trans. Dielect. Elect. Insul., **5**, 388–395, (1998).
- ⁴⁴ J. A. Rees. *Electrical breakdown in gases*. The Macmillan Press LTD, (1973).
- ⁴⁵ J. S. Townsend. *The Theory of Ionization of Gases by Collision*. Constable & Co. Ltd, (1910).
- ⁴⁶ A. Denat, J. P. Gosse, and B. Gosse. IEEE Trans. Elect. Insul., **23**, 545–554, (1988).
- ⁴⁷ D. W. Anderson. *Absorption of Ionizing Radiation*. University Park Press, (1984).

- ⁴⁸ A. Beroual, M. Zahn, A. Badent, K. Kist, A. J. Schwabe, H. Yamashita, K. Yamazawa, M. Danikas, W. D. Chadband, and Y. Torshin. *IEEE Electric. Insul. Mag.*, **14**, 6–17, (1998).
- ⁴⁹ O. Lesaint and M. Jung. *J. Phys. D: Appl. Phys.*, **33**, 1360, (2000).
- ⁵⁰ R. Gomer. *Field emission and field ionization*. American Institute of Physics, (1993).
- ⁵¹ A. de Bohan, B. Priaux, L. Ponce, R. Taieb, V. Véiard, and A. Maquet. *Phys. Rev. Lett.*, **11**, 113002, (2002).
- ⁵² H. M. Tetchou Nganso, S. Giraud, B. Piraux, Yu. V. Popov, and M. G. Kwato Njock. *J. Electron Spectrosc. Rel. Phen.*, **161**, 178-181, (2007).
- ⁵³ J. A. Anta, G. Marcelli, M. Meunier, and N. Quirke. *J. Appl. Phys.*, **92**, 1002–1008, (2002).
- ⁵⁴ N. F. Mott. *Phil. Mag.*, **19**, 835–852, (1969).
- ⁵⁵ J. C. Dyre. *J. Appl. Phys.*, **64**, 2456, (1988).
- ⁵⁶ J. F. Stanton and J. Gauss. *J. Chem. Phys.*, **111**, 8785-8788, (1999).
- ⁵⁷ P. A. Pieniazek, S. A. Arnstein, S. E. Bradforth, A. I. Krylov, and C. D. Sherill. *J. Chem. Phys.*, **127**, 164110, (2007).
- ⁵⁸ R. S. Mulliken. *J. Chem. Phys.*, **23**, 1833-1840, (1955).
- ⁵⁹ P.-O. Åstrand, K. Ruud, K. V. Mikkelsen, and T. Helgaker. *J. Phys. Chem. A*, **102**, 7686-7691, (1998).
- ⁶⁰ H. Polak and B. Jachym. *J. Phys. C: Solid State Phys.*, **10**, 3811–3818, (1977).
- ⁶¹ G. Jiang, J. Kuang, and S. Boggs. Evaluation of high field conduction models of polymeric dielectrics. In *Ann. Rep. Conf. Elec. Insul. Diel. Phen. (CEIDP)*, pages 187–190, (2000).
- ⁶² Ø. L. Hestad, S. Ingebrigtsen, H. S. Smalø, P.-O. Åstrand, and L. E. Lundgaard. In preparation, (2010).
- ⁶³ N. J. Felici. *IEEE Trans. Elect. Insul.*, **23**, 497–503, (1988).

Paper 5

Approximation of field, charge and extent of space charge limited field from a spheroid in a uniform background field

Ø. L. Hestad and S. Boggs

To be submitted.

Approximation of field, charge and extent of space charge limited field from a spheroid in a uniform background field

Øystein Hestad and Steven Boggs

November 12, 2010

Abstract

High field degradation of solids and liquids as a result of conducting defects takes place within a space charge limited field region generated by the stress enhancement. Formation of an electrical tree under such conditions requires that the space charge limited field region extend about $2 \mu\text{m}$ from the defect in the direction of the electric field. The space charge limited field also changes the surface charge on defect, which has implications for electromechanical forces which are cyclic for AC voltages. The ability to compute properties of the space charge limited field region without resorting to transient nonlinear finite element analysis is therefore of interest. Developing relevant approximations is difficult as a result of the highly nonlinear nature of the relevant phenomena. In this contribution, approximations are presented for the electric field on the surface of a spheroid in a uniform field (or semispheroid on a plane), in the regions of space charge limited field (near the tip) and without space charge limiting field (away from the tip). By integrating over the surface, the particle charge can be computed. In addition, approximations are presented for the maximum extent of the space charge limiting field region on axis of the spheroid, which is relevant to electrical tree initiation. The approximations are accurate for step voltages of finite rise time with exponentially increasing conductivity of the form $\sigma_0 \exp(k|E|^{1/n})$, where “n” can vary from 1 to 3, which covers the range of functional dependence found in the literature, and k and σ_0 are constants.

1 Introduction

Pre-breakdown and breakdown phenomena in liquid and solid insulation have been studied extensively during the last decades [1, 2, 3, 4, 5, 6]. In liquid insulation, a bush or tree like structure evolves in the insulation when stressed by a sufficiently strong inhomogeneous electric field [2]. The structure can be observed due to a refractive index which differ from the bulk insulation and is believed to consist of gas/plasma. For solid insulation, similar structures evolve when stressed by high over-voltages or after long time ageing by ac, dc or repeated impulses [4]. Streamers and electrical trees start at weak spots in the insulation, typically voids, protrusions at the electrodes, or conductive particles in the bulk of the insulation. For both solid and liquid insulation, the onset of

such pre-breakdown phenomena is typically linked to a critical field required for production of hot electrons and or UV photons [3, 7].

Several experimental studies of pre-breakdown phenomena in both solid and liquid insulation have been conducted with needle-plane geometry, where the needle electrode is intended to model a sharp metal particle in the bulk or a protrusion into the insulation [2, 7, 8, 9, 10]. This has led to a vast amount of experimental data for inception and propagation of electrical trees and streamers in highly divergent fields. In many cases, the geometrical (Laplacian) field is used to estimate the field necessary for inception and propagation of streamers and electrical trees. However, when sufficient voltage is applied to cause rapid degradation of the material, the field in the high field region will be governed by the space charge limited field (SCLF) [11, 6]. This is due to the exponential increase in conductivity with increasing electrical field typically observed for insulation materials [12]. An approximate value for the SCLF can be found based on the high-field conductivity of the material and the frequency of the applied voltage [6]. As the SCLF evolves with time and depends on the position in the SCLF-region, no existing approximation can predict accurately the field distribution within the SCLF-region.

The objective of this study is to find an approximation for the field and charge on a spheroid located in a uniform background field as a function of time, and the extent of the SCLF-region along the major axis of the spheroid. The geometry has been chosen because an analytical solution for the field distribution exists for the case with no space charge, and this geometry is a reasonable approximation for a protrusion on an electrode, conducting particle in the insulation, and needle-plane geometries often used for pre-breakdown experiments in solid and liquid insulation. The field, charge, and extension of the SCLF can be calculated accurately using finite element method (FEM). However, an analytical approximation would be beneficial as FEM is time consuming. Such an approximation might also improve the understanding of the phenomena.

FEM simulations yielding the charge on the spheroid can be compared directly with experiments performed in similar geometries using charge measurement techniques to evaluate the appropriateness of various conductivity models [13, 14]. An analytical approximation of the charge on the electrode could thus be used to find conductivity models that fit experimental results, followed by FEM simulations to validate and fine tune the models. To find an approximation for the charge on the spheroid, one must be able to predict accurately the field on the spheroid. The extent of the SCLF-region is important as an SCLF-extent of approximately $1.5 \mu m$ is needed for inception of electrical trees in XLPE [15]. Thus a good approximation of the extent of the SCLF along the axis combined with experimental data for various dielectric materials may enable us to predict the critical extension of the SCLF for more materials and evaluate the critical size of defects in the materials that would lead to inception of electrical trees.

This paper has been divided into five sections, where the first is this introduction. The next section introduces the SCLF. Then the FEM model used, the coordinate system (prolate spheroidal coordinates), and the analytical solutions of the Laplace equation are described. Section four presents the approximations developed for various conductivity models. Finally a short conclusion is provided.

2 Space charge limited field

When a dielectric is subjected to a high electric field, the conductivity of the material typically increases exponentially with the applied field [12, 6]. There are many proposed explanations for this, often involving lowering of the potential barrier localizing charge in the insulation, resulting in more available free charge, and/or increasing the mobility of charge carriers through hopping or tunnelling from site to site. In addition to increasing the bulk conductivity of the material, strong electric fields at the interface between electrode and insulation may cause injection of charge from the electrode through processes such as field emission (Fowler-nordheim), field ionization, and Schottky injection.

The SCLF was first described by Zeller et al. who used a simple model to investigate this phenomenon [16, 11]. In their model, they assume that the conductivity can be approximated by a step function with low conductivity below the SCLF and high conductivity above the SCLF. The abrupt jump in conductivity was explained by a mobility edge for electrons in the material, thus at fields above the SCLF the electrons are effectively delocalized. Clearly this is a crude approximation, as the conductivity will increase gradually with field. Nevertheless, such a simple model makes possible some useful analytical approximations. For a concentric sphere geometry, the space-charge density, ρ , is given in spherical coordinates by [11]

$$\rho(r) = \frac{2\epsilon_r\epsilon_0 F_c}{r}, \quad R < r < R_{sc} \quad (1)$$

where ϵ_r is the relative permittivity of the insulation, ϵ_0 is the permittivity of vacuum, F_c is the SCLF, R is the radius of the inner sphere, and R_{sc} is the extent/radius of the SCLF-region. The radius of the SCLF-region, R_{sc} , is given by [11]

$$R_{sc} = \frac{1}{2} \left(R + \frac{V}{F_c} \right) \quad (2)$$

where V is the potential between the concentric spheres. Zeller's approximation has also been used to derive analytical formulas for the temperature rise near high field protrusions and the electromechanical forces acting on the material in such high field regions [16]

As described previously, the high field conductivity typically increases exponentially with field, and can often be approximated by

$$\sigma(E) = \sigma_0 \cdot e^{(k \cdot E^{\frac{1}{n}})} \quad (3)$$

where σ_0 , k , and n are constants, and E is the electric field. n is typically either 1, 2 or 3, where $n = 1$ corresponds to standard hopping conduction, $n = 2$ can be explained by mechanisms such as Poole-Frenkel, Onsager-conductivity and some hopping conduction models, $n = 3$ has no established physical basis, but fits high field conduction current measurements in n-tridecane [14] and XLPE [13]. A simple statistical-mechanics approach based on the Poole-Frenkel mechanism, but with field dependent excitation and ionization energies, suggests that $n = 3$ for n-tridecane might be caused by the field dependence of the excitation energies for n-tridecane [17]. Clearly eq. 3 is a simplification, as temperature is not taken into account. However, for the present discussion we will focus on the field on

the apex, field on the spheroid surface, and the extent of the SCLF (R_{sc}), rather than on the degradation process itself. As the field has a much stronger influence on the conductivity than does the temperature, disregarding the temperature for the present purpose should not introduce a large error.

With a field dependent conductivity of the form given by eq. 3, an estimate of the SCLF can be found in several ways. One can look at the time scale on which charge must be able to move to limit the field (dielectric time constant) and compare this to the frequency of the applied voltage. The dielectric time constant must be comparable to the inverse of the voltage frequency [6],

$$\frac{1}{w} = \frac{\epsilon_r \epsilon_0}{\sigma(F_c)} \Rightarrow \sigma(F_c) = \epsilon_r \epsilon_0 w \quad (4)$$

where w is the frequency of the applied voltage and F_c is the SCLF. Another way of deriving this is by comparing the conductive term, $\sigma(E) \cdot E$, and the displacement term, $\epsilon_0 \epsilon_r \frac{dE}{dt}$, in the total current density. The SCLF will be reached when the two terms are comparable. Solving for the SCLF, F_c with a conductivity given by eq 3 gives:

$$F_c = \left(\frac{1}{k} \cdot \ln \left(\frac{\epsilon_r \epsilon_0 w}{\sigma_0} \right) \right)^n \quad (5)$$

The formula above shows that for an exponentially increasing conductivity, the space charge limited field depends on the frequency at which the voltage is applied. This is demonstrated in figure 1 where four conductivity models with the same SCLF at 10 MHz have been plotted versus field. The conductivity models have all been tuned to give a SCLF of 1 MV/m at 10 MHz, which is why they intersect each other and the horizontal line, $\epsilon_0 \epsilon_r \cdot 10 \text{ MHz}$, at 1 MV/m (eq. 4). The SCLF for 20 MHz and 1MHz for all four models can be found from the intersection of the horizontal lines corresponding to the respective frequencies and the conductivity versus field. Note that with a step conductivity, the SCLF will not depend on the frequency of the applied voltage.

For a more thorough discussion of the SCLF model, as well as its importance for degradation processes in dielectrics stressed by very high electric fields, the reader is referred to the original work by Hibma and Zeller [11] and the review paper by Boggs [6].

3 Geometry and coordinate system

3.1 Geometry, finite element model

The finite element software Comsol [18] was used to obtain numerical solutions of the Poisson equation for various conductivity models, thus providing the basis for comparison of analytical approximations with numerical solutions. This short section gives the details of the geometry used.

The 2D axisymmetric geometry consists of two parallel circular plane electrodes where a conductive semispheroid is placed on the axis of one of the planes (figure 2). The gap between the planes is filled with a dielectric material with a relative permittivity of two ($\epsilon_r = 2$) and a field dependent conductivity given either by an exponential dependence on the field (eq. 3) or as a step function. The minor radius, major radius, voltage waveform, and conductivity were varied.

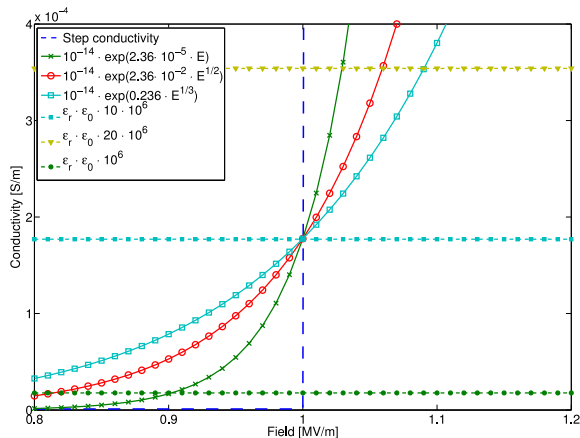


Figure 1: Four models for high field conductivity and $\epsilon_r \epsilon_0 \omega$ versus electrical field ($\epsilon_r = 2$). Note that the SCLF given by the intersections between the conductivity and $\epsilon_r \epsilon_0 \omega$ are low compared to typical insulators, but this plot gives the idea of how to obtain the SCLF and the frequency dependence of the SCLF.

3.2 Prolate spheroidal coordinates

The appropriate coordinate system for the geometry described in the previous section is prolate spheroidal coordinates (η, ξ, θ) , where constant η corresponds to a spheroid, constant ξ to a hyperboloid of revolution, and θ is the angle of revolution around the Z axis (figure 3). The Z axis goes through the foci of the spheroids. The square root of the metrics for this coordinate system are given by [19]

$$m_\eta = c_2 \sqrt{\frac{\eta^2 - \xi^2}{\eta^2 - 1}}, m_\xi = c_2 \sqrt{\frac{\eta^2 - \xi^2}{1 - \xi^2}}, m_\theta = c_2 \sqrt{(\eta^2 - 1)(1 - \xi^2)} \quad (6)$$

The surface of a spheroid with minor radius r and major radius h is given by $\eta_0 = h/c_2$ where $\pm c_2$ are the focal points of the spheroid given by $c_2 = \sqrt{h^2 - r^2}$.

3.3 Potential, electric field, and charge on the spheroid

The Laplace equation can be solved using prolate spheroidal coordinates for a spheroid located in a uniform background field. The potential with no space charge is given by [19]

$$V = c_2 \eta \xi E_0 - c_2 \eta \xi E_0 \frac{(\operatorname{arccoth}(\eta) - \eta^{-1})}{(\operatorname{arccoth}(\eta_0) - \eta_0^{-1})}, \quad (7)$$

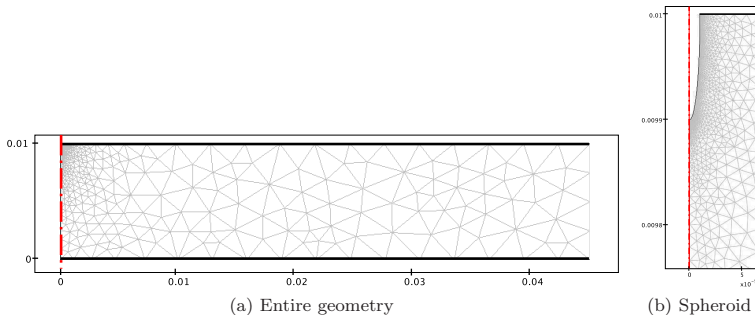


Figure 2: The figure shows the geometry used. The geometry consists of two parallel circular planes with 45 cm radius and axis through the z-axis. A semi-spheroid was placed on the upper plane electrode (in this case the dimension of the semi-spheroid was $r = 10 \mu m$, $h = 100 \mu m$). An enlargement of the semi-spheroid can be seen in subfigure (b). The gap between the two planes was 10 mm.

from which the field on the spheroid surface, and thus the charge on the spheroid, can be found. At the surface of the spheroid, the electric field is given by

$$E_{\eta_0} = -\frac{1}{m_\eta} \left(\frac{dV}{d\eta} \right)_{\eta=\eta_0} \quad (8)$$

The charge on the spheroid can now be found using Gauss' law [20]

$$Q = \epsilon_0 \epsilon_r \int_A E dA = \frac{\pi \epsilon_0 \epsilon_r (h^2 - r^2)^{\frac{3}{2}} E_0}{\sqrt{h^2 - r^2} - h \operatorname{arccoth} \left(\frac{h}{\sqrt{h^2 - r^2}} \right)} \quad (9)$$

These equations, combined with the equations derived for SCLF (eqs. 1, 2 and 5), are the starting point for finding approximations for the field/charge on the spheroid, as well as the extent of the space charge limited field when the conductivity is field dependent.

4 Approximations of field, charge and extent of SCLF

In the following sections the approximations developed for the field/charge on the spheroid and the extent of the SCLF along the Z axis from the spheroid apex will be described. First, an approximation for the relatively simple case of step-conductivity is given before an attempt to apply the approximations to more realistic conductivity.

4.1 Step-conductivity

In this section the field dependent conductivity is approximated to a step function where the conductivity starts to rise at 1 MV/m, (figure 1)

$$\sigma(|E|) = 10^{-14} + H(|E| - 1 \cdot 10^6) \quad (10)$$

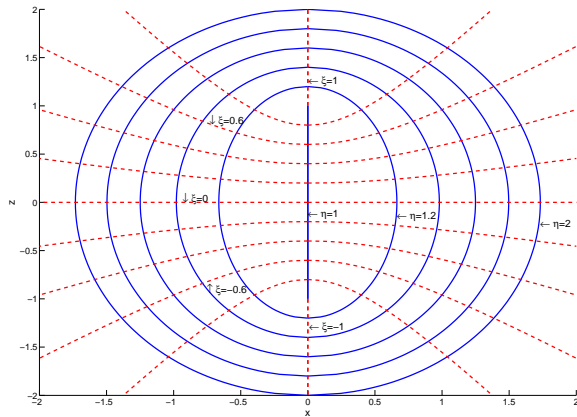


Figure 3: Schematic showing curves with constant ξ and η .

where $H(x)$ is a smoothed heaviside function with a continuous first derivative. Finite element simulations with the geometry given in section 3.1 and a conductivity given by eq. 10 were run so that the analytical approximations could be compared to results from simulations. A ramp voltage was applied to the plane electrode opposite the particle

$$V(t) = 1000 t \quad (11)$$

This formula for the applied voltage gives a background field of $E_0(t) = 100 \cdot V(t)$.

With conductivity of eq. 10, the approximate field on the surface of the spheroid can be found by dividing the spheroid into two regions. In the high-field region, the field is given by the SCLF, F_c , while as a first approximation, the field on the rest of the spheroid is given by the laplacian field (eq. 8). This can be seen in figure 4, where the laplacian field is compared to the field obtained with the conductivity given by eq. 10.

An approximation of the charge on the spheroid can now be found using this approximation for the field on the spheroid surface

$$Q_{sclf} = 2\pi\epsilon_0\epsilon_r \cdot \left(\int_{\xi=0}^{\xi=\xi_l} (m_\xi m_\theta E_{\eta_0}) d\xi + \int_{\xi=\xi_l}^{\xi=1} (m_\xi m_\theta F_c) d\xi \right) \quad (12)$$

where ξ_l is the position on the particle where the field reaches F_c . The left integral is over the part of the spheroid where the field is below the SCLF and the right integral is simply the integral of the constant SCLF, F_c , over the rest of the spheroid. The integral above can be solved using, for example, Maple,

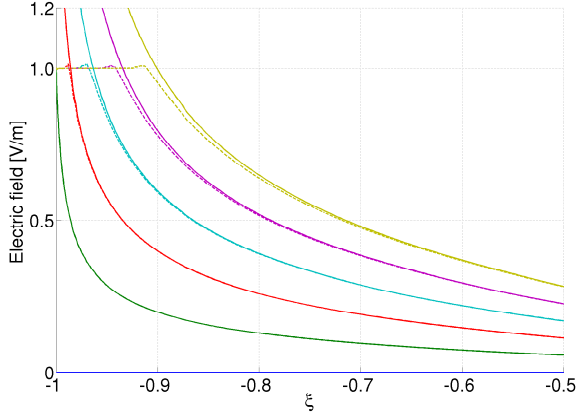


Figure 4: Electric field versus ξ . $\xi = -1$ at the apex of the spheroid. Dashed lines correspond to step conductivity and solid lines correspond to laplacian field. The field along the spheroid surface is plotted for six background fields: 0, 20000, 40000, 60000, 80000 and 100000 V/m.

giving the following result

$$\begin{aligned}
 Q_{sclf} = E_0 \left(\frac{\pi \epsilon_0 \epsilon_r (h^2 - r^2)^{3/2}}{\sqrt{h^2 - r^2} - h \cdot \operatorname{arccoth}\left(\frac{h}{\sqrt{h^2 - r^2}}\right)} \right) \xi_l^2 + \\
 F_c \pi \epsilon_0 \epsilon_r \cdot \left[\xi_l \cdot \left(r \cdot \sqrt{h^2 - \xi_l \cdot (h^2 - r^2)} - r^2 \right) + \right. \\
 \left. \frac{h^2 \cdot r}{\sqrt{(h^2 - r^2)}} \cdot \left(\arcsin\left(\frac{\xi_l \sqrt{h^2 - r^2}}{h}\right) - \arcsin\left(\frac{\sqrt{h^2 - r^2}}{h}\right) \right) \right] \quad (13)
 \end{aligned}$$

where E_0 is the background field. If the field does not reach the SCLF on the apex of the spheroid then $\xi_l = 1$, and eq. 13 turns into eq. 9. In order to use this equation, an expression for ξ_l must be found. This can be done by solving the following equation

$$E_{\eta_0} = F_c \quad (14)$$

Solving for ξ_l gives one positive and one negative root (same absolute value) corresponding to the two locations on the spheroid where the laplacian field is equal to the SCLF for a spheroid in a uniform background field. For the geometry where the spheroid is placed on one of the electrodes, only one of the two values corresponds to a physical location. If the field is low, this equation could give a value for ξ with an absolute value larger than 1. ξ has to be between -1 and 1 so this must be discarded, and instead $\xi = 1$ should be used for low fields. Figure 5 shows a plot of ξ_l versus background field for the geometry shown in figure 2 ($h=100 \mu\text{m}$ and $r=10 \mu\text{m}$) and with a SCLF of 1 MV/m.

Combining eqs 13 and 14, the charge on a spheroid in a material with field dependent conductivity can be approximated. In figure 6, the result obtained

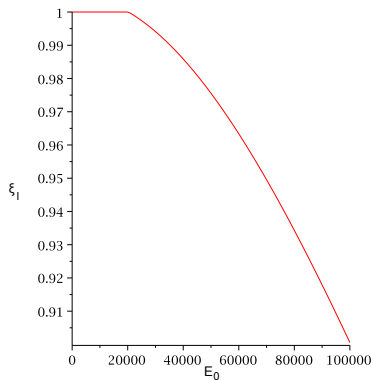


Figure 5: The position (ξ_l) on the spheroid where the field reaches the SCLF (F_c) as a function of background field (E_0). For low fields, $\xi_l = 1$, meaning that the field at the spheroid surface is below the SCLF.

from eq. 9 (constant conductivity) is compared to the result obtained using eq. 13 and 14. Figure 6 also compares the results obtained using the equations with the results obtained from finite element analysis (FEA).

Finding the extent of the SCLF along the z-axis starting from the apex of the spheroid can be carried out by adapting Zeller's approximation for concentric spheres (eq. 2) to the spheroid-plane geometry. To adapt eq. 2 one must find the voltage over the spheres and the radius of the inner sphere that best represents the geometry at the apex of the spheroid. The Laplacian field on the apex of the spheroid is given by

$$E_{La} = \frac{(h^2 - r^2)^{3/2} E_0}{r^2 \left(\sqrt{h^2 - r^2} - \operatorname{arccoth} \left(\frac{h}{\sqrt{h^2 - r^2}} \right) h \right)} \quad (15)$$

Based on eq. 15, the voltage over the concentric spheres, V_s , can be calculated assuming the spheroid has an "effective" radius R_{sp} and that the outer sphere is large compared to the inner sphere:

$$V_s = E_{La} \cdot R_{sp} \quad (16)$$

As a first approximation for the radius of the spheroid, one can use the radius of curvature at the apex $R_{apex} = r^2/h$. For very sharp spheroids, the curvature changes quickly as one moves away from the apex along the surface of the spheroid, and as the SCLF-region expands, it "sees" a larger part of the spheroid. Thus the radius given by r^2/h will be too small. An empirical correction factor must therefore be introduced, and the "effective" radius of the spheroid can be written as

$$R_{sp} = f \cdot \frac{r^2}{h} \quad (17)$$

where f is a dimensionless correction factor that depends on the "sharpness" of

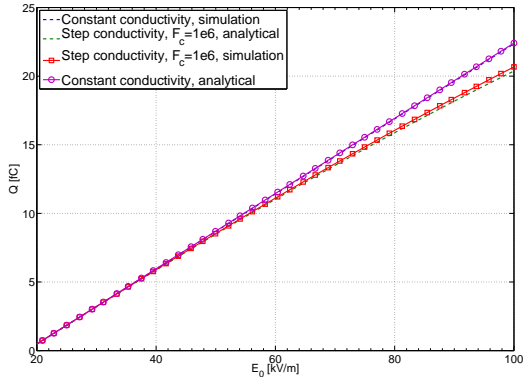


Figure 6: Charge on a semi-spheroid versus background field for a case with constant conductivity and a case where the conductivity limits the field to 1 MV/m. Results from Maple (analytical) and Comsol (simulation).

the spheroid. Using eqs. 16 and 17 in eq. 2 gives an approximation of R_{sc}

$$R_{sc} = \frac{1}{2} \left(R_{sp} + \frac{V_s}{F_c} \right) - R_{sp} = \frac{1}{2} \cdot f \cdot \frac{r^2}{h} \cdot \left(\frac{E_{La}}{F_c} - 1 \right) \quad (18)$$

In figure 7, this approximation has been compared to results from simulations. As expected, $f=1$ only gives a good approximation when the SCLF-region is very small ($R_{sc} < 1 \mu m$). The range where the approximation can be used is enhanced by using $f = 1.9 - \frac{r}{h}$, which gives a larger effective radius for sharp spheroids. Figure 7 shows that this gives a good approximation for ($R_{sc} < 5 \mu m$) for a large range of geometries.

4.2 Exponential conductivity

Replacing the step function for conductivity (eq. 10) with an exponential function (eq. 3) makes the problem of finding the field and charge on the spheroid more complex. As explained in section 2, the SCLF depends on frequency when the conductivity is not a step function of the field (see figure 1). The goal of this section is to derive an approximation capable of describing the field over the surface of the spheroid when a step voltage with a finite rise time is applied (figure 8). The step voltage gives a background field

$$E_0(t) = \begin{cases} \frac{V_{amp}}{d} \cdot \frac{t}{t_r}, & t < t_r \\ \frac{V_{amp}}{d}, & t \geq t_r \end{cases} \quad (19)$$

where t_r is the risetime of the voltage, V_{amp} is the voltage amplitude, and d is the distance between the plane electrodes. The approximation must therefore predict accurately the field on the surface of the spheroid while the voltage is rising, as well as after it reaches steady state. As a starting point, an approximation of the field on the apex of the spheroid is derived. An accurate prediction

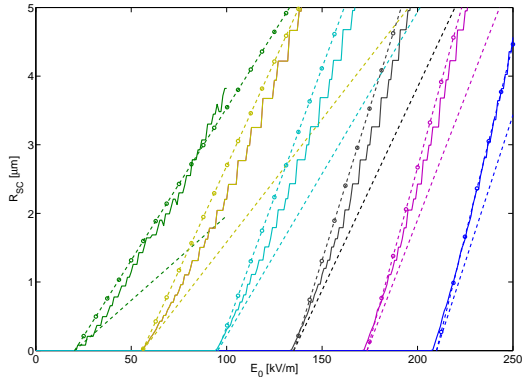


Figure 7: Comparison of R_{sc} obtained by simulation (solid line) with calculated values using eq. 18 with $f=1$ (dashed line) and $f=(1.9-r/h)$ (dashed line with open circles). The results were obtained with $h=100 \mu\text{m}$ and $r=10, 20, 30, 40, 50$ and $60 \mu\text{m}$.

of this field is important as this is the point stressed by the highest field and where the field is most distorted by the space-charge.

Most of the simulations performed to provide a basis for the approximations were carried out using the following conductivity formulas.

$$\sigma(E) = 10^{-14} \cdot \exp(2.36 \cdot 10^{-5} \cdot |E|) \quad (20)$$

$$\sigma(E) = 10^{-14} \cdot \exp(0.0236 \cdot \sqrt{|E|}) \quad (21)$$

$$\sigma(E) = 10^{-14} \cdot \exp(0.236 \cdot \sqrt[3]{|E|}) \quad (22)$$

Plots of the conductivity versus field for these three formulas are provided in figure 1, all of which give a SCLF of 1MV/m at 10 MHz.

In figure 9, the field on the apex of the spheroid with a conductivity given by eq. 20 is plotted versus time for voltage rise times ranging from 30 ns to 1 μs . The figure also shows the SCLF (as given by eq. 5) versus time. Figure 9 shows that eq. 5 gives a good estimate of the time at which the SCLF is reached at the apex, t_c , for a range of rise times. The field on the apex is given by the Laplacian field until it intersects the dotted line, which is the SCLF at this time/effective frequency. After this time, the field continues to increase as long as the background field/voltage is rising ($t < t_r$). Note that after t_r the field on the apex follows a curve given approximately by the formula for SCLF in eq. 5, which will be used to approximate the field after t_r .

A first approximation of the field on the apex for the time region $t_c < t < t_r$ is to calculate the derivative of the SCLF at the time when the SCLF is reached and assume the field rises at approximately this rate until the voltage levels off.

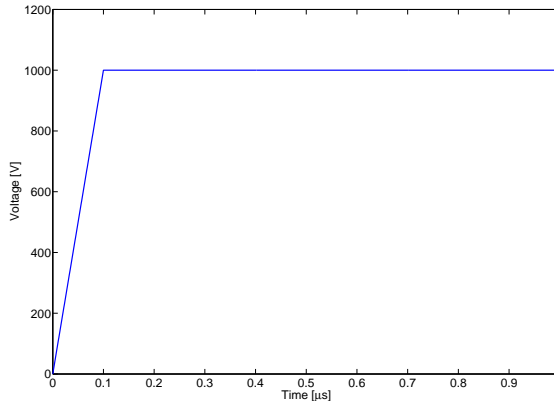


Figure 8: Step voltage with $t_r=100$ ns, amplitude of 1000 V and duration of $1 \mu\text{s}$

The approximation for the field at the apex can be written as

$$E_{\text{apex}}(t) = \begin{cases} E_{La}(t) & t < t_c \\ F_c(t_c) + \frac{dF_c}{dt}(t_c) \cdot (t - t_c) & t_c < t < t_r \\ F_c(t_0 + t - t_r) & t > t_r \end{cases} \quad (23)$$

Where E_{La} is the Laplacian field on the apex given in eq. 15, t_c is the time when the SCLF is reached at the apex of the spheroid and can be found by solving $E_{La}(t) = F_c(t)$ for t , F_c is the SCLF given by eq. 5, t_r is the rise time of the applied voltage, and t_0 is introduced to make the curve continuous ($1/t_0$ can be viewed as the effective radial frequency at $t = t_r$).

The main problem with eq. 23 is that the increase of the field with time after t_c is linear (see figure 10). This is only a good approximation for the first few ns after t_c . In order to obtain a better understanding of the phenomena that occur during the time from t_c to t_r , a series of formulas were fitted to results obtained from FEM simulations using the nonlinear curve fitter in Sigmaplot. To focus on this specific phenomenon (SCLF on apex when background field is increasing), simulations were run with a continuously rising voltage during the entire simulation. The duration of the simulation was increased to $2 \mu\text{s}$. Six different voltage ramp rates were used: 33 GV/s, 10 GV/s, 5 GV/s, 3.33 GV/s, 2.5 GV/s, and 2 GV/s. The equations for conductivity given above (eq. 20-22) were the starting point for the simulations, but a wide range of formulas of the form given by eq. 3 was used to find how the parameters n and k affect the time dependence of the field at the apex.

The field at the apex and the background field for a case with a conductivity given by eq. 20 and a voltage ramp rate of 10 GV/s have been plotted in figure 11. Three regions were observed from these simulations, as can be seen in the figure (times in parentheses correspond to the times of the differing regions in figure 11):

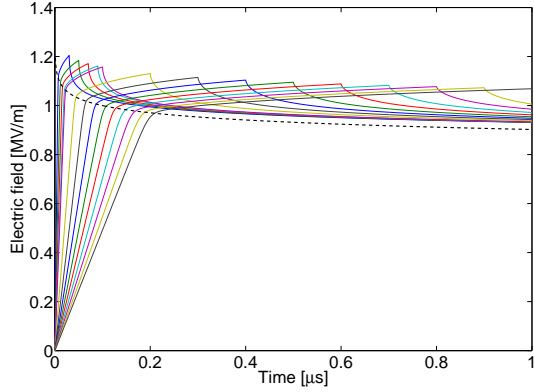


Figure 9: Results from simulations using eq. 20 and rise times from 30 ns to 1 μ s. F_c (eq. 5) has also been plotted (dotted line) to show that this equation gives a good estimate of the onset of the SCLF at the apex.

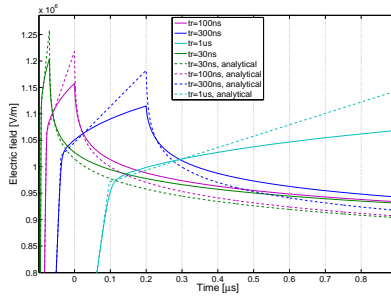


Figure 10: Results from simulations using the conductivity given in eq. 20 (solid lines) compared to results obtained using eq. 23

- ($t < 10$ ns) The field is given by the laplacian field (eq. 15).
- (10 ns $< t < 1$ μ s) When the SCLF is reached, the field increases much more slowly than predicted by the Laplacian formula.
- (1 μ s $< t < 2$ μ s) If the voltage is increased sufficiently a point is reached where the background field equals the SCLF. From this point, the rate at which the field at the apex increases is approximately equal to the rate at which the background field increases. This phenomenon will not be considered in this paper.

The solution for the field in the first time region ($t < t_c$) is known (eq. 15). The time between when the SCLF is reached (t_c) and when the voltage reaches

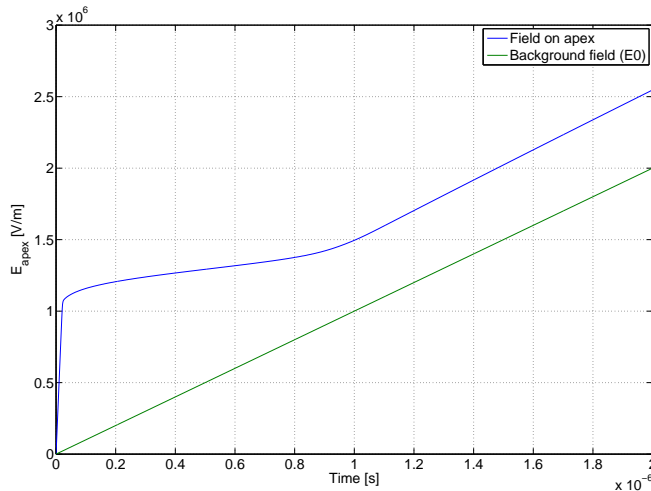


Figure 11: Field at the apex and background field versus time. The voltage increased at a rate of 10 GV/s. Minor axis= $10\mu\text{m}$, major axis= $100\mu\text{m}$, conductivity given by eq. 20

its maximum (t_r) is of primary interest. The region of interest ($t_c < t < t_r$) can be fitted to the following function:

$$\begin{aligned}
 E_{apex}(t) &= 2 \cdot \left(\frac{1}{k} * \ln \left(\frac{\epsilon}{\sigma_0 * t_c} \right) \right)^n - \left(\frac{1}{k} * \ln \left(\frac{\epsilon}{\sigma_0 * t} \right) \right)^n + \alpha \cdot (t - t_c) \cdot \frac{dE_0}{dt} \\
 &= 2 F_c(t_c) - F_c(t) + \alpha \cdot (t - t_c) \cdot \frac{dE_0}{dt}, \quad t_c < t < t_r
 \end{aligned} \tag{24}$$

The only unknown parameter in the equation above is α . Simulations were run to find how α depends on the conductivity and the geometry. The only parameter that has a marked influence on α is "n" in the conductivity formula (eq. 3). Parameters like the minor and major axis of the spheroid, k (in eq. 3), and the distance between the two planes (as long as it is much greater than the major axis of the particle) had only minor effects on α . α has been plotted versus the major radius of the spheroid for three different minor radii in figure 12. The difference between the maximum and minimum value for α was approximately 10%, so the effect of the geometry is relatively small compared to the effect of n (going from n=1 to n=2 more than doubles " α " for the same geometry).

To find a way to calculate α , a series of simulations was run to find a function that describes this parameter as a function of n. The best fit was obtained using a polynomial dependence on n (figure 13). Thus α can be approximated by

$$\alpha(n) = 0.124 \cdot n + 0.03 \cdot n^2 \tag{25}$$

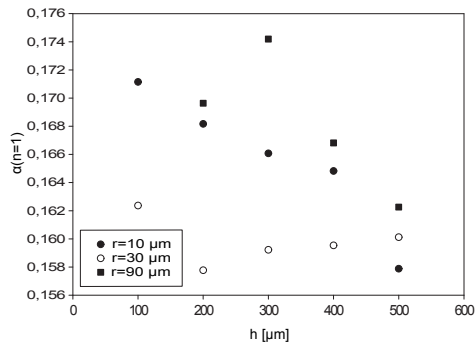


Figure 12: Plot showing the value of α in eq. 24 for different major and minor spheroid radii (h =major radius and r =minor radius). The simulations were run using a ramp rate of 10GV/s and a conductivity given by eq. 20. The gap distance between the two plane electrodes was 10 mm

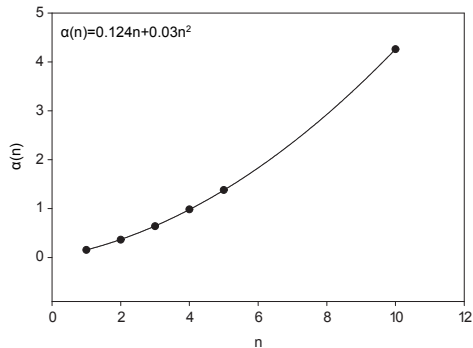


Figure 13: Plot showing the dependence of α in eq. 24 on n .

Inserting this into eq. 24 yields:

$$E_{apex}(t) = 2 F_c(t_c) - F_c(t) + (0.124 \cdot n + 0.03 \cdot n^2) \cdot (t - t_c) \cdot \frac{dE_0}{dt}, \quad t_c < t < t_r \quad (26)$$

At $t=t_c$, eq. 26 reduces to $F_c(t_c)$ as expected. The first term in the equation is simply a constant and is two times the SCLF at t_c . The second term links the evolution of the field at the apex with the frequency dependence of the SCLF. If the background field had not increased after $t=t_c$ this term would have reduced the field at the apex given by the effective frequency $\frac{1}{t}$. The last linear term takes into account that the external field is still increasing which increases the SCLF volume. Thus the field at the apex must increase to allow for the growth of the SCLF volume. This increase depends on the rate at which the external field increases and how the conductivity depends on the electric field.

In figures 14 to 16, the approximation given by eq. 26 is compared to simulations for a series of geometries, conductivity formulas, and voltage ramp rates.

All figures show the results from simulations as solid lines and the results using the approximation by dashed lines.

The approximation is good for a large range of h (major radius), r (minor radius), n , k , d (distance between the two planes) and voltage ramp rates. Using the approximation given in eq. 26 for the $t_c < t < t_r$ gives a formula for the field at the apex as a function of background field similar to eq. 19:

$$E_{apex}(t) = \begin{cases} E_{La}(t) & t < t_c \\ 2 \cdot F_c(t_c) - F_c(t) + \alpha(n) \cdot (t - t_c) \cdot \frac{dE_0}{dt}; & t_c < t < t_r \\ F_c(t_0 + (t - t_r)) & t > t_r \end{cases} \quad (27)$$

The first time period is given by the Laplacian field, eq. 15. When the SCLF is reached at the apex (at t_c), the approximation given by eq. 26 is used until the voltage stops rising (at t_r). To approximate the time region when the voltage is constant, the effective frequency ($1/t_0$) at the time when the voltage stops increasing is calculated. This is found by solving $F_c(t_0) = E_{apex}(t_r)$, where E_{apex} is given by eq. 26. This frequency decreases with increasing time and is approximated by $\frac{1}{t_0 + (t - t_r)}$. F_c in eq. 27 is assumed to be of the form given by eq. 3. In figure 17, a series of simulations compare the approximation in eq. 27 to data computed using Comsol. The approximation gives good results when $n=1$ (figure 17), but for $n=2$ and $n=3$, the approximation fails for $t > t_r$ (figure 18, dashed lines). The main problem for $n>1$ is that the formula for SCLF goes towards a lower value than given by the simulations, because the effective frequency for large times is $\frac{3}{t}$ not $\frac{1}{t}$ as used for $n=1$. Incorporating this into the equation for the SCLF (eq. 5) gives

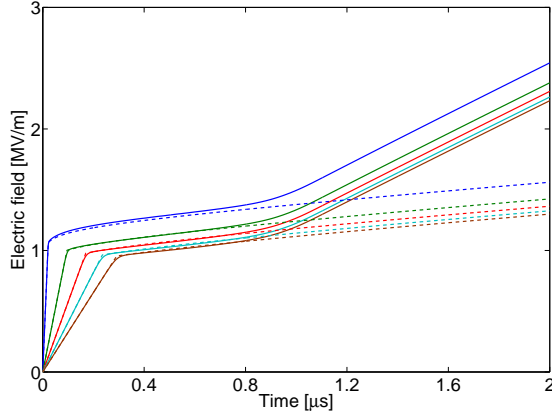
$$F_c = \left(\frac{1}{k} \cdot \ln \left(\frac{3\epsilon_r \epsilon_0}{\sigma_0 t} \right) \right)^n, \quad n > 1, t > t_r \quad (28)$$

Thus for conductivity with $n>1$, eq. 28 should be used to predict the evolution of the field after t_r . Figure 18 shows that this improves the approximation somewhat, although it seems evident that the effective frequency should be changed gradually from $1/t$ to $3/t$ after t_r .

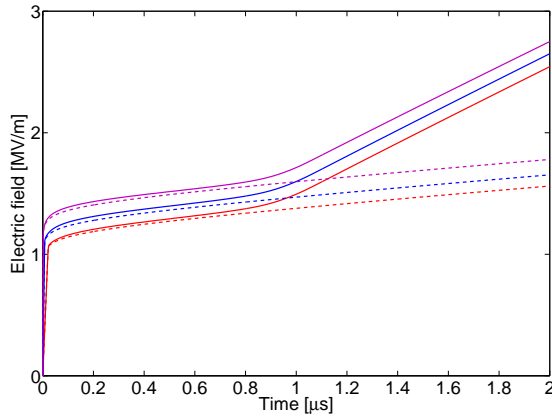
The approximation of the field on the apex is a good start towards predicting the field on the entire surface of the spheroid. There is nothing unique about the apex; thus any point on the spheroid within the SCLF-region should be predicted by a similar formula to eq 27. The formula for an arbitrary point on the spheroid should thus be given by

$$E_{surf}(t, \xi) = \begin{cases} E_{\eta_0}(t, \xi) & t < t_c \\ 2 \cdot F_c(t_c(\xi)) - F_c(t) + \alpha(n) \cdot (t - t_c(\xi)) \cdot \frac{dE_0}{dt}; & t_c < t < t_r \\ F_c(t_0(\xi) + (t - t_r)) & t > t_r \end{cases} \quad (29)$$

Note that eq. 29 is only valid for the part of the spheroid that falls within the SCLF-region. The part of the spheroid that falls outside of this can be approximated by the laplacian field ($E_{\eta_0}(t, \xi)$, eq. 8). In figure 19 this formula has been compared to simulations for $\xi=-1$ (the apex) and $\xi=-0.95$. The formula above assumes that the effective frequency of the SCLF at t_r is given by the field at the given location on the spheroid at that time. Figure 19 shows that this is not the case, the field at $\xi=-0.95$ falls approximately in the same way as at the apex. Thus the field at the apex governs how fast the field declines in



(a) Minor radius=10, 30, 50, 70, and 90 μm , major radius=100 μm



(b) Minor radius=10 μm , major radius=100, 300, and 500 μm

Figure 14: Field at the spheroid apex versus time for conductivity given by eq. 20 ($n=1$) and 10 GV/s voltage ramp. Comparison between results obtained from simulations (solid lines) and from the approximation outlined in the text above (dashed lines). The approximation is only good up to the point where the background field approaches the SCLF.

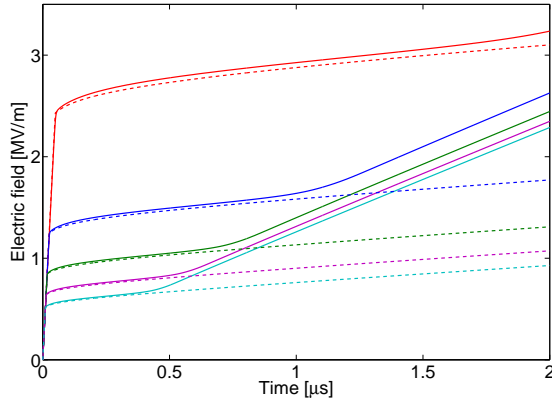


Figure 15: Field at the spheroid apex with conductivity given by eq. 3 with $\sigma_0 = 10^{-14}$, $n=1$, and $k=1E-5, 2E-5, 3E-5, 4E-5$ or $5E-5$. Minor radius= $10 \mu\text{m}$, major radius= $100 \mu\text{m}$, distance between planes= 10 mm , Comparison between results obtained from simulations (solid lines) and from the approximation outlined in the text above (dashed lines). The approximation is reasonably good for all the values of k corresponding to SCLF from 0.5 MV/m to 2.5 MV/m

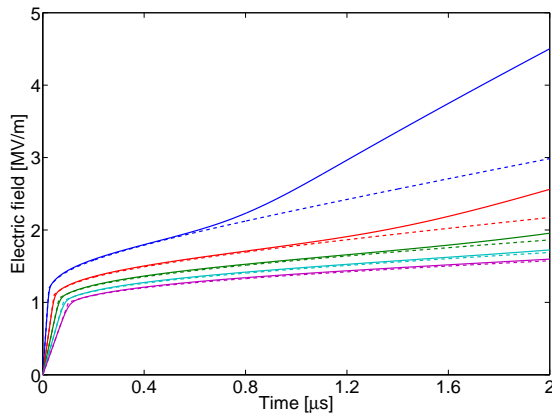


Figure 16: Field at the spheroid apex with conductivity given by eq. 22 ($n=3$). Minor radius= $10 \mu\text{m}$, major radius= $100 \mu\text{m}$, distance between planes= 10 mm . Comparison between results obtained from simulations (solid lines) and from the approximation outlined in the text above (dashed lines). Voltage ramp rate between 2 and 10 GV/s .

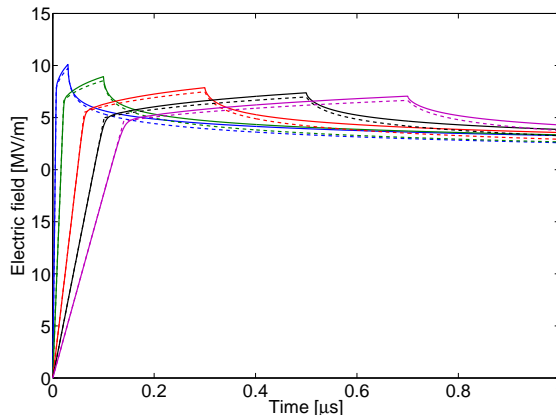


Figure 17: Field at the spheroid apex with conductivity given by eq. 20 ($n=1$) and a background field given by eq. 19 (step voltage). The rise times used were: 30, 100, 300, 500, and 700 ns. Full lines are based on simulations while dashed lines are based on the approximation given in eq. 27.

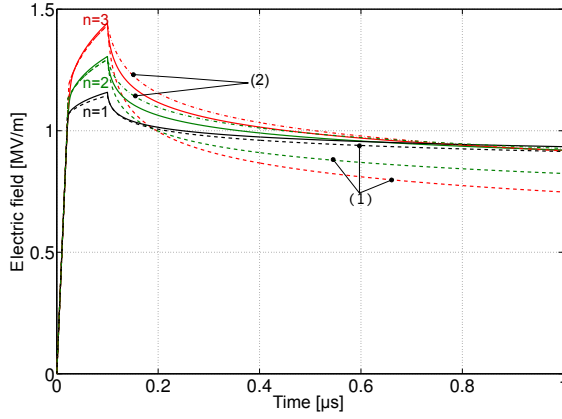
the SCLF region. Taking this into account a new approximation of the field on the surface of the spheroid can be found,

$$E(t) = \begin{cases} E_{surf}(t, \xi) & t < t_c \\ 2 \cdot F_c(t_c(\xi)) - F_c(t) + \alpha(n) \cdot (t - t_c(\xi)) \cdot \frac{dE_0}{dt}; & t_c < t < t_r \\ F_c(t_0(\xi = -1) + (t - t_r)) - F_c(t_0(\xi = -1)) + \\ 2 \cdot F_c(t_c(\xi)) - F_c(t_r) + \alpha(n) \cdot (t_r - t_c(\xi)) \cdot \frac{dE_0}{dt} & t > t_r \end{cases} \quad (30)$$

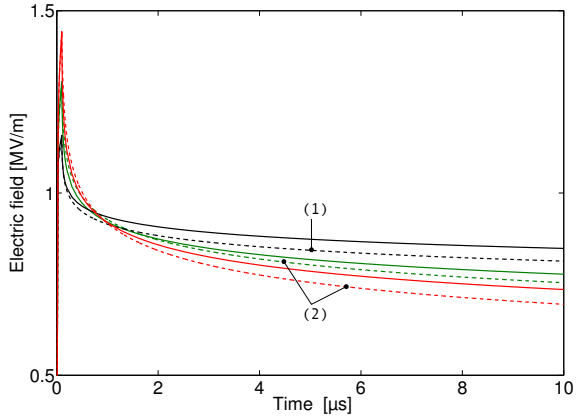
This equation has also been compared to the results obtained from simulations in figure 19.

Using the approximation found for the field on the apex surface, one can find an approximation for the charge on the surface of the spheroid in the same way as for step-conductivity. Thus one can integrate over the SCLF region, and over the region where the SCLF is not reached. As the formula above gives an approximation of the field inside the SCLF-region and one can simply use the laplacian field outside this region, the charge on the spheroid can be computed. This is, however, not a trivial task and requires the use of Maple or other computer tools. Matlab code that performs this task has been included in Appendix A. The transition between the SCLF region and the region outside must be smoothed somewhat, as the transition between them will not be as abrupt as one would expect with a step-conductivity. This can be done by requiring the field to decrease monotonically as one moves away from the apex of the spheroid. Figure 20 shows a comparison of simulations and approximation of charge on a spheroid.

Finally the problem of the extent of the SCLF with a conductivity that depends exponentially on the field will be treated. Finding an accurate approximation for this is nontrivial. However, the approach developed for step-



(a)



(b)

Figure 18: a) Field at the spheroid apex with conductivity given by eqs. 20-22 ($n=1-3$) and a background field given by eq. 19 (step voltage). The rise time used was 100 ns. Full lines are based on simulations while dashed lines are based on the approximation given in eq. 27. For $n=2$ and $n=3$, two approximations are shown, one where the effective frequency in the formula for the SCLF is assumed to be $1/t$ (1) and one where it is assumed to be $3/t$ (2). b) As for a), but with longer time span.

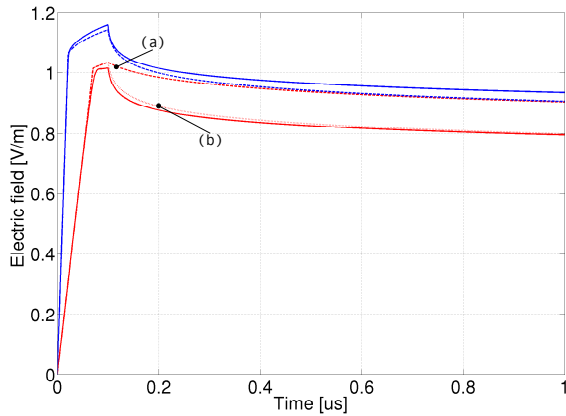


Figure 19: Field at $\xi=-1$ (apex) and $\xi = -0.95$ versus time, comparison between simulation (solid line) and the approximation in eq. 29 (a) and eq. 30 (b). Conductivity given by eq. 20 ($n=1$).

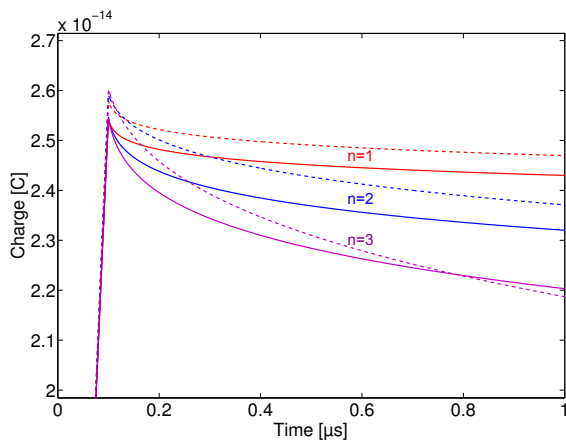


Figure 20: Charge on spheroid, finite element computations (solid lines) and approximation of the charge based on eq. 30. Conductivity given by eq. 20-22 ($n=1-3$), step voltage with $t_r=100$ ns, minor axis= $10 \mu\text{m}$ and major axis= $100 \mu\text{m}$.

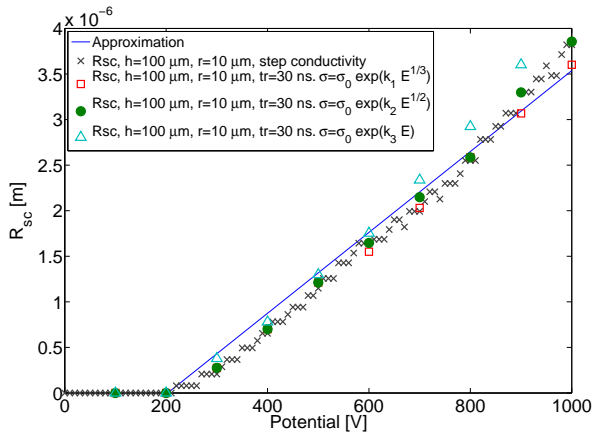


Figure 21: Extent of SCLF along the axis from the apex of the spheroid. Approximation (solid line) compared to finite element calculations obtained with step conductivity (eq. 10) and exponentially increasing conductivities given by eqs. 20-22 ($n=1-3$).

conductivity can be applied directly and gives a decent approximation for the extent of the SCLF for $n=1$ to 3. Figure 21 plots the extent of the field with step conductivity and the three field dependent conductivities given in eqs. 20-22 ($n=1-3$) which are compared to R_{sc} (eq. 18). When using this equation with the exponentially increasing conductivities, one must calculate F_c based on the equivalent frequency of the applied voltage.

5 Conclusion

Approximations for the field and charge on the surface of a spheroid in a uniform background field, and the extent of the SCLF from the apex of the spheroid, have been derived. The approximations have been tested for a variety of geometries and conductivity formulas, and generally give good results. Even so, the exact limitations of the approximations are not known, and they should therefore be used as a first approximation followed by finite element calculations to validate any conclusions drawn based on the approximations. Generally the approximation of the field on the spheroid give good results as long as the background field is increasing ($t < t_r$) for all conductivity formulas used, whereas formulas with $n=1$ gives the best fit after the time at which the background field stops increasing ($t > t_r$). There is still room for improvement of the approximation for the field and the charge on the spheroid for $n>1$ in the time range ($t > t_r$). Still the general shape when plotting charge and field on the spheroid follows the finite element calculations also for $n>1$.

The extent of the SCLF into the dielectric, R_{sc} , may be the most important result of this paper, as it is tied to the inception of electrical trees in polymers. The approximation found for R_{sc} is good up to at least $5 \mu\text{m}$, which is sufficient

as the critical extent in XLPE is about $1.5 \mu\text{m}$.

A Matlab code

```
% Input parameters, defines rise time etc..
% Rise time
tr=100e-9;
% constants in the conductivity formula sigma(E)=sigma0*exp(k*E^(1/n))
k=2.36e-5;
n=1;
sigma0=1e-14;
% Permittivity, relative * the vacuum permittivity.
epsilon=2*8.85e-12;
% Definition of the geometry
h=100e-6;
r=10e-6;
d=10e-3;
% dt and dxi
dt=1e-9;
dxi=1e-3;
%time vector
t=0:dt:10e-6;
% xi vector, from 0 to -1
xi=0:-dxi:-1;
%Background field:
E0=1000.*t./(d*tr);
% Formula for the SCLF as a function of t
Elim=(1./k.*log(epsilon./(sigma0.*t))).^n;
% Multiplication factor that the background field must be multiplied by to
% create the field on the apex (function of xi)
Esurf = xi.*((h.^2-r.^2).^(3/2)).*(((h.^2/(h.^2-r.^2)-xi.^2)/(h.^2/(h.^2-r.^2)-1))...
    .^(-1/2))/(r.^2)/(-acoth((h.*(h.^2-r.^2).^(-1/2))).*h+sqrt((h.^2-r.^2)));
% Creates a matrix with time vector along one axis and xi vector along the
% other, the values are the laplacian field given by the factor above time
% the background field
Esurf=[];
for i = 1:length(E0)
Esurf=[Esurf; Esurf.*E0(i)];
end
% Find the time when the laplacian field reaches the SCLF, function of xi
tlim=[];
for i = 1:length(xi)
    tlim=[tlim, max(find(Elim>Esurf(:,i)))];
end
% After tlim the field on the spheroid no longer increases like predicted
% by the laplacian formula. Thus the time region from tlim to the end of
% the time vector must be replaced by the formula found from curve fitting
% using sigmaplot:
for i=1:length(xi)
    Esurf(tlim(i):length(t),i)=2*Elim(tlim(i))-Elim(tlim(i):length(t))+...
        diff(E0)/diff(t).*(t(tlim(i):length(t))-t(tlim(i))).*(0.124*n+0.03*n^2);
end
% So far I have assumed that the voltage is rising during the entire time
% period, if this is the case Esurf given above will be the appropriate
% approximation for the field on the surface of the spheroid. Now I will
% assume that the voltage stays constant after tr (thus the background
% field is static from this time).
% First I find the index corresponding to tr (rise time):
trind=min(find(t>tr));
%Then I must find the effective frequency of the SCLF at the point apex at
%t=tr. The field on the apex will start to decrease with time after this
%point, according to an effective frequency given by: 1/(t0+(t-tr)).
```

```

%Actually the field on the part of the surface that is inside the
%SCLF-region will fall approximately like the field on the apex, the field
%on the rest of the spheroid is approximately given by the laplacian field.
if n>1
    Elim=(1./k.*log(epsilon./(sigma0.*0.33.*t)).^n;
end
t0ind=min(find(Esurf(trind, length(xi))≥Elim));
for i=1:length(xi)
    if tlim(i)≤trind
        Esurf(trind:length(t),i)=(1./k.*log(epsilon./(sigma0.*(t(t0ind)+...
            (t(trind:length(t))-t(trind))))).^n-(1./k.*log(epsilon./(sigma0.*(t(t0ind))))).^n+Esurf(trind:i,i));
    else
        Esurf(trind:length(t),i)=Esurf(trind,i);
    end
end
% Check that the function is decreasing for all t as xi is increasing from
% -1 towards 0 (the index is falling). This must be done because there is a
% region where the laplacian field approximation actually gives higher
% fields than the approximation above for the region inside the
% SCLF-region.
for i=(length(xi)-1):-1:1
    Esurf(find(Esurf(:,i)>Esurf(:,i+1)),i)=Esurf(find(Esurf(:,i)>Esurf(:,i+1)),i+1);
end
% The charge on the spheroid can now be found by integrating the field
% above over the surface of the spheroid, but for the integral I first
% need the square roots of the metrics for prolate-spheroidal coordinates
% (only need xi and theta):
c2=sqrt(h^2-r^2);
eta0=h./sqrt(h^2-r^2);
mxi=c2*sqrt((eta0^2-xi.^2)./(1-xi.^2));
mtheta=c2*sqrt((eta0^2-1).*(1-xi.^2));
m=mxi.*mtheta;
% mxi -> infinity and mtheta -> 0 as xi -> -1. Numerically this ends up as
% NaN, which creates problems. Solve this by replacing the number at xi=-1
% with the number at xi=-0.9999
m(length(m))=m(length(m)-1);
% Performs the integration, ends up with Q as a function of time
Q=[];
for i=1:length(t)
    Q=[Q,2*epsilon*pi*sum(m*dxi.*Esurf(i,:))];
end

```

References

- [1] J. C. Devins, S. J. Rząd, and R. J. Schwabe. Breakdown and prebreakdown phenomena in liquids. *J. Appl. Phys.*, 52:4531–4545, 1981.
- [2] A. Beroual, M. Zahn, A. Badent, K. Kist, A.J. Schwabe, H. Yamashita, K. Yamazawa, M. Danikas, W.D. Chadband, and Y. Torshin. Propagation and structure of streamers in liquid dielectrics. *IEEE Electric. Insul. Mag.*, 14:6–17, 1998.
- [3] A. Denat. High field conduction and prebreakdown phenomena in dielectric liquids. *IEEE Trans. Dielect. Elect. Insul.*, 13:518–525, 2006.
- [4] L. A. Dissado and J. C. Fothergill. *Electrical Degradation and Breakdown in Polymers*. Material and Devices Series 9. The Institution of Engineering and Technology, London, United Kingdom, 1992.
- [5] L. A. Dissado. Understanding electrical trees in solids: from experiment to theory. *IEEE Trans. Dielect. Elect. Insul.*, 9:483–497, 2002.
- [6] S. Boggs. Very high field phenomena in dielectrics. *IEEE Trans. Dielect. Elect. Insul.*, 12:929–938, 2005.
- [7] S. Rasikawan and N. Shimizu. Effect of additives on treeing initiation as a function of oxygen concentration in polyethylene. *IEEE Trans. Elect. Insul.*, 27:1089–1094, 1992.
- [8] R. Tobazeon. Prebreakdown phenomena in dielectric liquids. *IEEE Trans. Dielect. Elect. Insul.*, 1:1132–1147, 1994.
- [9] K. Tavernier, B. R. Varlow, and D. W. Auckland. Electrical tree modelling in non-linear insulation. In *Ann. Rep. Conf. Elec. Insul. Diel. Phen. (CEIDP)*, pages 661–664 vol. 2, 1998.
- [10] T. Baumann, B. Fruth, F. Stucki, and H. R. Zeller. Field-enhancing defects in polymeric insulators causing dielectric ageing. *IEEE Trans. Elect. Insul.*, 24:1071–1076, 1989.
- [11] T. Hibma and H. R. Zeller. Direct measurement of space-charge injection from a needle electrode into dielectrics. *J. Appl. Phys.*, 59:1614–1620, 1986.
- [12] D. Braun. Electronic injection and conduction processes for polymer devices. *J. Polym. Sci. B*, 41:2622–2629, 2003.
- [13] G. Jiang, J. Kuang, and S. Boggs. Evaluation of high field conduction models of polymeric dielectrics. In *Ann. Rep. Conf. Elec. Insul. Diel. Phen. (CEIDP)*, volume 1, pages 187–190 vol.1, 2000.
- [14] Ø. L. Hestad, L. E. Lundgaard, and P.-O. Åstrand. n-tridecane as a model system for polyethylene: Comparison of pre-breakdown phenomena in liquid and solid phase stressed by a fast transient. *Submitted*, 2010.
- [15] Z. Zheng and S. Boggs. Defect tolerance of solid dielectric transmission class cable. *IEEE Electric. Insul. Mag.*, 21:34–41, 2005.

- [16] H. R. Zeller and W. R. Schneider. Electrofracture mechanics of dielectric aging. *J. Appl. Phys.*, 56:455–459, 1984.
- [17] H. S. Smalø, Ø. L. Hestad, S. Ingebrigtsen, and P.-O. Åstrand. Field dependence on the molecular ionization potential and excitation energies compared to conductivity models for insulation materials at high electrical fields. *Submitted*.
- [18] Comsol Multiphysics® ver. 3.5a with AC/DC module. Comsol AB. Regnergatan 23. SE-111 40 Stockholm. Sweden. www.comsol.com.
- [19] W. R. Smythe. *Static and Dynamic Electricity, 3rd Ed.* Hemisphere Publishing Co, 1989.
- [20] K. Zhou and S. Boggs. Uniform field charge on a conducting particle standing on a ground plane. *IEEE Trans. Dielect. Elect. Insul.*, 16:1158–1159, 2009.